ISTANBUL TECHNICAL UNIVERSITY ★ GRADUATE SCHOOL OF SCIENCE ENGINEERING AND TECHNOLOGY

MIOCENE TO QUATERNARY GEODYNAMIC EVOLUTION OF THE BURDUR-FETHİYE SHEAR ZONE, SOUTH-WESTERN TURKEY

Ph.D. THESIS

İrem ELİTEZ

Department of Geological Engineering

Geological Engineering Programme

JUNE 2019

ISTANBUL TECHNICAL UNIVERSITY ★ GRADUATE SCHOOL OF SCIENCE ENGINEERING AND TECHNOLOGY

MIOCENE TO QUATERNARY GEODYNAMIC EVOLUTION OF THE BURDUR-FETHİYE SHEAR ZONE, SOUTH-WESTERN TURKEY

Ph.D. THESIS

İrem ELİTEZ
(505102302)

Department of Geological Engineering

Geological Engineering Programme

Thesis Advisor: Prof. Dr. Cenk YALTIRAK

JUNE 2019

İSTANBUL TEKNİK ÜNİVERSİTESİ ★ FEN BİLİMLERİ ENSTİTÜSÜ

BURDUR-FETHİYE MAKASLAMA ZONU'NUN MİYOSEN'DEN KUVATERNER'E JEODİNAMİK EVRİMİ, GÜNEYBATI TÜRKİYE

DOKTORA TEZİ

İrem ELİTEZ
(505102302)

Jeoloji Mühendisliği Anabilim Dalı

Jeoloji Mühendisliği Programı

Tez Danışmanı: Prof. Dr. Cenk YALTIRAK

HAZİRAN 2019

İrem ELİTEZ, a Ph.D. student of İTU Graduate School of Science Engineering and Technology student ID 505102302, successfully defended the thesis/dissertation entitled "MIOCENE TO QUATERNARY GEODYNAMIC EVOLUTION OF THE BURDUR-FETHİYE SHEAR ZONE, SOUTH-WESTERN TURKEY", which she prepared after fulfilling the requirements specified in the associated legislations, before the jury whose signatures are below.

Thesis Advisor :	**Prof. Dr. Cenk YALTIRAK** İstanbul Technical University	....
Jury Members :	**Prof. Dr. H. Serdar AKYÜZ** İstanbul Technical University	....
	Prof. Dr. Ş. Can GENÇ İstanbul Technical University	....
	Prof. Dr. Şükrü ERSOY Yıldız Technical University	....
	Prof. Dr. Faruk OCAKOĞLU Eskişehir Osmangazi University	....

Date of Submission : 15 May 2019
Date of Defense : 11 June 2019

“In questions of science, the authority of a thousand is not worth the humble reasoning of a single individual.”

Galileo Galilei

To my parents,

FOREWORD

First and foremost, I would like to express my deepest gratitude to my advisor, Prof. Dr. Cenk YALTIRAK for his continuous support of my research, my Ph.D. study and my life. The knowledge that he has provided me during my work is invaluable. He has always motivated me to do my best and given me the freedom to shape my own Ph.D.

I am grateful to Assoc. Prof. Gürsel SUNAL (İstanbul Technical University), Prof. Dr. Ali E. AKSU (Memorial University), Prof. Dr. H. Serdar AKYÜZ (İstanbul Technical University), Prof. Dr. Şükrü ERSOY (Yıldız Technical University) and Prof. Dr. Boris NATALIN (İstanbul Technical University) for their constructive comments. I would like to thank to Prof. Dr. Jeremy HALL (Memorial University) and Prof. Dr. Günay ÇİFCİ (9 Eylül University) for giving me the opportunity to take part in their project.

I thank to Şükrü ÖZÜDOĞRU and F. Eray DÖKÜ (Directors of the excavation team of the ancient city of Kibyra) for providing the opportunity to excavate a research trench and accommodation. Also, I thank to Tamer DUMAN (General Directorate of Mineral Research and Exploration - MTA) for the trench data.

I also thank to geologist Murat ŞAHİN (İstanbul Technical University) for his help in producing the GMT plots, Nureddin KAYMAKÇI (Middle East Technical University) and Ayberk UYANIK (Turkish Petroleum Corporation) for English editing, the archaeologists Mustafa ŞİMŞEK, Düzgün TARKAN, Mesut KAYA and the geological engineers Aybars ÖZMEN, Okan KARAKOÇ and Derya İpek GÜLTEKİN for their help in field and laboratory.

I am also grateful to Prof. Dr. Aral OKAY (İstanbul Technical University) for permission to use Mineral Separation Laboratory of the Eurasian Institute of Earth Sciences at İstanbul Technical University. I also would like to thank Stoyan GEORGIEV (Bulgarian Academy of Sciences) for U-Pb dating of the volcanic rocks and Chris HALL (University of Michigan) for $^{40}Ar/^{39}Ar$ dating.

I wish to thank my parents Nagihan and Adnan ELİTEZ who support me throughout my life.

Finally, I am grateful to TUBITAK ÇAYDAG (Project No: 107Y005 and 115Y424) and to the İstanbul Technical University Scientific Research Projects Coordination Department (Project No: 32511) for their financial support for the field studies and geochronological analysis.

May 2019

İrem ELİTEZ
(M.Sc. Geologist)

TABLE OF CONTENTS

Page

ABBREVIATIONS

AB	:	Acıgöl Basin
AD	:	Anno Domini
AKMB	:	Aksu, Köprüçay, Manavgat Basins
AL	:	Acıgöl
Al	:	Aluminium
AM	:	Anaximander Mountain
Ar	:	Argon
AVS	:	Acıpayam Volcanic Source
BB	:	Burdur Basin
BBF	:	Bandırma-Behramkale Fault
BFSZ	:	Burdur-Fethiye Shear Zone
BL	:	Burdur Lake
BMB	:	Büyük Menderes Block
BMG	:	Büyük Menderes Graben
Bt	:	Biotite
C	:	Calcite
Ca	:	Calcium
CIP	:	Common Intersection Point
Cl	:	Chlorine
DEM	:	Digital Elevation Model
DFS	:	Dynamic Frequency Selection
DSFZ	:	Dead Sea Fault Zone
E	:	East
EAFZ	:	East Anatolian Fault Zone
EB	:	Eşen Basin
EGB	:	Eğirdir Basin
EL	:	Eğirdir Lake
EMB	:	Edremit-Manyas Block
ESE	:	East-southeast
FB	:	Finike Basin

FBFZ	: Fethiye-Burdur Fault Zone
Fel	: Feldspar
Fm	: Formation
GA	: Gulf of Antalya
GF	: Ganos Fault
GG	: Gediz Graben
GIS	: Geographic Information System
GMT	: Generic Mapping Tools
GNKG	: Gökova-Nisyros-Karpathos Graben
GPS	: Global Positioning System
GYFZ	: Gökova-Yeşilüzümlü Fault Zone
IA	: Isparta Angle
ICP-MS	: Inductively Coupled Plasma - Mass Spectrometer
IMST	: Institute of Marine Sciences and Technology
K	: Potassium
KB	: Kasaba Basin
LA-ICP-MS	: Laser Ablation Inductively Coupled Plasma Mass Spectrometry
LIDAR	: Laser Imaging Detection and Ranging
Ma	: Million years
MB	: Menderes Block
MRB	: Marmaris-Rhodes Block
M-plane	: Movement plane
M-pole	: Movement pole
MSC	: Messinian Salinity Crisis
MSWD	: Mean square of weighted deviations
MTA	: General Directorate of Mineral Research and Exploration
MTF	: Manyas-Tuzla Fault
MUN	: Memorial University of Newfoundland
My	: Million years
N	: North
n	: Number
NAF	: North Anatolian Transform Fault
NE	: Northeast
NNE	: North-northeast
NW	: Northwest

Pb : Lead
PSFZ : Pliny-Strabo Fault Zone
RB : Rhodes Basin
RP : Rotation pole
S : South
SE : Southeast
SEP : Sırrı Erinç Plateau
SL : Stream length
sp. : Species
SRTM : Shuttle Radar Topography Mission
SSW : South-southwest
STEP : Subduction-Transform Edge Propagator
SW : Southwest
TB : Tefenni Basin
TEF : Thrace-Eskişehir Fault
Th : Thorium
U : Uranium
UB : Uşak Block
USGS : U.S. Geological Survey
W : West
WNW : West-northwest
WTB : Western Taurides Block
WTTF : Western Taurides Thrust Fault
VG : Volcanic glass
YFZ : Yeşilüzümlü Fault Zone

SYMBOLS

ccSTP	: Gas dissolved per cc of water at a standard temperature and pressure
km	: Kilometer
m	: Millimeter
mA	: Milliampere
mm/yr	: Millimeter per year
MWh	: Megawatt Hours
Mw	: Moment magnitude
µA	: Microampere
µm	: Micrometer
v_e	: East velocity
v_n	: North velocity
σ_{V_e}	: Standard deviation of east velocity
σ_{V_e}	: Standard deviation of north velocity
σ_{mag}	: Full covariance propagation to the velocity magnitude at a point
$\rho_{v_x v_y}$	: Correlation coefficient between east and north velocities
Φ	: Phi
λ	: Lambda
Ω	: Ohm

LIST OF TABLES

Page

LIST OF FIGURES

Page

MIOCENE TO QUATERNARY GEODYNAMIC EVOLUTION OF THE BURDUR-FETHİYE SHEAR ZONE, SOUTH-WESTERN TURKEY

SUMMARY

The tectonic framework of the eastern Mediterranean is based on an active subduction and small underwater hills/mountains on the oceanic crust moving toward the north. The Hellenic Arc, the Anaximander Mountains, the Rhodes and Finike basins, the compressional southern regions of the Western Taurides, and the extensional western Anatolian graben are the main interrelated tectonic structures that are shaped by the complex tectonic regimes. There are still heated debates regarding the structural properties and tectonic evolution of the southwestern Anatolia. GPS velocities and focal mechanisms of earthquakes demonstrate the absence of a single transform fault across the Burdur-Fethiye region; however, hundreds of small faults showing normal and left-lateral oblique slip indicate the presence of a regionally extensive shear zone in southwestern Turkey, which plays an important role in the eastern Mediterranean tectonics.

The 300-km-long, 75-90-km-wide NE-SW-trending Burdur-Fethiye Shear Zone developed during the formation of Aegean back-arc extensional system and the thrusting of Western Taurides. Today, the left-lateral differential motion across the Burdur-Fethiye Shear Zone varies from 3 to 4 mm/yr in the north to 8-10 mm/yr in the south. This finding could be attributed to the fact that while the subduction of the African Plate is relatively fast beneath the western Anatolia at the Hellenic Trench, it is slow or locked beneath the Western Taurides. Therefore, the GPS vectors and their distributions on land indicate remarkable velocity differences and enable us to determine the left-lateral shear zone located between the extensional and compressional blocks. Furthermore, this active tectonic regime creates differences in topography.

Southwestern Turkey is a tectonically active region where extensional, strike-slip, and compressional tectonics cooccur. Understanding the tectonic evolution of this region is crucial, but the controversial Neogene chronostratigraphy does not allow robust synthesis because of poor age control. A considerable number of studies suggested contradictory models of the evolution and Neogene stratigraphy of the Burdur-Fethiye Shear Zone. The Burdur-Fethiye Shear Zone includes several basins: the Karamık, Eğirdir, Acıgöl, Burdur, Tefenni, Acıpayam, Çameli, Gölhisar and Eşen basins. The field observations in this thesis revealed two distinct sedimentary sequences that unconformably overlie the pre-Neogene basement. The first sequence begins with middle-upper Miocene meandering- and braided-river sediments which transition upward into lacustrine sediments of the upper Miocene-lower Pliocene. This sequence is overlain by upper Pliocene-lower Quaternary alluvial fan conglomerates, mudstones and claystones. The basin deposits located along the Burdur-Fethiye Shear Zone consist of lacustrine sediments of a late Miocene lake that likely evaporated due to the Messinian salinity crisis.

Fault kinematic analysis and DEM and earthquake data indicate that the Burdur-Fethiye Shear Zone can be characterized as a heterogeneous left-lateral transtensional shear zone rather than a major fault system. The findings also suggest that the Burdur-Fethiye Shear Zone developed under the influence of progressive counterclockwise rotation of south-western Turkey, the Aegean graben system and the Cyprus and Hellenic arcs since the middle Miocene. All these basins represent restricted portions of ancient larger carbonate lakes. In the middle section of the zone, the lacustrine sediments are locally covered or cut by lamproites with sparse intercalations of tuff levels. New ^{40}Ar-^{39}Ar biotite and U-Pb zircon radiometric ages from volcanics and a tuff layer in this thesis demonstrate that the previously suggested Pliocene ages for these sediments are incorrect and that these Neogene sediments are middle Miocene in age.

A large number of ancient cities lie on the Burdur-Fethiye Shear Zone and many of them have been damaged by ancient earthquakes. One of these ancient cities is the ancient city of Kibyra. Most of previous studies suggest the Kibyra Fault depending on the damage in the city. However, the closest fault is located on the western side of the city and the earthquake damage was most likely caused by ground shaking. In this thesis, the existence of the supposed Kibyra Fault is discussed by integrating field studies, geological maps, trench data, digital elevation model and geomorphological analysis. In conclusion, it is understood that there is no evidence directly indicating a 35-km-long left-lateral fault in this region.

This thesis project demonstrates how deep structures, such as the continuation of the subduction transform edge propagator (STEP) fault between the Hellenic and Cyprus arcs in the continental area, can come into play as a shear zone on the brittle crust. The Burdur-Fethiye Shear Zone is located in the middle of this complex area. New field data, fault kinematic analyses, DEM and earthquake data and new ^{40}Ar-^{39}Ar biotite and U-Pb zircon radiometric ages are presented to characterize the tectonic controls. In addition, the aim of this thesis is to examine the existence of the Kibyra Fault, take a different approach to the active fault studies and emphasise the importance of active faults for socio-economic conditions.

BURDUR-FETHİYE MAKASLAMA ZONU'NUN MİYOSEN'DEN KUVATERNER'E JEODİNAMİK EVRİMİ, GÜNEYBATI TÜRKİYE

ÖZET

Doğu Akdeniz'in tektonik yapısı, aktif bir dalma-batma ve kuzey yönüne doğru ilerleyen okyanusal kabuk üzerinde bulunan küçük sualtı tepeleri/dağlarına dayanmaktadır. Helen Yayı, Anaximander Dağları, Rodos ve Finike basenleri, Batı Toroslar'ın sıkışan güney bölgeleri ve genişlemeli Batı Anadolu grabeni, karmaşık tektonik rejimlerle şekillenen birbiriyle ilişkili tektonik yapılardır. Güneybatı Anadolu'nun yapısal özellikleri ve tektonik evrimi ile ilgili hala hararetli tartışmalar bulunmaktadır. GPS hızları ve depremlerin odak mekanizmaları, Burdur ile Fethiye arasında KD-GB gidişli tek bir transform fay bulunmadığını kanıtlamaktadır. İleri sürünenin tam aksine, normal ve sol yanal oblik atım gösteren yüzlerce küçük fay, doğu Akdeniz tektoniğinde önemli bir rol oynayan güneybatı Türkiye'de bölgesel olarak geniş bir makaslama zonun varlığına işaret etmektedir.

Güneybatı Türkiye, Anadolu'nun Kuzey Anadolu Fayı ve Doğu Anadolu Fayı boyunca batıya kaçışı, Helen Yayı'nın geriye çekme (roll-back) etkisine bağlı KD-GB Ege yay ardı genişleme rejimi, Helen ve Kıbrıs yaylarının hareketi ile ilişkili STEP (subduction transform edge propagator) fay zonu ve Batı Toroslar sıkışma bölgesinin etkisi altındadır. Doğu Akdeniz'in Neojen tektonizması Afrika ve Arap levhalarının Avrasya Levhası'na doğru yaklaşması ile ilişkilidir. Afrika Levhası ile Ege-Anadolu Mikrolevhası arasındaki yakınsak sınır iki dalma-batma ile ilişkili yay ile karakterize edilmektedir: batıda Helen Yayı ve doğuda Kıbrıs Yayı. Bu iki yay arasında yaklaşık 400 km atım bulunmaktadır. Helen Yayı'nın altından devam eden dalma-batma, yay ardı bölgesi olan Ege Denizi ve Batı Anadolu'da geç Eosen'den beri gerilmeye neden olmaktadır. Helen ve Kıbrıs yayları arasındaki diferansiyel hareket, iki yayı birbirine bağlayan ve bir STEP fay zonu olarak karşımıza çıkan, dalan levhada bir yırtılma yaratır. Rodos Havzası boyunca kuzeydoğu yönünde ilerleyen STEP fay zonunun devamı güneybatı Anadolu'da, kırılgan kabukta bir makaslama zonu olarak karşımıza çıkar. Bu makaslama zonu Burdur-Fethiye Makaslama Zonu'dur.

Burdur-Fethiye Makaslama Zonu kuzeyde Şuhut-Çay ile güneyde Sarıgerme-Gelemiş arasında bulunan, 300 km uzunluğa ve 75 ile 90 km arasında değişen genişliğe sahip olan KD-GB uzanımlı transtansiyonel bir makaslama zonudur. Zon boyunca yükseklikler 0 ile 3000 metre arasında değişmektedir. Zonun batısını Uşak, Büyük Menderes, Muğla ve Marmaris-Rodos blokları, doğusunu ise Batı Toroslar Bloğu sınırlamaktadır.

Güneybatı Türkiye genişleme, yanal-atım ve sıkışma tektoniğinin beraber işlediği tektonik olarak oldukça aktif bir bölgedir. Bu bölgenin tektonik gelişimini anlamak oldukça önemlidir, fakat yetersiz yaş verisi nedeniyle tartışmalı bir hal alan Neojen kronostratigrafisi sağlam bir sentez olanağı vermemektedir. Yapılan dikkate değer sayıda çalışma Burdur-Fethiye Makaslama Zonu'nun Neojen stratigrafisi ve gelişimi ile ilgili birbiriyle çelişen pek çok değişik model öne sürmektedir. Burdur-Fethiye Makaslama Zonu üzerinde bulunan Karamık, Eğirdir, Acıgöl, Tefenni, Acıpayam,

Çameli, Gölhisar ve Eşen havzaların oluşumu zonun oluşumu ile ilişkilidir. Bu tez çalışmasında detaylı olarak ele alınan zon üzerinde Neojen sedimanlarının en yoğun gözlendiği bölge olan orta kesim Acıpayam, Çameli ve Gölhisar havzalarından oluşmaktadır. Bu bölgede egemen temel kayalar, zonun tamamında da egemen olan Likya Napları'na ait ofiyolitik melanj ve rekristalize kireçtaşlarıdır. Bunun yanı sıra Yeşilbarak Napı'na ait flişler de yer yer gözlemlenmektedir. Bu temel üzerine uyumsuzluk ile alt Miyosen-üst Oligosen yaşlı konglomera ve kumtaşları gelir. Arazi çalışmaları Neojen öncesi temeli uyumsuzluk ile örten iki adet sedimanter istif olduğunu göstermiştir. İlk istif en altta orta-üst Miyosen yaşlı konglomera ve kumtaşlarının egemen olduğu menderes ve örgülü akarsu sedimanlarıyla başlamaktadır. Bu istif yanal ve düşey geçişli olarak üstte kireçtaşı, marn ve kiltaşı gibi gölsel sedimanlardan oluşan üst Miyosen-alt Pliyosen yaşlı birimlere geçer. Bu istifi uyumsuzluk ile örten ikinci istif üst Pliyosen-alt Kuvaterner yaşlı alüvyal yelpaze ortamını işaret eden konglomera, çamurtaşı ve kiltaşından oluşmaktadır. Burdur-Fethiye Makaslama Zonu'nun orta kesiminde bulunan gölsel sedimanların Messiniyen tuzluluk krizi ile ilişkili olarak buharlaşmış bir geç Miyosen göl ortamına ait olduğu düşünülmektedir.

Bu çalışma kapsamında Burdur-Fethiye Makaslama Zonu'nun orta kesiminden elde edilen lamproit ve tüf seviyeleri yaşlandırılmıştır. Acıpayam Havzası'nın kuzeyinde bulunan lamproitler bu bölgede genellikle gölsel sedimanları kesmekte ya da üstlerine yerleşmektedir. Bunun yanı sıra gölsel sedimanların alt kesiminde yanal ve düşey geçişli olarak bulunan akarsu sedimanları da lamproitler tarafından lokal olarak kesilmiştir. Ayrıca çalışma alanın güneybatısında gölsel sedimanlar içerisinde bulunan bir tüf seviyesi bulunmuştur. ^{40}Ar-^{39}Ar biyotit ve U-Pb zirkon radyometrik yaşları akarsu sedimanlarının yaşının alt Messiniyen olduğunu göstermiştir. Ayrıca lamproitlerden alınan yaşlar ile gölsel sedimanlar içerisindeki tüf seviyesi korele edilerek bölge için yeni bir kronostratigafi oluşturulmuştur. Bu veriler ve gölsel sedimanların en üst kesiminde bulunan Messiniyen tuzluluk krizini temsil ettiği düşünülen şarap kırmızısı renge sahip kalişli seviyeler dikkate alınarak bölgedeki gölsel sedimanlar üst Miyosen-alt Pliyosen olarak yaşlandırılmıştır.

Burdur-Fethiye Makaslama Zonu 1 ile 10 km arasında değişen uzunluklara sahip normal ve oblik ana faylardan oluşmaktadır. Bu ana faylar zonun temelini oluşturan Likya Napı'nın eski faylarının ürünleridir. Zondaki birçok fay KB-GD, KD-GB ve KKD-GGB gerilme/oblik gerilme göstermektedir. Bu durum bölgede birbirine dik iki fay sistemi olduğu anlamına gelmektedir. Zonun orta kesiminde Neojen sedimanlar baskındır ve bu Neojen sedimanları içerisinde birçok küçük ölçekli fay ölçülmüştür. Yapılan kinematik analizler ile KD-GB, KB-GD, KKB-GGD ve KBK-DGD yönelimli stresler gözlemlenmiştir. Bilindiği gibi bölgenin güncel tektoniği Helen Yayı'nın geriye çekme (roll-back) etkisi ile ilişkili KD-GB yönelimli stres ve transtansiyonel makaslamanın neden olduğu KB-GD yönelimli streslerle kontrol edilmektedir. Bu nedenle ana faylar da hep bu doğrultularda gözlemlenmektedir. Bölgeye etki eden hem makaslama, hem içsel rotasyon hem de Anadolu'nun rotasyonu da küçük ölçekli faylardaki stres yönü değişimlerinin başlıca nedenidir.

Burdur-Fethiye Makaslama Zonu, Ege genişleme sistemini oluşturan yay-ardı gerilmesi ile Batı Toroslar'ın Akdeniz'e bindirmesi esnasında oluşan geniş bir fermuar gibidir. Bugün, Burdur-Fethiye Makaslama Zonu boyunca sol yanal diferansiyel hareket kuzeyde yaklaşık 3-4 mm/yıl ile güneyde 8-10 mm/yıl olarak değişmektedir. GPS vektörlerine hem paralel hem de dik topografik kesitler ve hız kesitleri oluşturulmuştur. Burdur-Fethiye Makaslama Zonu'nun batı kesiminde kuzeyden güneye doğru hızlarda yüksek bir artış olduğu görülmüştür. Zonun doğu kesiminde ise kuzeyden güneye hız azalması dikkati çekmektedir. Yani batıda topografya düşerken ve hızlar azalırken, doğuda tam tersi bir durum söz konusudur. Bunun nedeni batıdaki gerilme ve doğudaki sıkışma rejimleridir. GPS hızlarına dik alınan kesitlerde de batıdan doğuya doğru hızların düştüğü açıkça görülmektedir. Batı-doğu arasındaki hız farkı kuzeyde azken güneye doğru artmaktadır. Bu durum da bölgedeki makaslamanın bir kanıtı olarak yorumlanabilmektedir. Elde edilen bu verilerin en önemli nedeni Afrika Levhası'nın Helenik Yay'da Batı Anadolu'nun altına dalarken hızlı, Batı Toroslar'da ise yavaşlamış veya kitlenmiş olmasıdır. Bu nedenle de GPS vektörleri ve bunların kara alanındaki dağılımı dikkat çekici hız farkları gösterir. Bu aktif tektonik rejim topoğrafyada da farklılık yaratmaktadır. Bu değişim, GPS hızları ile daha iyi anlaşılan gerilen ve sıkışan bloklar ile arasındaki sol yanal makaslama alanını anlamamızı sağlamıştır.

Kinematik fay analizleri ve DEM ve deprem verileri Burdur-Fethiye Makaslama Zonu'nun tek bir ana faydan oluşan bir sistemden ziyade heterojen sol-yanal transtansiyonel bir makaslama zonu olduğunu göstermektedir. Bulgular ayrıca Burdur-Fethiye Makaslama Zonu'nun güneybatı Türkiye'nin saatin tersi yöndeki dönüşü, Ege graben sistemi ve Kıbrıs ve Helen yayları ile ilişkili olarak orta Miyosen'den beri geliştiğini ortaya koymuştur. Zon boyunca bulunan tüm havzalar eski büyük karbonat göllerinin parçalarıdır. Gölsel sedimanlar tüf seviyeleri ile seyrek olarak ardalanma gösteren lamproitler tarafından bölgesel olarak örtülmekte ya da kesilmektedir. Bu tez kapsamında, Acıpayam Havzası'nın kuzey kesiminde gözlemlenen lamproitlerden ve Çameli Havzası'nın güneybatısında bulunan bir tüf seviyesinden elde edilen ^{40}Ar-^{39}Ar biyotit ve U-Pb zirkon radyometrik yaşları daha önceki çalışmalarda Pliyosen olarak yaşlandırılan sedimanların orta Miyosen yaşlı olduklarını kanıtlamıştır.

Burdur-Fethiye Makaslama Zonu üzerinde oldukça fazla sayıda antik şehir bulunmaktadır ve bu antik şehirlerin çoğu eski depremlerde önemli ölçüde zarar görmüştür. Bu antik şehirlerde biri de Kibyra antik şehridir. Kibyra antik şehri ve çevresinde yapılmış önceki çalışmalar şehrin Kibyra Fayı olarak adlandırılan bir fay tarafından hasar gördüğünü kabul etmektedir. Fakat, bu şehre en yakın fay şehrin batı kesiminde bulunmaktadır ve şehirde meydana gelen deprem hasarının nedeni büyük olasılıkla yer sarsıntısıdır. Bu tez kapsamında Kibyra Fayı olarak adlandırılan fayın varlığı arazi çalışmaları, jeoloji haritaları, trenç verisi, sayısal yükseklik modeli ve jeomorfolojik analizlerin birleştirilmesi ile tartışılmıştır. Sonuç olarak, önceki çalışmalarda tanımlanan, Kibyra antik kentinin kuzey kesimindeki Çamköy'den başlayıp, antik kentin stadyumunu keserek güneydeki Yusufça'ya ilerleyen, yaklaşık 35 km uzunluğa sahip sol yanal Kibyra Fayı'nın aslında var olmadığı anlaşılmıştır.

Bu tez çalışması, Helen ve Kıbrıs yayları arasında bulunan STEP fayının kıtasal alanda devamı olarak izlenen derin yapıların, kırılgan kabuk üzerinde makaslama zonu olarak etkili olabileceğini göstermektedir. Burdur-Fethiye Makaslama Zonu bu kompleks alanın ortasında bulunmaktadır. Sonuç olarak, yeni arazi verileri, kinematik fay analizleri, DEM ve deprem verileri ve yeni ^{40}Ar-^{39}Ar biyotit ve U-Pb zirkon radyometrik yaşları Burdur-Fethiye Makaslama Zonu'nun oluşmasına ve gelişmesine neden olan tektonik aktiviteyi kontrol eden etmenleri ve zonun oluşumunun başlangıç zamanını ortaya koymuştur. Buna ek olarak, bu tezin amacı kapsamında Kibyra Fayı örneği üzerinden gidilerek aktif fay çalışmalarına farklı bir bakış açısı kazandırılmış ve aktif olduğu öne sürülen her fayın sosyo-ekonomik koşulları etkileyici yönleri olduğuna dikkat çekilerek çalışmaların bu titizlikle yapılması gerektiği vurgulanmıştır.

1. INTRODUCTION

1.1 Regional Geological Setting

The south-western Turkey and adjacent western Turkey form one of the most tectonically active areas of the eastern Mediterranean. Mostly northeast-southwest-striking active faults developed as the result of the counterclockwise rotation of the western segment of the Aegean-Anatolian Microplate and the N-S back-arc extension regime due to roll-back of the Hellenic Trench (Dewey and Şengör, 1979; Le Pichon and Angelier, 1979; McKenzie, 1978; Meulenkamp et al., 1988; Şengör, 1979; Şengör et al., 1985; Yılmaz et al., 2000).

The Hellenic and Cyprus Arcs are the convergent boundary of the African and Aegean-Anatolian plates in this region. These two arcs are connected by a STEP (subduction transform edge propagator) Fault Zone which is a tear in the subducting slab (Figure 1.1; Govers and Wortel, 2005). The NE-SW-trending STEP Fault Zone runs along the Pliny-Strabo Trenches. The continuation of the STEP Fault Zone to the northeast through the Rhodes Basin and into the southwest Anatolia appear as a shear zone on the brittle crust: the Burdur-Fethiye Shear Zone (Figure 1.1). The high-angle faults with extensional separations developed in the Rhodes Basin can be linked with the similarly trending and dipping faults onland on the southern part of the Burdur-Fethiye Shear Zone. These situations show that there is a continuity between the Pliny-Strabo Trenches in the southwest and the Burdur-Fethiye Shear Zone in the northeast (Aksu et al., 2009; Barka and Reilinger, 1997; Elitez et al., 2009; Hall et al., 2009, 2014; Huguen et al., 2001; Ocakoğlu, 2012; Taymaz and Price, 1992; ten Veen et al., 2004, 2009; Woodside et al., 2000; Yaltırak et al., 2010; Zitter et al., 2003).

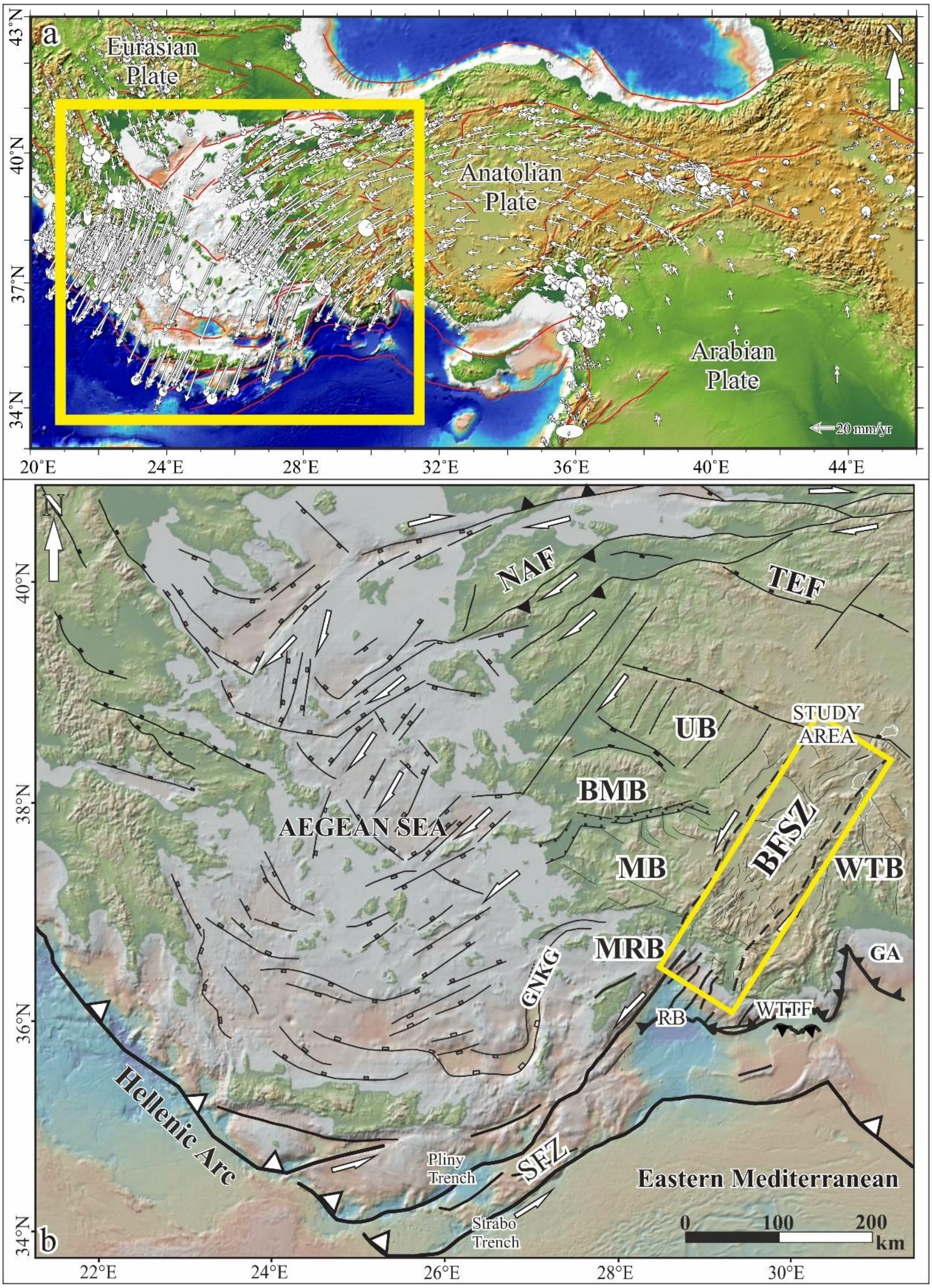

Figure 1.1 : (a) GPS vectors relative to fixed Eurasian Plate showing the counterclockwise rotation of the Anatolian Block (Kreemer et al., 2014). Yellow rectangle indicates Figure 1.1b. (b) Tectonic map of the Aegean Sea, western and southwestern Turkey showing the predominantly structures, compiled from Mascle and Martin (1990); Papanikolaou et al. (2002). NAF: North Anatolian Fault, TEF: Thrace-Eskişehir Fault, SFZ: STEP Fault Zone, BFSZ: Burdur-Fethiye Shear Zone, UB: Uşak Block, BMB: Büyük Menderes Block, MB: Muğla Block, GNKG: Gökova-Nisyros-Karpathos Graben, MRB: Marmaris-Rhodes Block, WTB: Western Taurides Block, WTTF: Western Taurides Thrust Fault, RB: Rhodes Basin, GA: Gulf of Antalya.

The study area of this thesis incorporates the Burdur-Fethiye Shear Zone which is a 75- to 90- km-wide and 300-km-long transtensional left-lateral shear zone between Şuhut-Çay on the northeast and Sarıgerme-Gelemiş on the southwest in south-western Turkey. The elevations range from 0 to 3000 m along the zone.

The western margin of the Burdur-Fethiye Shear Zone is delineated by the Büyük Menderes Graben, Muğla Block and Marmaris-Rhodes Block. The Büyük Menderes Graben is dominated by extensional tectonism. The Muğla and Marmaris-Rhodes blocks are situated to the south of the Büyük Menderes Graben. The Gökova-Nisyros-Karpathos Graben exists between the Muğla and Marmaris-Rhodes blocks. The Hellenic Arc is situated immediately southwest of the Marmaris-Rhodes Block. The eastern margin of the Burdur-Fethiye Shear Zone is delineated by the Western Taurides Block. The Finike and Rhodes basins are situated south of the Western Taurides Block.

The geology of the Burdur-Fethiye Shear Zone is comprised of Upper Oligocene to Recent sedimentary units that unconformably reside on the basement. These sedimentary units show local unconformities related to tectonic evolution and basin development. The basement rocks are composed of the Lycian Nappes, Yeşilbarak Nappe and Beydağları Para-autochthon (Figure 1.2). Also, there are volcanic successions with decreasing ages from north to south along the Burdur-Fethiye Shear Zone. These ages show that the zone is a deep tear zone between the western Anatolian extensional and the western Taurides compressional regimes since 15 Ma (Elitez et al., 2016b).

The zone consists of 1-2 km-long NE-SW-striking left-lateral normal oblique faults. These faults show evidence for left-lateral but total displacement across the zone is at maximum a few tens of kilometres. At the southern end of the zone, many NW-SE-striking faults indicate NE-SW-trending stress orientation due to the roll-back effect of the Hellenic Trench in the zone.

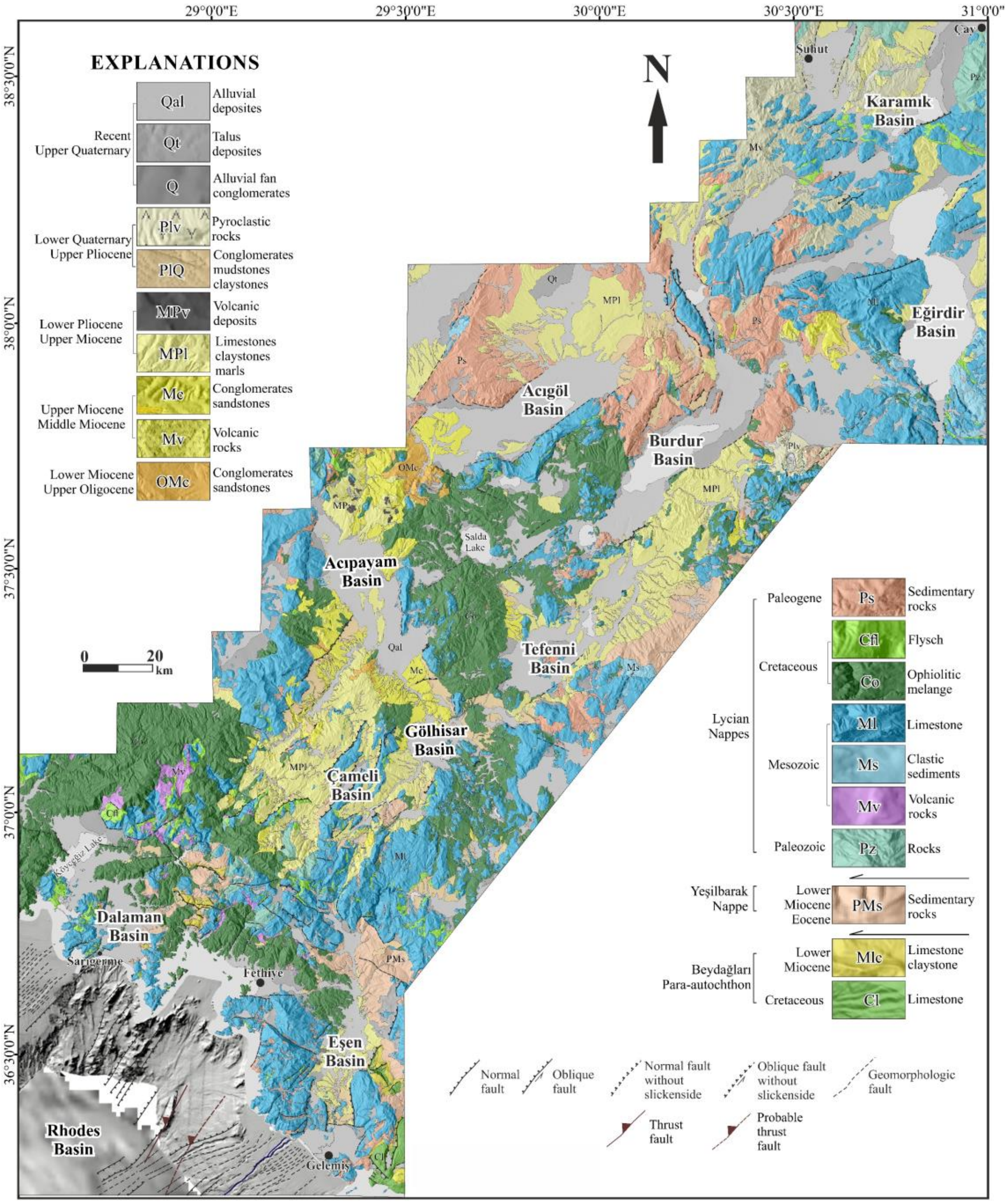

Figure 1.2 : Geological map of the Burdur-Fethiye Shear Zone. Contacts bounding the basement rocks were drawn by integrating the 1:500000 Denizli and Ankara sheet geological maps by the General Directorate of Mineral Research and Exploration (Şenel, 2002), field observations, DEMs and satellite images.

1.2 Thesis Objectives and Structure

This thesis forms part of the TÜBİTAK ÇAYDAG (Project No: 107Y005 and 115Y424) and the Istanbul Technical University Scientific Research Projects Coordination Department (Project No: 32511). A multidisciplinary approach including geological mapping, stratigraphy, geomorphology, tectonics, structural geology, paleoseismology, geophysics, modelling and archaeogeology ensured the achievement of the thesis objectives. A total of approximately 150 days were spent in the field since 2008. An area of 169 topographic sheets of 1/25000 scale was mapped (Figure 1.3). The geometry and style of the structures, such as major faults, were determined using a combination of digital elevation models (DEMs), aerial photos and field data. Active deformation analysis involves detailed mapping and GPS data. The Neogene stratigraphy of the region was identified by the help of radiometric ages.

Despite numerous references to south-western Turkey, the Burdur-Fethiye Shear Zone and the basins along this zone are scattered throughout the literature, no detailed geological structural investigation of the region has been undertaken. Most of the previous studies were based on the Burdur-Fethiye Fault Zone, which was characterized as a narrow NE-SW-trending left-lateral fault by Barka et al. (1997), and age determinations of the randomly collected fossil samples from the different stratigraphic levels. Most of the researchers suggest tectonic interpretations without detailed field data. Also, there are some stratigraphic problems in literature. Although this thesis marks both structural architecture and tectonostratigraphy of the Burdur-Fethiye Shear Zone using field studies, radiometric ages, GPS slip vectors, trench data and fault-plane solutions, it is necessary to extend these observations to a regional plate-tectonic scale.

The major aims of this thesis are:

- to create a detailed geological map of the Burdur-Fethiye Shear Zone
- to characterise the stratigraphy and facies relationships
- to resolve the conflicting chronostratigraphic interpretation of the Neogene successions
- to characterise the faults and deformations along the zone
- to characterise the active faulting and recent deformation along the zone
- to discuss the evolutionary differences of previous studies about the region.

This thesis consists of the five articles (Chapter 2-6), two comments (Chapter 7 and 9) and two replies (Chapter 8 and 10) which were published in the SCI indexed journals following the introduction chapter (Chapter 1). Lastly, a conclusions chapter (Chapter

11) is provided. Each chapter has its own introduction, results and discussions sections. Data and material not used in the text are presented in the appendices.

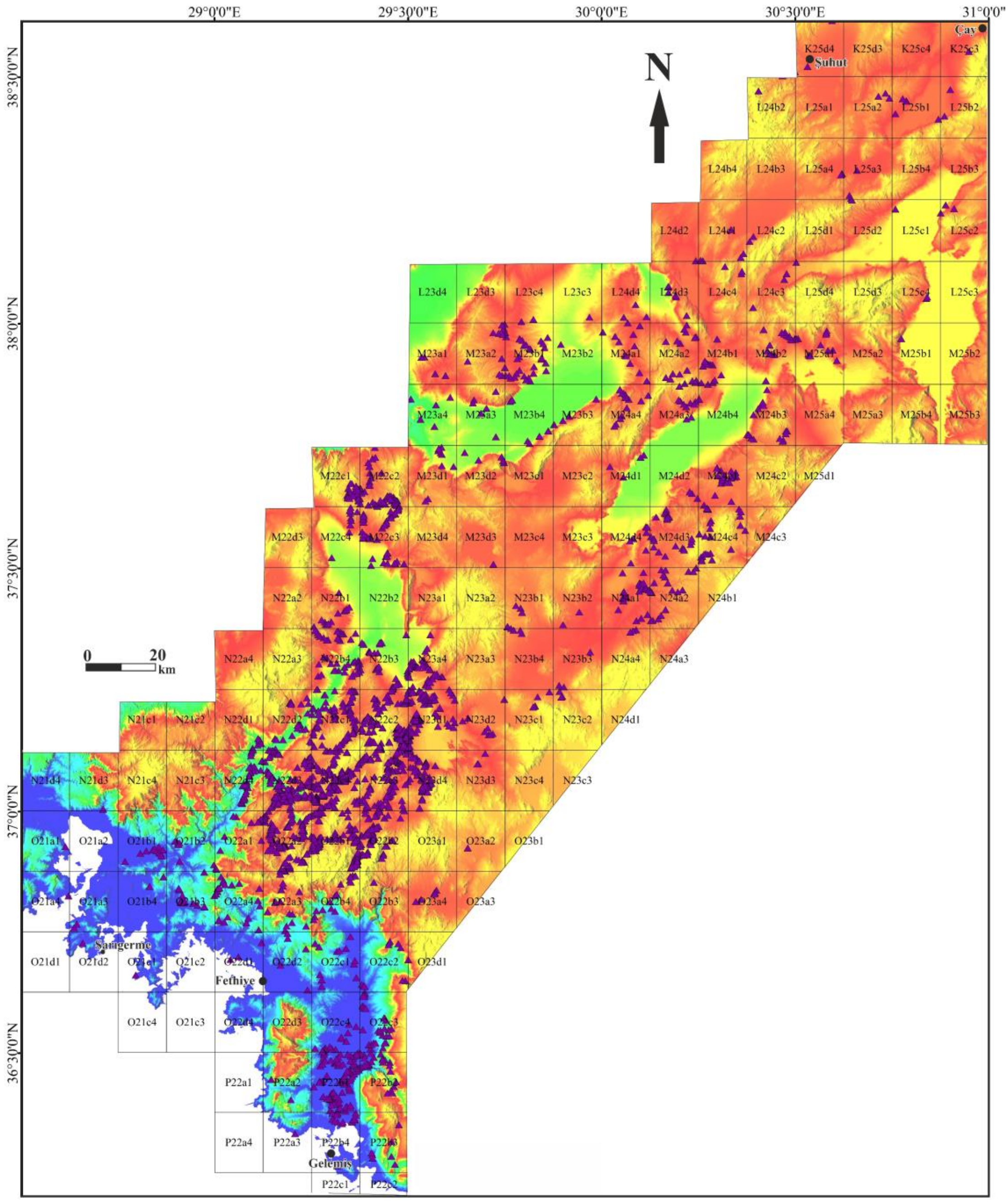

Figure 1.3 : Topographic sheets used in the thesis. Purple triangles indicate the measurement locations.

2. EXTENSIONAL AND COMPRESSIONAL REGIME DRIVEN LEFT-LATERAL SHEAR IN SOUTHWESTERN ANATOLIA (EASTERN MEDITERRANEAN): THE BURDUR-FETHİYE SHEAR ZONE [1]

2.1 Introduction

The geographical domains where intra-continental transform faults, back-arc extension and continental collision work together are the most attractive research areas in the world. A large number of Global Positioning System (GPS) sites in Anatolia, Aegean Sea and Greece in eastern the Mediterranean can shed light on our understanding of the relative plate motions and tectonic deformations associated with the convergence of the African and Eurasian plates (Figure 2.1). The Pliocene-Quaternary tectonic evolution of the Aegean-Anatolian-Microplate has become a highly controversial topic in terms of GPS data and interpretations. The microblock modelling has gained popularity with the development of geodetic measurement technologies, providing the much needed framework for discussions on the regional kinematic evolution and tectonic boundaries across the eastern Mediterranean region (Barka and Reilinger, 1997; Kahle et al., 1998; Mc Clusky et al., 2000; Reilinger et al., 2006; Aktug et al., 2009; Özeren and Holt, 2010; Reilinger et al., 2010; Tiryakioğlu et al., 2013; Kreemer et al., 2014). The first such study for the southwestern Anatolia and the surrounding areas was carried out by Barka and Reilinger (1997). These authors suggested that using a limited number of GPS sites, a NE-SW-striking left-lateral fault should exist between two different velocity patterns in southwestern Anatolia (Barka and Reilinger, 1997). This view was reconfirmed in further GPS studies (Erdoğan et al., 2009; Reilinger et al., 2010; Tiryakioğlu et al., 2013). An increased number of GPS stations across the eastern Mediterranean indicated that a significant velocity difference suggesting the supposed NE-SW-striking single left-lateral fault does not exist (Aktuğ et al., 2009). In recent years, tectonic research on

[1] This chapter is based on the paper "Elitez, İ., Yaltırak, C., and Aktuğ, B. (2016). Extensional and compressional regime driven left-lateral shear in south-western Anatolia (eastern Mediterranean): The Burdur-Fethiye Shear Zone. Tectonophysics, 688, 26-35."

land in southwestern Anatolia (Elitez and Yaltırak, 2014 a, c; Elitez et al., 2015), marine research in the Rhodes Basin (Hall et al., 2009; 2014a), the studies about Anaximander Mountain (Aksu et al., 2009), the Finike Basin (Aksu et al., 2009, 2014) and the Gulf of Gökova (Tur et al., 2015) necessitate a discussion about the recent mechanism of the left-lateral transtensional system referred to as the Burdur-Fethiye Shear Zone (Elitez and Yaltırak, 2014a) within the context of the GPS data.

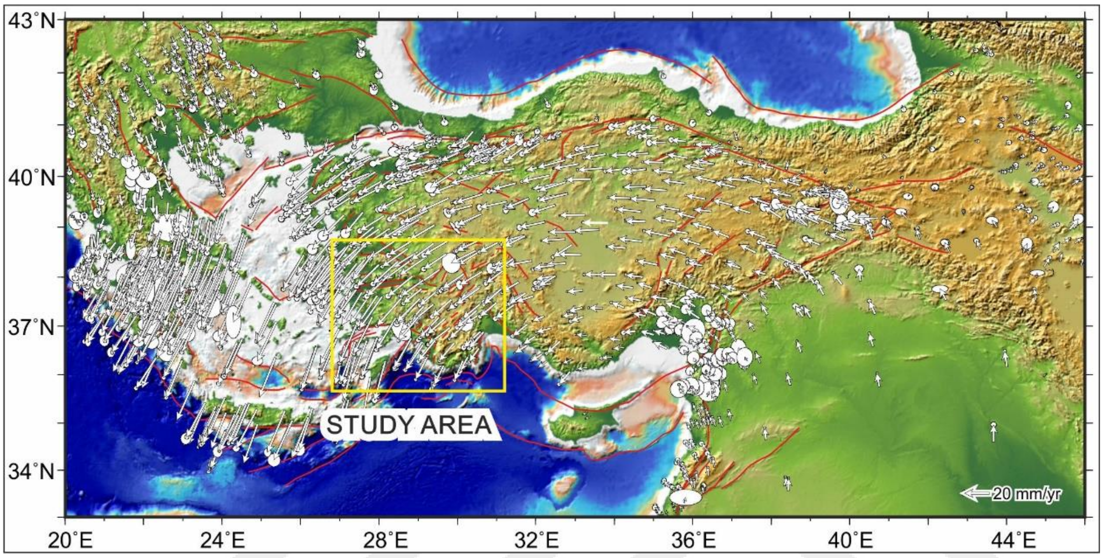

Figure 2.1 : GPS vectors relative to the fixed Eurasian Plate showing the counterclockwise rotation of the Anatolian Block (Kreemer et al., 2014).

2.2 GPS Data and Analysis

Several studies that quantify the Pliocene-Quaternary deformation across southwestern Turkey have been published (Reilinger et al., 2006; Aktuğ et al., 2009; Erdoğan et al., 2009; Tiryakioğlu et al., 2013). The study area in southwestern Turkey has also been specifically studied with GPS measurements (Aktuğ and Kılıçoğlu, 2006). The use of combined velocity fields has been a common practice to remove any possible reference frame effects (Aktuğ et al, 2009; Nocquet et al., 2012; Aktuğ et al., 2013). Recently, a global combined velocity field has been published within Global Strain Rate Project (Kreemer et al., 2014), which incorporates the published GPS velocities in the region (Reilinger et al., 2006; Aktuğ et al., 2009; Erdoğan et al., 2009; Tiryakioğlu et al., 2013). In addition, realizing an Anatolia-fixed frame requires the identification of the sites within Anatolia, and represents its west-directed escape and counterclockwise rigid rotation of its western sector since the Pliocene. The most complete study dealing with the rotation of Anatolia, including a discussion about its internal deformation, was given in Aktuğ et al. (2013). In this study, we used the Euler pole of Anatolia with respect to Eurasia (Φ= 31.682°, λ= 31.613 and Ω=1.380°/Myr), to remove the effect of Anatolian rotation, so to express the velocity field in an Anatolia-fixed frame (Figure 2.2).

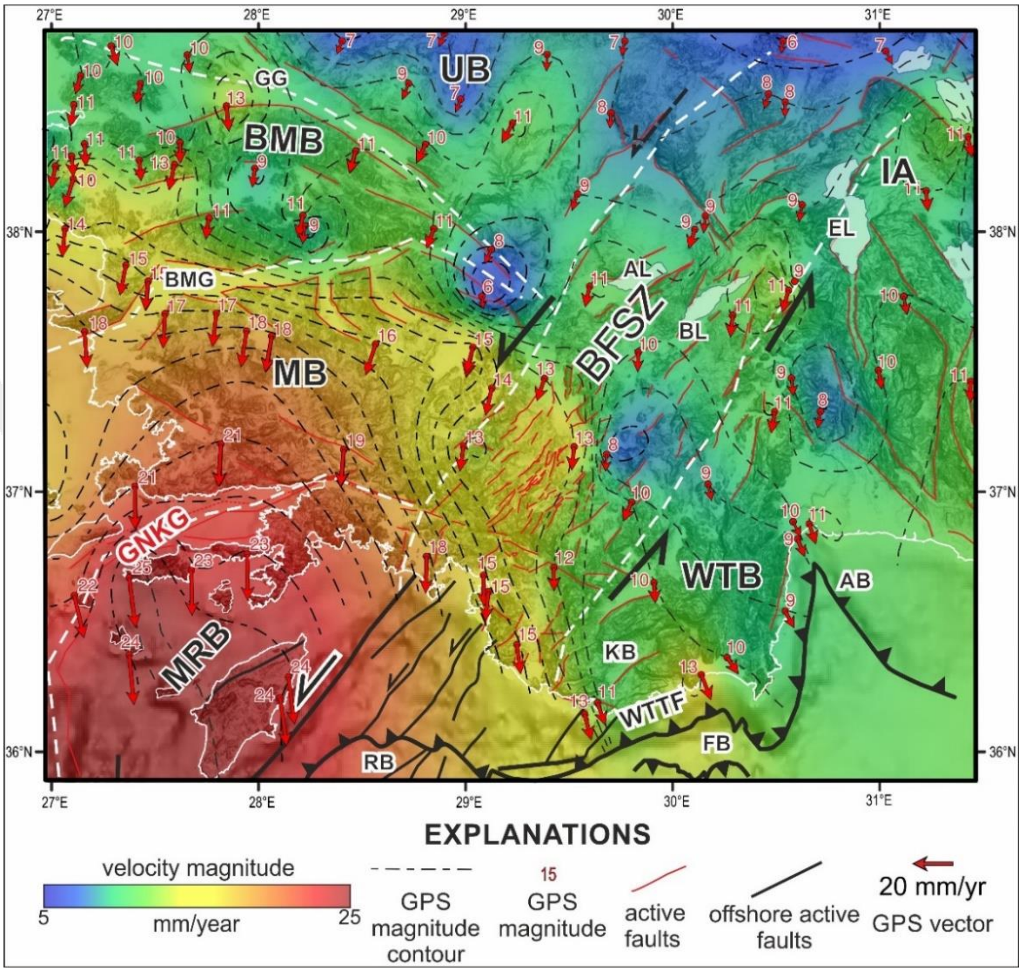

Figure 2.2 : Anatolia-fixed GPS velocities and magnitude colour-contour map. Red lines show active faults from Elitez et al. (2015) and Tur et al. (2015). UB: Uşak Block, BMB: Büyük Menderes Block, GG: Gediz Graben, BMG: Büyük Menderes Graben, MB: Muğla Block, GNKG: Gökova-Nisyros-Karpathos Graben, MRB: Marmaris-Rhodes Block, BFSZ: Burdur-Fethiye Shear Zone, WTB: Western Taurides Block, WTTF: Western Taurides Thrust Fault, IA: Isparta Angle, RB: Rhodes Basin, FB: Finike Basin, KB: Kasaba Basin, AB: Antalya Basin, AL: Acıgöl, BL: Burdur Lake, EL: Eğirdir Lake.

The continuous magnitude colour maps in Figures 2.2 and 2.3 were produced through the surface interpolation of the velocity magnitudes at a spatial resolution of 0.5'x0.5' using the Generic Mapping Tools (GMT) version 5.1.2. We used the algorithm of continuous curvature splines with adjustable tension, which provides a "minimum curvature" solution when the tension is zero (Smith and Wessel, 1990). A value of

0.01 was chosen for the tension parameter to avoid the oscillation artifacts and false local extrema, and at the same time to ensure a smooth surface. The errors of the velocity components were propagated to the uncertainties of the velocity magnitudes. A full covariance propagation to the velocity magnitude at a point can be expressed as

$$\sigma_{mag} = \sqrt{\frac{1}{v_e^2 + v_n^2}\left(v_e^2\sigma_{V_e}^2 + v_n^2\sigma_{V_n}^2 + 2v_e v_n \rho_{v_x v_y}\sigma_{V_e}\sigma_{V_n}\right)} \tag{2.1}$$

where v_e, v_n, σ_{V_e}, σ_{V_e} and $\rho_{v_x v_y}$ are the east velocity, north velocity, the standard deviation of east velocity, standard deviation of north velocity and the correlation coefficient between east and north velocities.

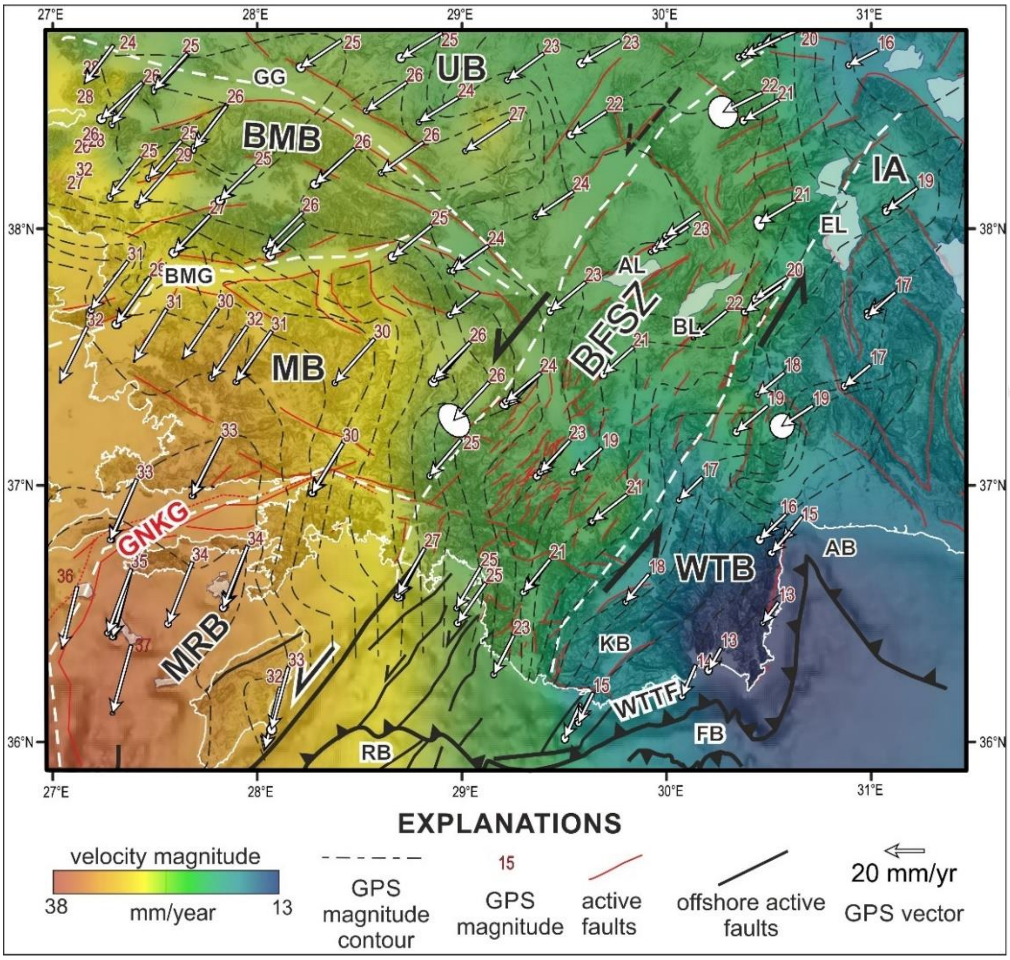

Figure 2.3 : Eurasia-fixed GPS velocities and magnitude colour-contour map. Red lines show active faults from Elitez et al. (2015) and Tur et al. (2015). UB: Uşak Block, BMB: Büyük Menderes Block, GG: Gediz Graben, BMG: Büyük Menderes Graben, MB: Muğla Block, GNKG: Gökova-Nisyros-Karpathos Graben, MRB: Marmaris-Rhodes Block, BFSZ: Burdur-Fethiye Shear Zone, WTB: Western Taurides Block, WTTF: West Taurides Thrust Fault, IA: Isparta Angle, RB: Rhodes Basin, FB: Finike Basin, KB: Kasaba Basin, AB: Antalya Basin, AL: Acıgöl, BL: Burdur Lake, EL: Eğirdir Lake.

The errors of the velocity magnitudes were also interpolated by using the same interpolation algorithm to give a numerical measure of the spatial resolution of the GPS derived velocity magnitudes with respect to their uncertainties (Figure 2.4). The uncertainties of the velocity magnitudes are at ~1-1.5 mm/yr level, a little higher than the those of velocity components except for three data points where they reach 3 mm/yr, as seen in Figure 3. Using the combined velocity field given in Kreemer et al. (2014), a total of nine velocity and topographic profiles were constructed parallel and perpendicular to the GPS velocities (Figures 2.5 and 2.6). Thus, it has become possible to correlate velocities, topography and fault patterns (Figures 2.2, 2.3 and 2.6).

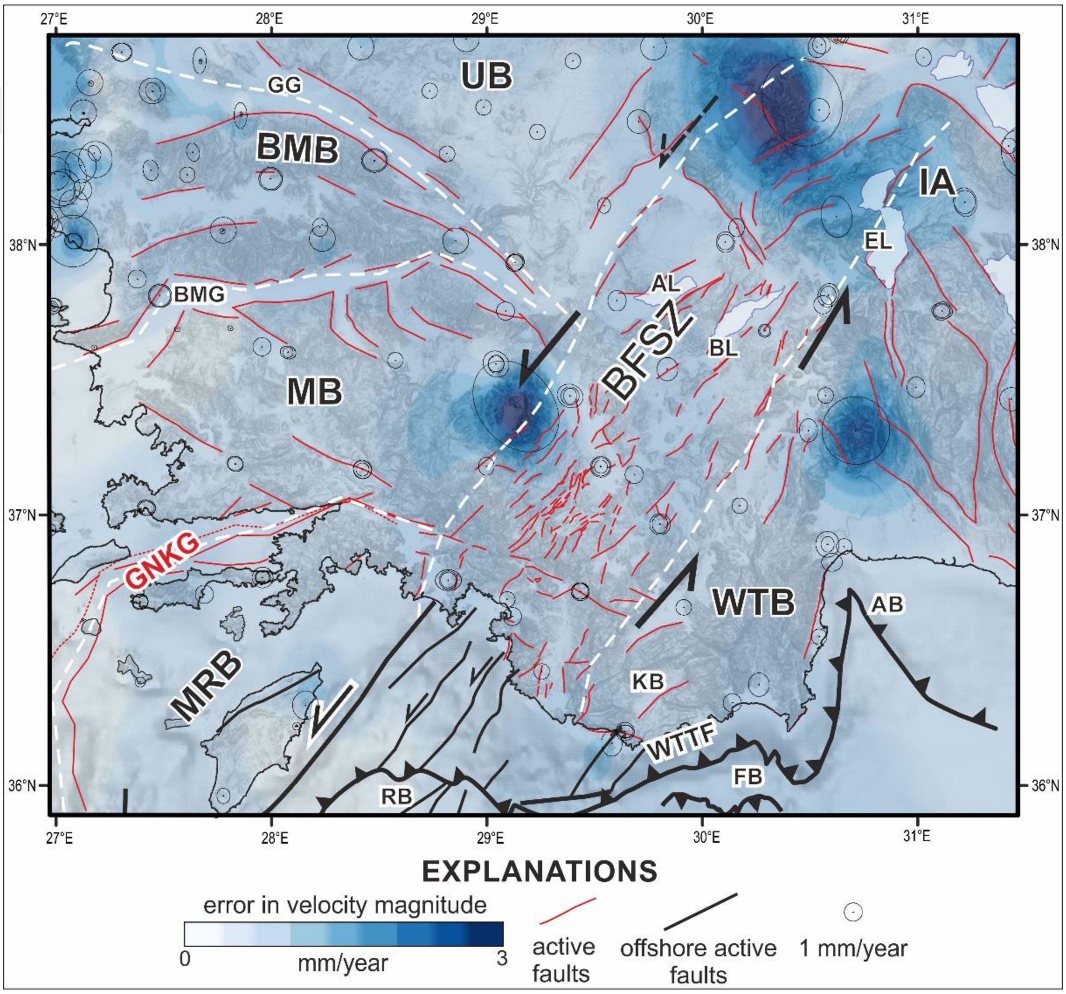

Figure 2.4 : The velocity magnitudes at GPS data points (in ellipses) and interpolated errors in colour contours. UB: Uşak Block, BMB: Büyük Menderes Block, GG: Gediz Graben, BMG: Büyük Menderes Graben, MB: Muğla Block, GNKG: Gökova-Nisyros-Karpathos Graben, MRB: Marmaris-Rhodes Block, BFSZ: Burdur-Fethiye Shear Zone, WTB: Western Taurides Block, IA: Isparta Angle, RB: Rhodes Basin, FB: Finike Basin, KB: Kasaba Basin, AB: Antalya Basin, AL: Acıgöl, BL: Burdur Lake, EL: Eğirdir Lake.

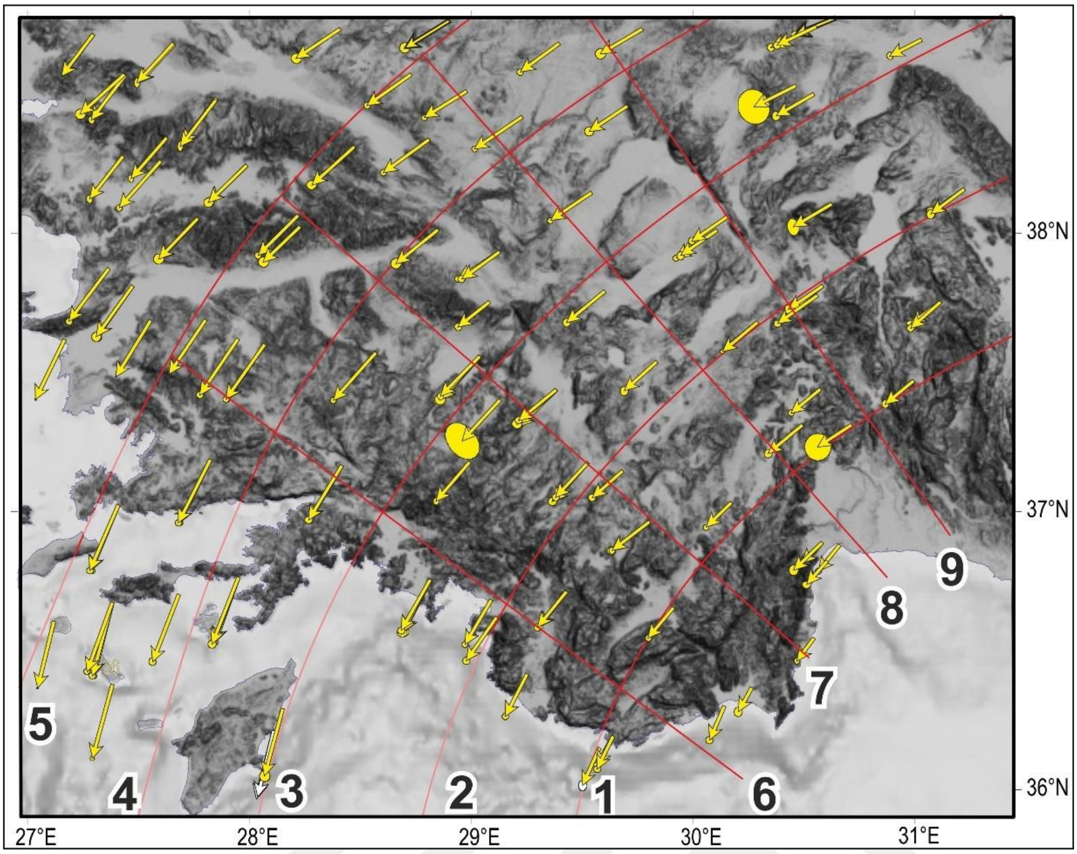

Figure 2.5 : GPS velocities and topographic section profiles.

2.3 Seismo-Tectonic Frame

From a tectono-stratigraphic and kinematic point of view, southwestern Turkey is a problematic area in the eastern Mediterranean regime. The Aegean graben system (e.g., McKenzie, 1978; Le Pichon and Angelier, 1981; Şengör, 1979; Şengör et al., 1985; Taymaz et al., 1991; Seyitoğlu et al., 2004; Çemen et al., 2006; Ersoy et al., 2010; Gessner et al., 2013, Tur et al., 2015), compressional Western Taurides uplift (Aksu et al., 2009; 2014; Hall et al., 2009; 2014a) and unidentified structural area between these two domains are controversial (Alçiçek et al., 2005; 2013; ten Veen, 2004; Alçiçek and ten Veen, 2008; Gürer et al., 2004; Över et al., 2010; Kaymakçı et al., 2014; Elitez and Yaltırak 2014 a, c; Elitez et al., 2015). Barka and Reilinger (1997) suggested a single left-lateral fault similar to the East Anatolian Fault between the Aegean graben system and the compressional western Tauride uplift. Subsequent mapping studies showed the inexistence of a single left-lateral fault (Gürer et al., 2004; Alçiçek et al., 2005; 2013; Alçiçek and ten Veen, 2008; Över et al., 2010; Kaymakçı et al., 2014; Elitez and Yaltirak 2014 a, c).

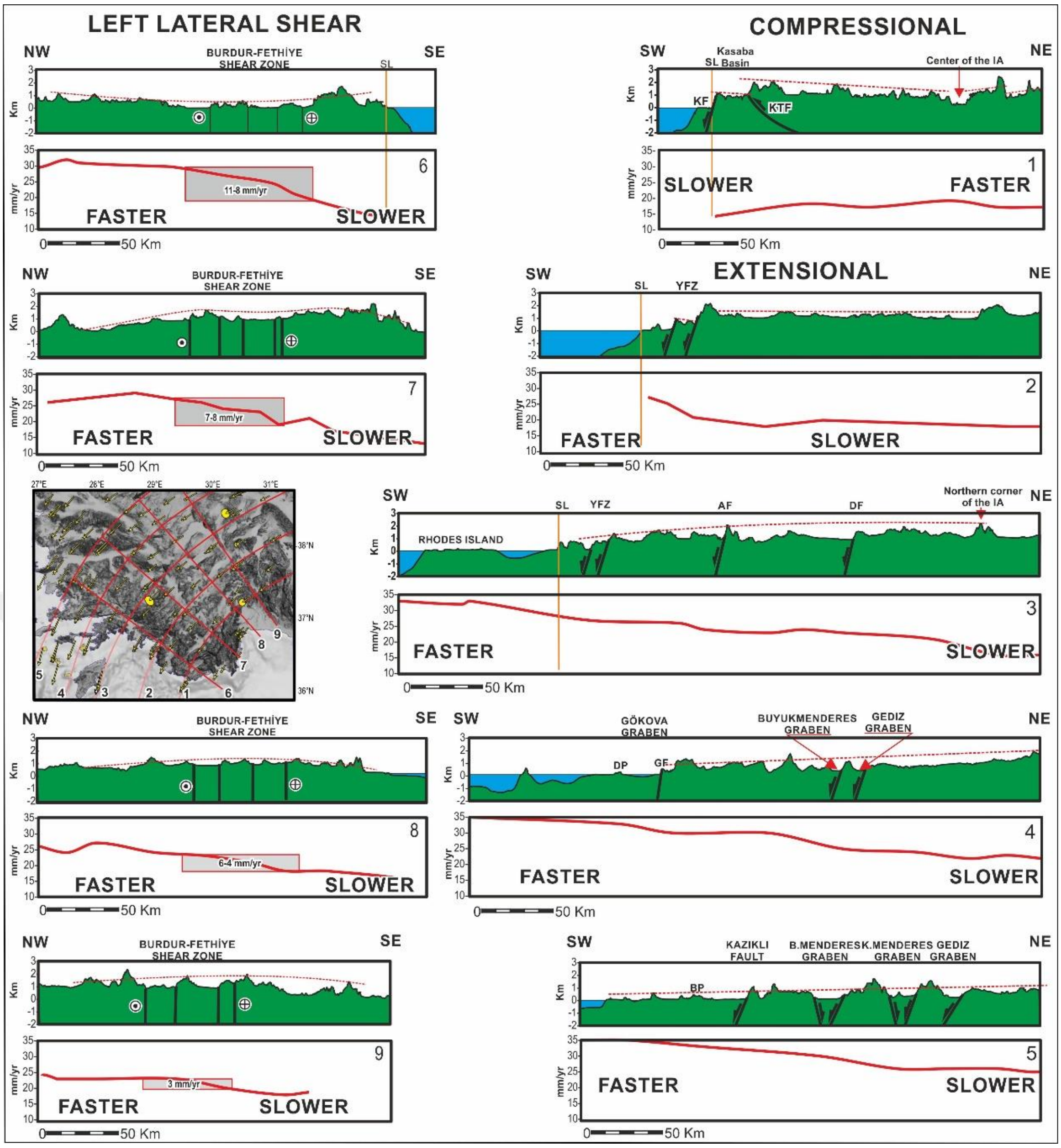

Figure 2.6 : GPS velocity and topographic profiles. Small map shows the locations of the profiles on Digital Elevation Model. YFZ: Yeşilüzümlü Fault Zone, IA: Isparta Angle, SL: Sea level.

However, the geological map prepared by integrating new techniques and field studies has demonstrated that there is instead a 75- to 90-km-wide left-lateral transtensional shear zone between the Aegean graben system and the compressional western Tauride uplift (Elitez and Yaltırak 2014a, c; Elitez et al., 2015). The zone, which we named the Burdur-Fethiye Shear Zone, links with the Pliny-Strabo Fault Zone in the marine areas defined as a component of the Subduction-Transform Edge Propagator (STEP) fault (Hall et al., 2014a). To the west of the Burdur-Fethiye Shear Zone, the graben system is opening similar to the fingers of a hand, and the rigid blocks bounded by these grabens are formed by the counterclockwise rotation of southwestern Anatolia and the roll-back effect of the Hellenic Trench (e.g., Tur et al., 2015). This rotation is observed as counterclockwise changes in the directions of the GPS vectors (Figures 2.2 and 2.3). The extensional regime can be described as the difference of the vector magnitudes along the same direction between Uşak Block and Marmaris Rhodes Block. This difference is approximately -10 mm/yr in the Eurasia-fixed frame (Figure 2.3). Muğla and Marmaris blocks move faster than the Uşak Block towards the southwest. Additionally, the earthquake activity in western Anatolian grabens shows that the opening of grabens is controlled by oblique normal faults (Figure 2.7). The earthquakes that occurred in the Gediz, Büyük Menderes and Gökova-Nisyros-Karpathos grabens indicate the significant rotations of the extension vectors (Figure 2.7). While the extension is NE-SW in the Gediz Graben located between the northernmost Uşak Block and Büyük Menderes Block, it becomes NW-SE in the southernmost Gökova-Nisyros Graben, and even becomes to E-W in Karpathos Graben. Tur et al. (2015) explain that the arc-shaped Gökova-Nisyros-Karpathos Graben rotated counterclockwise relative to a pole on land, thus the extension direction in the graben has changed. All of the significant earthquakes in this region are shallow, compatible with the tectonic and structural geometries. The dominant system in the uppermost 20 km of the crust in the region is a slightly oblique extensional regime (Figure 2.7). The compressional regime is still active in the southern part of the Burdur-Fethiye Shear Zone in the marine area, Anaximander Mountain, Finike Basin and Sırrı Erinç Plateau (Hall et al., 2009; 2014a, Aksu et al., 2009; 2014). Likewise, the Gulf of Antalya, which is a part of the Western Taurides, is also active as a compressional structure (Hall et al., 2014b). In the marine area, the earthquakes are deep with mainly strike-slip and thrust components (Figure 2.7). Aksu et al. (2009) show that a large thrust carries the Western Taurides to the south. The earthquake depths in the vicinity of this structure, named the Western Taurides thrust fault range between 20 and 100 km (Figure 2.7). Near the footwall surface, it is observed that the shallow earthquakes are generated by oblique normal faults. In the Gulf of Antalya and the southern side of the Western Taurides, the earthquakes are thrust and oblique earthquakes (Figure 2.7). Earthquakes with pure normal first motion are also observed in the Western Taurides. It is known that shallow normal fault earthquakes can occur on the footwall of the huge thrust faults (Shanker et al., 2011).

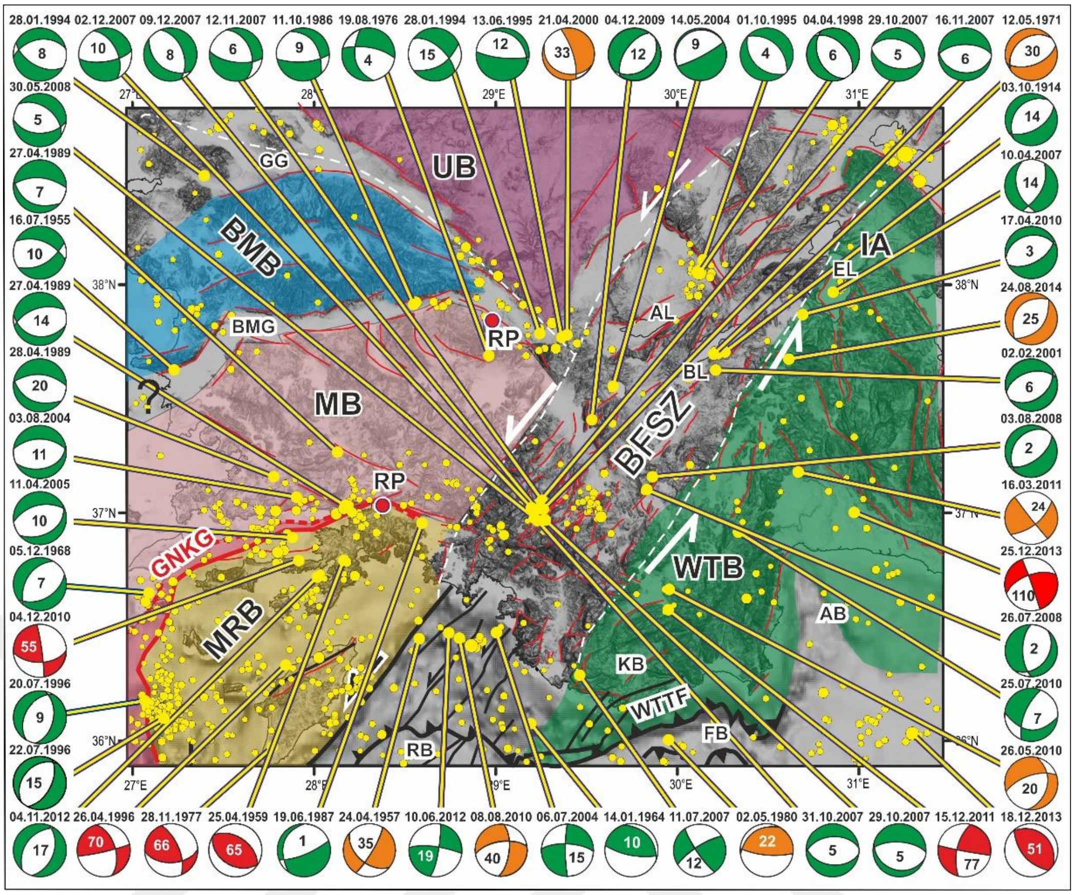

Figure 2.7 : Seismotectonic map of southwestern Turkey, southeastern Aegean Sea and eastern Mediterranean Sea. Fault plane solutions from Kiratzi and Louvari (2003); Benetatos et al. (2004); Yolsal et al. (2007); Yolsal and Taymaz (2010); Över et al. (2010, 2013a); Yolsal-Cevikbilen and Taymaz (2012), USGS (2015). EQ focal mechanism solution colours show depths: green 20≤ km, orange 21-50 km, red 51≥ km. Different colours show different zones and blocks. Red lines show active faults on land. Black lines show offshore faults. BFSZ from Hall et al. (2014a), Elitez et al. (2015), Elitez and Yaltırak (2014c); Anaximander Mounts and Rhodes Basin from Aksu et al. (2009), Hall et al. (2009; 2014a). Faults of Gökova region from Tur et al. (2015). Red lines show main faults. GNKG: Gökova-Nisyros-Karpathos Graben, BFSZ: Burdur Fethiye Shear Zone, WTTF: Western Taurides Thrust Fault, BMG: Büyük Menderes Graben, GG: Gediz Graben, UB: Uşak Block, BMB: Büyük Menderes Block, MB: Muğla Block, MRB: Marmaris-Rhodes Block, WTB: Western Taurides Block, IA: Isparta Angle, RB: Rhodes Basin, FB: Finike Basin, KB: Kasaba Basin, AB: Antalya Basin, AL: Acıgöl, BL: Burdur Lake, EL: Eğirdir Lake, RP: Rotation Pole (red point). Earthquakes (yellow points) Mw≥5 from ISG database.

2.4 GPS Velocities and Topography

The Burdur-Fethiye Shear Zone and surrounding blocks specify three different tectonic regions: (1) the compressional Western Taurides, (2) the extensional western Anatolia grabens and (3) the left-lateral transtensional shear zone. The variation of the GPS velocity magnitudes helps the identification and the interpretation of these regions (Figures 2.2 and 2.3). In order to separate the effects of two different mechanisms (with or without counterclockwise rotation of Anatolia), both Eurasia-fixed and Anatolia-fixed magnitude colour maps were created. The Eurasia-fixed magnitude colour map includes GPS velocities varying between 13 and 38 mm/yr (Figure 2.3), and the Anatolia-fixed magnitude colour map includes GPS velocities varying between 6 and 25 mm/yr (Figure 2.2). The Eurasia-fixed GPS velocities increase from 20 mm/yr on the northwestern part of the Burdur-Fethiye Shear Zone to 25 mm/yr on the southwestern part, while the 5 mm/yr difference explains the NE-SW-trending extension (Figure 2.3). Likewise, the Anatolia-fixed GPS velocities increase from 7 mm/yr on the northwestern part of the zone to 15 mm/yr on the southwestern part (Figure 2.2). The topographic and Eurasia-fixed velocity profiles perpendicular or parallel to the GPS vectors in this area are shown in Figures 2.5 and 2.6. The region to the northwest of the Burdur-Fethiye Shear Zone moves faster to southwest in comparison with the zone itself (from green to red in Figure 2.3). Additionally, the vectors show counterclockwise deviations towards the south (Figure 2.3). Comparison between the topographic profiles parallel to the GPS vectors (Figure 2.5) and the velocity magnitudes (Figure 2.6) show that in association with southwest descent of the SW-NE topographic profiles 2, 3, 4 and 5, the GPS velocities show notable increase in the same direction. This is the effect of the back-arc extension regime that causes the increase in the velocity of Anatolian sector of the Aegean-Anatolia Microplate toward the southwest. The velocity decreases towards the southwest on the profile from the Western Taurides region in the southeast of the zone (section 1), while the topography rises (Figure 2.6), which can be explained by a compressional region in concordance with the active thrust fault that defines the shelf edge of Finike and Rhodes basins (Aksu et al., 2009; 2014). On the profiles perpendicular to the Burdur-Fethiye Shear Zone (sections 6-9), the breakups related to the lateral movement are effective on the parts associated with the shear zone (Figure 2.6). The velocity difference is 3-4 mm/yr on the northern side of the region and 8-10 mm/yr on the southern side (Figure 2.3). The velocity profiles also show a decrease from south to north along the zone (Figures 2.3 and 2.6). The only reason for such smooth change of the velocity differences across the zone is that the Burdur-Fethiye Shear Zone is a wide structural area located on a Cretaceous ophiolitic zone comprised of many faults (Hall et al., 2014a; Elitez et al., 2015; Tur et al., 2015). The remarkable point is that the velocity difference in the northeastern part is relatively low compared with the southwestern part. Because the velocity difference is low between the Aegean extension and Western Taurides compression systems, which collectively define a convex morphology, the velocity difference increases toward the southern part of the zone and a concave morphology is observed (Figure 2.6). This phenomenon probably explains why the southern part of the zone is wider (90 km) than the northern part (75 km). In the system that accelerates toward the south and opens similar to a fan, the vertical components of the normal faults increase toward the south. For example, there is a 1500 m vertical offset in the Tortonian lacustrine sediments located on the footwall and hanging wall of the Yeşilüzümlü Fault Zone (Elitez and Yaltırak, 2016).

2.5 Transtensional Shearing and Field Observations

Several remarkable models in literature provide significant clues regarding the evolution of the shear zones. According to Ramsay and Huber (1983), the shearing leads to more deformation in the central part of a zone and the strain ellipses show different extension directions. Hull (1988), Mitra (1991) and Means (1995) define Type 1 (strain hardening) shear zones that thicken with time. Vitale and Mazzoli (2008) state that the strain intensity increases from the margins to the centre in the heterogeneous systems. The experimental transtensional model of Schreurs and Colletta (1998) show that the normal faults develop between earlier formed major strike-slip faults while the deformation increases. Some of these faults exhibit oblique slips in the progress of time; the high angles of the faults begin to decrease during the deformation and small transtensional basins form.

The Burdur-Fethiye Shear Zone is characterized by several basins bounded by NE-SW-trending major faults. Elitez and Yaltırak (2014c) identify the region as an active shear zone in the light of the model of Schreurs and Colletta (1998). These major faults are mainly 1- to 10-km-long NE-SW-striking normal and oblique faults (Figure 2.8), and they are the products of the old faults of Lycian Nappes, which form the basement of the Burdur-Fethiye Shear Zone.

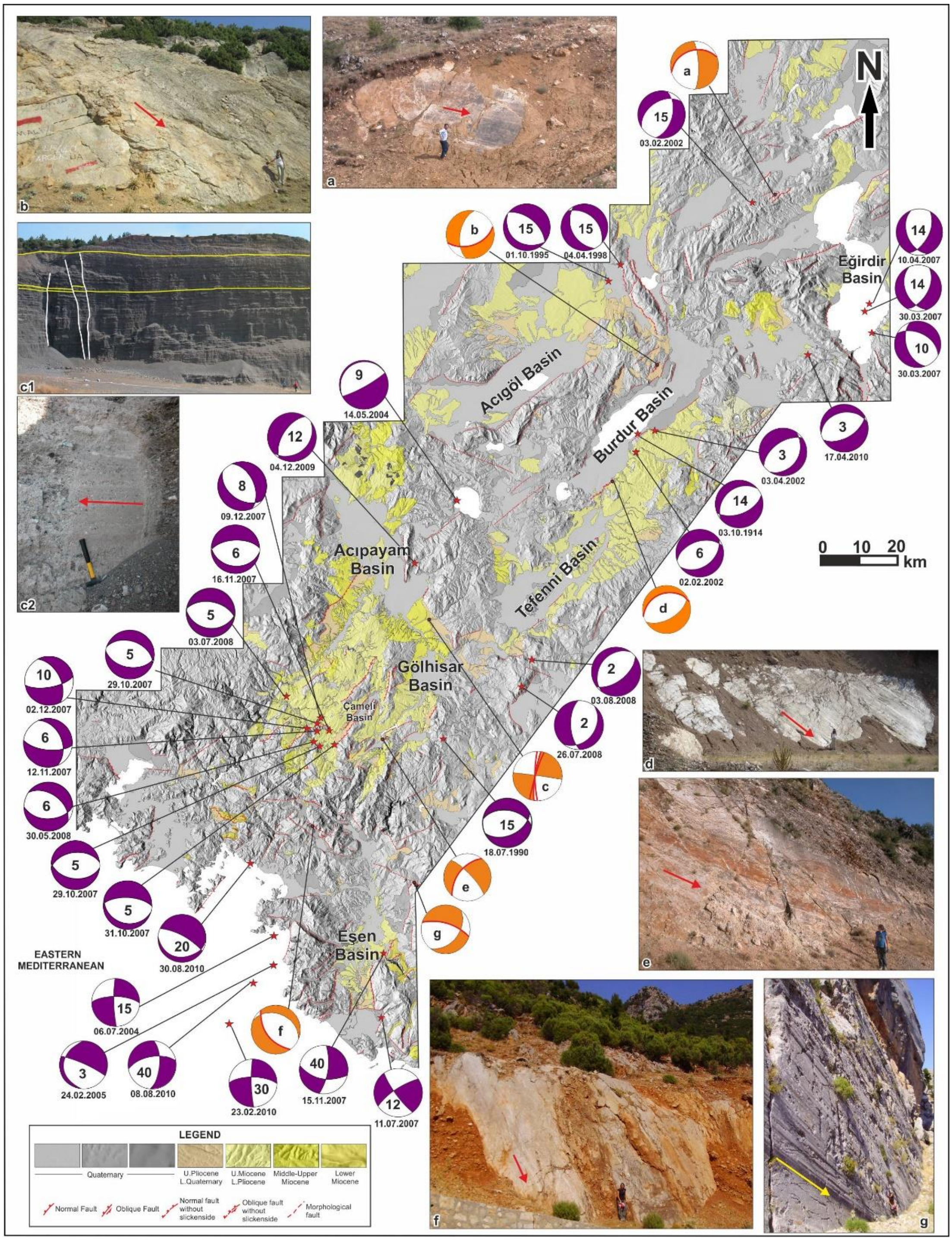

Figure 2.8 : Miocene-Quaternary map of the Burdur-Fethiye Shear Zone and several faults as examples of strike-slip and oblique faults. Earthquake focal mechanism solutions are shown in purple and fault plane solutions of the faults are shown in orange. Numbers indicate depths of earthquakes and letters indicate photographs. Earthquake data from Över et al. (2010, 2013a, b) and USGS (2015).

Although the minor faults also exhibit normal and oblique characteristics, limited reverse and strike-slip movements are observed in the region (e.g., Figures 2.8c1 and 2.8c2). Most of the earthquake solutions along the zone show NE-SW, NNE-SSW and NW-SE extensions/oblique extensions that indicate two different normal fault systems perpendicular to each other in the zone (Figure 2.8). The NE-SW-striking normal fault solutions and major faults in the same directions represent the deformations observed in the transtensional shear zones suggested by Schreurs and Colletta (1998). Additionally, NW-SE-striking faults, such as the Gökova-Yeşilüzümlü Fault Zone (Figures 2.8g and 2.8f), the Dinar Fault Zone and the Keçiborlu-Çobansaray Fault Zone (Elitez et al., 2015), and the focal mechanism solutions are consistent with the NE-SW-trending stress orientation due to the roll-back effect of the Hellenic Trench in the zone (Figure 2.7).

2.6 Discussion and Conclusions

The studies across the southwestern Anatolia suggest different fault models and discussions by accepting the view of a single left-lateral fault and representing block boundaries related to this fault (Alçiçek, 2001; Gürer et al., 2004; Alçiçek et al., 2005; 2013; Alçiçek and ten Veen, 2008; Över et al., 2010; 2013 a, b; Kaymakçı et al., 2014). The geological map used as the source in this paper was produced using an ArcGIS database by integrating a digital elevation model, high-resolution satellite images and field studies that indicate exact formation contacts and fault relationships (Elitez et al., 2015; Elitez and Yaltırak, 2016). During this study, 263 1-10 km long NE-SW-striking normal and left-lateral oblique normal faults and 74 NW-SE-striking normal and left-lateral oblique normal faults were identified and mapped along the NE-SW-trending 75-90 km wide and 300 km long Burdur-Fethiye Shear Zone (Figure 2.8). The previous fault maps of this region have the scale of 1/100000 and smaller. Therefore, many minor faults and second-order structures were either omitted or incorrectly mapped as major faults with the lengths of tens of kilometers (e.g., Gürer et al., 2004; Alçiçek et al., 2005, 2013; ten Veen, 2004; Alçiçek and ten Veen, 2008; Över et al., 2010; 2013 a, b; Kaymakçı et al., 2014). This 75-90 km wide and 300 km long shear zone could not have been noticed by the researchers due to the local scopes of their studies. The Burdur-Fethiye Shear Zone, consisting of normal and left lateral oblique normal faults, was identified as a transtensional zone by Elitez and Yaltırak (2014a), which is at odds with previous models (e.g., Barka and Reilinger, 1997; ten Veen et al., 2009). The main shortcoming of the NE-SW extensional graben system approach, suggested based on the characteristics of the faults and earthquake focal mechanism solutions (Alçiçek, 2001; Alçiçek et al., 2005; 2013; ten Veen, 2004; Alçiçek and ten

Veen, 2008; Över et al., 2010; 2013 a, b), is its kinematic incompatibility with the surrounding systems (Figure 2.1). The tectonics of the region are dominated by the NE-SW and N-S extensions across the Aegean graben system, the NE-SW extension of the Island of Kos, the E-W extension of the Island of Karpathos, the compression in the Rhodes Basin, and the NW-SE extension on the Island of Rhodes (Figure 2.7). Under such circumstances, the GPS vectors do not show direction changes indicating these extensions (Figure 2.3). In order to suggest a kinematic model explaining the GPS vectors and current deformation, an integrated approach which clarifies the tectonic structure of the whole region is needed. In this framework, the Burdur-Fethiye Shear Zone is a left-lateral deformation transition zone, driven by the relative velocity differences due to the roll-back effect of the Hellenic Trench and the compressional region of the Western Taurides, but mostly due to the westward escape of the Anatolian sector of the Aegean-Anatolian Microplate. The development mechanism of the zone can be explained by the separation between Aegean and Cyprus slabs with a transform fault in the Miocene and the surfacing of this deep structure on the brittle crust as a shear zone (Figure 2.9). The data in the magnetotelluric study of Gürer et al. (2004) clearly identifies the shear zone (Elitez et al., 2015). The continuation of the Burdur-Fethiye Shear Zone in the marine areas (i.e., Pliny-Strabo Fault Zone) has the characteristics of a STEP fault (Özbakır et al., 2013; Hall et al., 2014a). It encompasses the deformation between the Aegean extensional regime and the Western Taurides compressional regime and is characterized by shallow earthquakes on the brittle crust, oblique normal faults and young basins that are bounded by these faults (Figure 2.7; Elitez et al., 2015). The GPS velocity vectors show a spatial velocity difference correlated with the fault directions and an acceleration from southeast to northwest among the parallel vectors.

According to the GPS vectors obtained from the Burdur-Fethiye Shear Zone and its immediate environs, the formation mechanism of the dividing blocks and the graben between these blocks should be associated to the back-arc extension regime. The region including the Aegean graben system moves faster towards southwest than the westward extrusion of Anatolia (+4 - +12 mm/yr). In this case, rather than a N-S extension regime in western Anatolia, the NE-SW back-arc extension regime and the counterclockwise rotation have an effect on the formation of the fan-shaped geometry of the Aegean graben. The opening of the Gulf of Gökova in the Pliocene-Quaternary is part of this mechanism (Tur et al., 2015).

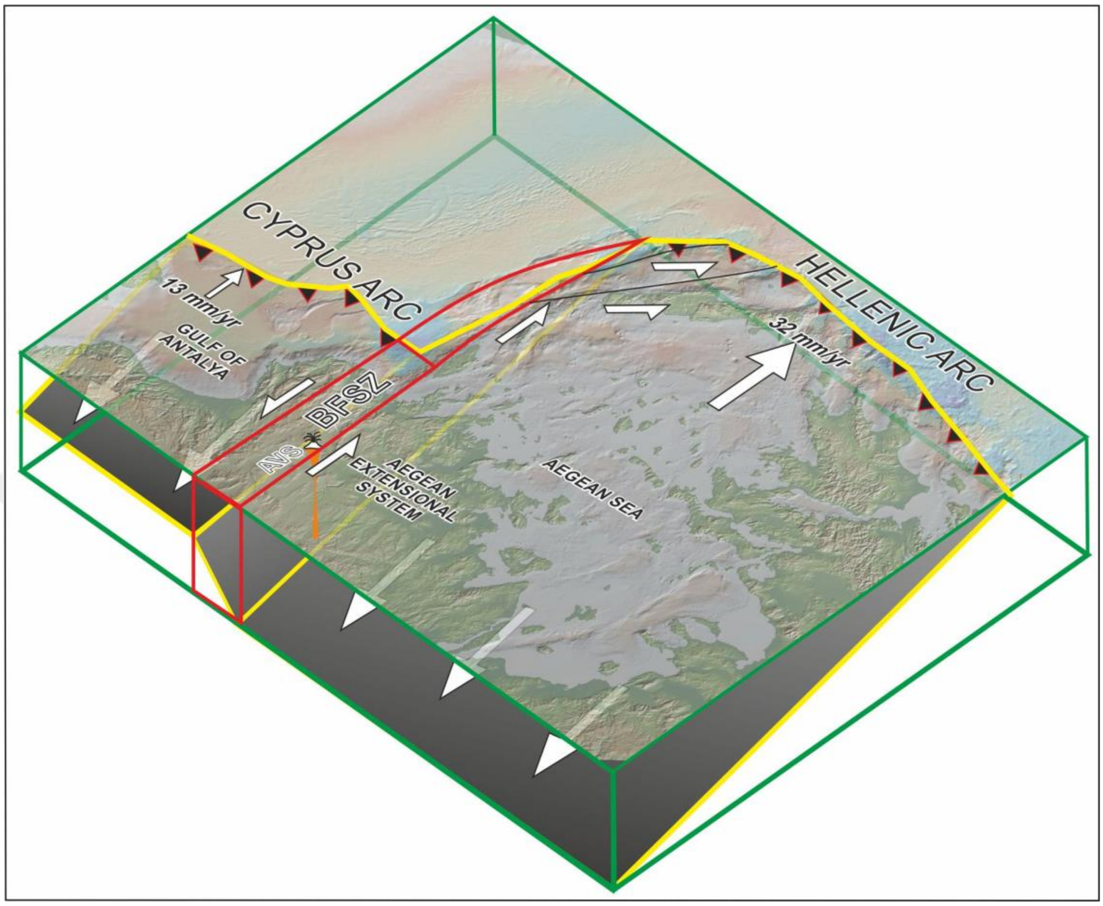

Figure 2.9 : 3D tectonic block model of the southwestern Turkey and Aegean Sea. Red lines show the Burdur-Fethiye Shear Zone on land, the offshore parts of either Pliny-Strabo Fault System or southeastern Aegean STEP fault. AVS: Acıpayam Volcanic Source, BFSZ: Burdur-Fethiye Shear Zone.

The velocity of the westward motion of the Anatolian sector of the Aegean-Anatolian Microplate decreases across the Western Taurides and the 4-6 km topography with an ~2000 m elevation, creating a remarkable contrast behind the deepest depressions of the eastern Mediterrenean, the Rhodes (>4000 m) and Finike (>3000 m) basins. The uplifted region moves 10 mm/yr slower toward the southwest than the Anatolian sector of the Aegean-Anatolian Microplate. The cause of this slowing down is the compressional regime in this region, where the Western Taurides has been uplifting related to the Western Taurides thrust fault (WTTF) (Figure 2.3). By all means, this region is expected to form a transfer zone due to the relative motion between two parallel systems – one is extensional, the other is compressional. The Burdur-Fethiye Shear Zone is a left-lateral shear zone located along a 75-90 km width and 300 km length area between the western Anatolian extensional and the Western Taurides compressional regimes, and also the propagation of the STEP fault into the upper plate (Figures 2.7, 2.8 and 2.9; Hall et al., 2014a). The lamproite upwelling (Paton, 1992) occurred along this deep tearing zone is observed in Acıpayam region in the middle section of the zone (Figure 2.9). In addition to the chemical composition and ages of these lamproites, the distribution of the basins and the effects of the faults (Elitez and Yaltırak, 2016) demonstrate that the zone has been active since the late Miocene. Current GPS velocities on land enable understanding especially of formation mechanisms of the southwestern Anatolia, the Aegean extension system, the Western Taurides thrust fault and their relationships with the Hellenic Trench, the Anaximander Mountains and the Cyprus Arc, allowing quantification of the plate motions in the eastern Mediterranean. According to the geodetic data, the Burdur-Fethiye Shear Zone is an intercontinental transform structure. This zone is the single example of the experimentally revealed model of Scheuers and Colletta (1998), which involves parallel normal faults in a transtensional shear zone. The STEP fault (Govers and Wortel, 2005) develops between two subducting slabs with different dip angles as a consequence of the separation by a strike-slip displacement. The continuation of a STEP fault on land can be observed as a shear zone in the brittle crust (Figure 2.9). At this stage, it is not necessary to expect the existence of a single Burdur-Fethiye fault.

3. MIOCENE TO QUATERNARY TECTONOSTRATIGRAPHIC EVOLUTION OF THE MIDDLE SECTION OF THE BURDUR-FETHİYE SHEAR ZONE, SOUTH-WESTERN TURKEY: IMPLICATIONS FOR THE WIDE INTER-PLATE SHEAR ZONES[2]

3.1 Introduction

South-western Turkey is one of the most tectonically active areas in the eastern Mediterranean region (Figure 3.1). This region is dominated by westward motion of Anatolia along the North Anatolian Fault and East Anatolian Fault (Dewey and Şengör, 1979; Şengör, 1979; Şengör et al., 1985), a NE-SW Aegean back-arc extension regime due to roll-back of the Hellenic Arc (Le Pichon and Angelier, 1979; McKenzie, 1978; Meulenkamp et al., 1988; Yılmaz et al., 2000) and the subduction transform edge propagator (STEP) fault zone related to the motion of the Hellenic and Cyprus arcs (Govers and Wortel, 2005; Hall et al., 2014a). The Burdur-Fethiye Shear Zone is a tectonic structure in south-western Turkey bounded by the southern part of the Aegean extensional province on the west (dark-blue region in Figure 3.2) and the Western Taurides Block on the east (green region in Figure 3.2). This shear zone is a 75- to 90-km-wide left-lateral transtensional zone that extends approximately 300 km between Şuhut-Çay on the northeast and Sarıgerme-Gelemiş on the southwest on land and to the Pliny-Strabo Fault Zone (Figure 3.2; Taymaz and Price, 1992; Barka and Reilinger, 1997; Woodside et al., 2000; Huguen et al., 2001; Zitter et al., 2003; ten Veen, 2004; ten Veen et al., 2008; Aksu et al., 2009; Hall et al., 2009, 2014a; Yaltırak et al., 2010; Ocakoğlu, 2012; Elitez and Yaltırak, 2014c; Elitez et al., 2015; Elitez et al., 2016b). In previous studies, these NE-SW-striking left-lateral faults, which were apparently present between Burdur and Fethiye in south-western Turkey, were named the Burdur Fault, Fethiye-Burdur Fault, Fethiye-Burdur Fault Zone, Burdur-Fethiye Fault Zone or Burdur-Fethiye Shear Zone (e.g. Barka et al., 1995; Eyidoğan and Barka,

---

[2] This chapter is based on the paper "Elitez, İ., and Yaltırak, C. (2016). Miocene to Quaternary tectonostratigraphic evolution of the middle section of the Burdur-Fethiye Shear Zone, south-western Turkey: Implications for the wide inter-plate shear zones. Tectonophysics, 690, 336-354."

1996; Barka and Reilinger, 1997; Glover and Robertson, 1998; ten Veen, 2004; Verhaert et al., 2004, 2006; Alçiçek et al., 2006; Bozcu et al., 2007; ten Veen et al., 2008; Över et al., 2010, 2013a; Elitez and Yaltırak., 2014c; Hall et al., 2014a, b; Elitez et al., 2015).

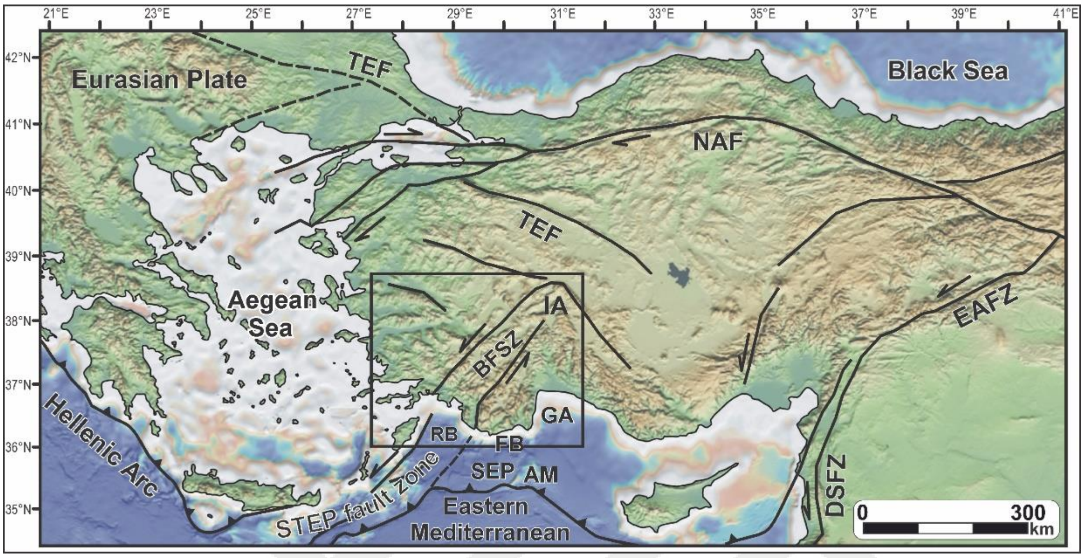

Figure 3.1 : Simplified tectonic map of Turkey compiled from Yaltırak et al., 2012 (TEF: Thrace-Eskişehir Fault, NAF: North Anatolian Transform Fault, EAFZ: East Anatolian Fault Zone, DSFZ: Dead Sea Fault Zone, IA: Isparta Angle, BFSZ: Burdur-Fethiye Shear Zone, RB: Rhodes Basin, GA: Gulf of Antalya, FB: Finike Basin, AM: Anaximander Mountain, SEP: Sırrı Erinç Plateau). Rectangle indicates Figure 3.2.

The Burdur-Fethiye Shear Zone is characterized primarily by left-lateral offset with a normal component (Dumont et al., 1979; Şaroğlu et al., 1992; Taymaz and Price, 1992; Price and Scott, 1994). Barka et al. (1995) stated that this zone is a major boundary fault separating western Anatolia from the Isparta Angle. Eyidoğan and Barka (1996) suggested that the western flank of the Isparta Angle is made up of the Burdur-Fethiye Fault Zone and is the north-eastern continuation of the Pliny-Strabo Fault Zone. In addition, Barka and Reilinger et al. (1997) suggested a GPS-based geodetic slip rate of 1.5-2 cm/yr along the Burdur-Fethiye Shear Zone. Akyüz and Altunel (1997; 2001) concluded that one segment of the Burdur-Fethiye Fault Zone display 50 cm of recent left-lateral offset of the stadium in the ancient city of Kibyra, which is located in Gölhisar (Figure A.1). The existence of this offset is disputed, according to Elitez and Yaltırak (2014b). In contrast, Kaymakçı et al. (2014) and Özkaptan et al. (2014) asserted that the Fethiye-Burdur Fault Zone may be a deep structure that formed along the ancient northern trace of the STEP fault, based on palaeomagnetic and kinematic studies. Nevertheless, recent studies have begun to provide the precise location of the Burdur-Fethiye Shear Zone (Elitez and Yaltırak, 2014c; Hall et al., 2014a; Elitez et al., 2015; Elitez et al., 2016b; this study).

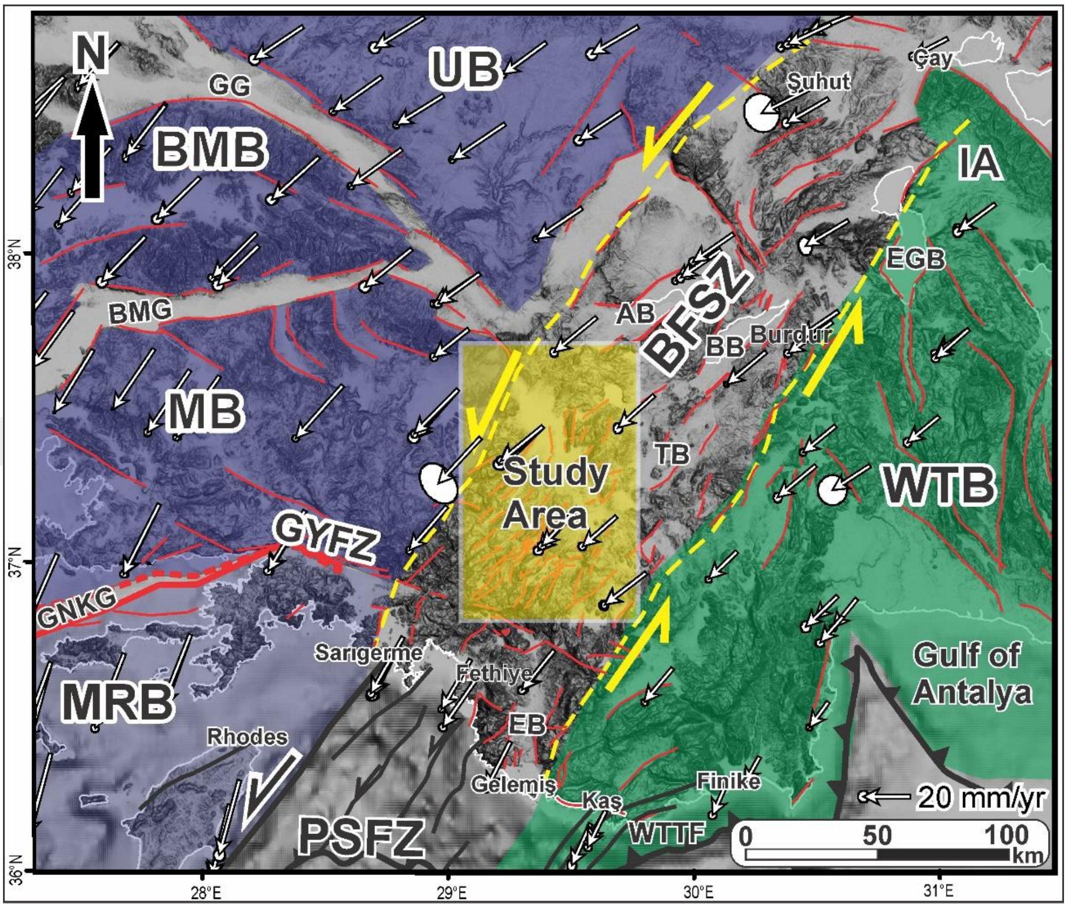

Figure 3.2 : Regional fault map of south-western Anatolia compiled from Tur et al. (2015). Yellow rectangle indicates location of the study area. Dark-blue region denotes the NE-SW extensional domain (MRB: Marmaris-Rhodes Block, MB: Menderes Block, BMB: Büyük Menderes Block, UB: Uşak Block, GG: Gediz Graben, BMG: Büyük Menderes Graben, GNKG: Gökova-Nisyros-Karpathos Graben). Green region denotes the NNE-SSW compressional domain (WTB: Western Taurides Block, IA: Isparta Angle, WTTF: Western Taurides Thrust Fault). GPS vectors are from Kreemer et al. (2014). BFSZ: Burdur-Fethiye Shear Zone, PSFZ: Pliny-Strabo Fault Zone, GYFZ: Gökova-Yeşilüzümlü Fault Zone, AB: Acıgöl Basin, BB: Burdur Basin, TB: Tefenni Basin, EGB: Eğirdir Basin, EB: Eşen Basin.

The Burdur-Fethiye Shear Zone is dominated by numerous minor faults of normal, oblique and left-lateral strike-slip offset and major 1- to 10-km-long, NE-SW-striking, normal and left-lateral oblique normal faults. The Acıpayam, Çameli and Gölhisar basins are located in the middle section of this shear zone (Figure 3.2). In previous studies, the area including these basins was designated the Çameli Basin (e.g., Alçiçek 2001; Alçiçek et al., 2004, 2005, 2006; Över et al., 2010). Despite several studies, the tectonic evolution of the region remains poorly understood. For example, Alçiçek (2001) and Alçiçek et al. (2004, 2005, 2006) suggested a three-stage graben model involving three rifting pulses during the late Miocene to latest Pliocene, whereas Över et al. (2010) suggested a model involving late Cenozoic NW-SE-, NE-SW- and ~N-S-trending extensions. In addition, Alçiçek and ten Veen (2008) asserted that the Acıpayam Basin is a late early Miocene piggy-back basin and that extension formed the Çameli Basin during the Tortonian.

The terrestrial Neogene sediments in the study area were generally assigned to the Çameli Formation (Erakman et al., 1982; Bilgin et al., 1990). Later, the Çameli Formation was divided into three members, specifically, the Derindere, Kumafşarı and Değne members, which consist of alluvial-fan, fluvial and lacustrine deposits, respectively (Alçiçek, 2001; Alçiçek et al., 2004, 2005, 2006). However, the ages and stratigraphic positions of these members are controversial (e.g., Elitez et al., 2015, 2016a). Recent studies identified three formations: the Gölhisar, İbecik and Dirmil formations (Elitez et al., 2009; Elitez, 2010; Hall et al., 2014a; Elitez and Yaltırak, 2014c; Elitez et al., 2015).

In this paper, we focus on the Miocene to Quaternary tectonostratigraphic evolution of the middle section of the Burdur-Fethiye Shear Zone. The main purposes of this study were to present a revised Neogene stratigraphy, characterize the Burdur-Fethiye Shear Zone and reconstruct the tectonic evolution of the middle section of the Burdur-Fethiye Shear Zone by integrating field observations, DEMs, GPS data, fault kinematics and fault-plane solutions of earthquakes compiled from the literature (Över et al., 2010; USGS earthquake catalogue, 2015).

3.2 Material and Methods

Precise geological mapping is one of the most important issues in geological studies. Documenting the spatial distribution of geologic bodies and their contacts plays a crucial role in interpreting the tectonic evolution of any region. Although traditional field techniques are still accepted as the most fundamental tools in preparing geological maps, we suggest that the integration of digital technologies with classical methods significantly increases the resolution and quality of such products.

The following steps were followed in the integration of the digital data with the traditional field observations. First, we created the digital elevation model (DEM) of the region of interest by interpolating the digital contours of 1:25000-scale topographic maps at a ground pixel resolution of 10 m. Non-commercial Google Earth satellite imagery and geological maps of previous studies were superimposed on the interpolated DEMs in the second stage. The integration of all spatial data was performed using the GIS software product ESRI ArcGIS Desktop 10.1®. We performed preliminary interpretation of major structures, i.e., tectonic lineaments and stratigraphic contacts, following the second stage. These preliminary maps were spatially controlled and precisely coordinated during the field studies using mobile tablets and/or phablets with GPS receivers. These devices were also used for measuring and recording the geologic structures of the study area. Finally, all the digitally collected measurements and observations were added to the GIS database, and we finalised our geological map to contain all the available information.

Kinematic analyses of major and minor faults were performed to evaluate the deformation in the region. The minor faults were grouped into four sets based on the geomorphologic properties of the study area and geologic-tectonic features of the surrounding regions. Then, the minor faults with their striae and slip directions were grouped based on the stratigraphic positions (ages) of the formations and cross-cutting relations in the field. The faults that are indicative of different stress regimes were grouped using Angelier’s M-pole girdle solution method (1979, 1984). This method is a version of Arthaud’s M-plane method (1969) and one of the most appropriate methods for analysing complex fault sets and reactivated old structures. Aleksandrowski (1985) modified these two methods to create a way to identify fault sets of different ages using movement planes (M-planes).

The M-plane girdle solution method is based on movement planes. Planes that were produced by or reactivated under similar stress regimes have the same kinematic properties (Aleksandrowski, 1985). Although the plane attitudes appear to differ from one another, the M-planes of the faults intersect at a point generally indicating the maximum (or rarely the minimum) principal stress direction (the ideal situation). Regardless of the plane attitudes, if the M-planes intersect at a point and the M-poles create a great circle, then the faults were produced or affected by the same stress regime. All the minor faults in the study area were grouped using the M-plane method.

The stress tensors of each set were identified. Finally, the sets were interpreted based on their stratigraphic and regional conditions.

The kinematic analysis of the minor and major faults and the fault-plane solutions of earthquakes were performed using FaultKin 7.4.1 (Marrett and Allmendinger, 1990; Allmendinger et al., 2012) and Win-Tensor (Delvaux and Sperner, 2003) software based on a subset of the data (380 faults and 10 earthquakes), including fault-plane orientations, slickenside lineations and sense-of-movement information. When comparing the intersection points of the M-planes and the principle stress directions of the fault sets, the principle stress directions display small amount of deviations due to the Win-Tensor software. However, this situation does not affect the kinematic interpretation of the study area. The earthquake data are from Över et al. (2010) and a 2015 USGS earthquake catalogue spanning the time period of May 1971 to September 2015.

3.3 Geomorphological Features

The middle section of the Burdur-Fethiye Shear Zone crosses an old Neogene basin. Today, this region includes three modern basins: the Acıpayam (375 km^2), Çameli (20 km^2) and Gölhisar (120 km^2) basins (Figure A.1 in Appendix A). The topography consists of high, steep mountains at elevations of 1000-2000 metres. These mountains are underlain primarily by ophiolitic mélange and limestones of the basement. An area of gentle topography dominated by a wide drainage system of the tributaries of the Dalaman River is located at the base of the mountains. This area is underlain primarily by Neogene sediments. The topography west of the village of Kelekçi is characterised by plains and deep valleys with an average elevation of ~1000 m (Figure A.1 in Appendix A). Similar valleys are also present south of the town of Gölhisar, and small alluvial plains are located between the hills.

3.4 Stratigraphy

In this study, we focused on an area straddling the middle section of the Burdur-Fethiye Shear Zone, where Neogene sediments predominate. The ages of the geological units in the study area span a wide time period between the Palaeozoic and Quaternary. The study area is underlain by four sedimentary packages that unconformably overlie the basement rocks: (1) upper Oligocene-lower Miocene, (2) middle Miocene-lower Pliocene, (3) upper Pliocene-lower Quaternary, and (4) upper Quaternary units (Figures A.1 and A.2 in Appendix A; Figure 3.3).

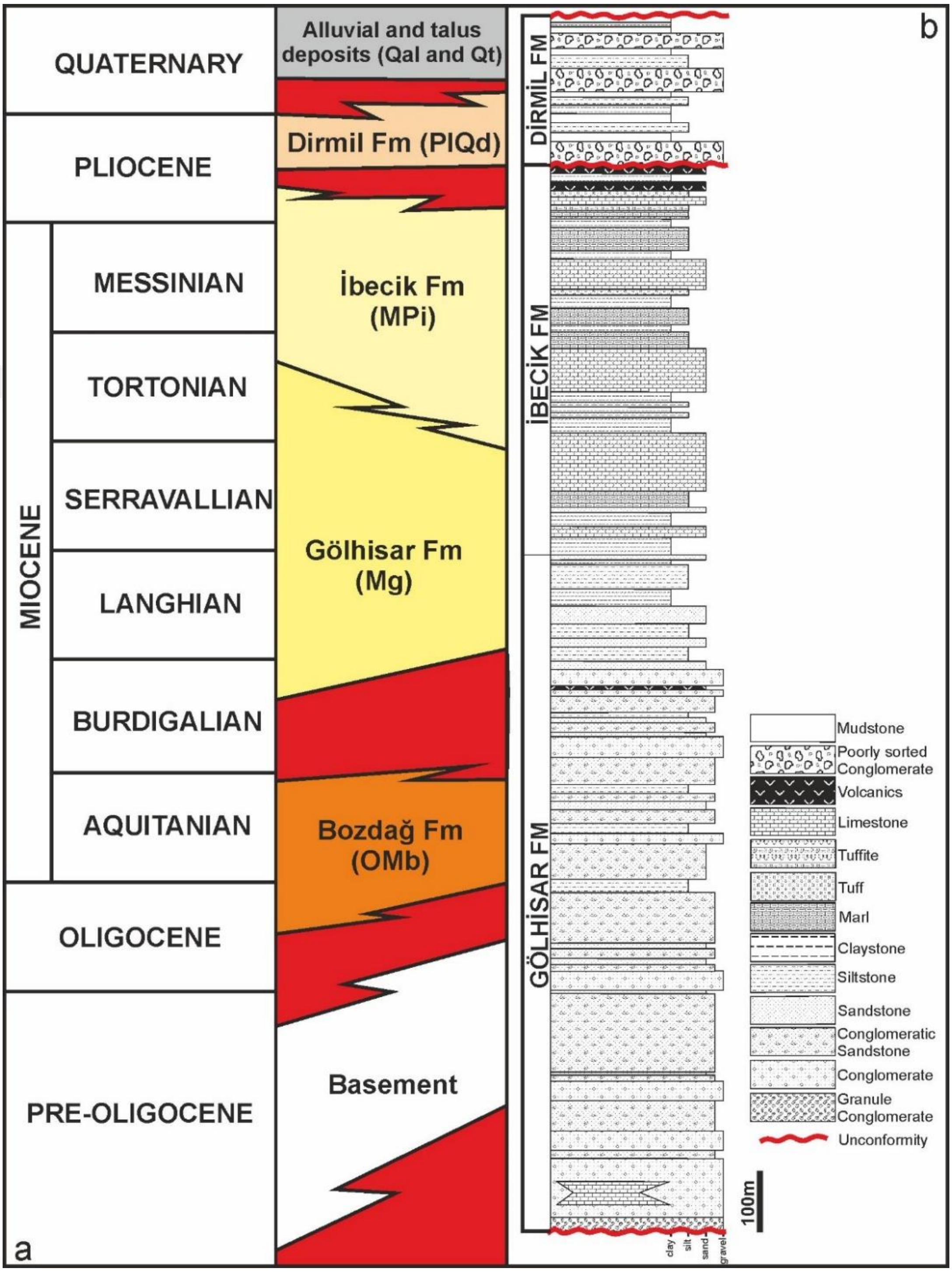

Figure 3.3 : (a) Generalized stratigraphic section of the study area compiled from Elitez et al. (2015). (b) Generalized stratigraphic sequence of the Gölhisar, İbecik and Dirmil formations.

3.4.1 Basement rocks

The basement rocks of the region are composed of the Yeşilbarak Nappe (Önalan, 1979) and Lycian Nappes (Graciansky, 1967; Brunn et al., 1970; Önalan, 1979; Ersoy, 1990). The Yeşilbarak Nappe (PMs) is composed of Eocene-lower Miocene turbiditic sandstone, claystone, siltstone, shale and mudstone and tectonically overlain by the Lycian Nappes. The Lycian Nappes consist of Palaeozoic rocks (PZ), Mesozoic volcanic rocks (Mv), Mesozoic sedimentary rocks (Ms), Mesozoic limestones (Ml), Cretaceous ophiolitic mélange (Co), Cretaceous flysch (Cfl) and Palaeogene sedimentary rocks (Ps) (Figure A.1 in Appendix A). The Palaeozoic rocks are exposed on the south-western side of the study area and include limestone, dolomite, radiolarite, chert, shale and sandstone (Şenel, 1997c). The Mesozoic rocks, which are generally exposed in the topographically high areas (Figure A.1 in Appendix A), are composed of limestone, radiolarite, chert, dolomite, sandstone, conglomerate and basalt. The Cretaceous ophiolitic mélange is characterized by harzburgite, serpentinite, dunite, radiolarites and localized limestone blocks and underlies a large portion of the study area (Figure A.1 in Appendix A). The Cretaceous flysch is generally exposed in the south-western part of the study area. This unit, which has turbiditic characteristics, comprises sandstone claystone, cherty limestone and conglomerate (Şenel, 1997c). The Palaeogene sedimentary rocks comprising conglomerate, sandstone, siltstone and shale, are generally exposed in the western and north-western portions of the study area.

3.4.2 Bozdağ Formation

The Bozdağ Formation unconformably overlies the basement rocks and is unconformably overlain by the Gölhisar Formation (Figure 3.3a). The formation is composed of alternating conglomerate, sandstone and mudstone. This unit was named by Göktaş et al. (1989).

The best exposures of the Bozdağ Formation are located in the northern portion of the study area, near Söğütköy. In addition, the unit crops out northeast of Kelekçi and in a valley between the villages of Ören and Mevlütler (Figure A.1 in Appendix A).

This unit consists of medium to thickly bedded, locally massive, dark-grey, grey, light-brown, yellowish, and reddish conglomerate, sandstone and mudstone. Its thickness is ~500 m.

Fossils of algae such as Schizotrix sp. and Scytonema sp. are found at the base of the Bozdağ Formation. An upper Oligocene-lower Miocene age is assigned to the formation due to its stratigraphic position (Şenel, 1997c). The Bozdağ Formation was deposited in a coastal environment under terrestrial influence.

3.4.3 Gölhisar Formation

The Neogene succession starts with green, greenish grey to grey, reddish, brown and purple conglomerates and sandstones. These rocks were designated as the Derindere and Kumafşarı members by Alçiçek (2001) and as the Gölhisar Formation by Elitez and Yaltırak (2014c), with its type locality in Gölhisar (Figure A.1 in Appendix A and Figure 3.4).

The Gölhisar Formation crops out mostly north of Gölhisar and south of Acıpayam. It is also exposed on the northern and southern sides of the study area (Figure A.1 in Appendix A).

The unit tectonically or unconformably rests on basement rocks and grades vertically and horizontally into the İbecik Formation (Figure 3.5). It consists of thick beds of granule conglomerate at the bottom and grades upward into conglomerate, conglomeratic sandstone, sandstone and siltstone (Figure 3.3b). The conglomerates are predominantly composed of sub-rounded serpentinite, radiolarite and limestone pebbles supported by a matrix of sand and fine pebbles. The pebble compositions vary depending on the characteristics of the local basement rocks. The sequence is dominated by pebbles of the ophiolitic mélange and limestone (Figure 3.4) around Gölhisar (Figure A.1 in Appendix A). Grey and greenish grey ophiolitic pebbles are observed between Kumafşarı and Çavdır, whereas reddish and purple pebbles derived from the ophiolitic mélange are observed in the south-western part of the region (Figure 3.6). Around Acıpayam and north of Yeşilyuva, the pebbles are composed primarily of reworked material derived from the Bozdağ Formation and ophiolitic mélange. A ~60-m-thick limestone is exposed in a localized area southwest of Acıpayam. A similar limestone in a similar stratigraphic position is exposed north of Gölhisar. This limestone at this locality is a ~40-m-thick lens within the Gölhisar conglomerates.

The formation is ~900 m thick. Şenel et al. (1989) suggested an early-middle Miocene age of the limestones in the unit. The fossil data are poor, and the formation has been assigned a middle-late Miocene age based on stratigraphic relationships (Elitez et al., 2009; Elitez, 2010; Elitez and Yaltırak, 2014c; Elitez et al., 2015). It is a possible that the bottom of the Gölhisar Formation may be early Miocene at these localities. The Gölhisar Formation contains sedimentary facies reflecting both meandering- and braided-river systems, and the limestone lenses indicate a reef depositional environment.

Figure 3.4 : Conglomerates and sandstones of the Gölhisar Formation (coordinates 37°9'55.98"N, 29°30'1.20"E).

Figure 3.5 : Transition between the İbecik and Gölhisar formations (coordinates 37°14'56.90"N, 29°27'25.70"E).

Figure 3.6 : Reddish sequence of the Gölhisar Formation in the south-western part of the region (coordinates 37°5'32.40"N, 29°6'4.20"E).

3.4.4 İbecik Formation

The İbecik Formation contains white, beige and yellowish sandstone, siltstone, claystone, marl, tuff and limestone. Alçiçek (2001) designated the sequence as the Değne Member, whereas Elitez and Yaltırak (2014c) designated it as the İbecik Formation based on outcrops near the village of İbecik (Figure A.1 in Appendix A). The İbecik Formation, which underlies a large part of the study area, is best exposed along the NE-SW road from Yapraklı Dam to a small hill to the northeast. The formation grades laterally and vertically into the Gölhisar Formation at the bottom and is unconformably overlain by the Dirmil Formation (Figure 3.7). The bottom of the formation consists of beige sandstones and whitish grey claystones that grade upwards into white and greyish fractured marls and limestones (Figure 3.3b). In the northern part of the study area, there are intercalating vertical transition with tuffs (Figure 3.8). The uppermost part of the formation consists mostly of red-wine-coloured claystones and hard, locally fractured, thickly bedded, whitish yellow and red-wine-coloured silty carbonates including caliche (Figure 3.9). This upper part has a thickness of ~200 m and records a period of aridity.

Figure 3.7 : Unconformity between the İbecik and Dirmil formations (coordinates 37°3'44.00"N, 29°31'54.95"E).

Figure 3.8 : Alternating tuff and claystone (coordinates 37°36'15.12"N, 29°27'20.88"E).

The sediments of the İbecik Formation are locally covered or cut by volcanic rocks at elevations of approximately 1300 to 1600 metres north of Yeşilyuva (Figures A.2d in Appendix A and Figure 2.10). The total thickness of the İbecik Formation is ~850 m. Paton (1992) classified these volcanic rocks as lamproites and from them obtained 40Ar/39Ar radiometric dates of 4.59±0.57, 5.66±0.63, 5.89±0.41, 6.52±0.33, 6.28±0.48 and 6±1.54 Ma (Tortonian-early Pliocene). Vertebrate fossils discovered at an elevation of 1400 m in the village of Elmalıyurt (36°53'18.34"N 29°21'33.73"E) indicate a Vallesian age of the marls and thin coal beds of the İbecik Formation (Saraç, 2003). The total thickness of the İbecik Formation is ~850 m. The evolution stages of the lacustrine deposits indicate a likely age-range of the İbecik Formation of late Miocene to early Pliocene (Elitez, 2010; Elitez and Yaltırak, 2014c). The sedimentary facies indicate deposition in a shallow, warm lake and shoreline environments, mainly beach and delta.

Figure 3.9 : Red-wine-coloured carbonated sequence in the upper part of the İbecik Formation (coordinates 37°6'42.51"N, 29°23'42.44"E).

3.4.5 Dirmil Formation

The Dirmil Formation, named by Elitez (2010), is predominantly composed of copper-coloured conglomerates and mudstones and localized siltstones and claystones. The best outcrops are observed north of Altınyayla (Dirmil) on the down-dropped side of the Kuşdili Fault (Figure 3.11a) and southwest of the Çameli Basin on the down-dropped side of the Asar Fault (Figure 3.11b). West of the Dalaman River and south of the Acıpayam Basin, the copper-coloured Dirmil Formation is clearly exposed on the high-elevation plains (Figure A.1 in Appendix A).

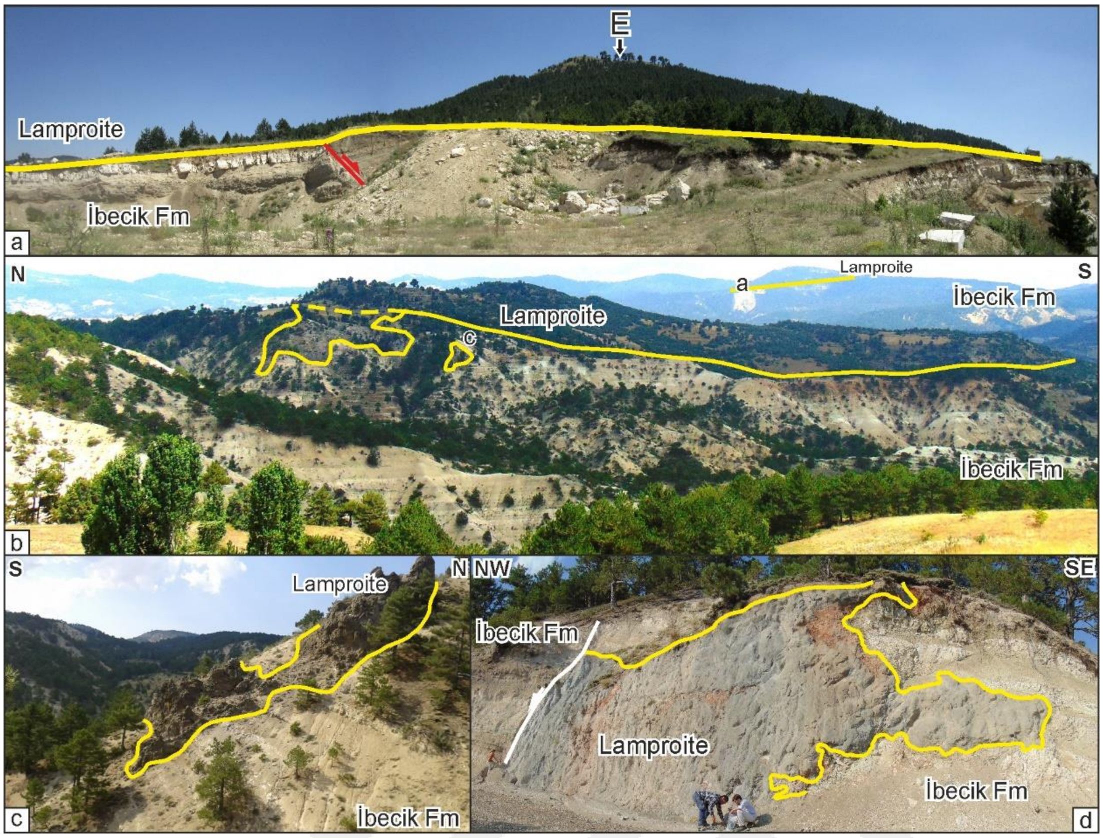

Figure 3.10 : Volcanic rocks located on the northern side of the study area. (a) Contact between the İbecik Formation and lamproite at ~1550 m. Red line denotes normal faulting (coordinates 37°38'52.67"N, 29°26'40.49"E). (b) Contacts between the İbecik Formation and lamproites. a and c show the locations of Figures 3.10a and 2.12c, respectively (coordinates 37°39'33.55"N, 29°21'40.18"E). (c) Lamproite cutting the İbecik Formation (coordinates 37°39'43.19"N, 29°22'11.68"E). (d) Normal faulting and lamproite cutting the İbecik Formation (coordinates 37°40'3.43"N, 29°21'53.31"E).

The formation unconformably overlies Gölhisar and İbecik formations (Figures 3.4a-c and 3.9). This fault-controlled deposition is observed primarily on the folded and tilted Miocene sequence located in front of the basement rocks (Figure A.2a-c in Appendix A). The conglomerates are poorly sorted and consist of mud-supported, angular to sub-angular pebbles. The conglomerates and mudstones of the Dirmil Formation are locally present as 10-15-m-thick infills of paleo-valleys.

The Dirmil Formation is approximately 250 m thick. Based on its stratigraphic position and micromammal fossils (e.g. Mimomys pliocaenicus, Apodemus dominans and Micromys praeminutus; Erten, 2002) in the village of Cevizli, the formation is assigned a late Pliocene-early Quaternary age in this study. The sediments of the unit are interpreted as having been deposited in an alluvial fan environment.

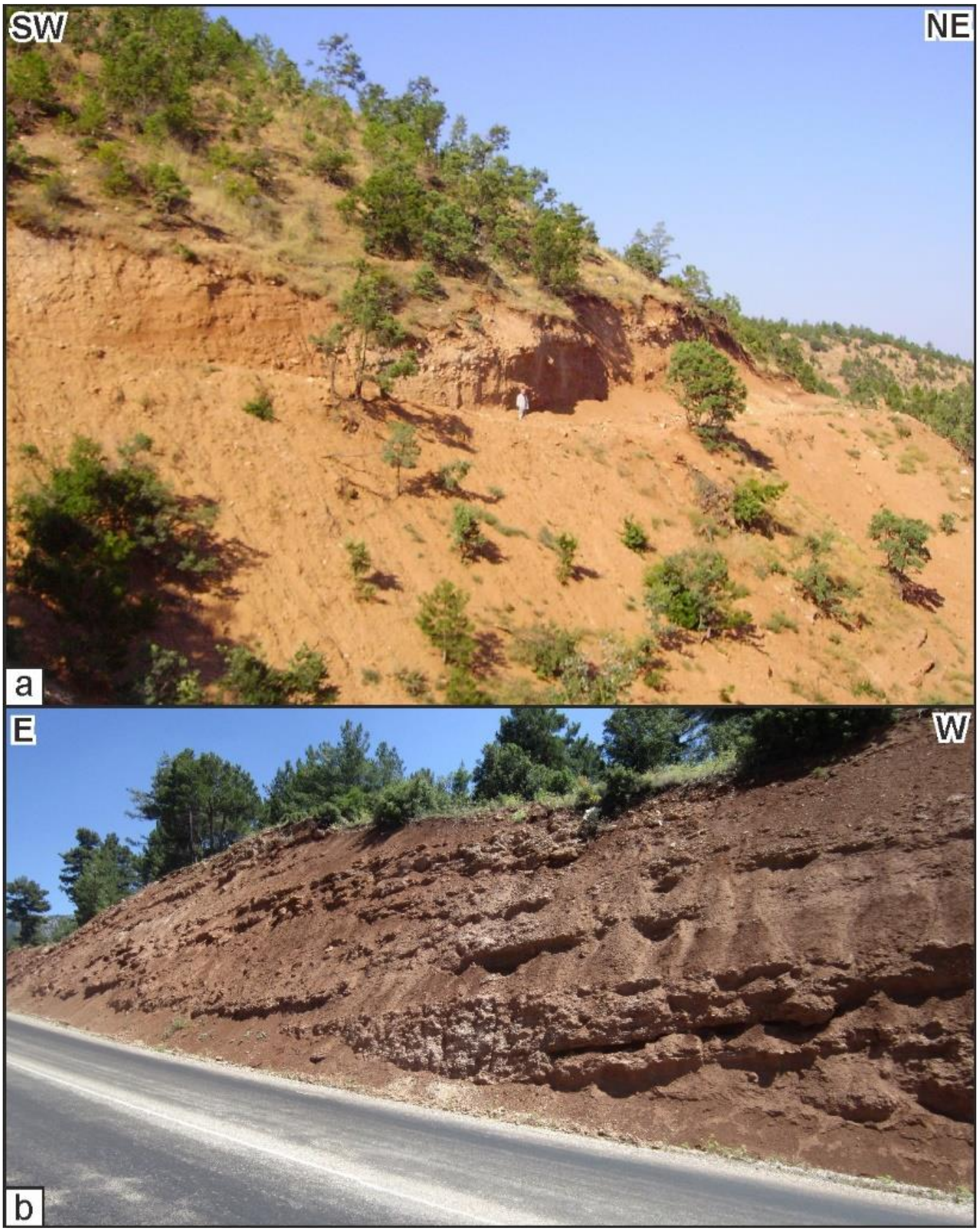

Figure 3.11 : (a) Alluvial fan deposits of the Dirmil Formation located on the down dropped side of the Kuşdili Fault (coordinates 37°3'2.30"N, 29°33'10.48"E). (b) Alluvial fan deposits of the Dirmil Formation located on the down-dropped side of the Asar Fault (coordinates 36°59'59.64"N, 29°16'15.60"E).

3.4.6 Alluvial and talus deposits

The youngest units in the study area are lower Quaternary-Holocene alluvial and talus deposits. The alluvial deposits are composed of uncemented sand, silt and gravel. They make up the materials filling the Acıpayam, Çameli and Gölhisar basins and are also observed along the beds of local rivers (Figures A.1 and A.2b in Appendix A). The talus deposits are predominantly composed of basement-derived gravels and blocks. They are present on the down-dropped sides of the major faults and at the bases of hills (Figure A.1 in Appendix A).

3.5 Structural Architecture

To evaluate the kinematics of the region, we started by mapping the clear lineaments on the contour-derived DEM. The major faults display significant geomorphologic expression both on the DEM and in the field. In this way several faults were mapped during the field studies; however, only 14 of the major faults were identified and named. The dip directions, dip angles and rakes of 9 major faults (Table 3.1, Figure 3.12 a-j) were measured in the field. Although no striations were observed on five of these major faults, their geologic and geomorphologic features are suggestive of normal or oblique (normal and left-lateral) faulting with dips to the northwest (Çiğdemli, Sarıkavak, Kuşdili) and southeast (Çameli, Acıpayam) (e.g., Figure 3.12 k-l).

Table 3.1 : Best exposure coordinates and measurements of the major fault planes.

Figures	Fault Name	Best Exposures		Dip direction	Dip angle	Rake
		Latitude (N) degree, minute, second	Longitude (E) degree, minute, second			
3.12b	Kumafşarı	37°20'9.30"N	29°32'56.16"E	295°	50°	-80°
3.12c	Western Kibyra	37°10'30.48"N	29°28'28.56"E	126°	51°	-70°
3.12d	İbecik	36°59'29.46"N	29°25'4.26"E	308°	58°	-15°
3.12e	Gürsu	36°57'23.16"N	29°18'41.64"E	118°	70°	-120°
3.12f	Kızılyaka	37°2'57.84"N	29°21'39.96"E	315°	60°	-80°
3.12g	Asar	37°0'31.80"N	29°18'37.98"E	288°	50°	-90°
3.12h	Kalınkoz	37°7'18.60"N	29°20'34.86"E	309°	55°	-63°
3.12i	Karabayır	36°55'38.16"N	29°10'44.40"E	308°	83°	-45°
3.12j	Narlı	36°59'26.10"N	29°2'53.70"E	336°	34°	-50°

Normal and left-lateral oblique normal faults are the main structural features in the study area (Figure A.1 in Appendix A; Table 3.1). The major faults are mainly NE-SW-striking faults parallel to the main trend of the Burdur-Fethiye Shear Zone. The dip angles vary between 34^o and 83^o (Table 3.1). The 371 minor faults indicate not only normal and oblique characteristics but also rare reverse and strike-slip offset and create a seemingly chaotic structural fabric. In these chaotic areas, the movement planes (M-planes) correspond to the intersections of various M-plane populations and reflect various principle stress axes. Therefore, the M-plane method (Arthaud, 1969; Aleksandrowski, 1985) was used to assign the faults to various stages of deformation. First, the minor faults were divided into four sets according to their regions across the zone (I, II, III, IV in Figure 3.13). Because insufficient number of minor faults offset in the Dirmil Formation, only the M-planes of minor faults offsetting the Gölhisar and İbecik formations were plotted separately for each region using FaultKin 7.4.1. (Marrett and Allmendinger, 1990; Allmendinger et al., 2012), and their common intersection points (CIPs; Aleksandrowski, 1985) were plotted (Figure 3.14). Based on CIPs, the individual sets of the M-planes were plotted. The stress axes of the minor faults and 10 earthquakes were calculated using an improved version of the right dihedron method (Angelier and Mechler, 1977), and the focal mechanisms (Figure 3.15) were generated by using Win-Tensor software (Delvaux and Sperner, 2003).

3.5.1 Major faults

The study area is dominated by the NE-striking major faults between the basement rocks and Neogene and post-Neogene deposits. Although there are many major faults in the region, only nine major faults display measurable kinematic indicators in the field (Table 3.1). These faults are characterised by NW-SE oblique extension in the region (Figure 3.12a). Because no fault planes or striations were observed, five faults (the Çameli, Kuşdili, Çiğdemli, Sarıkavak, Acıpayam faults) were classified as normal or left-lateral oblique normal based on cross-cutting relationships and offset features. The geomorphologically distinct lineaments observed in the DEMs and other satellite and airborne imagery were classified as geomorphologic faults (Figure A.1 in Appendix A). The NE-striking major faults in the study area, which dip to the northwest or southeast, are the Kumafşarı, Western Kibyra, Kuşdili, İbecik, Gürsu, Çameli, Kızılyaka, Asar, Kalınkoz, Karabayır, Narlı, Sarıkavak, Çiğdemli and Acıpayam faults.

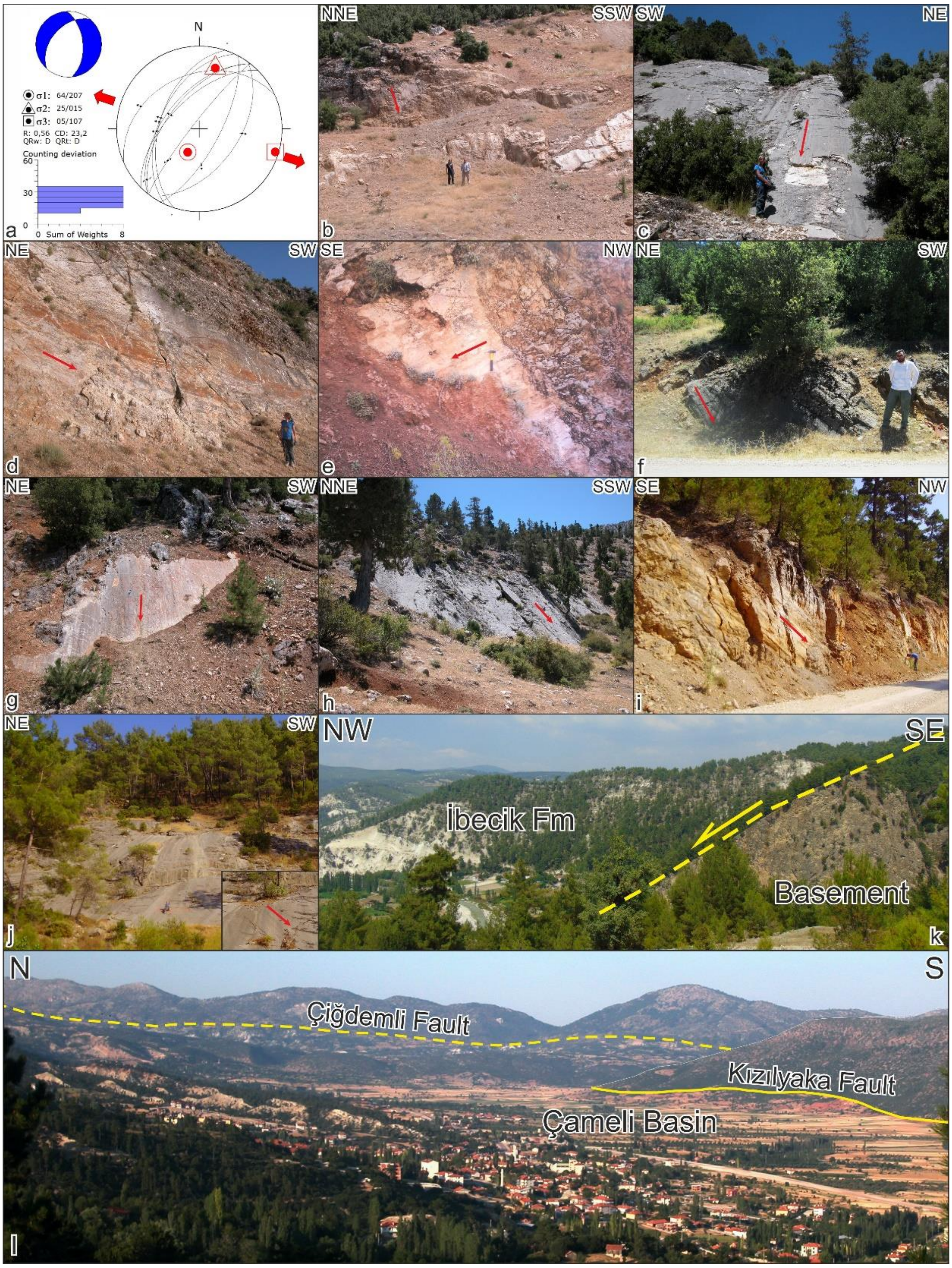

Figure 3.12 : (a) Principle stress axes and focal mechanism of the major faults. (b-j) Major faults with striations (see Table 3.1). (k) Sarıkavak Fault juxtaposing Mesozoic basement and the İbecik Formation (coordinates 37°1'11.64"N, 29°11'37.32"E). (l) Çiğdemli and Kızılyaka faults (coordinates 37°4'15.06"N, 29°20'9.18"E).

The Kumafşarı Fault is located on the southeast margin of the Acıpayam Basin (Figure A.1 in Appendix A). This fault is a ~3-km-long, NW-dipping major normal fault with a left-lateral slip component that juxtaposes basement rocks against Quaternary sediments (Figure 3.12b). On the western boundary of the Gölhisar Basin, a left-lateral oblique normal fault, designated the Western Kibyra Fault, is observed (Figure 3.12c). The ~6-km-long trace of the Western Kibyra Fault locally offsets basement rocks (Figure A.2c in Appendix A) and locally juxtaposes basement rocks against lacustrine sediments of the İbecik Formation (Figure A.1 in Appendix A). On the southeastern side of the Gölhisar Basin, the Kuşdili Fault, which is ~3 km long, separates the between basement from alluvial fan deposits of the Dirmil Formation (Figure A.1 in Appendix A). Slickensides are lacking; however, geologic and geomorphologic indicators indicate normal faulting (Figure A.2c in Appendix A). Another left-lateral oblique normal fault, the İbecik Fault, is observed at İbecik in the southern part of the study area (Figure A.1 in Appendix A and Figure 3.12d). The 1-km-long NW-dipping İbecik Fault forms the contact between Mesozoic limestone and the İbecik Formation (Figure A.1 in Appendix A). Approximately 10 km southwest of the İbecik Fault, the Gürsu Fault juxtaposes basement rocks against the İbecik Formation (Figure A.1 in Appendix A). The Gürsu Fault is a right-lateral oblique normal fault dipping to the southeast (Figure 3.12e).

The Çameli and Kızılyaka faults play a significant role in the formation of the Çameli Basin (Figure A.2b in Appendix A). These major faults are both NE-SW-striking left-lateral oblique normal faults bounding the Çameli Basin (Figure A.1 in Appendix A). The Çameli Fault is a 13-km-long SE-dipping structure. It appears to be a contact between the Quaternary fill of the Çameli Basin and the İbecik Formation. The Kızılyaka Fault is an 8-km-long NW-dipping fault (Figure 3.12f). It extends to a 3-km-long normal fault named the Asar Fault (Figure 3.12g) at the south-western side. Both the Kızılyaka and Asar faults juxtapose Mesozoic limestones against alluvial fan deposits of the Dirmil Formation (Figure A.1 in Appendix A). North of the Çameli Basin, the NW-dipping Kalınkoz Fault is observed (Figure 3.12h). This feature is a 13-km-long left lateral oblique fault juxtaposing Mesozoic limestone and the İbecik Formation (Figures A.1 and A.2a in Appendix A). On the south-western side of the study area, the Karabayır Fault juxtaposes Palaeozoic basement and the İbecik Formation (Figure A.1 in Appendix A). This major fault is a left-lateral oblique normal fault that dips to the northwest (Figure 3.12i) and is ~1 km long. Farther northwest, two northwest-dipping faults, the Narlı and Sarıkavak faults, are present (Figure A.1 in Appendix A). The 4-km-long Narlı Fault offsets the basement rocks, whereas the 12-km-long Sarıkavak Fault juxtaposes the basement against the Neogene units (Figure A.1 in Appendix A). The Narlı Fault is a left-lateral oblique normal fault (Figure 3.12j). Although no striations were observed, the Sarıkavak Fault was classified as normal based on the positions of the adjacent geologic units (Figure 3.12k).

The ~5,5-km-long Çiğdemli Fault is another major fault located northeast of the Çameli Basin (Figure 3.12l). Its fault plane was not directly observed; however, local relationships between units indicate that it is a northwest-dipping normal fault (Figure A.1 in Appendix A). On the north-western side of the study area, southwest of the Acıpayam Basin, the Acıpayam Fault locally juxtaposes basement rocks against Neogene sediments and locally offsets Neogene sediments (Figure A.1 in Appendix A). The plane of this fault is not exposed. According to the paleoseismological study by Kürçer et al. (2016), the Acıpayam Fault is a Quaternary normal fault with a minor left-lateral strike-slip component.

3.5.2 Minor fault subsets

The 371 minor faults observed in the study area are grouped based on their locations in the Neogene formations across the zone (Figure 3.14). The movement planes of each minor fault were used to divide a heterogeneous fault-slip dataset into homogeneous subsets using the M-plane method (Aleksandrowski, 1985). We thereby obtained 19 individual bundles of M-planes (Figure 3.15). Figure 3.15 shows that the minor faults simultaneously developed under four major extensional regimes: NE-SW, NNW-SSE, NW-SE and WNW-ESE.

In the northern part of the study area, north of the Acıpayam Basin (I in Figure 3.13), although a few faults offset the Gölhisar Formation and display NNE-SSW extension (I-g in Figure 3.15), the majority of the minor faults with measurable slickensides offset the İbecik Formation and display NW-SE extension (I-i in Figure 3.15; e.g. Figure 3.16a). The Gölhisar Basin and surroundings (II in Figure 3.13) are characterised by deformations linked to NNW-SSE (IIa-g and IIb-g in Figure 3.15) and WNW-ESE (IIc-g and IId-g in Figure 3.15) extensions, and also strike-slip characteristics (IIe-g in Figure 3.15) involving the Gölhisar Formation. Although most of the Neogene minor faults in the study area are normal faults, a few pure left-lateral faults offset the Gölhisar Formation (e.g. Figures 3.16b and c). The minor faults offsetting the İbecik Formation south and southwest of Gölhisar display NE-SW extension (IIa-i, IIb-i, IIc-i, IId-i in Figure 3.15; e.g. Figure 3.17a).

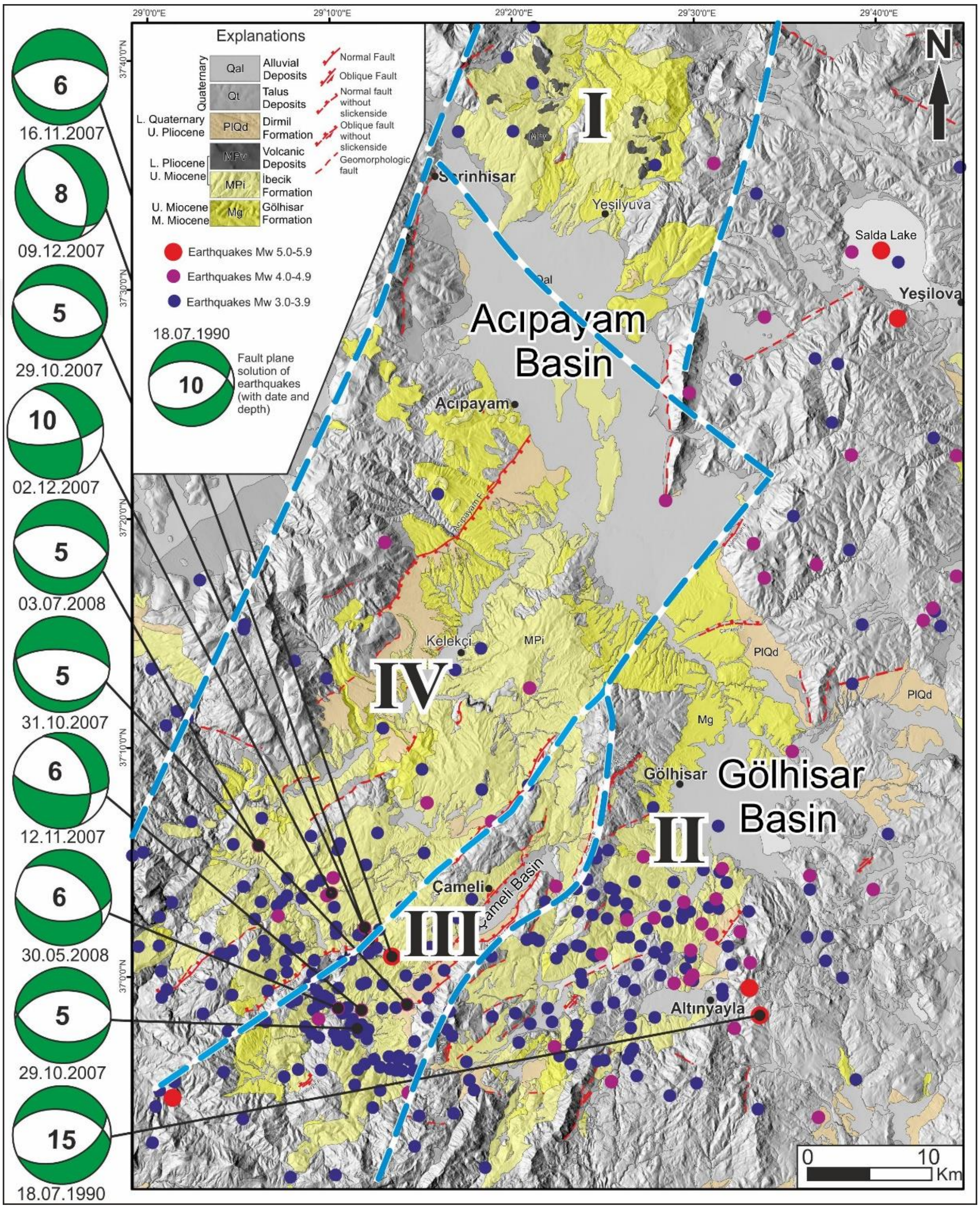

Figure 3.13 : Seismotectonic and middle Miocene-Quaternary geological map of the study area. Fault-plane solutions of earthquakes are shown in green, and numbers indicate depths of hypocentres. Earthquake data are from Över et al. (2010) and USGS (2015). Roman numerals denote regions of the minor fault sets, and blue dashed lines denote the approximate boundaries of the regions.

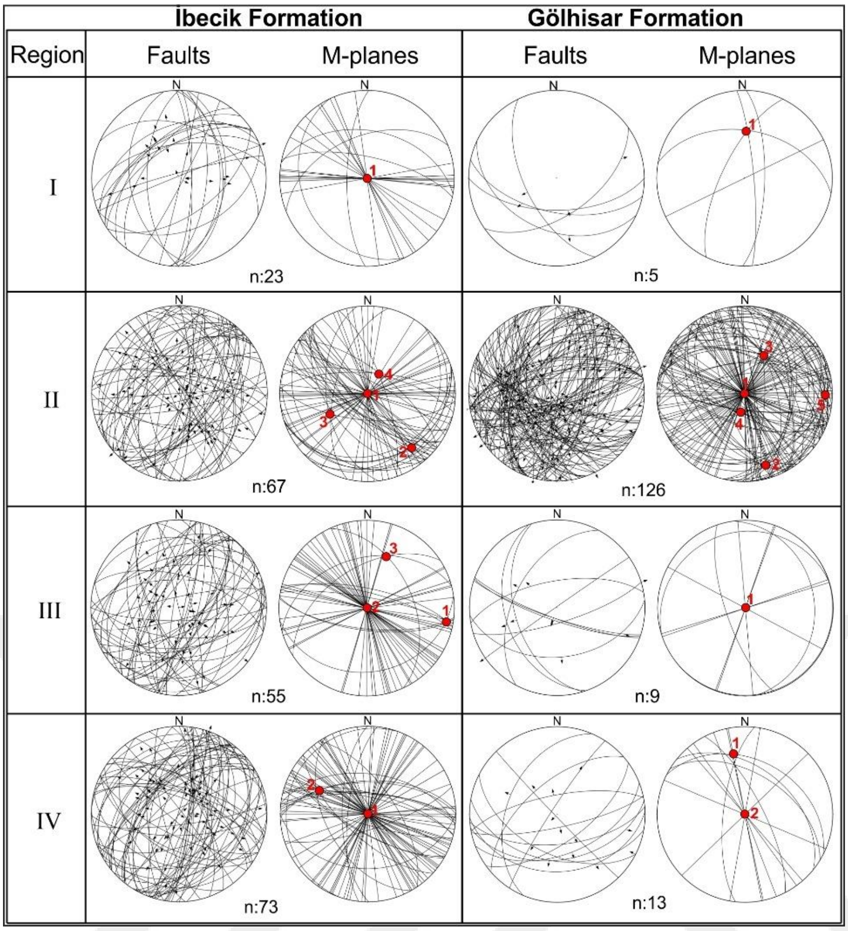

Figure 3.14 : Minor faults and M-plane patterns corresponding to the regions and Neogene formations, obtained using FaultKin 7.4.1 (Marrett and Allmendinger, 1990; Allmendinger et al., 2012). Red circles denote common intersection points (CIPs) of M-planes (Aleksandrowski, 1985).

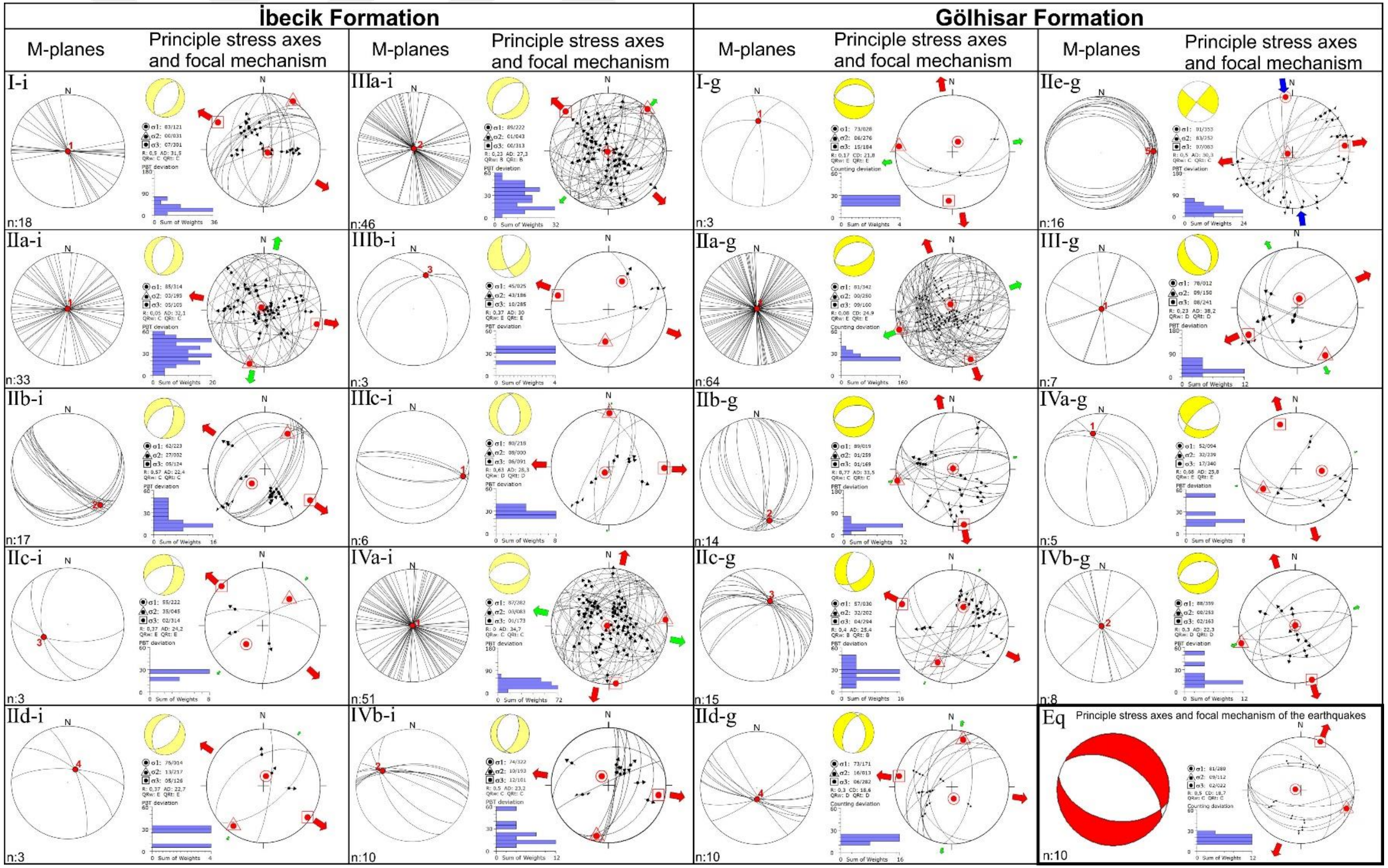

Figure 3.15 : Individual bundles of M-planes taken from Figure 3.14, and principle stress axes and lower-hemisphere, equal-area projections of focal mechanisms obtained using Win-Tensor (Delvaux and Sperner, 2003).

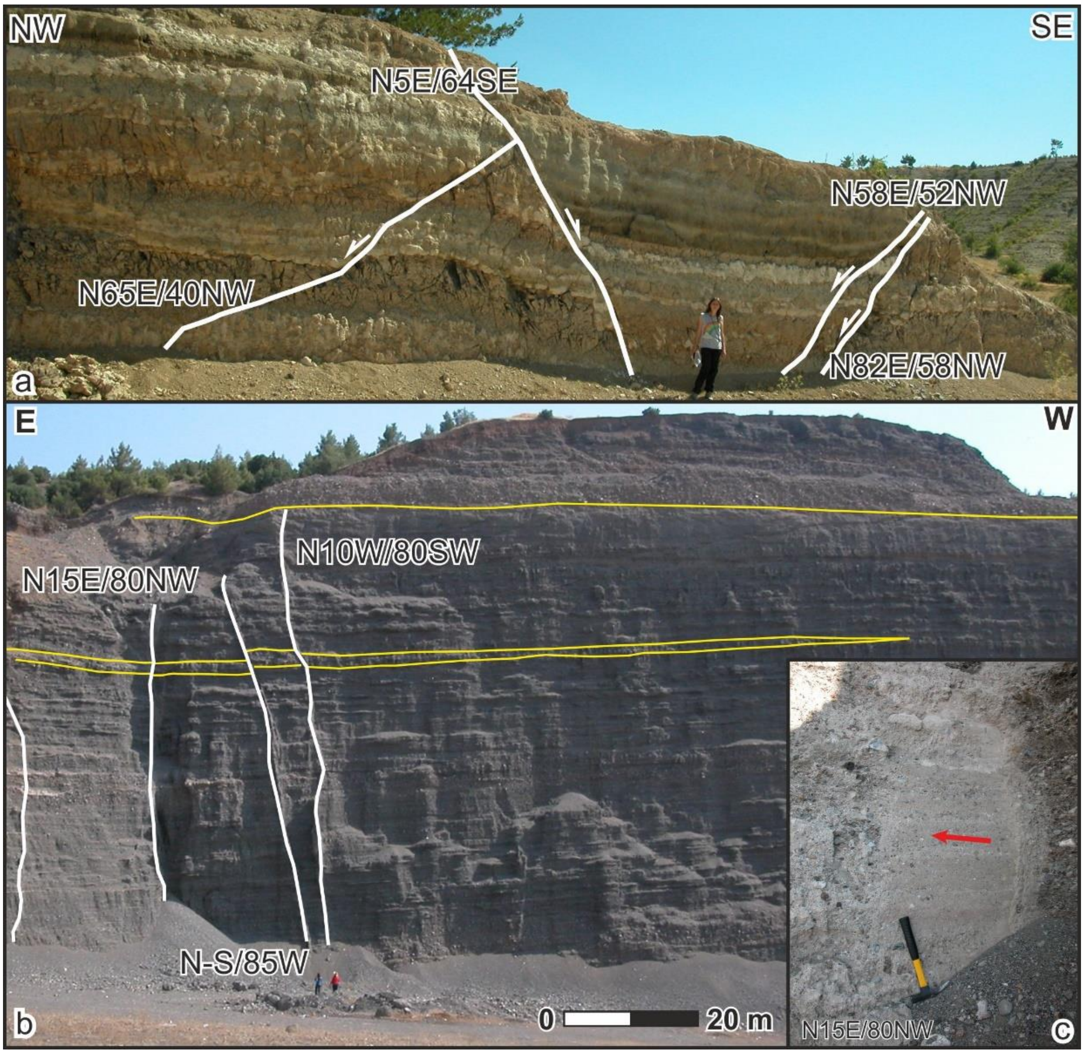

Figure 3.16 : Minor faults offsetting Neogene sediments. (a) Normal faults offsetting the İbecik Formation (coordinates 37°33'55.38"N, 29°23'35.58"E). (b) Left-lateral faults (white lines) and bedding (yellow lines) in the Gölhisar Formation (coordinates 37°16'22.26"N, 29°33'47.70"E). (c) Plane of a left-lateral fault in Figure 3.16b.

The Çameli Basin and surrounding area are dominated by NW-SE, NNW-SSE and NE-SW extensions (IIIa-i, IIIb-i, IIIc-i, III-g in Figure 3.15). Because the İbecik Formation is exposed across most of this area, the minor faults generally offset its lacustrine deposits (e.g., Figure 3.17b). North and northwest of this region, NW-SE and NNW-SSE extensions are prominently manifested as minor faults offsetting the İbecik Formation (IVa-i and IVb-i in Figure 3.15). Similarly, although a few minor faults offsetting the Gölhisar Formation indicate NNW-SSE extension (IVa-g and IVb-g in Figure 3.15), the normal faults juxtaposing the Gölhisar and İbecik formations (e.g., Figure 3.17c) and pure left-lateral faults offsetting the Gölhisar Formation (e.g., Figure 3.17d) are also exposed.

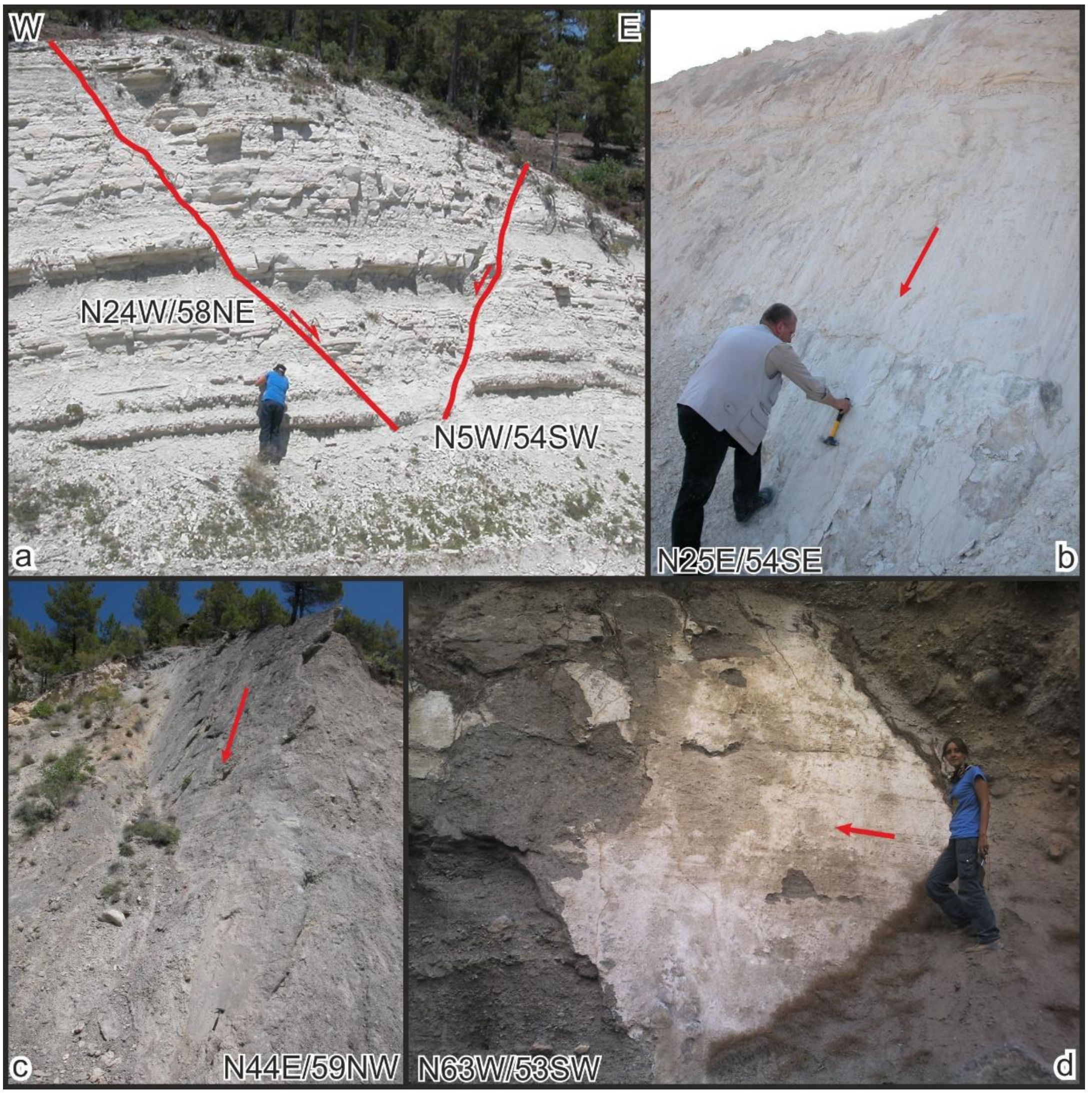

Figure 3.17 : (a) Two normal faults offsetting the İbecik Formation (coordinates 37°2'27.72"N, 29°27'35.94"E). (b) Plane of a normal fault offsetting the İbecik Formation (coordinates 37°8'40.50"N, 29°23'57.48"E). (c) Fault juxtaposing the İbecik and Gölhisar formations (coordinates 37°10'30.06"N, 29°16'2.16"E). (d) Plane of a left-lateral fault plane offsetting the Gölhisar Formation (coordinates 37°13'14.52"N, 29°11'54.12"E).

3.6 Discussion

3.6.1 Tectonic framework and kinematic data of the study area

South-western Turkey is a highly tectonically active region with distinct deformations related to various types of structural features. All these deformations are linked to one another. In particular, the extensional tectonism of the Aegean graben system, the Isparta Angle and the transpression-dominated forearc region of the Cyprus and Hellenic arcs have exerted significant effects on the evolution of the Burdur-Fethiye

Shear Zone and therefore on our study area (Figure 3.1). Similarly, the stratigraphy of each basin along the Burdur-Fethiye Shear Zone cannot be evaluated separately. A mixed deformation pattern that includes normal faults common on the Aegean side, thrusting common on the eastern side and oblique motions in the middle section dominates the Burdur-Fethiye Shear Zone (Hall et al., 2014a). The Aegean system, located west of the study area (dark-blue region in Figure 3.2), has been formed by counterclockwise rotation of south-western Anatolia and roll-back of the Hellenic Trench (Tur et al., 2015). Therefore, the Aegean region is dominated by NE-SW and N-S extensions. East and southeast of the study area (green region in Figure 3.2), compression in the Gulf of Antalya, Anaximander Mountains, Finike Basin and Sırrı Erinç Plateau is still active (Aksu et al., 2009, 2014; Hall et al. 2009, 2014a, b).

The first hypothesised structural feature in the region was a major left-lateral fault named the Fethiye-Burdur Fault Zone (Barka et al., 1995). Based on our studies, a single major throughgoing fault system with a distinct main displacement zone (e.g., the North Anatolian or East Anatolian faults) does not exist. Instead, there are numerous 1 to 10 km-long faults in the region. In this study, the fault kinematic analysis was performed using the measurements of dip directions, dip angles and rakes of fault planes at 380 locations. The dip angles of the 9 major faults range from 34º to 83º, and these faults display slickenlines with rakes between -15º and -120º (Table 3.1). Both the major and minor faults in the region generally show pure normal faulting and normal faulting with a left-lateral component. In addition, there are several right-lateral oblique normal faults and a few minor reverse faults in the region. The fault-plane solutions of 10 earthquakes indicate extensional and oblique displacements, and the records of 329 earthquakes indicate that most of these earthquakes occurred in the southern part of the study area (Figure 3.13).

Recent models of the evolution of the middle section of the Burdur-Fethiye Shear Zone in previous studies can be divided into three scenarios:

1. Formation of a graben during early Tortonian to early Pleistocene time as a result of a NW-SE-oriented extensional system (Alçiçek, 2001; Alçiçek et al., 2004, 2005, 2006).

2. Miocene-Pliocene to Holocene NW-SE, NE-SW and NNE-SSW extensions related to the Cyprus and Hellenic arcs (Över et al., 2010).

3. NE-SW-trending left-lateral shearing involving the Aegean graben system, Isparta Angle, Cyprus and Hellenic arcs and counterclockwise rotation of Anatolia since the middle Miocene (Elitez and Yaltırak, 2014c; Hall et al., 2014b; Elitez et al., 2015; Elitez et al., 2016b).

Local studies in the region suggest an evolution controlled by an extensional regime. Alçiçek (2001) and Alçiçek et al. (2004, 2005, 2006) asserted that the Neogene basin, designated the Çameli Basin by them, developed as half-grabens due to NW-SE extension along NE-SW-trending normal faults. The geological maps in these studies show bedding, dipping to the southeast towards NW-dipping normal faults (e.g., Alçiçek et al., 2005; their figure 2). There is no geologic or geomorphologic evidence in the field to support the presence of these faults (see both Figure A.1 in Appendix A and their figure 2 in Alçiçek et al., 2005). Kinematic analysis of a few minor faults indicates NW-SE, NE-SW and NNE-SSW extensional regimes in the study area (Över et al., 2010). However, the different extension directions obtained from the minor faults may not represent different tectonic phases. The major faults previously interpreted as normal faults typically show an oblique sense of offset in the study area (Figure 3.12, Table 3.1). The fault sets that exhibit various extension directions (Figure 3.15) formed as a result of left-lateral oblique movement. The beds dip in all directions (Figure A.1 in Appendix A), and folded structures exist (Figure A.2 in Appendix A). Such structures are probably products of both rotation and shear deformation. The palaeomagnetic study by Özkaptan et al. (2014) along the suggested Burdur-Fethiye Fault Zone, which was characterized as a narrow NE-SW-trending left-lateral fault by Barka et al. (1997), indicates that the sense of rotation is almost the same along the fault. Considering this view, the answer to the question "Fethiye-Burdur Fault Zone: a myth?" asked by Kaymakçı et al. (2014) is "yes, it is a myth". The explanation is that both studies were performed along a narrow fault zone of ~10 km.

Extensions within a left-lateral shear regime may cause tectonic and morphological misinterpretations. The basement of the study area is composed of the ophiolitic mélange of the Lycian Nappes. The NE-SW-striking major faults are the products of old faults within the Lycian Nappes. Therefore, many major faults instead of a single major fault are observed in a wide area. The strikes of the major faults and the extension directions and fold axes in the region are nearly parallel to the zone and manifest as structures produced by progressive deformation within shear zones, as revealed by Schreurs and Colletta (1998) and Fossen et al. (2013). According to the shear zone model developed by Ramsay and Huber (1983), the strain ellipses display different extension directions across a zone and more deformation in the centre. Concordantly, the heterogeneous systems show an increase in strain intensity from the margins to the centre of the shear zone (Vitale and Mazzoli, 2008) and can widen with time (Type I; Means, 1984, 1995; Hull, 1988). In the transtensional model by Schreurs and Colletta (1998), normal faults develop between older major strike-slip faults with increasing deformation, some of these faults develop oblique slips, the high angles of the faults begin to decrease during the deformation and small transtensional basins develop, as seen in the study area (Figures A.2a-c in Appendix A and Figure 3.18). In the transtensional folding model by Fossen et al. (2013), there are hinge-parallel extensions in the brittle upper crust and fold axis rotations with increasing strain. The stereonet plots of the bedding in the İbecik and Gölhisar formations indicate nearly NE-trending fold axes (Figure 3.19). In such shear zones, displacements on the major faults are small because the displacement is spread across a wide zone. The amount of shear displacement related to rotation in the region and relative motion of the blocks around the zone is ~40 km (Yaltırak, 2003). In this case, the average displacement per kilometre along the Burdur-Fethiye Shear Zone should be ~400 m. Present-day GPS-based velocities reflect a similar situation (Elitez et al., 2016b). Considering the 40 km of displacement during the last 15 My, it is understandable that no remarkable continuous lateral structures developed. Therefore, NW-SE extension affecting the region leaves significant geomorphologic traces in the region. Because the local rotations related to tilted fault blocks, folding and slow shearing are common in the Miocene sediments, it is difficult to determine the main rotation of the sedimentary sequences. The stress directions obtained from the minor faults in the study area indicate NE-SW, NW-SE, E-W, NNW-SSE extensions and NE-SW left-lateral oblique extension (Figure 3.15). An examination of the stress directions of the strain ellipsoids, which experienced 20º of counter clockwise rotation since 15 Ma in the left-lateral shear model (Ramsay and Huber, 1983), indicates that they are compatible with the stress directions obtained from the kinematic analysis (Figure 3.15).

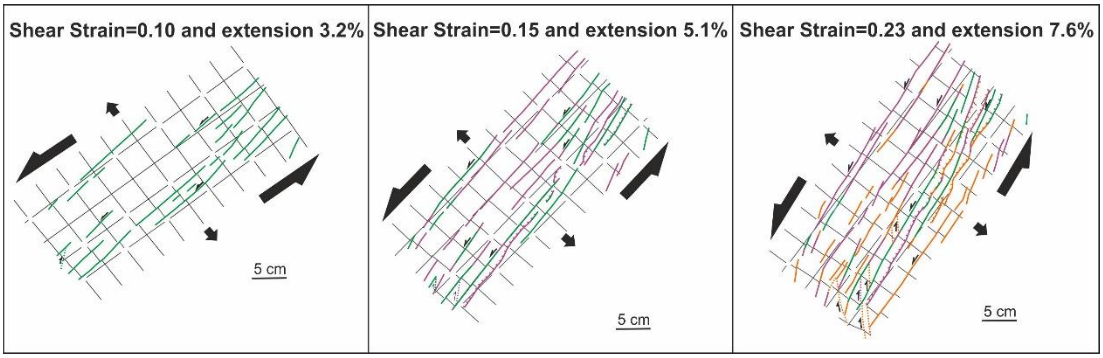

Figure 3.18 : Fault evolution in a left-lateral transtensional system modified from Schreurs and Colletta (1998). Newly generated faults are shown by different colours (green, purple and orange, respectively).

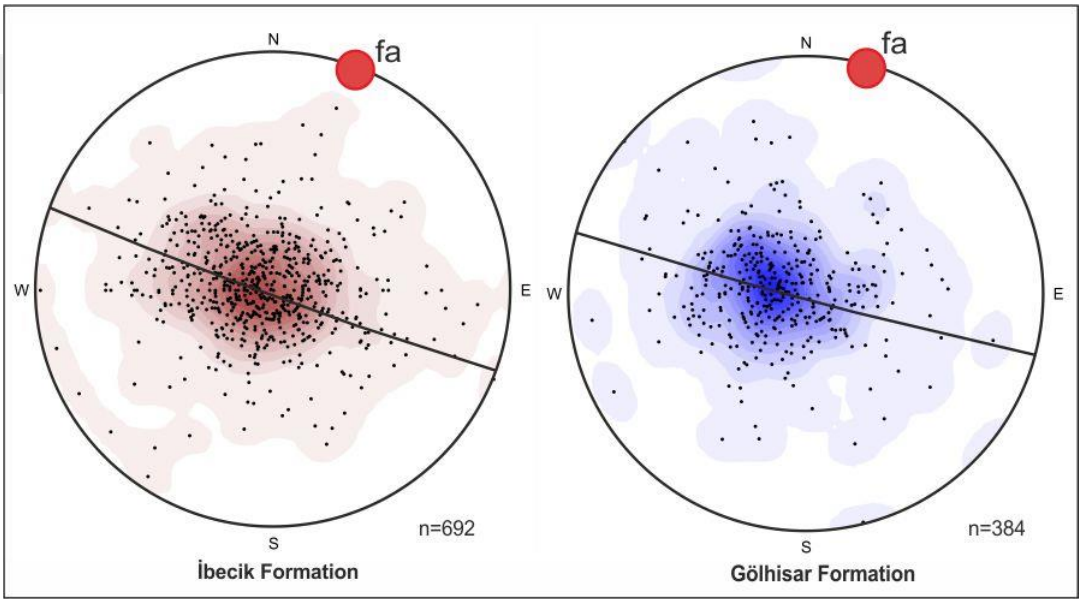

Figure 3.19 : Stereoplots of the beddings and fold axes in the Neogene sediments (fa: fold axis).

The 329 earthquakes of moment magnitude (Mw)≥3 after 1971 (USGS earthquake catalogue, 2015) generally occurred in the southern part of the region and they had relatively shallow hypocentres, generally less than 10 km deep (Figure 3.13). The largest recorded earthquakes since 1971 are the earthquakes of 12 March 1971 (Mw 5.7 and Mw 5.6; Yeşilova and Salda Lake), 18 July 1990 (Mw 5.5; Altınyayla), 21 November1990 (Mw 5.0; Altınyayla), 13 November 1994 (Mw 5.4; south-western part of the study area), 29 October 2007 (Mw 5.3; Çameli) and 16 November 2007 (Mw 5.1; Çameli). Ten fault-plane solutions of recent earthquakes in the region show N-S and NE-SW pure normal and oblique mechanisms (Figure 3.13). In the western part of the Burdur-Fethiye Shear Zone, the GPS-based slip rates range from 22 mm/yr in the north to 27 mm/yr in the southwest (Figure 3.2). These rates differ by 5 mm/yr and indicate NE-SW extension related to the roll-back of the Hellenic Trench. In the eastern part of the zone, the GPS-based velocities range from 19 mm/yr on the north to 15 mm/yr on the south, which Aksu et al. (2009) suggested are related to compression of the region. The GPS velocity differences across the zone are 3-4 mm/yr in the northernmost part and 8-10 mm/yr in the southernmost part (Elitez et al., 2016b). In the study area, this difference is 6-7 mm/yr.

The transtensional shear systems led to the formation of various faults and basins, internal rotation of the structures across the zone and formation of the fold axes parallel to the extension direction. The presence of a major fault, the Burdur-Fethiye Fault Zone, was suggested in previous studies. However, our GPS data and the clear structural patterns in the region indicate the presence of a transtensional shear system.

3.6.2 Regional kinematic model

Based on the seismotectonic, geodetic and structural data, the structural properties of the two significant regions clarify the development of structures in the study area. The Menderes Block, situated west of the study area (Figure 3.2), is dominated by the extensional regime and is characterized by NE-SW-, N-S- and NW-SE-trending depressions (Tur et al., 2015). The GPS-based vectors obtained within the Menderes Block indicate 24 mm/yr and 34 mm/yr of south-westward movements in the northern and southern parts, respectively (Figure 3.2). This differential motion indicates NE-SW extension. In addition, there is an approximately 5° angular difference between the vectors, necessitating counter clockwise rotation of the block. Tur et al. (2015) suggested that this rotation is generated by back-arc extension and forms the grabens in the Menderes Block. East of the study area, the mechanism of uplift of the Western Taurides Block indicate compression between the Rhodes Basin and the Gulf of Antalya (Aksu et al., 2009, 2014; Hall et al. 2009, 2014a, b). The thrust faults bounding the Rhodes and Finike basins were formed by southwest migration of the Aegean region (Aksu et al., 2009; Hall et al., 2009; 2014a). At the centre of the Isparta Angle, there are thrust faults that offset early Miocene deposits and extend from the Gulf of Antalya to south of Isparta (Hall et al., 2014b). The GPS velocities indicates 4 mm/yr decrease from Isparta Angle to Kaş (Figure 3.2) and corresponding uplift (Elitez et al., 2016b). This differential motion indicates NE-SW compression related to the Western

Taurides thrust fault (WTTF, Figure 3.2). The Menderes Block moves south-westward 4 mm/yr faster on the north and 10 mm/yr faster on the south than the Western Taurides Block. This velocity difference explains the NE-SW-trending extension between the two blocks, which has produced the formation of the Burdur-Fethiye Shear Zone. Because the Menderes Block is moving more rapidly, this shear is left-lateral. Studies have shown that, the Aegean is a region of NE-SW back-arc extension (dark-blue region in Figure 3.2) due to roll-back of the Hellenic Trench (Le Pichon and Angelier, 1979; McKenzie, 1978; Meulenkamp et al., 1988; Yılmaz et al., 2000). In addition, a NNE-SSW compressional regime (green region in Figure 3.2) is still active in the south-eastern portion of the zone (Aksu et al., 2009; 2014; Hall et al., 2009; 2014a). The Burdur-Fethiye Shear Zone is an active left-lateral transtensional shear zone located between these tectonic regimes from the Miocene to Recent and is also the propagation of the subduction-transform edge propagator (STEP) fault into the upper plate (Hall et al., 2014a; Elitez et al., 2016b). There is general agreement that the western limb of the Isparta Angle (Burdur-Fethiye Shear Zone) in south-western Turkey underwent 30^{o}-40^{o} of counter clockwise rotation of during the Miocene (Kissel and Poisson, 1987). In addition, the zone is predominantly compressional due to the relative movement of African and Anatolian blocks (Le Pichon and Angelier, 1979), and this motion is expressed on land by the northward buckling of the western Taurides Mountains (Aksu et al., 2009; Hall et al., 2009). In the late Miocene, the Isparta Angle experienced a compression phase with thrusting along its western and eastern limbs (Barka et al., 1995; Barka and Reilinger, 1997). Paleomagnetic data indicates that the Western Taurides Block underwent 20^{o} of counter clockwise rotation between 16 and 5 Ma (van Hinsbergen et al., 2010b; Koç et al., 2016). These counter clockwise and clockwise rotations are related to the northward motion of the African Plate and evolution of the "Λ" shaped Isparta Angle (Hall et al., 2014b) since the late Miocene. The counter clockwise rotation of the western Taurides initiated the development of the Burdur-Fethiye Shear Zone and progressively changed the orientation of the faults and basins in south-western Turkey since the middle Miocene.

The southern Menderes Block has been affected by NE-SW extensional tectonics since the middle Miocene (Bozkurt and Park, 1994; Sözbilir, 2001; Seyitoğlu et al., 2004; van Hinsbergen and Boekhout, 2009). In addition, the fold and thrust structures in the Rhodes Basin has experienced a counter clockwise rotation (Aksu et al., 2009; Hall et al., 2009; 2014b), while the Western Taurides experienced a 20º of counter clockwise rotation since the middle Miocene (van Hinsbergen et al., 2010b; Koç et al., 2016). Based on the Miocene-Quaternary tectonics of south-western Turkey and the kinematic analysis of the region, the orientation of the western limb of the Isparta Angle (early Burdur-Fethiye Shear Zone) was ENE-WSW in the middle Miocene (1 in Figure 3.20). Meanwhile, the western part of the Isparta Angle moved northward and rotated 20º counterclockwise. According to Koç et al. (2016), while the middle part of the Isparta Angle underwent no rotation, the eastern part the Köprüçay Basin rotated ~20º-30º clockwise and the Manavgat Basin underwent ~25-35º of counter clockwise rotation since the early-middle Miocene. These rotations were clearly related to bending and northward movement of this region. Consequently, the Menderes Block is moving south-westward west of the Burdur-Fethiye Shear Zone, while the Isparta Angle is moving northward. The key issue is to identify the structural changes associated with the movement of the Isparta Angle. Yaltırak (2003) suggested a tectonic model to explain the relationship between the evolution of the Thrace-Eskişehir Fault and that of the Isparta Angle from the middle Miocene to the early Pliocene (Figure 3.21). According to this model, while the Isparta Angle was moving northward, western Anatolia was moving westward and rotating counterclockwise along the Thrace-Eskişehir Fault. Thus, as it is now, western Anatolia was rotating counterclockwise and moving toward the Hellenic Arc from the middle Miocene to early Pliocene.

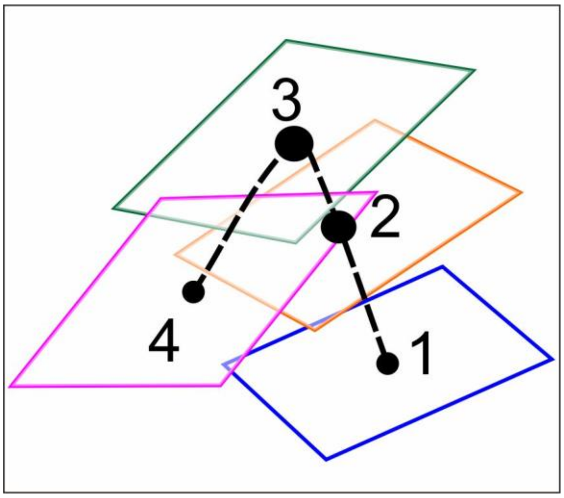

Figure 3.20 : Counterclockwise rotation and palinspastic migration in the middle section of the Burdur Fethiye Shear Zone. Parallelograms show the positions of the study area in different time-intervals (see Figure 3.22).

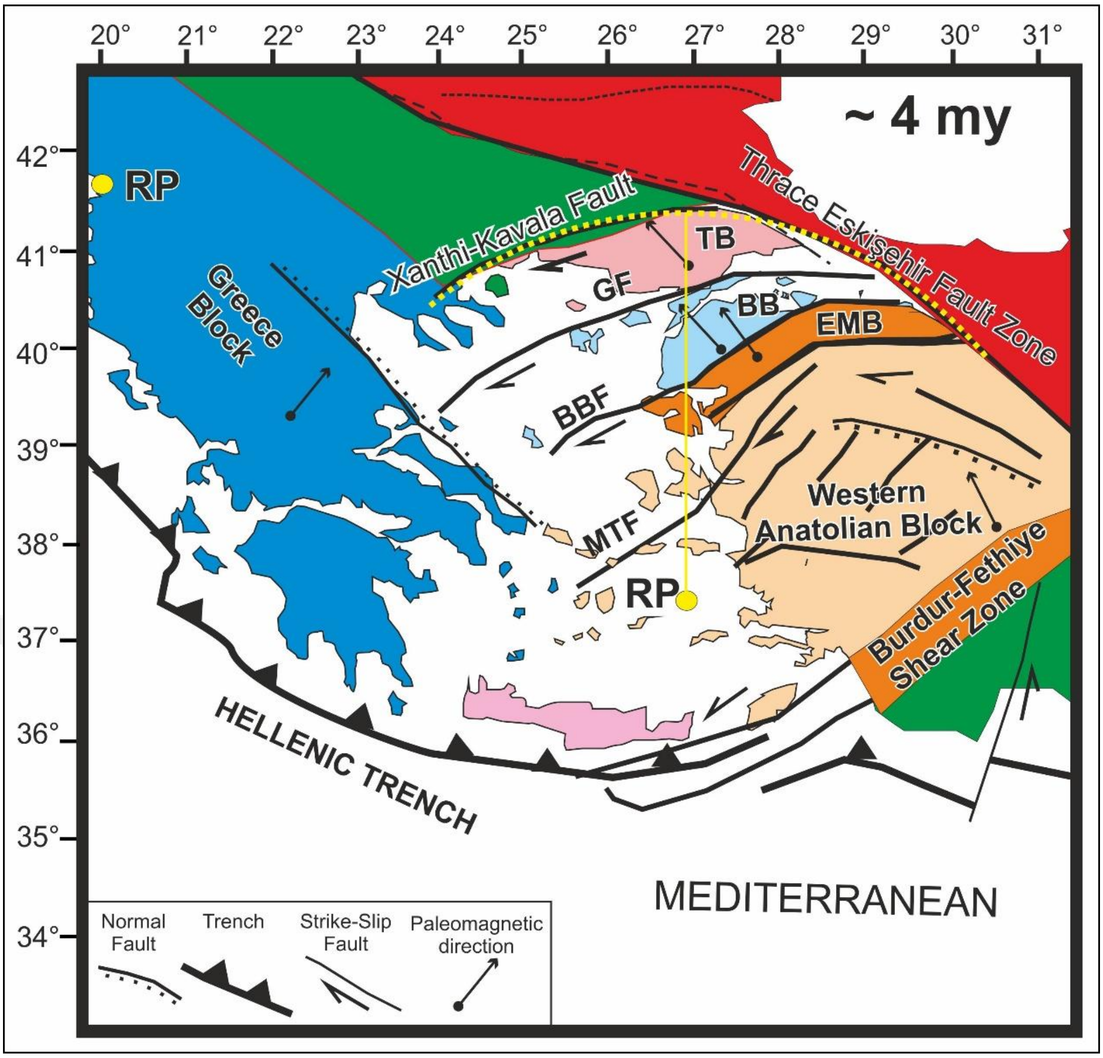

Figure 3.21 : Early Pliocene palinspastic map and tectonic block model of the Aegean region before North Anatolian Fault and westward tectonic escape. Dashed line shows the Thrace-Eskisehir Fault Euler Circle. RP: rotation pole; BBF: Bandırma-Behramkale Fault; GF: Ganos Fault; MTF: Manyas-Tuzla Fault; TB: Thrace Block; BB: Biga Block; EMB: Edremit-Manyas Block (compiled from Yaltırak, 2003; Sakınç and Yaltırak, 2005).

A palinspastic model of the region (Figure 3.22) was constructed by combining the recent GPS data, the palaeomagnetic data published by van Hinsbergen et al. (2010b) and Koç et al. (2016), the Euler pole calculated by Yaltırak (2003) and the palaeomagnetic data compiled by Yaltırak (2003), which indicate middle Miocene to early Pliocene rotation of western Anatolia. The Pliocene and Quaternary faults, GPS velocities and rotations during the latest 5 My were considered in preparing Figure 3.22. The western Anatolian Block is shown bounded by Thrace-Eskişehir Fault and Burdur-Fethiye Shear Zone. While rotating the western Anatolian Block along at circle corresponding to movement along the Thrace-Eskişehir Fault back in time, both the

Isparta Angle and western Anatolian block move southward (Figure 3.20; 5-15 Ma in Figure 3.22). Thus, the rotational and dimensional changes along the zone become clear (Figure 3.20). Today, the Burdur-Fethiye Shear Zone displays both internal rotation of a transtensional system and left-lateral displacement decreasing to the northeast (Hall et al., 2014a) under the effects of the Aegean graben system, Cyprus and Hellenic arcs and counter clockwise rotation of the south-western Turkey (Appendix B).

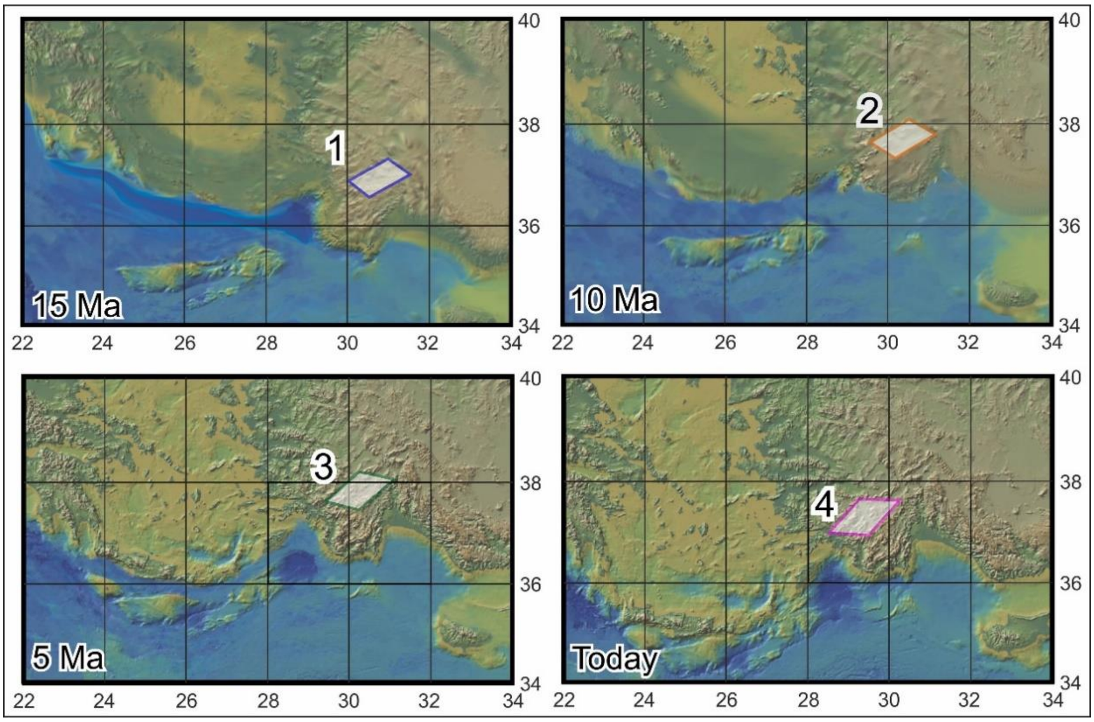

Figure 3.22 : Palinspastic evolution of Western Anatolia, Aegean Region and Burdur-Fethiye Shear Zone. Parallelograms show the study area.

3.7 Dating of the Sedimentary Sequence

To explain the Miocene-Quaternary evolution of the middle section of the Burdur-Fethiye Shear Zone, the rock units and their relationships in the Acıpayam, Çameli and Gölhisar basins and in south-western Turkey must be clarified. There are a few basins containing younger rocks along the Burdur-Fethiye Shear Zone, such as the Burdur, Tefenni, Eşen and Acıgöl basins (Figure 3.2). These basins represent portions of larger carbonate lakes. According to most studies, the lacustrine deposits in these basins are of Pliocene age, except in small areas north and east of the Acıpayam Basin (e.g. Şenel, 2002; Alçiçek, 2001; Alçiçek et al., 2004, 2005, 2006, 2008; Kazancı et al. 2012). In contrast, other studies suggested the presence of three different Neogene formations with ages ranging from middle Miocene to early Quaternary (Elitez et al., 2009; Elitez, 2010; Elitez and Yaltırak, 2014c; this study).

The most important stratigraphic problem in south-western Turkey is the age-ranges of the Neogene sediments. Some studies suggest different ages of the same fossils in the same localities. For example, the upper portions of the sedimentary sequence in the study area were dated at 1.8 Ma (Alçiçek et al., 2005; 2005, 2006) and 2.2 Ma (van den Hoek Ostende et al., 2015b). A new study reports new mammal fossils at the Ericek locality in the Çameli Basin (van den Hoek Ostende et al., 2015b). Although the age interval of these fossils is equivalent to that of the younger part of the MN15 zone (3.6-3.8 Ma), the authors suggested an age of 3.4 Ma as a best estimate. 40Ar/39Ar radiometric dates obtained by Paton (1992) provide additional important information about the age of the Neogene sediments. Dated volcanic rocks cut or overlie the lacustrine marls, claystones and limestones of the İbecik Formation in the northern part of Acıpayam Basin at elevations of ~1500-1600 m, and the rocks yield an age of Tortonian to early Pliocene (Figures A.1 and A.2 in Appendix A). In addition, mammal fossils dated at 10.8-8.5 Ma (Saraç, 2003) are located in the lacustrine sediments south of Elmalıyurt. The İbecik Formation is exposed at ~1300 m in the north-western Çameli Basin at ~1750 m in the southern part of the study area (Elmalıyurt) and at ~200 m in the northern part of the Eşen Basin south of the study area. This elevation difference of ~1550 m indicates that rapid uplift started in the Miocene (Aksu et al., 2009; Hall et al., 2009), and the widespread exposures of the same unit indicate the presence of an extensive warm lake in the late Miocene. However, the red-wine-coloured beds at the top of the İbecik Formation indicate a period of aridity related to the Messinian salinity crisis (MSC; Hsü et al., 1973). These caliche levels are observed at many locations and imply that this warm lake started to evaporate during the Messinian, and they can be regarded as representing the dry floor of the Messinian lake. After the Messinian, the lake began to break up into smaller lakes as a result of the activity along the Burdur-Fethiye Shear Zone. This late Miocene lake was probably formed by the regional tectonics and covered the entire region. It started to evaporate following the MSC, specifically, at the beginning of the Pliocene.

On the north-western side of the study area, limestone lenses are interbedded with the conglomerates of the Gölhisar Formation west of Acıpayam. Alçiçek and ten Veen

(2008) asserted that this unit was deposited in a piggy-back basin in the early Miocene. The unit in this locality is composed of poorly sorted brownish and red alluvial fan conglomerates containing well-rounded ophiolite and marble pebbles, and an 80-m-thick carbonaceous sequence including coral, gastropod and bivalve fossil levels overlies this unit. According to our studies, a lower Miocene marine sequence does not overlie the upper Oligocene-lower Miocene conglomerates along the Burdur-Fethiye Shear Zone. The Gölhisar Formation unconformably overlies the upper Oligocene-lower Miocene conglomerates in a valley north of the village of Ören (Figure A.1 in Appendix A). The most significant constituents of these conglomerates are well-cemented, massive beds composed of well- to sub-rounded cobbles and pebbles. Bed thicknesses vary between 4 and 50 m. In the Denizli Basin, there is no early Miocene marine limestone (Alçiçek et al., 2007). The sequence begins with lower-middle Miocene conglomerates and clayey limestones of the Kızılburun Formation and grades upwards into the middle-upper Miocene claystones, siltstones, marls, mudstones and clayey limestones of the Sazak Formation (Alçiçek et al., 2007; Wesselingh et al., 2008). The upper unit (Kolankaya Formation) is composed of mudstones, siltstones, sandstones, claystones, marls, clayey limestones and conglomerates and is also older than late Miocene (Wesselingh et al., 2008). The Acıpayam Basin was not connected to the Denizli Basin during the early Miocene. The reported fossils in Kale (Denizli) are early Miocene (Akdeniz, 2011). The Beyağaç Basin represents the most likely connection between the Kale and Acıpayam basins. The middle-upper Miocene sequence in the Beyağaç Basin is similar in terms of sedimentary characteristics to those of the Gölhisar and İbecik formations, and thus this sequence is time equivalent to the Neogene sequence along the middle section of Burdur-Fethiye Shear Zone. The local unconformities in the Gölhisar Formation around Acıpayam are the types of contacts encountered along tectonically active basin margins. Therefore, the conglomerates south of the Mevlütler locality were correlated with the Oligocene-lower Miocene conglomerates in Acıgöl and Kale-Tavas in previous studies (Şenel, 1997c; Akdeniz, 2011). Even in the best-case scenario, the marine fossils at the Acıpayam locality (Akdeniz, 2011) are related to a small marine inflow from the Kale Basin. Therefore, the age of the bottom of the Gölhisar Formation may be regarded as early Miocene.

In light of field studies, the Gölhisar and İbecik formations represent the period between 15 and 3.7 Ma, and the Dirmil Formation has an age of 2.2 Ma and later. The palaeomagnetic rotation data (Yaltırak, 2003; van Hinsbergen et al, 2010b; Koç et al., 2016) and volcanism (Paton, 1992) indicate that the Burdur-Fethiye Shear Zone has been active and a part of Mediterranean tectonics since the early-middle Miocene. Furthermore, the paleo-drainage system and sediment provenance recorded along the middle section of the Burdur-Fethiye Shear Zone indicate deposition from the middle Miocene to Quaternary in south-western Turkey, thereby confirming the age estimates in our study (Elitez et al., 2016a).

3.8 Conclusions

- The Burdur-Fethiye Shear Zone (BFSZ) is a left-lateral transtensional shear zone that developed under the progressive influence of the roll-back of the Hellenic Trench, the compressional region of the Western Taurides and the westward escape of Anatolia since the middle Miocene.
- The Burdur-Fethiye Shear Zone is dominated by 1-10-km-long NE-SW-striking normal and oblique-left-lateral faults and NE-SW-trending basins.
- The Acıpayam, Çameli and Gölhisar basins are located along the middle section of the Burdur-Fethiye Shear Zone, where Neogene deposits are dominant.
- The Neogene stratigraphy of the region indicates a time of deposition between the middle Miocene and early Pliocene.
- The Acıpayam, Çameli and Gölhisar basins represent the parts of an extensive warm late Miocene lake that probably evaporated during the Messinian salinity crisis.
- The Acıpayam, Çameli and Gölhisar basins were generated by the transtensional Burdur-Fethiye Shear Zone.
- The kinematic analysis of the minor faults yields NE-SW, NNW-SSE, WNW-ESE and NE-SW-trending stress orientations. It is known that the recent tectonics of the region is dominated by a NE-SW-trending stress orientation due to the roll-back of the Hellenic Trench within the zone and a NW-SE-

trending stress orientation due to the transtensional shear. The shearing, internal rotation and counter clockwise rotation of Anatolia changed the stress directions.

- The structural evolution and kinematics of the study area is attributed to progressive deformation that has been active since the late Miocene.

4. A CRITICAL REVIEW OF THE KIBYRA FAULT (BURDUR-FETHİYE SHEAR ZONE, SW TURKEY)[3]

4.1 Introduction

South-western Turkey is a tectonically very active region dominated by Aegean back-arc extension regime (Le Pichon and Angelier, 1979; Mckenzie, 1978; Meulenkamp, et al., 1988; Yılmaz et al., 2000), westward motion of Anatolia (Dewey and Şengör, 1979; Şengör, 1979; Şengör et al., 1985) and the subduction transform edge propagator (STEP) fault zone (Govers and Wortel, 2005; Hall et al., 2014a). In the previous studies, the NE-SW striking faults between Burdur and Fethiye in south-western Turkey (Figure 4.1) were named the Burdur Fault, Fethiye-Burdur Fault, Fethiye-Burdur Fault Zone, Burdur-Fethiye Fault Zone or Burdur-Fethiye Shear Zone (e.g. Barka and Reilinger, 1997; Barka et al., 1995; Bozcu et al., 2007; Elitez and Yaltırak, 2014c; Elitez et al., 2015; Eyidoğan and Barka, 1996; Glover and Robertson, 1998; Hall et al., 2014a; Över et al., 2010, 2013a; ten Veen, 2004; ten Veen et al., 2009; Verhaert et al., 2004; Verhaert et al., 2006;) after the pioneering work of Dumont et al. (1979). However, recent studies showed that there is a left-lateral transtensional zone, which was named the Burdur-Fethiye Shear Zone, between the western Anatolian extensional and the Western Taurides compressional regimes (Elitez et al., 2016b; Elitez and Yaltırak, 2016)

The *so called* Kibyra Fault is thought to be located in the middle section of the Burdur-Fethiye Shear Zone, between northeast of Çamköy and İbecik villages (Figure C1 in Appendix C) and destroyed the ancient city of Kibyra. The existence and activity of Kibyra Fault was suggested first by Akyüz and Altunel (1997, 2001). They observed a damage in the stadium of the ancient city and attributed it the activity of a NNE-SSW striking left-lateral fault that collapsed seat rows on the eastern side of the stadium.

[3] This chapter is based on the paper "Elitez, İ., Yaltırak, C., Kürçer, A., Özdemir, E., and Güldoğan, Ç. U. (2017). A critical review of the Kibyra Fault (Burdur-Fethiye Shear Zone, SW Turkey). Geodinamica Acta, 29:1, 91-102."

They proposed that this fault cut and displaced Pliocene deposits on both eastern and western sides of the stadium.

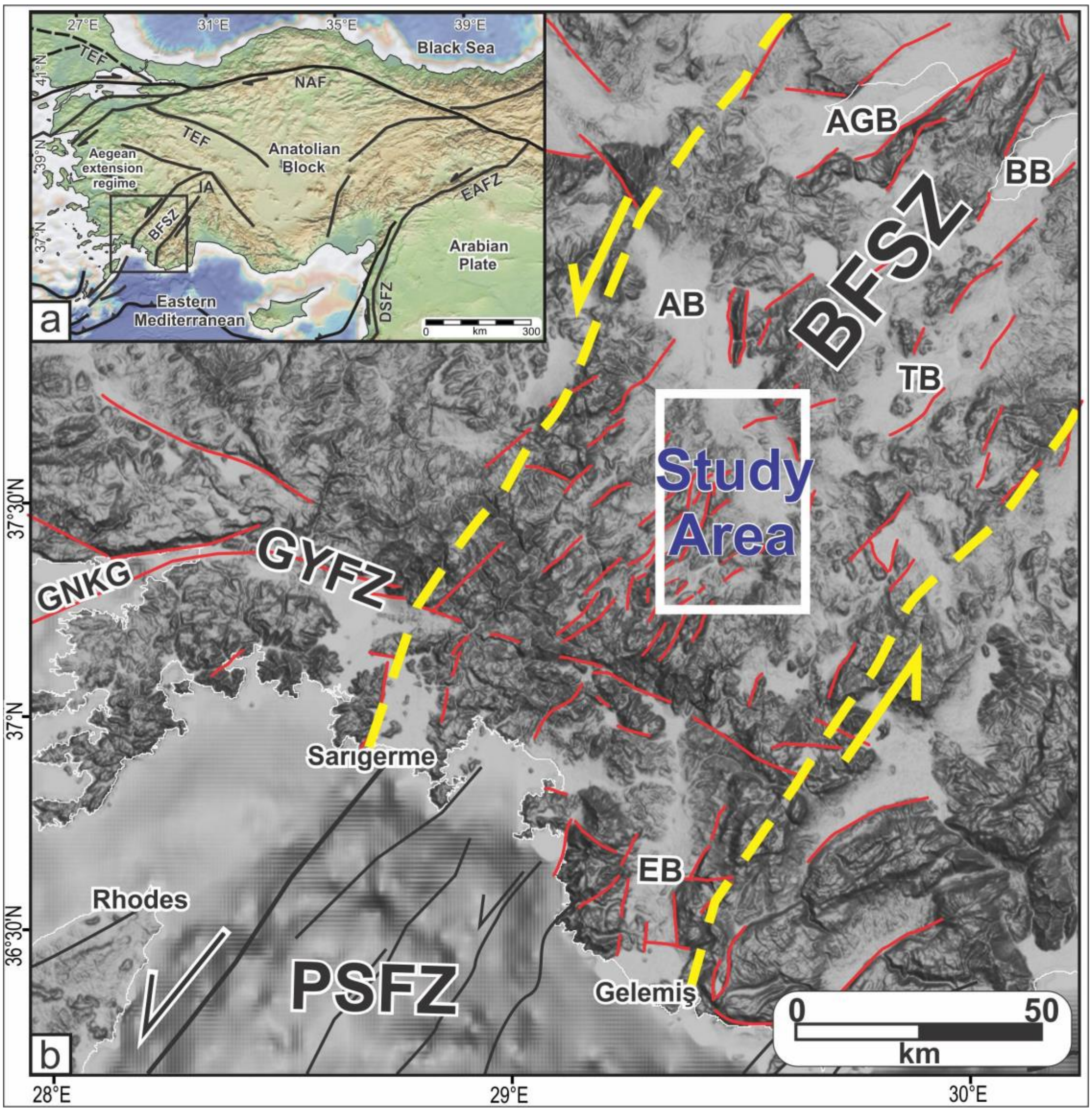

Figure 4.1 : Simplified tectonic map of south-western Turkey compiled from Yaltırak et al. (2012). TEF: Thrace-Eskişehir Fault, NAF: North Anatolian Transform Fault, EAFZ: East Anatolian Fault Zone, DSFZ: Dead Sea Fault Zone, IA: Isparta Angle, BFSZ: Burdur-Fethiye Shear Zone. Rectangle indicates Figure 4.1b. (b) Simplified fault map of the southwestern Turkey and location of the study area. BFSZ: Burdur-Fethiye Shear Zone, PSFZ: Pliny-Strabo Fault Zone, GYFZ: Gökova-Yeşilüzümlü Fault Zone, AB: Acıpayam Basin, AGB: Acıgöl Basin, BB: Burdur Basin, TB: Tefenni Basin, EB: Eşen Basin, GNKG: Gökova-Nisyros-Karpathos Graben.

Alçiçek et al. (2004), Alçiçek et al. (2005) and Alçiçek et al. (2006) mapped this fault and extended it to the northeast of Çamköy and southwest of Gölhisar. Karabacak (2011) described Kibyra Fault as a N20°E trending, at least 35 km-long fault between İbecik Village in the south and Çamköy Village in the north based on aerial photo study, geological field evidence and offset features. The author argued that slickensides on fault planes, deflected stream beds and terraces, fault-parallel elongated ridges are the surface evidences for the existence and kinematics of left-lateral Kibyra Fault (Karabacak et al., 2013). On the other hand, Elitez and Yaltırak (2014b) argued that there is no fault cutting the ancient stadium of Kibyra and the deformation is the result of the differential deformation of the heterogeneous foundation of the stadium.

The active fault mapping directly affects the settlement suitability, urban planning and economic aspects of engineering structures and their siting. Therefore, in this paper, we focus on the importance of active fault mapping which is very crucial for seismic hazard studies and has the potential to lead scientific and also socio-economic problems. In this context, the main purpose of this study is to verify the existence of supposed Kibyra Fault in the field by integrating geomorphological, paleoseismological (trench excavation), and field observations.

4.2 Materials and Methods

In this study, the geological and geomorphological properties of the region between Çamköy and İbecik (Gölhisar, SW Turkey) and surrounding area are described based on both recent and classical methods. Remote Sensing methods that involve use of Digital Elevation Models and satellite and airborne images are effective and efficient ways of revealing geomorphological properties of regions. In this context, we integrated Digital Elevation Model (DEM), DigitalGlobe images provided by Google Earth, available geological maps, and field observations obtained during our field studies between 2008 and 2015. Using all these information and techniques a detailed geological map has been prepared and the trace of supposed Kibyra Fault is also plotted on these geological map (Figure C1 in Appendix C), based on the information obtained from the publications mentioned above. In order to observe the fault trace, deflected streams and ridge offsets were surveyed and two trenches were excavated in the ancient stadium of Kibyra and Yusufça village. These localities were chosen because the supposed Kibyra crosses over these localities. In addition, the longitudinal river profiles and stream length-gradient (SL) indices (Hack, 1973) of individual rivers at different locations were constructed using the GIS software product ESRI ArcGIS Desktop 10.1 (Appendix D and E).

4.3 Tectonic Framework

The Kibyra Fault is supposed to be located in the Gölhisar basin which is developed within a NE-SW trending left-lateral shear zone. The pre-Neogene basement of the study area includes Mesozoic limestones, Cretaceous ophiolitic melange and Cretaceous flysch of Lycian Nappes and Paleogene sedimentary rocks which lie unconformably on the Lycian Nappes (Brunn et al., 1970; Collins and Robertson, 1997, 1998; Ersoy, 1990; Önalan, 1979). The sedimentary sequence unconformably covers the pre-Neogene basement, begins with Middle-Upper Miocene fluvial conglomerate-sandstone units of the Gölhisar Formation and passes vertically and laterally into the Upper Miocene-Lower Pliocene lacustrine limestone-claystone sequence of the İbecik Formation. The Upper Pliocene-Lower Quaternary alluvial fan conglomerates and mudstones of the Dirmil Formation unconformably overlie these units (Elitez and Yaltırak, 2014c; Elitez et al., 2015). Recent talus deposits are mainly observed along the front of the fault scarps or high hills and flood plain deposits of the present river network are situated unconformably on top of all the pre-Holocene sequences.

Numerous small-scale to mesoscopic faults can be observed in the region and they are mainly NE-striking normal faults with or without slight left-lateral strike-slip components (Hall et al., 2014a). In addition to these small-scale faults several major faults also exist in the region. In this regard, we have determined three types of major faults in the region; (1) faults which can be recognized from digital elevation models (DEM) and contain measurable kinematic indicator in the field, (2) faults which can be recognized on the DEM and can also be defined by cross-cutting relationships and off-set features, (3) photo-lineaments which are morphologically distinct linear features and can be recognized on DEMs and other satellite or airborne imagery (Figure C1 in Appendix C). Most of these faults are striking NE-SW and dipping NW directions, SE-dipping faults are also common as well. The Kalınkoz Fault is a NE-SW striking NW dipping normal fault located to the north of Çameli Basin which is delimited at the northwest by the Çameli Fault and at by the Kızılyaka Fault at the southeast. Both Çameli and Kızılyaka faults are NE-striking left lateral oblique-slip normal faults. The NNE-striking, WNW-dipping Çiğdemli Fault (Figure 4.2a) is a normal fault situated at the northeast of Çameli Basin. The Miocene deposits in front of the fault are steeply dipping due west (Figure 4.2b). Although, no kinematic indicator has been observed on the fault planes, there are other geological evidences which implies that the Çiğdemli Fault might be a normal fault with left lateral strike-slip component. Other normal faults in the study area are Kuşdili Fault, located in the southern part of Gölhisar Basin and Çamköy Fault located in the northern part of the study area (Figure C1 in Appendix C). The Kuşdili Fault is a NE-SW striking NW dipping fault that occur between pre-Neogene basement units and alluvial fan deposits of Dirmil Formation (Figure C1 in Appendix C) (Elitez and Yaltırak, 2014c). In the northern part of the study area, there is an asymmetric valley. The southern flank of this valley has a steep slope and the attitudes of the exposed Miocene deposits are the same on the both sides of the valley. This morphology indicates a normal fault which we named as Çamköy Fault (Figure 4.2d). A NE-striking left lateral oblique-slip normal fault exists at the western boundary of the Gölhisar Basin. Contrary to the other researchers, we have given 'western Kibyra' name to this fault (Figure C1 in Appendix C) because the ancient city of Kibyra is located on the hanging wall. Quaternary talus deposits comprising limestone blocks and boulders are observed in front of the western fault scarp (Figure 4.2c) indicating present activity of the fault. The İbecik Fault which is located in the southern part of the study area is discussed in the next section.

The largest known earthquakes in the Gölhisar Basin are AD 23 and 417 earthquakes that damaged the Kibyra (Guidoboni et al., 1994). The largest recorded earthquakes (M_w 5.0 and M_w 5.5) occurred in 1990 (USGS earthquake catalogue, 2015). The earthquakes are commonly occurred at the southern part of the Gölhisar Basin (Figure 4.3). Considering the presence of widespread alluvial fan deposits of the Dirmil Formation in front of the Çiğdemli and Kuşdili faults, talus deposits in front of the Kibyra Fault and current seismicity in the region, it can be claimed that at least one of these three faults must be responsible from the earthquake tremors and destruction of ancient city of Kibyra.

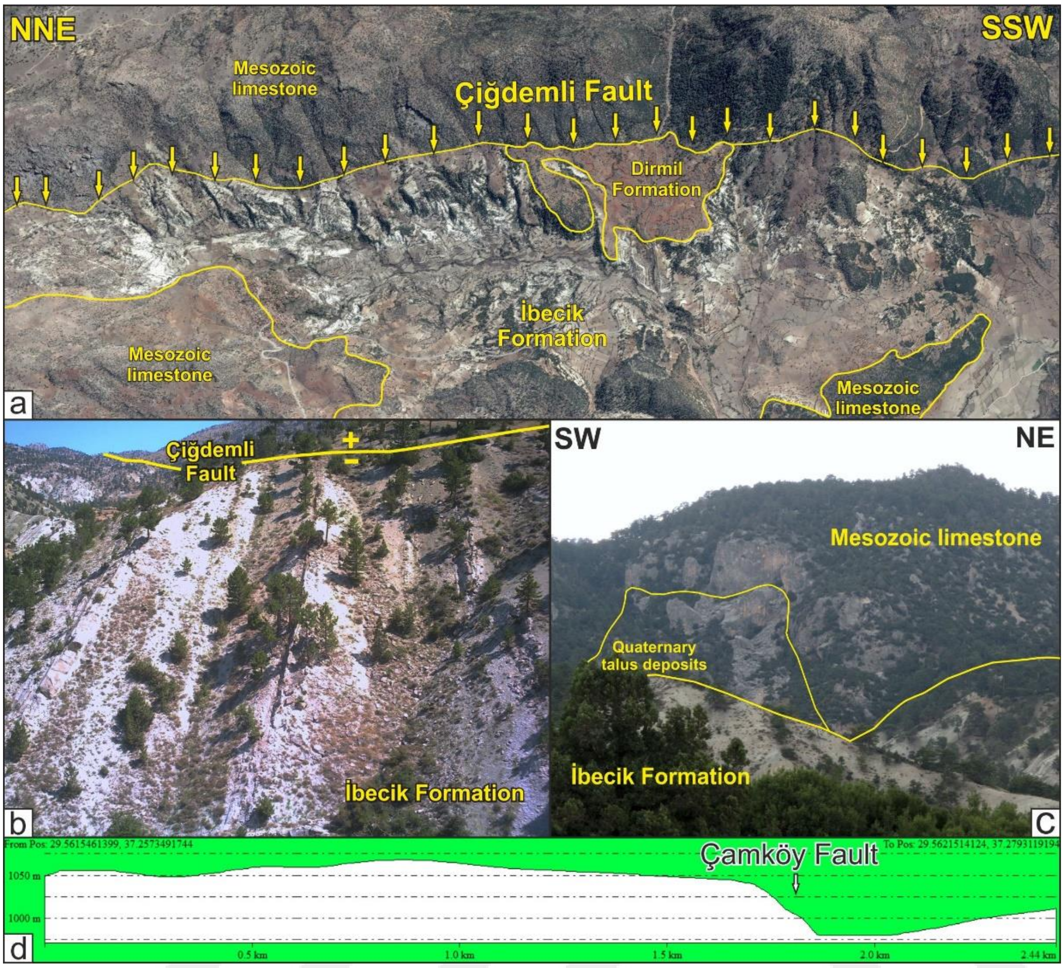

Figure 4.2 : (a) 3D satellite image of the Çiğdemli Fault. Yellow arrows indicate the fault trace. (b) Claystones and limestones of İbecik Formation with high angles. (c) Quaternary talus deposits in front of the Kibyra Fault which was located to northwest of Kibyra. (d) S-N topographic profile of the location where Çamköy Fault exists.

4.4 Faults in the Study Area

It was suggested that the Kibyra Fault is a 35-km-long fault, located between northeast of Çamköy village, cuts the ancient stadium of Kibyra and extends to the İbecik village in the southwest (Akyüz and Altunel, 1997, 2001; Alçiçek et al., 2006; Karabacak, 2011). At the northern tip of the supposed Kibyra Fault, several N-S trending strike-slip faults can be observed (Figure 4.4a). According to Alçiçek et al. (2006), these faults are Quaternary dextral strike-slip faults that cut the tilted Pliocene conglomerates and extend into the ancient stadium of Kibyra. Karabacak (2011) argued that these vertical faults cut the Quaternary deposits and the horizontal motion is consistent with the motion of the fault in the İbecik village.

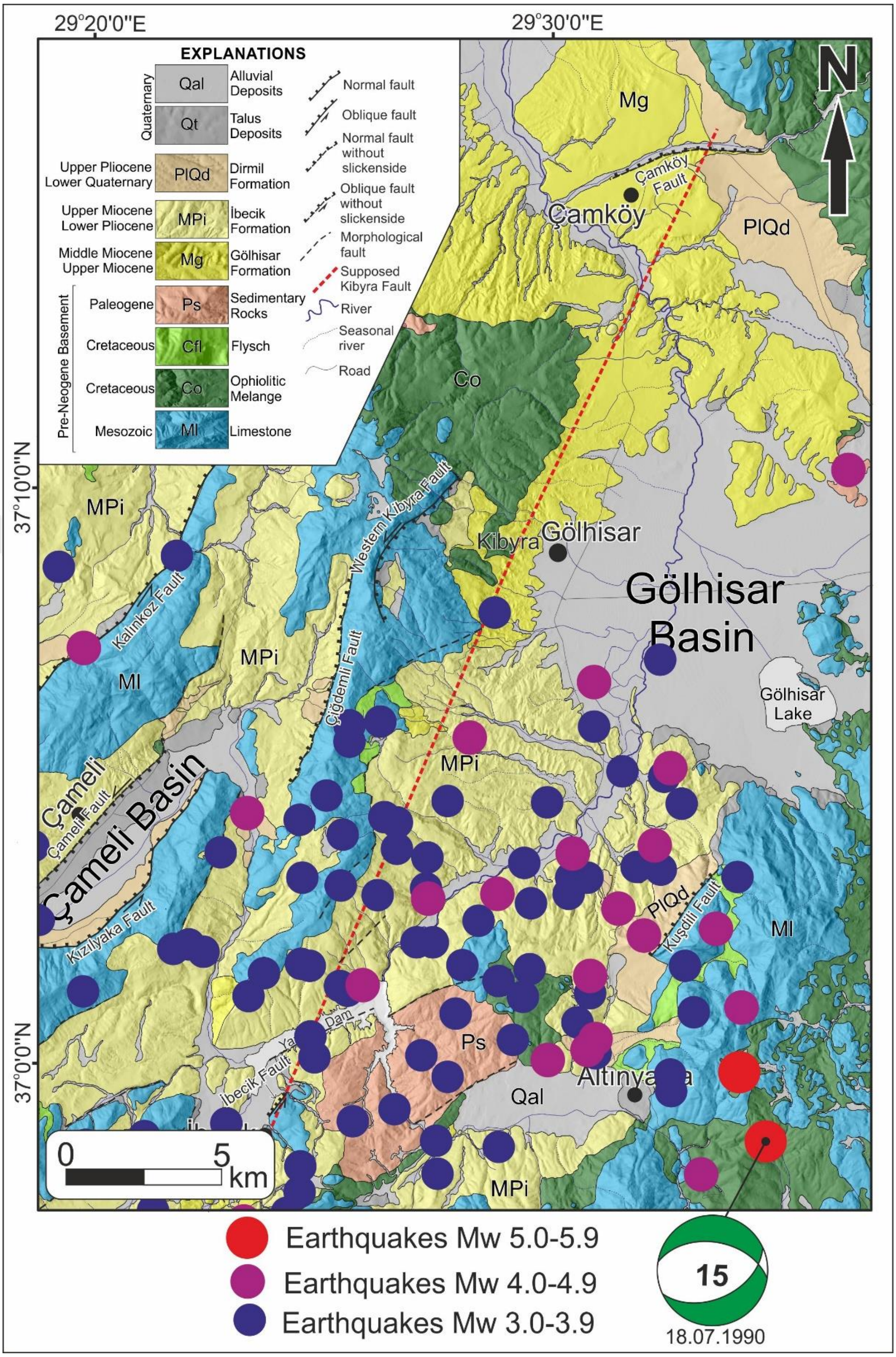

Figure 4.3 : Seismotectonic map of the study area. Earthquake data from USGS (2015).

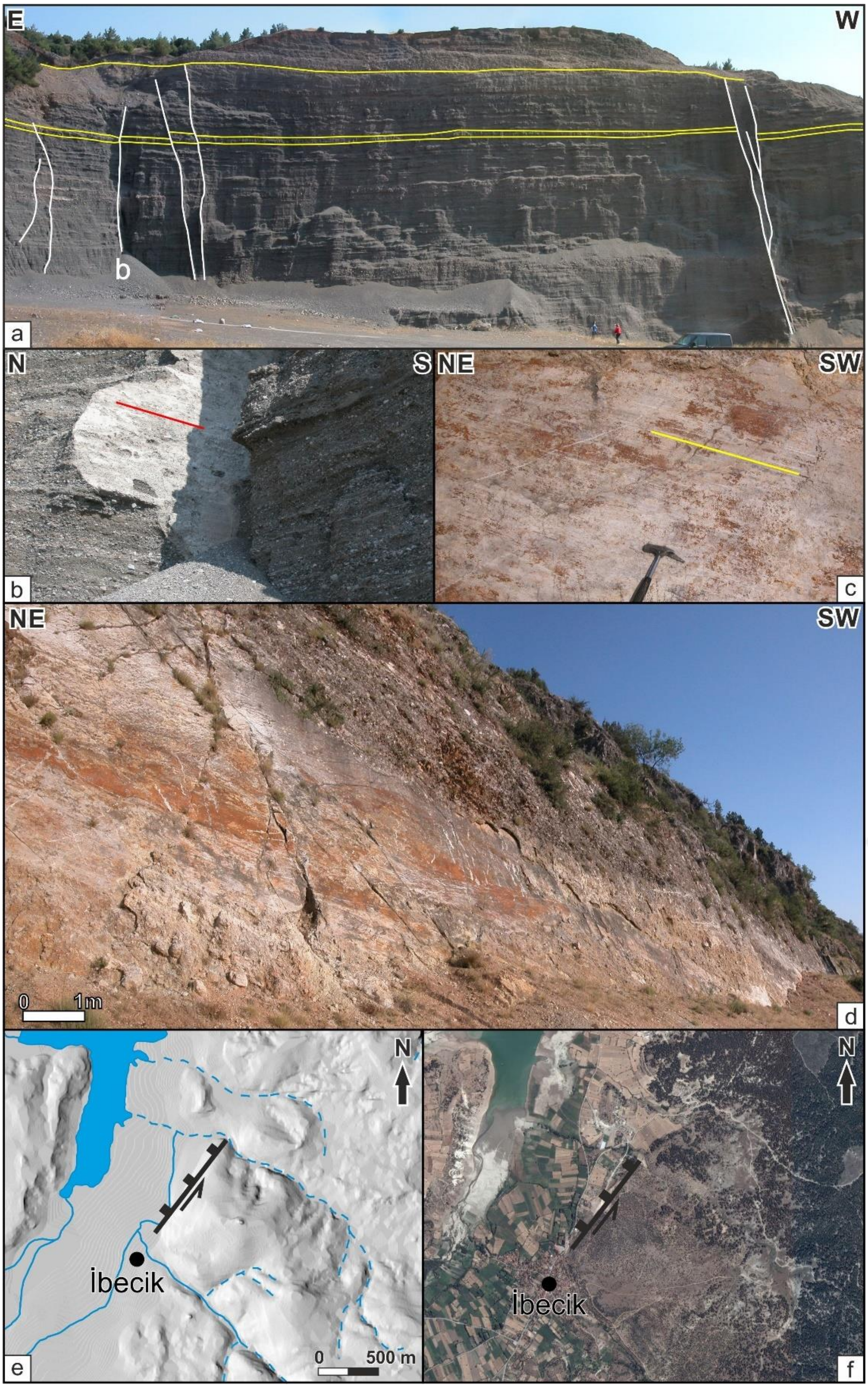

Figure 4.4 : (a) Miocene conglomerates and strike-slip faults. Yellow lines indicate the layers. b indicates the location of Figure 4.4b. (b) Fault plane of the strike-slip fault shown in Figure 4.4a. Red line indicates the striation. (c) Fault plane of the İbecik Fault shown in Figure 4.4d. Yellow line indicates the striation. (d) View of the İbecik Fault in the field. (e) View of the İbecik Fault on DEM. (f) View of the İbecik Fault on satellite image.

Our field study observations conflict with these studies. In the northeast, the ~30 m thick conglomeratic sequence which is composed of the middle-upper Miocene Gölhisar Formation includes several N-S and NNE-SSW trending pure strike-slip faults (Figure 4.4b). These faults do not cut the whole sequence, the upper ~5 m thick sediments cover all these strike-slip faults (Figure 4.4a). Therefore, these faults can neither be Quaternary faults nor a part of the supposed Kibyra Fault.

Furthermore, when examining the fault in İbecik village, it represents a different character from the northeastern faults. This fault, which we named as İbecik Fault (Figure 4.4d), is a 1 km-long, N38°E/58°NW left lateral oblique normal fault with slickenside pitches around 15° and observed between the lacustrine claystones of İbecik Formation and Mesozoic limestones of Lycian Nappes (Elitez and Yaltırak, 2014c; Elitez et al., 2015). The alignment of the trace of fault is obviously expressed on DEMs and satellite images (Figure 4.4e, f). It does not extend no further than few hundred meters to northeast or southwest therefore, it cannot be the continuation of the supposed İbecik Fault.

4.4.1 The ancient city of Kibyra

For the existence and current activity of the Kibyra Fault is claimed to be the collapsed seat rows in the stadium of Kibyra. Kibyra, especially the ancient stadium, display abundant architectural relics and collapsed features most probably due to the earthquakes in 23 and 417 Guidoboni et al. (1994). The first geo-archaeological studies in the ruins were undertaken by Akyüz and Altunel (1997, 2001). They suggested up to 50 cm sinistral offset along the seat rows of the Kibyra stadium and claimed that the Kibyra Fault is a N15E striking fault. Alçiçek et al. (2006) argued that there are vertical offsets reaching up to 50 cm. Karabacak (2011) and Karabacak et al. (2013) attributed the structural deformation on the constructions of Kibyra to a left-lateral fault passing through stadium. They used the asymmetric damage on the seat rows as the evidence for the left-lateral offset along the fault. Elitez and Yaltırak (2014b) argued that there is no displacement on the lowermost seat row and the ground below them. Likewise, on the eastern wall of the stadium along the course of the supposed Kibyra Fault no displacement occurred. Based on this information Elitez and Yaltırak (2014b) proposed that the damage was most likely caused by weak artificial foundation fill rather than any fault crossing the ancient city.

The stadium of Kibyra is located on a N-S elongated, west facing concave ridge (Figure 4.5a). The topography shows that the western side of this ridge was most probably excavated before the construction of the stadium (Figure 4.5b). Two types of artificial fill materials were derived from this part of the ridge. One of them is a poorly cemented partly consolidated material. This material was spread in the eastern side of the ridge in order to form a platform for the eastern seat rows and today it is clearly apparent on the eastern slope of the stadium (Figure 4.5c). The other type of material comprise conglomeratic blocks (Figure 4.5d) which are used for the construction of the eastern wall on which the eastern seat rows were placed (Özüdoğru et al., 2011). On the southern side of the stadium, there are 20 seat rows and the lowermost row is half-buried. It is an important counter evidence that the supposed Kibyra Fault crosses the southern seat rows, however, no displacement occurred on this lowermost row (Figure 4.6). In order to verify this observation, a 1.3 m deep trench was excavated in front of the half-buried row by the help of the responsible archaeologists (Figure 4.6; Elitez and Yaltırak, 2014b). The trench revealed that the stadium floor is covered by approximately 1.3 m thick fill material and there is no displacement on the lowermost row nor deeper levels, therefore, no fault exists along the collapsed seat rows contrary to Akyüz and Altunel (1997, 2001), Karabacak (2011) and Karabacak et al. (2013).

4.4.2 Paleoseismologic study

Another trench was excavated by the General Directorate of Mineral Research and Exploration (MTA) for paleoseismic investigation. The trench site is located north of Yusufça (Figure C1 in Appendix C and Figure 4.7) and also close to river pattern change in front of Kara Hill, and deflected stream channels and a ridge in the eastern side of Yusufça which are supposed to indicate the activity of the Kibyra Fault (Karabacak, 2011) (see locations 2 and 3 in supplementary material). The trench was excavated in an ancient stream bed and extended up to slopes of a small hill out of the stream bed (Figure 4.7a, b, c). The ~32-m-long, ~2 m deep trench exposes three different deposits. These include pre-Neogene basement rocks, channel-swamp deposits and soil cover. At the base of the trench, mainly southeast dipping conglomerates and sandstones alternating with clay beds (Figure 4.7d) are exposed. The pebbles were derived from the ophiolitic sequences and limestones of the pre-Neogene basement. These sediments are overlain by (probably) Holocene channel-swamp deposits and followed by ~50 cm thick soil cover. No trace of fault was observed in the trench (Figure 4.7d).

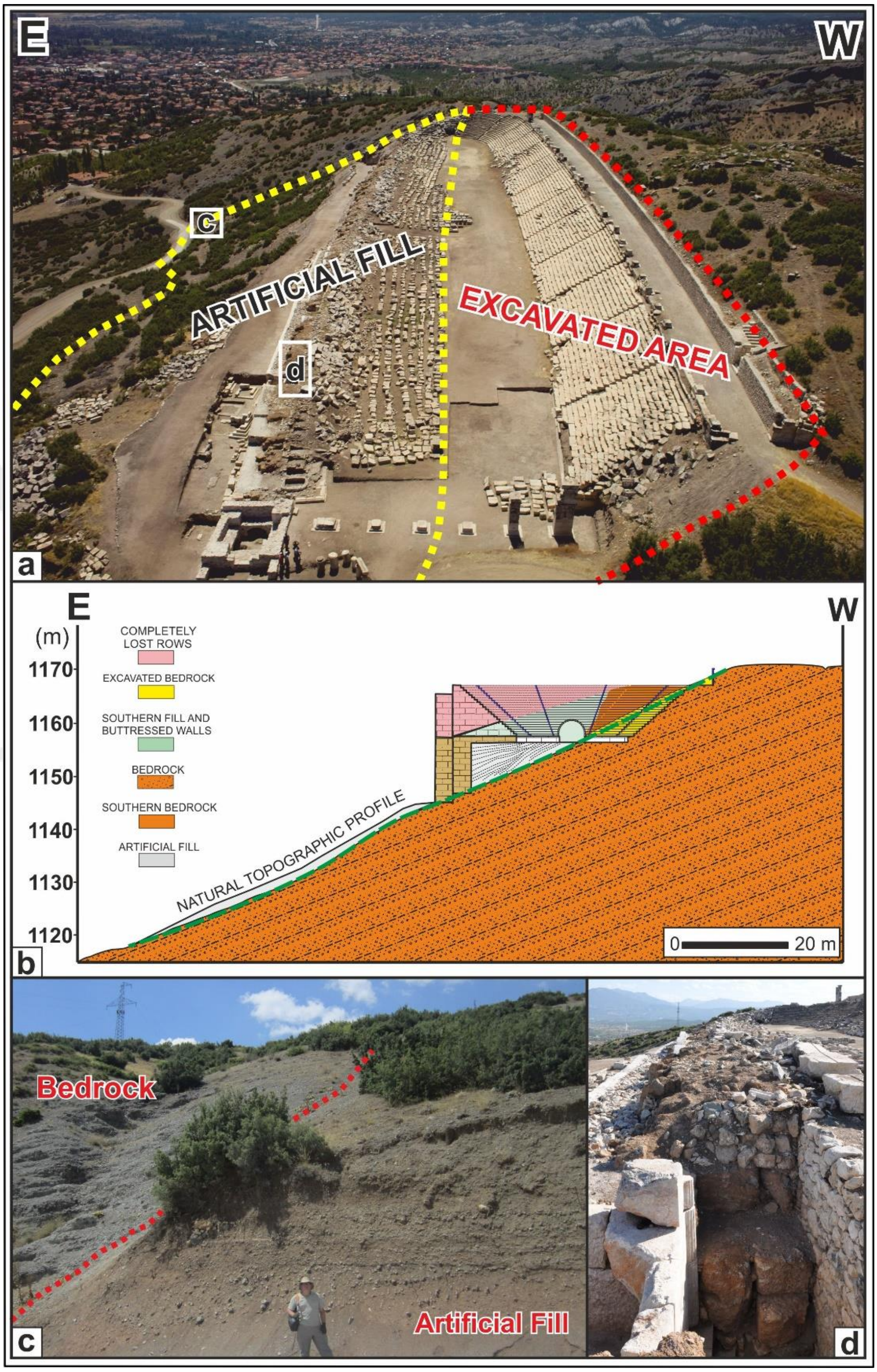

Figure 4.5 : (a) Aerial photo of the ancient stadium of Kibyra. Yellow dashed line indicates the artificial fill area. Red dashed line indicates the excavated area. c and d indicate the locations of Figures 4.5c and 6d. (b) E-W cross-section of the southern part of the ancient stadium. (c) Boundary between bedrock and artificial fill. (d) Conglomerate blocks used during the construction of the eastern seat rows.

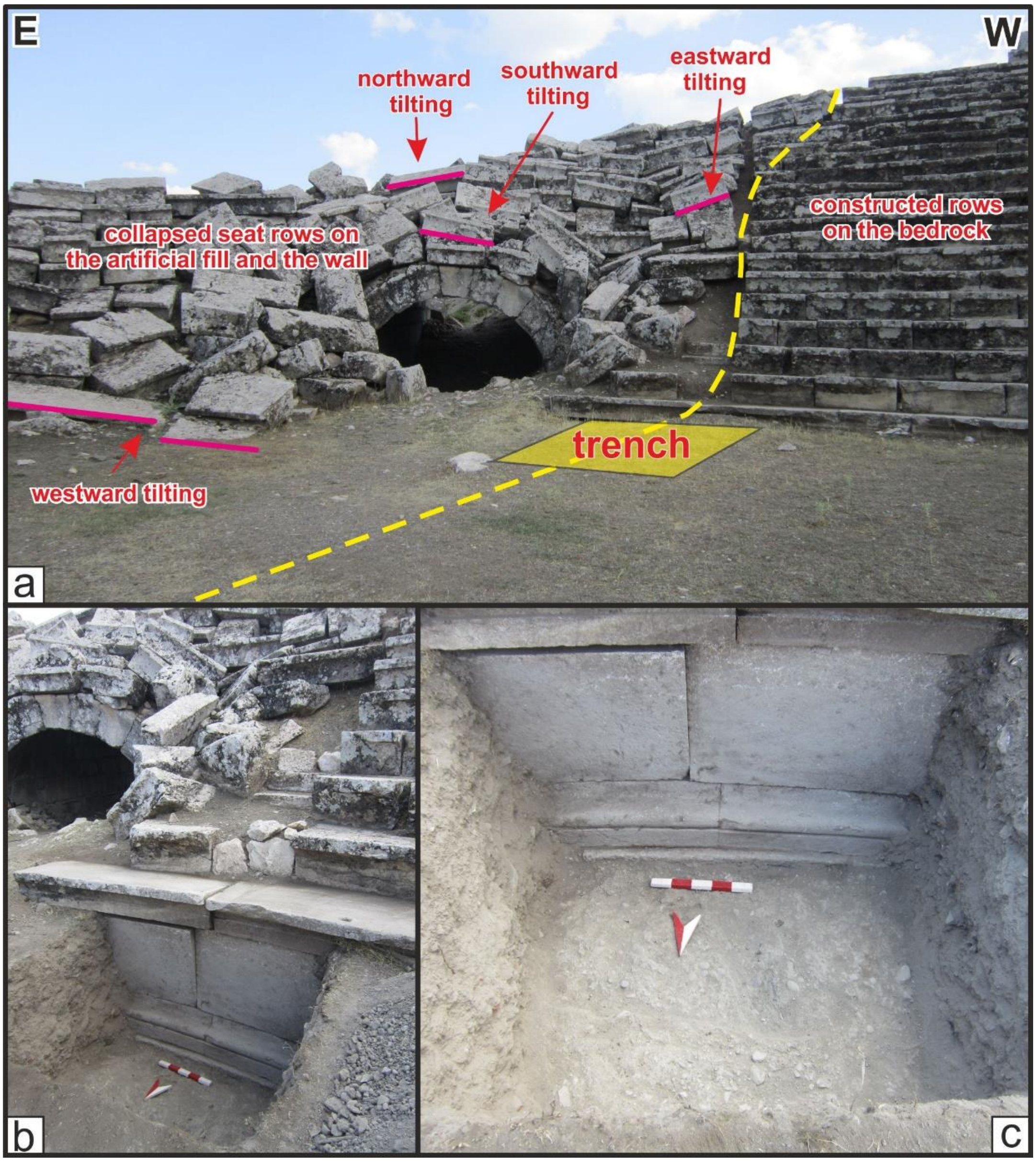

Figure 4.6 : (a) Trench excavated in front of the southern seat rows. Yellow dashed line indicates the supposed Kibyra Fault. (b) and (c) show the lowermost row and bottom of the stadium from different directions. Scale in the trench is 50 cm.

4.5 Discussion

In this study, we evaluated the existence of the Kibyra Fault by integrating remotely sensed data, field observations and paleoseismological trench excavations.

The southwestern Turkey is a tectonically very active region and contains numerous seismically active faults. The alignments of these faults are markedly expressed on the DEMs, satellite and airborne imagery. Most of these faults are exposed in the field which provide ample evidence for determining their characteristics and kinematics.

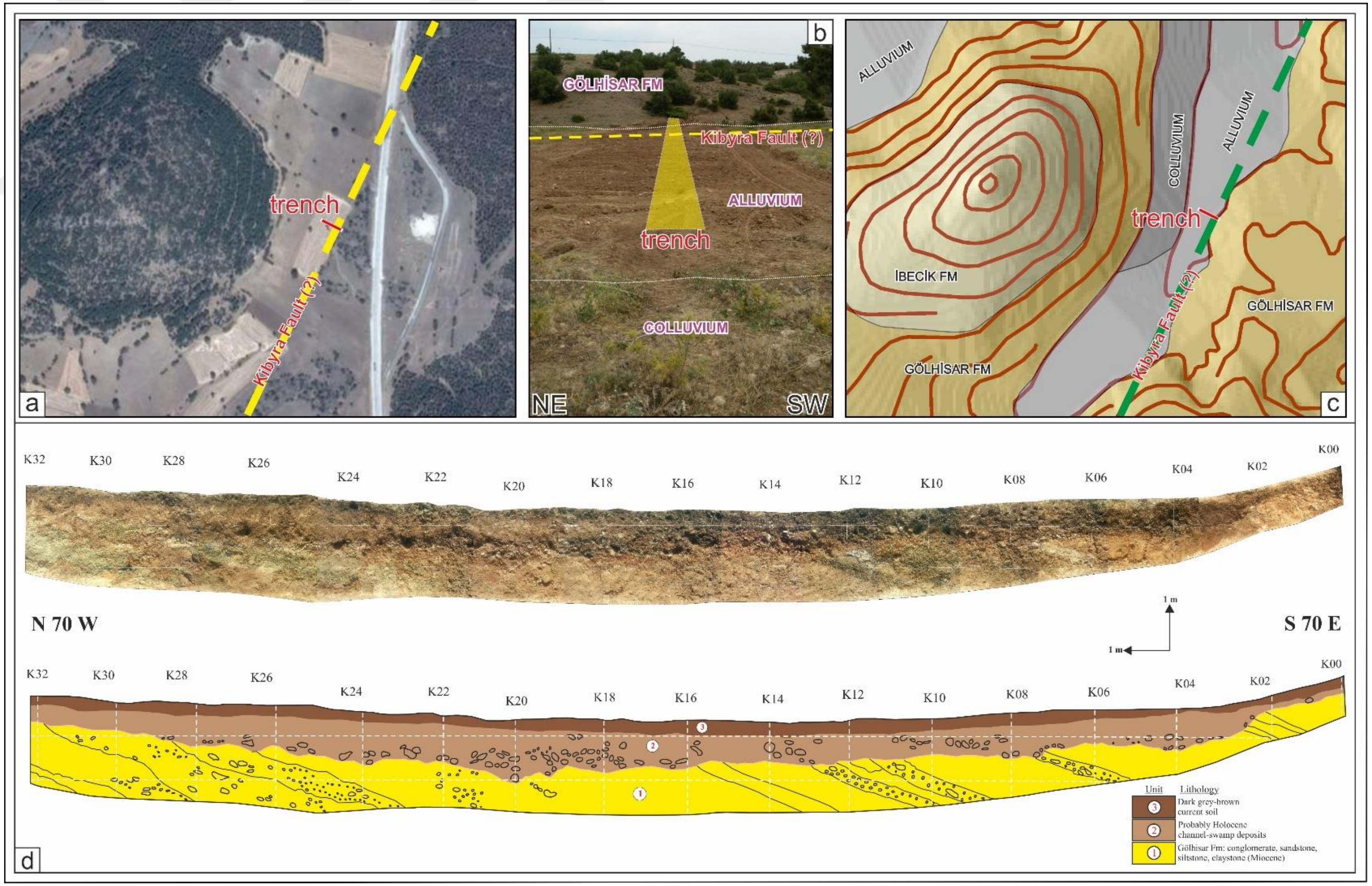

Figure 4.7 : (a) Satellite image of the trench site. Yellow dashed line indicates supposed Kibyra Fault. (b) Trench direction and geological units in the trench site. Yellow dashed line indicates supposed Kibyra Fault. (c) Simplified geological map and digital elevation model of the trench site. Green dashed line indicates supposed Kibyra Fault. (d) Northern wall of the trench (Coordinate: 37°13'11.45"N 29°31'55.35"E).

The most cited paper about the tectonic framework of the SW Turkey includes Barka et al. (1995) which proposed the concept of Fethiye-Burdur Fault Zone (FBFZ) that inspired the proponents of FBFZ such as Akyüz and Altunel (2001) who considered the Kibyra Fault as one of the segments of this fault zone. Later, Alçiçek et al. (2006), Karabacak (2011) and Karabacak et al. (2013) adopted the same concept for the supposed Kibyra Fault. However there is no single evidence for the existence of such a NE-SW-trending left-lateral fault zone which could be a part of a large shear zone, the so called Fethiye-Burdur Fault Zone with normal and strike-slip components (Elitez et al., 2015; Hall et al., 2014a).

It is customary that in order to examine the existence and characteristics of a fault, a number of geological and geomorphological evidences are required. Therefore, the NW-SE topographic profiles were constructed and also the SL indices and lithologies have been superimposed onto the river longitudinal profiles (supplementary material). Based on the SL indices linked to relative rock resistance, several rivers have anomalously high SL index values on relatively soft rocks of İbecik and Gölhisar formations. These high indices are most probably associated with the faults, folding and/or contacts between different rock units. The anomalies along supposed Kibyra Fault are observed in a few locations. However, these high indices cannot be interpreted as tectonic signals. These anomalies are mostly related to the faults in the geological units.

Apart from geological data geomorphological evidences are very crucial for the recent activities of faults. High resolution satellite images and digital elevation models provide invaluable information for detection and delineation of active faults in a region. In addition to these data, paleo- and archeo-seismological data are prime importance for determining the late Quaternary to Recent activities of faults and their earthquake recurrence intervals. In this study we have used all these methodologies in order to verify the existence and recent activity of the Kibyra Fault. However, we could not encounter single convincing evidence along the trace of supposed Kibyra fault from İbecik village in the south to Çamköy in the north (Figure C1 in Appendix C) which is the proposed trace of the fault (Akyuz and Altunel, 1997, 2001; Alçiçek et al., 2005; Alçiçek et al., 2004; Alçiçek et al., 2006; Karabacak, 2011; Karabacak et al., 2013). Based on these data we came to a conclusion that there is no Kibyra Fault at least at the location firstly proposed by Akyüz and Altunel (1997, 2001).

It is important to note here that, apart from their scientific importance, presence of active faults in a region has important socio-economic consequences in terms of site selection of engineering structures and settlements. Nowadays many lineaments, which are characterized as active faults, are asserted in the geological studies and take part in literature. Unfortunately, some of these faults are derived from incorrect interpretation or unsupported data (e.g. ten Veen et al., 2009; also see Elitez et al., 2015). The supposed Kibyra Fault is one of the examples of such faults.

4.6 Conclusions

- The faults which are located in the northeastern and southwestern parts of the study area are parallel to each other but have pure left-lateral and normal fault with left-lateral strike-slip components respectively. Therefore, kinematically it is almost impossible that they cannot be parts of a single continuous fault.
- No cross-cutting and offset relationships that could indicate the presence of supposed Kibyra Fault is observed neither in the trenches located in the stadium of Kibyra and nor along the proposed trace of the fault around Yusufça village.
- The detailed geomorphological observations show that there is no linear feature that might indicate a 35 km-long fault.
- There is no appreciable stream deflections nor ridge offsets along the supposed fault trace to indicate a single trace of a left lateral fault.
- The supposed Kibyra Fault does not exist.

5. A NEW CHRONOSTRATIGRAPHY (^{40}Ar-^{39}Ar AND U-Pb DATING) FOR THE MIDDLE SECTION OF THE BURDUR-FETHİYE SHEAR ZONE, SW TURKEY (EASTERN MEDITERRANEAN)[4]

5.1 Introduction

Southwestern Turkey is a tectonically complex and active region in the Anatolian Microplate. Various hypotheses have been proposed for the tectonic evolution of this region, where structures formed associated with: 1) the westward escape of the Anatolian Microplate (Dewey and Şengör, 1979; Şengör, 1979; Şengör et al., 1985); 2) the NE-SW back-arc extension of the Aegean region (McKenzie, 1978; Le Pichon and Angelier, 1979; Meulenkamp et al., 1988; Yılmaz et al., 2000); 3) the subduction-transform edge propagator fault zone related to the motion of the Hellenic and Cyprus arcs (Govers and Wortel, 2005; Hall et al., 2014a); and 4) the compressional region of the Western Taurides (Aksu et al., 2009, 2014; Hall et al., 2009, 2014a, 2014b). The Burdur-Fethiye Shear Zone is a transtensional left-lateral shear zone 75-90 km wide and 300 km long, located along the southeastern boundary of the large Aegean extensional region and forming the western part of the Isparta Angle (Figure 5.1; Hall et al., 2014a; Elitez et al., 2016b). The middle section of this shear zone consists of an ancient basin fill including the middle Miocene to lower Pliocene sequence, accumulated in fluvial and lacustrine environments and deformed by left-lateral transtensional shearing (Elitez et al., 2016b; Elitez and Yaltırak, 2016). Today this region includes the Acıpayam, Çameli, and Gölhisar basins and their modern basin fill consisting of Pliocene-Quaternary units (Elitez and Yaltırak, 2016). In most previous studies the local fluvial, lacustrine, and alluvial fan deposits were mapped together and assigned a Pliocene age (e.g., Şenel, 1997c, 2002). Such terrestrial sediments were first named the Çameli Formation (Erakman et al., 1982), but were subsequently divided

---

[4] This chapter is based on the paper "Elitez, İ., Yaltırak, C., and Sunal, G. (2018). A new chronostratigraphy (^{40}Ar-^{39}Ar and U-Pb dating) for the middle section of the Burdur-Fethiye Shear Zone, SW Turkey (eastern Mediterranean). Turkish Journal of Earth Sciences, 27 (5), 405-420."

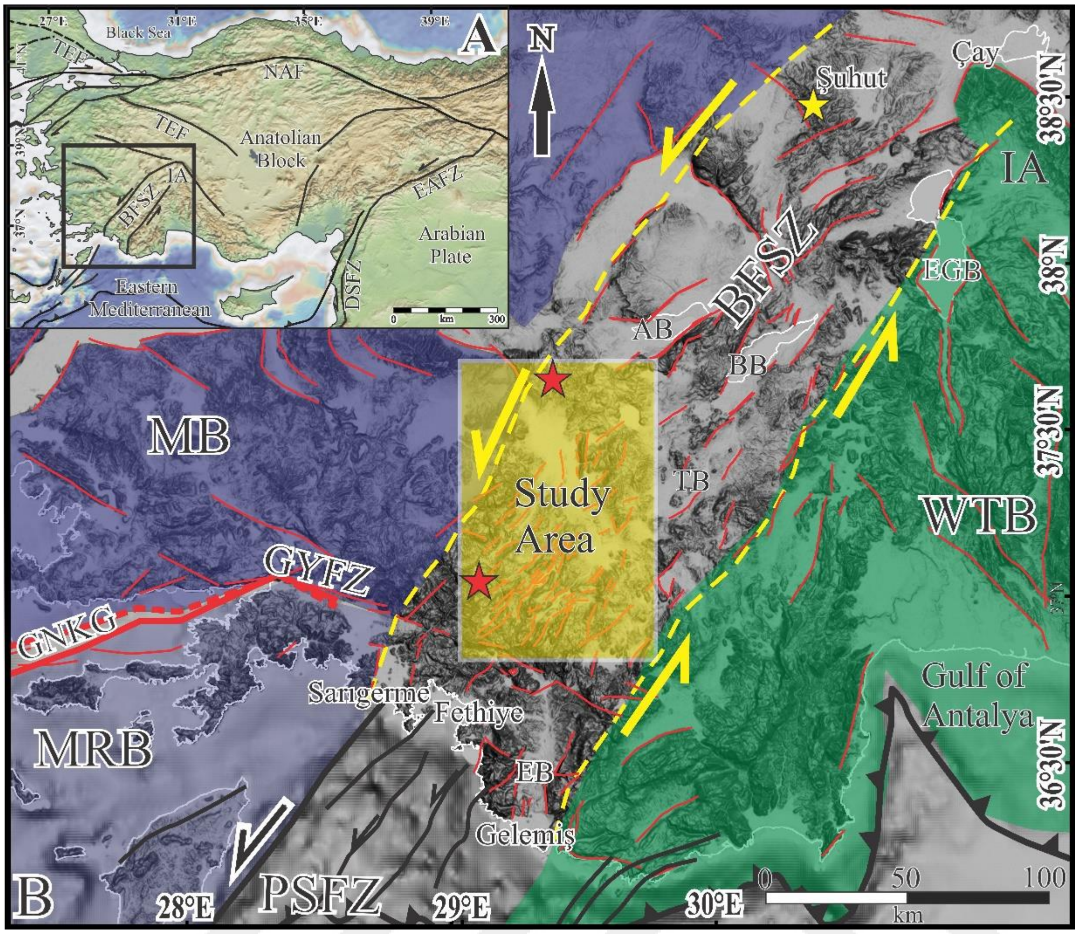

Figure 5.1 : A) Simplified neotectonics map of Turkey compiled from Yaltırak et al. (2012) TEF: Thrace-Eskişehir Fault, NAF: North Anatolian Fault Zone, EAFZ: East Anatolian Fault Zone, DSFZ: Dead Sea Fault Zone, IA: Isparta Angle, BFSZ: Burdur-Fethiye Shear Zone. Rectangle indicates Figure 5.1B. B) Regional fault map of southwestern Anatolia compiled from Tur et al. (2015). Yellow rectangle indicates location of the study area. Dark blue region denotes the NE-SW extensional domain. (MRB: Marmaris-Rhodes Block, MB: Menderes Block, GNKG: Gökova-Nisyros-Karpathos Graben). Green region denotes the NNE-SSW compressional domain (WTB: Western Taurides Block, IA: Isparta Angle). BFSZ: Burdur-Fethiye Shear Zone, PSFZ: Pliny-Strabo Fault Zone, GYFZ: Gökova-Yeşilüzümlü Fault Zone, AB: Acıgöl Basin, BB: Burdur Basin, TB: Tefenni Basin, EGB: Eğirdir Basin, EB: Eşen Basin. Red stars indicate locations of dated samples in this study. Yellow star indicates location of dated samples of Prelević et al. (2015).

into three members: the basal alluvial-fan Derindere Member, the middle fluvial Kumafşarı Member, and the upper lacustrine Değne Member (Alçiçek et al., 2004, 2005, 2006). Later, Elitez and Yaltırak (2014c, 2016) mapped these three sediment successions as the Gölhisar, İbecik, and Dirmil formations. Based on micromammal fauna, the lacustrine sediments of the İbecik Formation were assigned an age of 10.8-8.5 Ma (Saraç, 2003) or ~3.4 Ma (van den Hoek Ostende et al., 2015b), while the upper section of the sedimentary sequence was dated as 1.8-2.2 Ma (e.g., Alçiçek et al., 2005, 2006; van den Hoek Ostende et al., 2015a). Recent studies showed that this significant time gap caused the development of an angular unconformity between lacustrine and alluvial fan sediments (Elitez and Yaltırak, 2016; Elitez et al., 2016a). In the northern part of the study area, there are volcanic rocks that cut and/or overlie the lacustrine sediments. A small number of $^{40}Ar/^{39}Ar$ radiometric dates from these volcanic rocks were obtained by Paton (1992) and reported ages range between Tortonian and early Pliocene. Further, however, these sediments were assigned to the middle Miocene-upper Pliocene based on previously dated volcanic rocks, reliable micromammal fossil records, and stratigraphic relationships (Elitez and Yaltırak, 2014c, 2016).

The above review of the existing literature shows that the chronostratigraphy of the Acıpayam, Çameli, and Gölhisar basins and their environs is controversial. The chronostratigraphy of these basins remains one of the most important problems in the region because of its vital role in the tectonic and kinematic history of southwestern Anatolia, including the Burdur-Fethiye Shear Zone. The data we obtain can redefine all the events along the Burdur-Fethiye Shear Zone. Based on the ages of these sediments, the timing of tectonic events both in western and southwestern Anatolia will be modified and the geological construction of the region will be reinterpreted. In an attempt to resolve the conflicting chronostratigraphic interpretation of the Neogene successions across the Acıpayam, Çameli, and Gölhisar basins and environs, we collected seven volcanics and a tuff sample for radiometric dating. U-Pb zircon and ^{40}Ar-^{39}Ar biotite methods were applied on the samples and the results show that lacustrine sediments are upper Miocene in age rather than Pliocene.

5.2 Description of Local Stratigraphic Units

5.2.1 Basement rocks

The Neogene Acıpayam, Çameli, and Gölhisar basins developed over Paleozoic to early Miocene basement rocks. These basement rocks are composed of Lycian nappes (Brunn et al., 1970; Graciansky, 1972; Önalan, 1979; Ersoy, 1990) and Yeşilbarak nappe (Önalan, 1979) and consist of Paleozoic rocks, Mesozoic volcanic rocks, Mesozoic sedimentary rocks, Mesozoic limestones, Cretaceous ophiolitic mélange, Cretaceous flysch, Paleogene sedimentary rocks, and Eocene-lower Miocene turbiditic sedimentary rocks. The Paleozoic rocks comprising limestones, dolomites, radiolarites, cherts, shales, and sandstones (Şenel, 1997c) are generally exposed in the southwestern part of the study area (Figure F1 in Appendix F). The Mesozoic volcanic rocks, including basalts, spilitic basalts, and rarely radiolarites, cherts, and shales (Şenel, 1997c), crop out on the southwestern side of the study area. The Mesozoic sedimentary rocks consist of sandstones, mudstones, and conglomerates and can be observed in two small areas in the northwestern and southwestern parts of the study area. The Mesozoic limestones, composed of locally recrystallized pelagic and neritic limestones, generally cover topographically high areas (Figure F1 in Appendix F). The Cretaceous ophiolitic mélange mainly comprises harzburgites, serpentinites, dunites, and radiolarites and covers an extensive area (Figure F1 in Appendix F). The Cretaceous flysch is turbiditic in nature and is characterized by sandstones, claystones, cherty limestones, and conglomerates (Şenel, 1997c). These rocks outcrop as small exposures in the study area (Figure F1 in Appendix F). The Paleogene sedimentary rocks include conglomerates, sandstones, siltstones, and shales and are exposed on the western and northwestern parts of the study area. The Eocene-lower Miocene turbiditic sediments consist of sandstones, claystones, siltstones, shales, and mudstones.

5.2.2 Bozdağ Formation

The Neogene basin fills start with alternating conglomerates, sandstones, and mudstones of the Bozdağ Formation (Göktaş et al., 1989). The Bozdağ Formation unconformably overlies the basement rocks and is unconformably overlain by the Gölhisar Formation (Figure F1 in Appendix F). The best exposures of the unit are located in the northern portion of the study area, northeast of Kelekçi and in the valley between the villages of Ören and Mevlütler (Figures F1 and F2 in Appendix F). The Bozdağ Formation consists of medium to thick-bedded, locally massive, dark-gray, gray, light-brown, yellowish, and reddish conglomerates, sandstones, and mudstones. It is approximately 500 m thick. Based on its stratigraphic position and algae fossils such as *Schizotrix* sp. and *Scytonema* sp., Şenel (1997c) dated the formation as upper Oligocene-lower Miocene. The Bozdağ Formation contains sedimentary facies representing a coastal environment under terrestrial influence.

5.2.3 Gölhisar Formation

The Gölhisar Formation contains green, greenish gray-to-gray, reddish brown, brown, and purple conglomerates and sandstones. This unit was identified by Elitez (2010). The best outcrops and cross-sections are observed north of Gölhisar, south of

Acıpayam, and along the new Acıpayam-Çameli main road (Figure F1 in Appendix F). The Gölhisar Formation unconformably or occasionally tectonically rests on the basement rocks and grades vertically and horizontally into the İbecik Formation (Figure F2 in Appendix F). The succession starts with thick beds of granule conglomerates at the bottom and grades upward into conglomerates, conglomeratic sandstones, sandstones, and siltstones. The pebble composition of conglomerates varies depending on the characteristics of the local basement rocks (e.g., serpentinite, radiolarite, and limestone pebbles). However, around Acıpayam and north of Yeşilyuva, the pebbles are composed primarily of reworked material derived from the Bozdağ Formation.

The thickness of the unit is ~900 m. Lack of fossil data does not allow a proper dating. Therefore, the age of the formation is thought to be middle-late Miocene due to its stratigraphic position (Elitez, 2010; Elitez and Yaltırak, 2014c, 2016). The Gölhisar Formation was deposited in a meandering and/or braided river system. The limestone lenses at the bottom of the unit indicate a reefal environment near Acıpayam and northern of Yeşilova.

5.2.4 İbecik Formation

The İbecik Formation (Elitez, 2010) is predominantly composed of white, beige, and yellowish sandstones, siltstones, claystones, marls, tuffs, and limestones. The best cross-sections are observed near the village of İbecik, along the NE-SW road from the Yapraklı dam to a small hill to the northeast (Figure F1 in Appendix F). The İbecik Formation grades laterally and vertically into the Gölhisar Formation at the bottom and is unconformably overlain by the Dirmil Formation. The succession starts with beige sandstones and whitish grey claystones that grade upwards into white and greyish fractured marls and limestones. The uppermost part of the İbecik Formation includes mostly red wine-coloured claystones and hard, locally fractured, thickly bedded, whitish yellow and red wine-coloured silty carbonates including caliche. The thickness of this upper part is ~200 m and it records a period of aridity. There are intercalating vertical transition with tuffs rich in biotite. Especially in the southernmost part of the study area, biotites of 2-3 mm in size are observed. They are commonly found among the marl levels of the İbecik Formation. The İbecik Formation is ~850 m thick. In the northern part of the study area, the sediments of the İbecik Formation are covered or cut by Denizli lamproites (Paton, 1992) at elevations of 1300-1600 m (Figures F1 and F2 in Appendix F).

Based on vertebrate fossils at 1400 m elevation south of the village of Elmalıyurt (36°53′18.34″N, 29°21′33.73″E), the marls and thin coal beds of the İbecik Formation are assigned a Vallesian age (Saraç, 2003). The evolutionary stages of the lacustrine deposits indicate a continuous deposition from late Miocene to early Pliocene (Elitez, 2010; Elitez and Yaltırak, 2014c, 2016). The İbecik Formation contains sedimentary facies reflecting a shallow, warm lake and shoreline environments, including beach and delta.

5.2.5 Dirmil Formation

The Dirmil Formation is made of copper-coloured conglomerates, mudstones, local siltstones, and claystones. This unit was named by Elitez (2010). The unit crop outs mostly north of Altınyayla (or Dirmil) on the footwall of the Kuşdili normal fault and southwest of the Çameli Basin, on the footwall of the Asar normal fault. West of the Dalaman River and south of the Acıpayam Basin, these copper-coloured rocks are clearly exposed on high-elevation plains (Figure F1). The Dirmil Formation unconformably rests on the folded and tilted Gölhisar and İbecik formations. This fault-controlled deposition is observed primarily in front of the basement rocks (Figure F1). The conglomerates of the unit are poorly sorted and consist of angular to subangular pebbles supported by a matrix of mud. The total thickness of the Dirmil Formation is ~250 m. Based on its stratigraphic position and micromammal fossils (e.g., *Mimomys pliocaenicus*, *Apodemus dominans*, and *Micromys praeminutus*; Erten, 2002), a late Pliocene-early Quaternary age is assigned to the formation (Elitez and Yaltırak, 2016). The sediments of the unit indicate an alluvial fan depositional environment.

5.3 Sampling and Methods

Six lamproites and one tuff sample were collected from the study area. Lamproites cut both the İbecik and the Gölhisar formations, but we only observed intercalating lamproite levels in the İbecik Formation (Figures F1 and F2 in Appendix F), indicating the synchronous nature of the volcanism with the İbecik Formation. Samples 4, 5, 6, 8, and 9 cut or cover the İbecik Formation (Figures F1 and F2 in Appendix F; Figures

5.2a and 5.2b). One lamproite sample cutting the Gölhisar Formation was collected (i.e. S7; Figure F1 in Appendix F; Figure 5.2c). A tuff level was collected from the İbecik Formation (i.e. S3; Figure F1 in Appendix F; Figures 5.2d, and 5.2e).

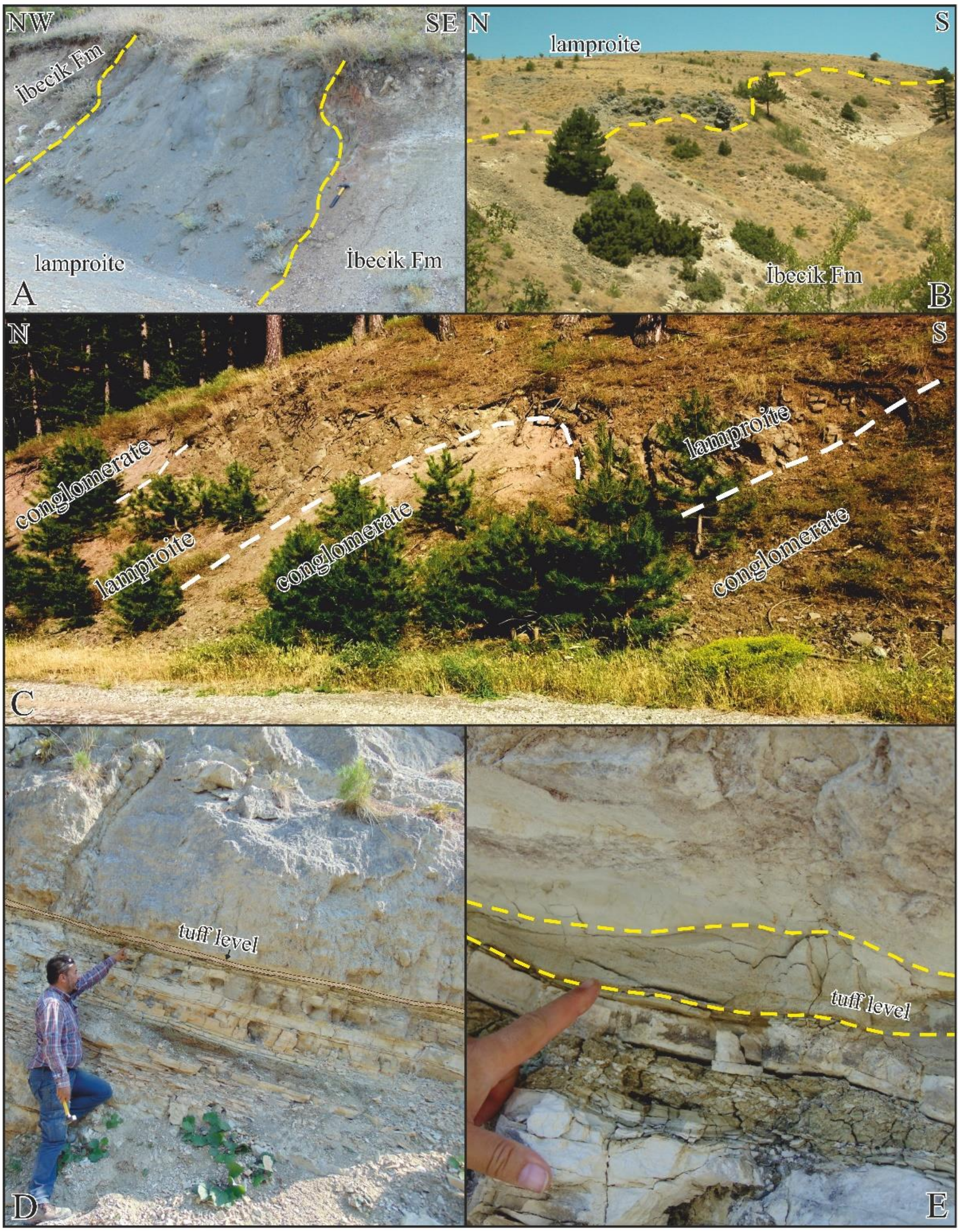

Figure 5.2 : Examples from the outcrops of target volcanic rocks in the study area. A) Lamproite cutting the İbecik Formation (sample 5; 37°39′52.63″N, 29°22′32.92″E). B) Lamproites overlying the İbecik Formation (37°37′5.34″N, 29°21′1.38″E). C) Lamproites cutting the Gölhisar Formation (sample S7; 37°37′21.07″N, 29°28′28.45″E). D, E) Tuff level observed in the Ibecik Formation (sample S3; 37°2′14.60″N, 29°4′48.29″E).

In the region, lamproite samples are generally mildly to highly altered. Therefore, we tried to collect less altered samples. However, each sample has a different degree of alteration. The tuff sample comes from the southern part of the region (Yolçatı village; Figures F1 and F2 in Appendix F). The tuff layer is a pyroclastic fall deposit 2-12 cm thick. It is rich in idiomorphic biotite and feldspar minerals (Figure 5.3). This tuff layer accumulated between two marl layers. Different lithologies with different thicknesses can be observed in the road cut (Figures 5.2d and 5.2e). There are white lacustrine limestones, marls, and claystones. The tuff layer can be traced all along the road cut, indicating very extensive and continues deposition. Both biotite and zircon were extracted from this sample for age determination.

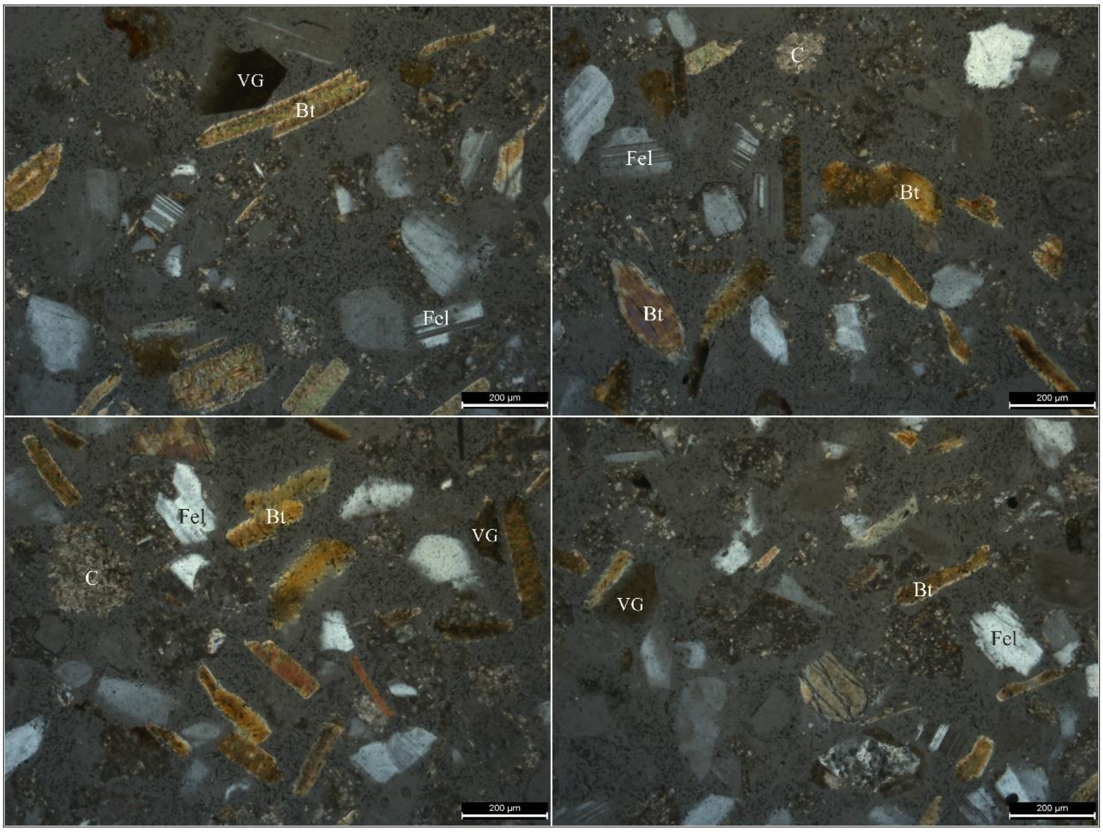

Figure 5.3 : Photomicrograph showing mineral content of sample S3 under polarized optical microscope (Bt: biotite, VG: volcanic glass, Fel: feldspar, C: calcite).

5.3.1 ^{40}Ar-^{39}Ar dating

All samples were initially processed for geochronological analysis at the Mineral Separation Laboratory of the Eurasian Institute of Earth Sciences at İstanbul Technical University. Initially rock samples were crashed to reduce grain size, and then sieved for grain classification. The grain size between 125 and 250 µm was washed and dried at 105 °C. Biotite minerals were separated repeatedly using a Frantz geomagnetic separator between 4 and 6 mA to at least 95% purity.

Samples were wrapped in Al foil and irradiated for 90 MWh at location 8B at the McMaster Nuclear Reactor at McMaster University in Hamilton, Canada, in irradiation package mc52. Standard hornblende MMhb-1 was used as a neutron fluence monitor with an assumed age of 520.4 Ma (Samson and Alexander, 1987). All samples were incrementally heated with a Coherent Innova 5 W continuous argon-ion laser until complete fusion was achieved. Samples were loaded into 3 adjacent wells of 2 mm in diameter and each laser power setting was degassed for 30 s.

Ar isotopes were measured using a VG1200S mass spectrometer with a source operating at 150 µA total emission and equipped with a Daly detector operating in analogue mode. Mass discrimination was monitored daily using ~4×10^{-9} ccSTP of atmospheric Ar. Fusion system blanks were run every five fusion steps and blank levels from argon masses 36 through 40 (~2×10^{-14}, ~3×10^{-14}, ~1×10^{-14}, ~3×10^{-14}, and 2×10^{-12} ccSTP, respectively) were subtracted from sample gas fractions. Corrections were also made for the decay of ^{37}Ar and ^{39}Ar, as well as interfering nucleogenic reactions from K, Ca, and Cl as well as the production of ^{36}Ar from the decay of ^{36}Cl.

5.3.2 Zircon U-Pb LA-ICP-MS dating

The whole-rock sample was crushed in a jaw crusher (crushing to <0.3-0.5 cm) and milled in a disk mill (<0.6-1 mm). After milling, the sample was washed and separated into heavy and light fractions, then dried. The heavy fraction was sieved and the non- to slightly magnetic fraction was separated using a magnetic separator. Heavy liquids (bromoform – 2.9 g/cm^3 and methylene iodide – 3.32 g/cm^3) were used to collect the zircon concentrates. The zircons were picked manually under a binocular microscope. The grains were then mounted in epoxy resin and polished. Cathodoluminescence and back-scattered images were produced at Belgrade University using a scanning SEM JSM-259 6610.

Laser ablation-inductively coupled plasma-mass spectrometry (LA-ICP-MS) analyses were carried out at the Geological Institute of the Bulgarian Academy of Science. Spatial resolution was 35 µm and frequency was 8 Hz. The U-Pb fractionation was corrected using the GEMOC GJ-1 and raw data were processed using GLITTER4.

^{207}Pb/^{206}Pb, ^{208}Pb/^{232}Th, ^{206}Pb/^{238}U, and ^{207}Pb/^{235}U ratios were calculated. Th disequilibrium correction was made for the results of the LA-ICP-MS. Th gets fractionated from U, imparting a disequilibrium in ^{230}Th (an intermediate product in the ^{238}U decay series) that has to be corrected to get an accurate age for younger magmatic rocks (Guillong et al., 2014). U-Pb concordia ages were calculated and plotted using ISOPLOT (Ludwig, 2003).

5.4 Results

Geochronological studies were carried out by two different methods to reveal the chronostratigraphy of the middle section of the Burdur-Fethiye Shear Zone. Dating results are presented in Figures 5.4, 5.5, 5.6 Tables 5.1, 5.2 and G1. Six lava samples and a tuff sample were dated using the ^{40}Ar/^{39}Ar method. An additional tuff sample was also dated by zircon U-Pb method. Eleven ^{40}Ar/^{39}Ar dates were obtained from lamproites (samples S4-S9) located in the northern part of the study area (Figures F1, and F2 in Appendix F; Figures 5.2a-c; Table 5.1). Two duplicated biotites were dated for each sample to get better results. However, the results show a wide scatter ranging from 5.83 to 12.32 Ma (Figure 5.4), with several ages indicating large error margins (Table 5.1), high MSWD values, and/or low percentages of released argon (Figure 5.4). Therefore, these ages were disregarded during evaluation of the chronostratigraphy of the region.

Sample S4 gave two biotite ages, one of which was geologically inconsistent. Furthermore, another age had a large error range (8.23 ± 3.48 Ma; Figure 5.3 and Table 5.1). Sample S5 yielded ages of 5.06 ± 1.44 and 5.69 ± 2.34 Ma, respectively (Figure 5.4 and Table 5.1). These ages are similar considering their error margins. Sample S6 also yielded similar ages from two different biotite separates (6.08 ± 0.48 and 6.43 ± 0.29 Ma; Figure 5.4 and Table 5.1). These ages are one million years older than the ages obtained for S5. Sample S7 gave similar ages but the first age revealed a higher MSWD value and a low fraction of ^{39}Ar released (Figure 5.4 and Table 5.1). Therefore, we accepted 6.94 ± 0.35 Ma as the age of the sample. Similar to sample S7, sample S8 yielded ages around 6.9 Ma (6.98 ± 0.31 and 6.88 ± 0.22). The results of sample S9 show a plateau profile ranging between 7.92 ± 0.55 and 6.87 ± 0.38 Ma. After excluding outliers, we calculated 6.81 ± 0.30 Ma as a weighted average age for the lamproite dykes (Figure 5.4). We dated one sample using both ^{40}Ar/^{39}Ar and U-Pb LA-

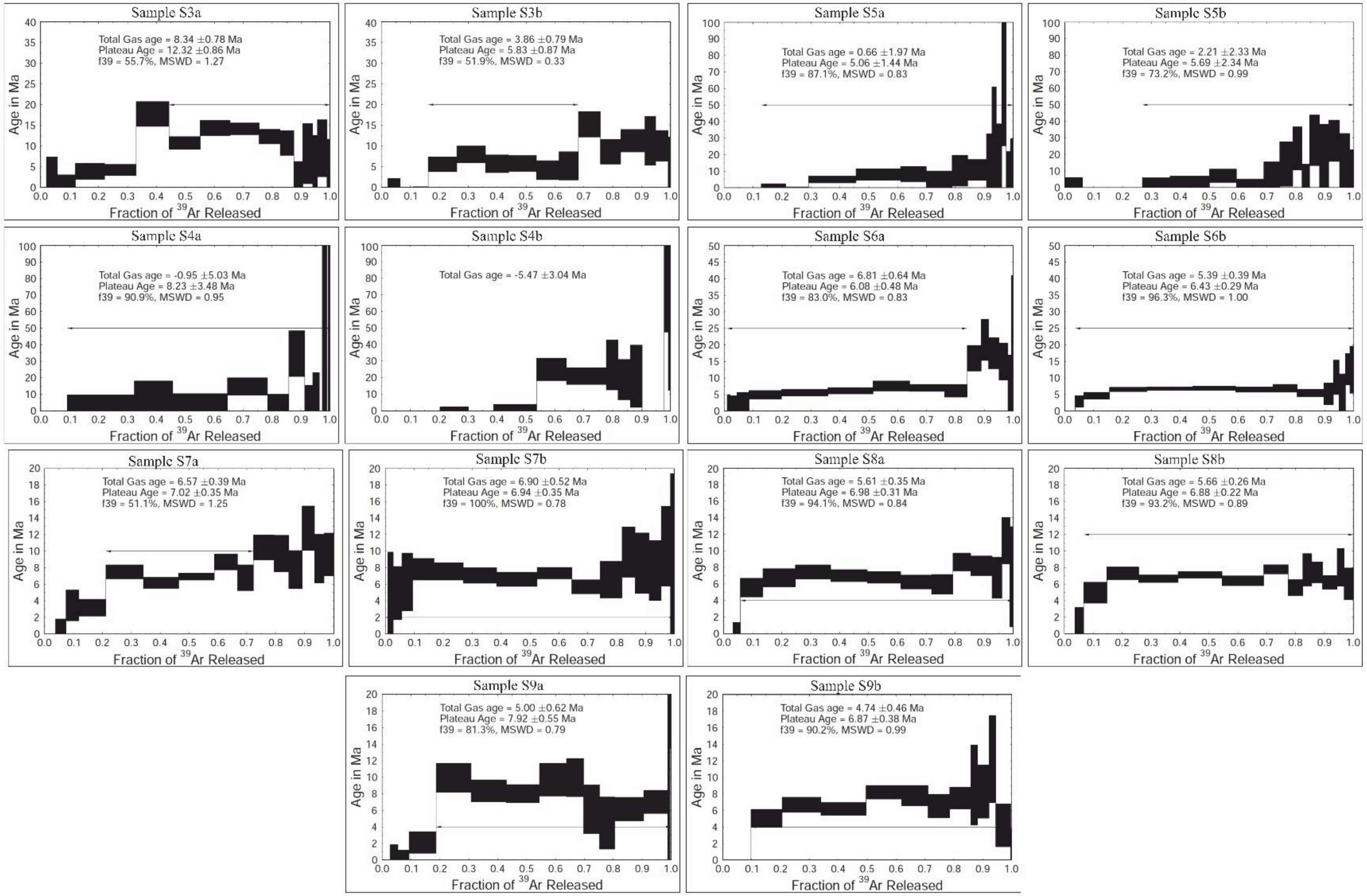

Figure 5.4 : Diagrams of plateau ages obtained from biotites of lamproites samples. Ar isotopes were measured in the Argon Geochronology Laboratory, University of Michigan, Ann Arbor, MI, USA (analyst: Chris Hall).

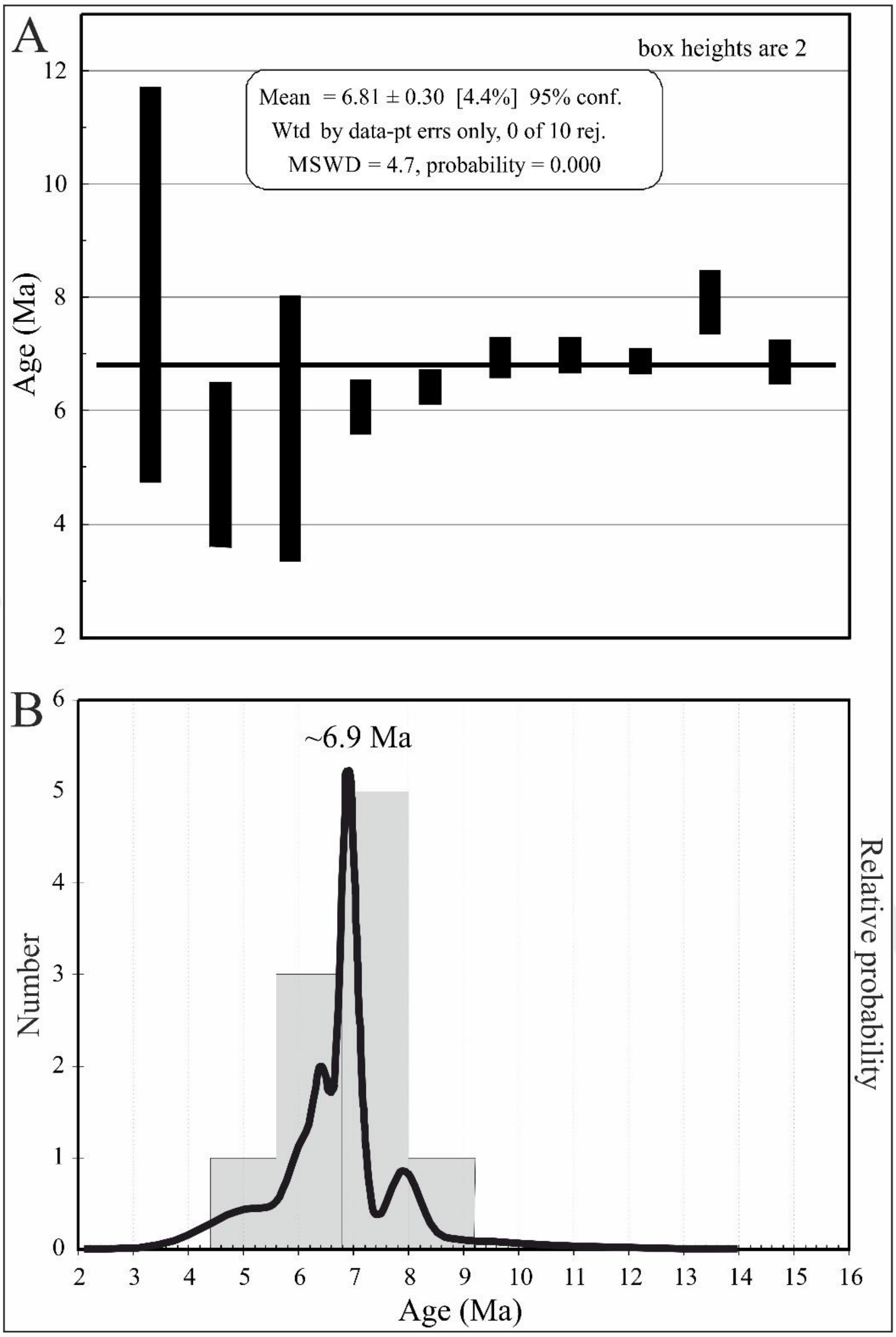

Figure 5.5 : $^{40}Ar/^{39}Ar$ age range plots of the individual samples except tuff sample. A) Mean age calculation of the ages (Ludwig, 2003). B) Relative probability distribution of the ages.

ICP-MS methods from a tuff layer in the İbecik Formation in the southwestern part of the study area (S3; Figures F1 and F2 in Appendix F; Figures 5.2d and 5.2e). This sample location consists entirely of laminated shales, marls, and limestone beds. The dated sample is a thin tuff lamina, consisting of mica, feldspar, quartz, and minor zircon (2-3 mm thick) intercalated with the lacustrine limestone. In the outcrop, the base contact of the tuff level is a sharp boundary (Figures 5.2d and 5.2e). This thin level is an entirely atmospheric fall-out deposit and the rest of the sequence consists of fine-grained lacustrine sediments. $^{40}Ar/^{39}Ar$ ages of sample S3 are very different from one another. The first age data are very poor and excluded. It showed a high MSWD value and low fraction of ^{39}Ar released. Another separate gave 5.83 ± 0.87 Ma. Figure 5.6a shows cathodoluminescence images of the zircon crystals extracted from sample S3. The zircons are perfectly idiomorphic and exhibit slight to well-expressed oscillatory zoning, typical for crystallization in magmatic conditions. The zircon grains in the sample are predominantly medium to short prismatic and some of them reveal a complex internal structure with recrystallized cores and inclusions of apatites. Thirty-one spots were analysed and most of them yielded concordant ages (between 90% and 107%; Table 2). Some of the zircon zones yielded discordant ages, probably due to lead loss. The concordia age obtained from the zircons is 6.93 ± 0.041 Ma (Figure 5.6b) as crystallization age. Both zircon U-Pb and biotite ^{40}Ar-^{39}Ar ages are identical in error ranges and correspond to a Messinian interval.

Table 5.1 : Brief characterization of samples and their ages (*40Ar/39Ar dating; **U-Pb dating).

Sample	Locality	Rock	Mineral	Age, Ma
S3a* S3b*	37°2′14.60″N, 29°4′48.29″E	Tuff	Biotite	12.32 ± 0.86 5.83 ± 0.87
S4a* S4b*	37°40′2.71″N, 29°21′53.05″E	Lamproite	Biotite	8.23 ± 3.48 -
S5a* S5b*	37°39′52.63″N, 29°22′32.92″E	Lamproite	Biotite	5.06 ± 1.44 5.69 ± 2.34
S6a* S6b*	37°36′12.49″N, 29°27′21.85″E	Lamproite	Biotite	6.08 ± 0.48 6.43 ± 0.29
S7a* S7b*	37°37′21.07″N, 29°28′28.45″E	Lamproite	Biotite	7.02 ± 0.35 6.94 ± 0.35
S8a* S8b*	37°35′18.78″N, 29°26′20.69″E	Lamproite	Biotite	6.98 ± 0.31 6.88 ± 0.22
S9a* S9b*	37°37′2.42″N 29°27′18.40″E	Lamproite	Biotite	7.92 ± 0.55 6.87 ± 0.38
S3**	37°2′14.60″N, 29°4′48.29″E	Tuff	Zircon	6.933 ± 0.041

Table 5.2 : Zircon LA-ICP-MS data of sample S3.

					Isotopic ratios							Apparent ages (Ma)				
Spot	Th (ppm)	U (ppm)	Pb (ppm)	Th/U	$^{207}Pb/^{206}Pb$	± 1σ	$^{207}Pb/^{235}U$	± 1σ	$^{206}Pb/^{238}U$	± 1σ	Rho	$^{206}Pb/^{238}U$	± 2σ	$^{207}Pb/^{235}U$	± 2σ	Concordance
1	933.13	1173.52	1.34	0.80	0.04859	0.03344	0.00685	0.00465	0.00102	0.00005	0.51669	6.58	0.64	6.93	9.36	95%
2	1548.03	2579.09	2.99	0.60	0.04607	0.01395	0.00663	0.00198	0.00104	0.00003	0.52244	6.72	0.39	6.71	3.99	100%
3	3174.95	3293.75	3.95	0.96	0.04298	0.01159	0.00629	0.00165	0.00106	0.00004	0.53016	6.83	0.52	6.36	3.33	107%
4	2846.23	2223.47	2.93	1.28	0.04592	0.01248	0.00677	0.00182	0.00107	0.00003	0.52369	6.89	0.39	6.85	3.67	101%
5	2464.87	2183.70	2.81	1.13	0.04608	0.00894	0.00680	0.00130	0.00107	0.00003	0.53256	6.89	0.39	6.88	2.62	100%
6	1909.99	2053.28	2.50	0.93	0.04575	0.01430	0.00676	0.00208	0.00107	0.00003	0.52041	6.90	0.39	6.84	4.19	101%
7	759.53	1219.00	1.38	0.62	0.04587	0.02033	0.00679	0.00298	0.00107	0.00004	0.52002	6.91	0.52	6.87	6.00	101%
8	628.52	1058.23	1.18	0.59	0.04633	0.01482	0.00686	0.00215	0.00107	0.00003	0.51995	6.91	0.39	6.94	4.33	100%
9	2898.74	2211.67	2.91	1.31	0.04571	0.00994	0.00680	0.00146	0.00108	0.00003	0.52948	6.95	0.39	6.88	2.94	101%
10	1995.09	1541.33	2.09	1.29	0.04732	0.02662	0.00704	0.00392	0.00108	0.00004	0.51540	6.95	0.52	7.12	7.89	98%
11*	1196.98	1229.28	1.54	0.97	0.05246	0.01510	0.00782	0.00222	0.00108	0.00003	0.52215	6.96	0.39	7.91	4.47	88%
12	1655.50	1782.37	2.22	0.93	0.04627	0.01018	0.00690	0.00150	0.00108	0.00003	0.52864	6.96	0.39	6.98	3.02	100%
13	1378.51	1709.69	2.03	0.81	0.04550	0.01079	0.00679	0.00158	0.00108	0.00003	0.52616	6.97	0.39	6.87	3.18	101%
14*	2354.34	3038.96	3.70	0.77	0.05849	0.00871	0.00873	0.00128	0.00108	0.00002	0.52804	6.97	0.26	8.82	2.58	79%
15	1863.29	2827.69	3.35	0.66	0.05135	0.01154	0.00767	0.00170	0.00108	0.00003	0.52876	6.98	0.39	7.75	3.42	90%
16	1132.48	2033.75	2.29	0.56	0.04603	0.01480	0.00688	0.00217	0.00108	0.00003	0.51999	6.98	0.39	6.96	4.37	100%
17	3093.72	2312.65	3.13	1.34	0.04629	0.00995	0.00695	0.00147	0.00109	0.00003	0.52962	7.01	0.39	7.03	2.96	100%
18	1809.53	1496.46	2.00	1.21	0.04459	0.00979	0.00670	0.00145	0.00109	0.00003	0.52783	7.02	0.39	6.78	2.92	104%
19	1436.70	1597.15	2.04	0.90	0.04588	0.01632	0.00697	0.00244	0.00110	0.00005	0.52840	7.09	0.64	7.05	4.91	101%
20	1181.09	1086.60	1.43	1.09	0.04487	0.02206	0.00687	0.00333	0.00111	0.00004	0.51729	7.15	0.52	6.95	6.71	103%

*Highly discordant analyses.

Table 5.2 (continued): Zircon LA-ICP-MS data of sample S3.

Spot	Th (ppm)	U (ppm)	Pb (ppm)	Th/U	Isotopic ratios						Rho	Apparent ages (Ma)				Concordance
					$^{207}Pb/^{206}Pb$	± 1σ	$^{207}Pb/^{235}U$	± 1σ	$^{206}Pb/^{238}U$	± 1σ		$^{206}Pb/^{238}U$	± 2σ	$^{207}Pb/^{235}U$	± 2σ	
21*	1317.21	1329.23	1.59	0.99	0.01226	0.01416	0.00183	0.00208	0.00108	0.00004	0.50813	6.96	0.52	1.85	4.21	376%
22*	7374.26	6693.73	9.19	1.10	0.09434	0.00637	0.01392	0.00090	0.00107	0.00002	0.55468	6.89	0.26	14.03	1.80	49%
23*	2477.10	2162.38	2.78	1.15	0.06162	0.00969	0.00909	0.00141	0.00107	0.00002	0.52700	6.89	0.26	9.18	2.84	75%
24*	3895.93	3659.24	4.80	1.06	0.08341	0.01098	0.01231	0.00156	0.00107	0.00003	0.54393	6.89	0.39	12.42	3.13	56%
25*	1083.17	1900.45	2.60	0.57	0.13619	0.01353	0.02016	0.00192	0.00107	0.00003	0.55619	6.92	0.39	20.26	3.82	34%
26*	834.13	954.61	1.24	0.87	0.11212	0.01787	0.01672	0.00259	0.00108	0.00004	0.54866	6.97	0.52	16.83	5.17	41%
27*	2201.48	1651.83	2.57	1.33	0.13287	0.01632	0.01994	0.00235	0.00109	0.00004	0.55896	7.01	0.52	20.04	4.67	35%
28*	1029.26	1121.67	1.67	0.92	0.14675	0.02497	0.02208	0.00359	0.00109	0.00005	0.55246	7.03	0.64	22.17	7.12	32%
29*	1832.31	2009.34	2.66	0.91	0.09232	0.01782	0.01402	0.00262	0.00110	0.00005	0.54854	7.09	0.64	14.13	5.24	50%
30*	1856.05	1951.93	2.82	0.95	0.11241	0.01223	0.01753	0.00183	0.00113	0.00003	0.54906	7.29	0.39	17.64	3.65	41%
31*	1113.52	1340.18	3.74	0.83	0.36478	0.03775	0.07754	0.00697	0.00154	0.00008	0.58120	9.93	1.03	75.83	13.09	13%

*Highly discordant analyses.

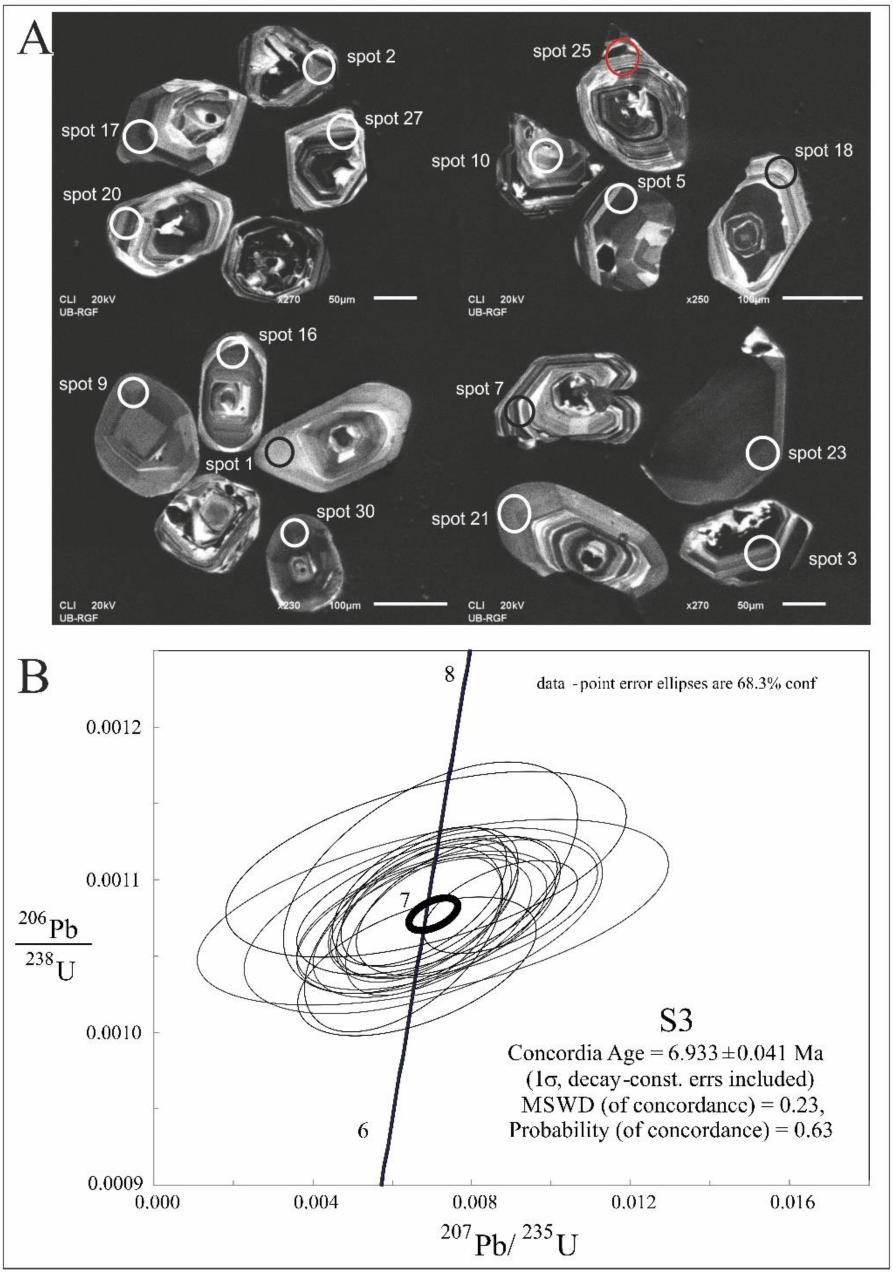

Figure 5.6 : A) Cathodoluminescence images of zircon crystals from sample S3. B) U-Pb LA-ICP-MS data for zircons from the tuff level in the İbecik Formation.

5.5 Discussion and Conclusions

The late Miocene-Pliocene terrestrial sediments occupy wide areas on the geological maps of southwestern Anatolia (see Şenel, 1997c, 2002). The timing of tectonism in this region has been determined based on limited terrestrial fossil ages (e.g., Erten, 2002; Saraç, 2003; Alçiçek et al., 2005; van den Hoek Ostende et al., 2015b). In general, the upper Pliocene carbonate sequences have not been recorded in Neogene geological history in the Mediterranean literature, except for Anatolia (e.g., Popov et al., 2006; Snel et al., 2006; Rossi et al., 2015; Guerra-Merchán, 2014; Cornée et al., 2016; Frigui et al., 2016). On the contrary, pre-Messinian and especially Tortonian carbonate environments are widespread in all Mediterranean regions (e.g., Buchbinder, 1979; Jacobs et al., 1996; Brachet et al., 1998; Krijgsman et al., 2002; Tsaparas and Marcopodouluo-Dicantoni, 2005; Hüsing et al., 2009; Braga, 2016; Brandano et al., 2016; Moisette et al., 2018). The pre-Miocene sequences and the records of the Messinian salinity crisis (Hsü et al., 1973), holding an important place in the Tertiary geology of the Mediterranean, are almost absent in southwestern Anatolia (e.g., Şenel, 1997c, 2002). This situation was first noted in the northern Aegean and Marmara seas (Sakınç et al., 1999; 2000; Sakınç and Yaltırak, 2005; Snel et al., 2006), where Pliocene carbonate sequences do not exist and terrestrial conglomerates and alluvial fan sediments unconformably rest on the Miocene sequences. Based on the presence of Mediterranean fauna and the ages of cross-cutting basalts, Sakınç and Yaltırak (2005) suggested that the lower part of the limestones in the Alçıtepe Formation (northwestern Anatolia) were deposited during the Tortonian. These authors also suggested that the upper parts of the Alçıtepe Formation, including the brackish species, were deposited during the Messinian and that they can be considered as evidence for the inflow from the Paratethys to the Northern Aegean region during the Messinian.

The new radiometric ages provided in this study allowed a more reliable comparison between the northern Aegean region (i.e. northwestern Anatolia) and southwestern Anatolia. The carbonate deposition (i.e. the Alçıtepe Formation) in northwestern Anatolia and the Sea of Marmara has a time-equivalent deposition in southwestern Anatolia (i.e. the İbecik Formation). Likewise, the Dirmil Formation is similar in terms of sedimentary characteristics to the late Pliocene-early Quaternary Conkbayırı Formation (Şentürk and Karaköse, 1987; Yaltırak, 2002) in the Gelibolu Peninsula, the Samanlıdağ Formation in the Armutlu Peninsula (Alpar and Yaltırak, 2002), and the Karacabey Formation in the Manyas Plain (Yaltırak and Alpar, 2002). Accordingly, this sequence is time-equivalent to the Neogene sequence along the middle section of the Burdur-Fethiye Shear Zone. This left-lateral transtensional shear system created various basins. Today, these basins include the remnants of larger carbonate lakes. In previous studies, these lacustrine deposits were assigned to the Pliocene, except for the Acıpayam Basin (e.g., Şenel, 2002; Alçiçek et al., 2004, 2005, 2006, 2008; Kazancı et al., 2012). Paton (1992) dated the basaltic dykes cutting limestones as upper Miocene in the north of Acıpayam Basin. This interpretation led to the separation of the same unit into two different formations (e.g., Şenel, 2002). The different age assignments for the same rocks at two different sides of the same basin created great confusion in the literature and led to misinterpretation of the geological history of the region.

Paton (1992) studied the Denizli lamproites and dated them using the $^{40}Ar/^{39}Ar$ whole-rock method with radiometric ages of 4.59 ± 0.57, 5.66 ± 0.63, 5.89 ± 0.41, 6.52 ± 0.33, 6.28 ± 0.48, and 6 ± 1.54 Ma (i.e. Tortonian-early Pliocene). At the same time, some researchers reported mammal fossils located in the south of the Acıpayam Basin and gave an age interval between 10.8 and 1.8 Ma (e.g., Saraç, 2003; Alçiçek et al., 2005; van den Hoek Ostende et al., 2015b). Elitez et al. (2016a) and Elitez and Yaltırak (2018) claimed that the geographic locations of these samples and positions of the fossils are not reliable. Therefore, stratigraphic relationships remain ambiguous.

Across the northern part of the Acıpayam Basin at elevations of ~1500-1600 m, the volcanic rocks cut and/or overlie lacustrine sediments of the İbecik Formation (Figure F2 in Appendix F). In this study, we dated biotites from seven samples of these volcanics using the ^{40}Ar-^{39}Ar method. However, some of the samples yielded bad results, most probably due to alteration of the samples. Furthermore, we could constrain the age range of the volcanics. The ^{40}Ar-^{39}Ar data yielded ages of 5.06 ± 1.44, 6.08 ± 0.48, 6.43 ± 0.29, 6.98 ± 0.31, 6.88 ± 0.22, and 6.87 ± 0.38 Ma (6.81 ± 0.30 Ma weighted average; Figures 5.4 and 5.5). In addition, we obtained two important age data: 1) biotites from a lamproite dyke cutting the conglomerates of the Gölhisar Formation (Figure 5.2c) yielded the $^{40}Ar/^{39}Ar$ age of 6.94 ± 0.35 Ma, and 2) the zircon age from a tuff level intercalated with the lacustrine deposits of the İbecik Formation (Figures 5.2d and 5.2e) yielded a precise U-Pb age of 6.93 ± 0.041 Ma (Figure 5.5; Tables 5.1 and 5.2). The same sample also gave a 5.83 ± 0.87 Ma biotite ^{40}Ar-^{39}Ar age (Sample S3b; Figure 5.5 and Table 5.1).

The İbecik Formation grades laterally and vertically into the Gölhisar Formation at its base. This uppermost part of the river deposits of the Gölhisar Formation indicates a lower Messinian age (Figure 5.7). The red wine-coloured beds at the top of the İbecik Formation indicate a period of aridity, probably related to the Messinian salinity crisis, and imply intense evaporation during the Messinian (Elitez and Yaltırak, 2016). The $^{40}Ar/^{39}Ar$ and U-Pb ages demonstrated that the Burdur-Fethiye Shear Zone has been active since the middle Miocene. According to the results presented in this paper, it is well established that there was a lamproite upwelling related to the evolution of the Burdur-Fethiye Shear Zone during the Messinian. New $^{40}Ar/^{39}Ar$ and U-Pb dates unequivocally demonstrate that the lacustrine sediments located both along the northern and southern sectors of the study area are upper Miocene-lower Pliocene in age (Table 5.1) and that the widespread exposures of the lacustrine sediments indicate the presence of an extensive late Miocene warm lake. This lake intensively evaporated during the Messinian salinity crisis. After the Messinian, the lake began to break up into smaller lakes associated with the evolution of the Burdur-Fethiye Shear Zone. The Acıpayam, Çameli, and Gölhisar basins were the parts of this large pre-Messinian lake.

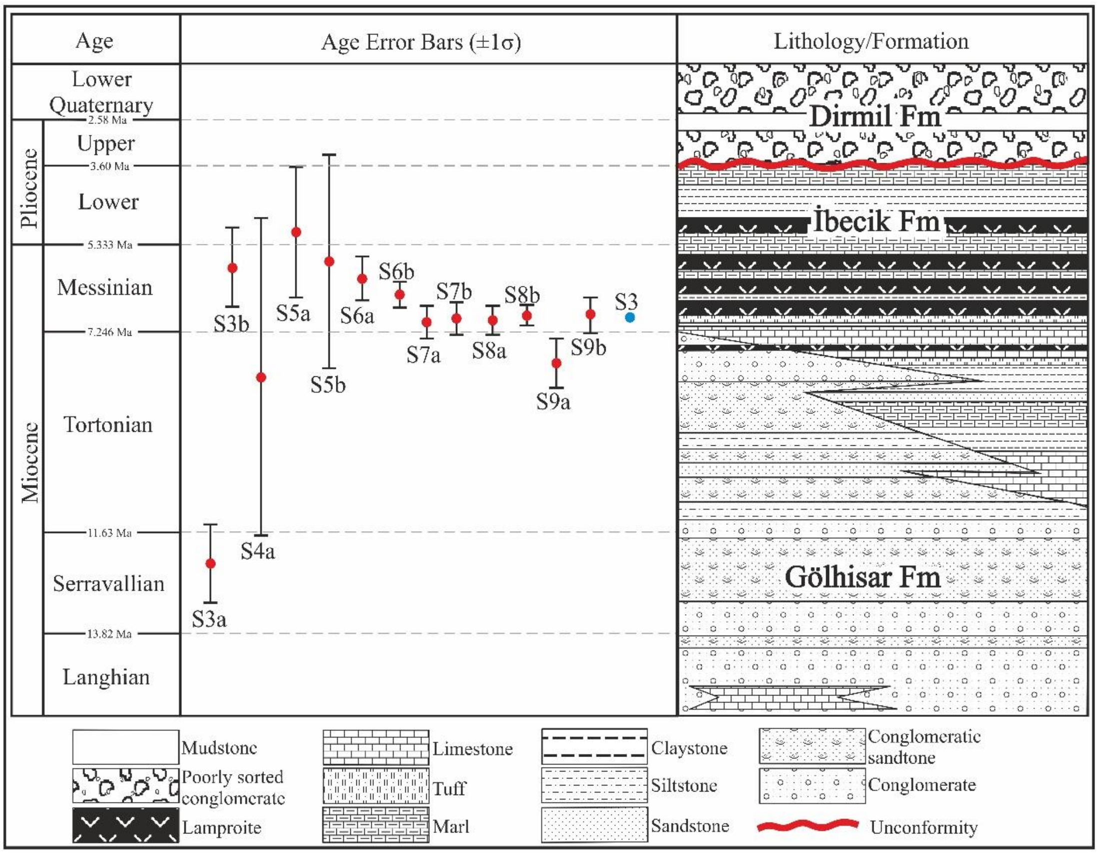

Figure 5.7 : Generalized stratigraphic sequence of the Gölhisar, İbecik, and Dirmil formations, and age distributions of the dated samples in the sequence.

In conclusion, the Pliocene age indicated for the lacustrine sediments in previous studies should be revised in the light of these new radiometric ages. These new ages strongly suggest that the 1.2-km-thick river facies of the Gölhisar Formation located under the lacustrine sediments of the İbecik Formation were deposited during the middle-upper Miocene. The volcanic and volcanosedimentary sequences grade laterally into the river sediments around Şuhut in the northern part of the Burdur-Fethiye Shear Zone (Figure 5.1). The river sediments in that region are equivalent to the sediments of the Gölhisar Formation and the ages of the volcanic and volcanosedimentary sequences are between 15 and 8 Ma (Akal et al., 2013; Prelević et al., 2015). The decreasing radiometric ages of the volcanic rocks from north to south indicate that the Burdur-Fethiye Shear Zone is a deep tear zone between the western Anatolian extensional and the western Taurides compressional regimes since 15 Ma (Elitez et al., 2016b). This study clearly documented that the lamproites in the north and the tuffs in the southernmost part of the Gölhisar-Çameli-Acıpayam basin are of the same age as the limestones in the north. Thus, the northern limestones bearing lamproite intrusions and the southern limestones including tuff layers are the same age (Figure F1 and F2 in Appendix F). These ages indicate that the lacustrine basins on the Burdur-Fethiye Shear Zone and the timing of sedimentation are older.

The new data presented here show that the Burdur-Fethiye Shear Zone initiated during the middle Miocene in an area where there were carbonate lakes of late Tortonian-early Pliocene age. New radiometric ages are in stark contrast with the late Pliocene-early Pleistocene age for these deposits claimed by previous studies and geological maps. Finally, our results allow correlations to be established between the lacustrine sediments in the middle part of the Burdur-Fethiye Shear Zone with sedimentary sequences of the other basins in southwestern Turkey (e.g., lacustrine sediments at ~200 m in the northern part of the Eşen Basin and at ~1200 m around Acıgöl and Burdur basins).

6. THE FETHİYE-BURDUR FAULT ZONE: A COMPONENT OF UPPER PLATE EXTENSION OF THE SUBDUCTION TRANSFORM EDGE PROPAGATOR FAULT LINKING HELLENIC AND CYPRUS ARCS, EASTERN MEDITERRANEAN[5]

6.1 Introduction

The Neogene tectonics of the eastern Mediterranean are dominated by the convergence of the African and Arabian plates with the Eurasian Plate, with the Aegean-Anatolian Microplate caught between (Figure 6.1; Dewey and Şengör, 1979; Dewey et al., 1986; Le Pichon and Kreemer, 2010; McKenzie, 1972). The convergent boundary between the lower African plate and the upper Aegean-Anatolian microplate is characterised by two subduction-related arcs — the Hellenic Arc in the west and the Cyprus Arc in the east, offset from each other by 400 km.

Subduction of the African Plate has, more or less, ceased across the Cyprus Arc (Papazachos and Papaioannou, 1999), with continuing con-vergence of the African and Aegean-Anatolian accommodated across several ‘principal deformation zones’ such as the Misis-Kyrenia Fault Zone, the Amanos-Larnaka Fault Zone and the Latakia-Tartus Ridge, and equivalents to the west (e.g., Aksu et al., 2005; Hall et al., 2005). Subduction continues below the Hellenic Arc (Shaw and Jackson, 2010), where the subducting plate is rolling back, causing extension in the back-arc region of the Aegean Sea and western Anatolia since the late Eocene (Gautier et al., 1999). The differential motion of the Hellenic and Cyprus arcs is related to a tear in the subducting slab, causing a Subduction Transform Edge Propagator (‘STEP’) fault zone (Govers and Wortel, 2005) along the transfer zone that connects the two arcs. This large-scale plate situation can be discerned from mantle tomography.

[5] This chapter is based on the paper “Hall, J., Aksu, A. E., Elitez, İ., Yaltırak, C., and Çifçi, G. (2014). The Fethiye-Burdur Fault Zone: A component of upper plate extension of the subduction transform edge propagator fault linking Hellenic and Cyprus Arcs, Eastern Mediterranean. Tectonophysics, 635, 80-99”.

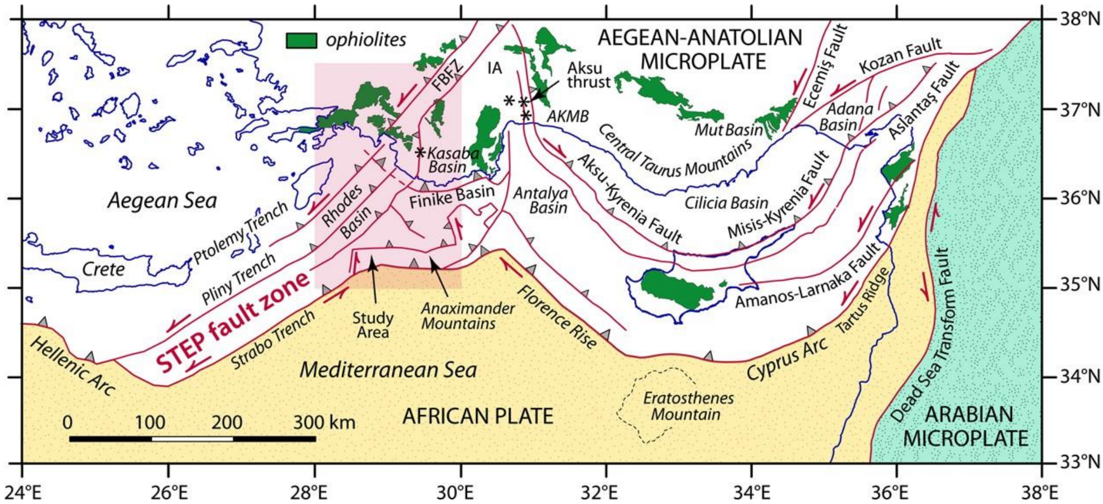

Figure 6.1 : Simplified tectonic map of the eastern Mediterranean Sea and surrounding regions, showing major plate/microplate boundaries, ophiolitic rocks and major tectonic elements. AKMB = Aksu, Köprüçay, Manavgat Basins, FBFZ = Fethiye-Burdur Fault Zone, IA = Isparta Angle, STEP = Subduction Transform Edge Propagator (Govers and Wortel, 2005), * = Neogene-Quaternary volcanics. Half arrows indicate transform/strike-slip faults. Light red inset = Rhodes Basin and environs illustrated in Figure 6.2.

From the length of the subducting slab and nappe stacking in exposed geology, Faccenna et al. (2003) and van Hinsbergen et al. (2005) estimated that over 2000 km of subduction has occurred below the Aegean since the Jurassic. Piromallo and Morelli (2003) showed that descending (African and Arabian) plate slabs below the eastern Mediterranean area continue into the lower mantle, the models from which Faccenna et al. (2006) used to show that the deep slab descending from the Bitlis suture of the Arabian-Eurasian plate collision is detached (confirming the conclusions of Hafkenscheid et al., 2006), whereas that below the Hellenic Arc is still attached to the surface plate. In the area lying between these (i.e., below the Cyprus Arc), van Hinsbergen et al. (2010c) show that the subducting slab is detached from the African plate below western Anatolia, and Biryol et al. (2011) show that, while the slab at great depth is still continuous, at shallow depth, there is a gap, or tear, at the Hellenic/Cyprus Arc junction, confirming earlier findings of de Boorder et al. (1998) and Govers and Wortel (2005), with possible tears elsewhere farther east along the Cyprus Arc also. The continuity of the slab at great mantle depth suggests that continuous unbroken subduction was succeeded by successive slab detachments, and consequent tears, as continental collision proceeded from east to west: the Arabian Plate has collided with the Eurasian Plate and its deep slab is now detached; the African Plate is starting to collide with the Aegean-Anatolian Microplate below the Cyprus Arc, with some detachment initiated; whereas at the Hellenic Arc, subduction continues and no detachment has occurred. Thus, deep tomographic evidence of slab tear at the boundary of Hellenic and Cyprus Arcs is clear, and appears to be rather simple, although not necessarily well resolved.

How the deep slab tear links to surface deformation is a significant question of lithosphere tectonics. Consideration of the development of metamorphic core complexes in the Aegean region (Jolivet et al., 2013; Le Pourhiet et al., 2012) and the ages of volcanism related to asthenospheric flow into slab gaps or tears (Pe-Piper and Piper, 2007) indicate that the slab tear between the Aegean and Cyprus arcs may be as old as 15-20 my, though evidence of accelerated roll-back of the Aegean subduction since 15 my has been interpreted to be related to initiation of the tear at around 15 my, or later (van Hinsbergen et al., 2010c). The most obvious surface structures associated with the STEP fault are the Ptolemy, Pliny and Strabo Trenches, which define a fault zone at least 50 km wide (Özbakır et al., 2013), with sinistral strike-slip faulting along NE-SW lineaments interpreted from marine geophysical studies (Le Pichon and Angelier, 1979), and inferred from adjacent land studies (Zachariasse et al., 2008) and first motions of recent earthquakes (Shaw and Jackson, 2010). Contraction across the STEP fault zone appears to be accommodated on separate thrusts (Özbakır et al., 2013; Shaw and Jackson, 2010). The age of inception of such faulting is not clear from published marine surveys of the trenches, but sinistral transtension initiated at 4-5 Ma is observed in Rhodes (ten Veen and Kleinspehn, 2002) and inferred by Zachariasse et al. (2008). Tracing the STEP fault zone to the northeast is difficult: the Pliny and Strabo Trenches strike into the Rhodes Basin, across which the dominant structural trend swings northwards from NE-SW to NNE-SSW (Hall et al., 2009). In addition, there are a number of major bathymetric features of ENE-WSW trend (like those interpreted on Rhodes by ten Veen and Kleinspehn, 2002; and in the marine area by ten Veen et al., 2004) that occur in the area of the Anaximander Mountains (Aksu et al., 2009) and converge toward the NNE-SSW structures at the southwestern margins of the Rhodes Basin, where the basin merges with the northeastern end of the Pliny-Strabo Trenches. Following the NNE-SSW structures of the Rhodes Basin (Hall et al., 2009) to the northnortheast, leads to the possibility that the STEP fault might link with the Fethiye-Burdur Fault Zone (e.g., Barka and Reilinger, 1997; Dumont et al., 1979), and/or to the Eşen Çay basin (Alçiçek, 2007; ten Veen, 2004; ten Veen et al., 2009) to the east. Ocakoğlu (2012) surveyed part of the marine area offshore Fethiye Bay and provided first insights into the possible fault linkages from the Pliny and Strabo Trenches with the Fethiye-Burdur Fault Zone.

A STEP fault zone is defined by a tear in the subducting slab, thus it exists, by definition, in the lower plate at a convergent margin, but the associated deformation must propagate into the overlying plate. In this case, the Pliny and Strabo Trenches at the surface already lie in the overlying plate, since the plate boundary (sensu stricto) must lie beneath the Mediterranean Ridge accretionary wedge to the south. The STEP fault represents a transfer fault (maybe not strictly a transform fault) which allows the rollback and back-arc extension of the Aegean to be detached from the deformation of the Cyprus arc. Thus, the relative displacement should gradually decrease along the strike of the STEP fault into the upper plate. Assuming that the Cyprus and Hellenic arcs were once collinear, about 400 km of offset of the arcs has occurred, an offset compatible with the reconstructions of van Hinsbergen and Schmid (2012). van Hinsbergen et al. (2010a) and van Hinsbergen (2010) argue that around 60 km of NE-SW extension occurred around the Menderes massif during its exposure as a core complex, but no such extension is found farther east (e.g., in the Beydağları autochthon), so that a sinistral strike-slip offset of around 60 km along a NE-SW lineament (or some equivalent structure) would be required to balance the geometry. It is unclear where that displacement occurs, but part of it might lie along the Fethiye-Burdur Fault Zone. Barka and Reilinger (1997) estimate that current sinistral motion required by GPS measurements across the Fethiye-Burdur Fault Zone is around 1.5-2cm yr^{-1}. Further to this, proceeding northeastwards, the depth to the STEP fault in the lower plate increases, thus increasing the possibilities for a variety of structures in the upper plate to distribute the strain associated with what already appears to be a wide zone of deformation in the area of the Pliny and Strabo Trenches.

Thus, a key question that we address in this contribution is the manner in which the STEP fault propagates into the upper plate. Specifically, we assess the nature of the connection from the Pliny and Strabo Trenches through the Rhodes Basin to the Fethiye-Burdur Fault Zone, with particular attention to the offshore extrapolation of the latter, and extending the interpretation of Ocakoğlu (2012). Our assessment is based on previously unpublished marine multi-channel seismic reflection data acquired offshore Fethiye and adjacent areas of the Rhodes and Finike Basins, and the Anaximander Mountains. We also review possible propagation of the STEP fault zone more widely across the Rhodes Basin and Anaximander Mountains. In comparing interpretation of our offshore data with results from geological mapping onland, we also address related issues of the evidence of continued contractional tectonics offshore into Pliocene-Quaternary time, and the rapid subsidence of the Rhodes and Finike Basins in this same time period.

6.2 Background

Özbakır et al. (2013) show that the NE-SW-trending Pliny and Strabo Trenches lie in a zone of oblique sinistral convergence, but with strain partitioned into strike-slip faults and fold/thrusts (Figure 6.1). Based on mapping and earthquake first motions, they conclude that faults running along the Pliny and Strabo Trenches are either Riedel (R) or P shears, i.e., sinistral strike-slip faults. Compression appears to be accommodated by thrusting and folding separate from the strike-slip faulting. Thrusting is more widely distributed: it is observed in the Rhodes Basin (Hall et al., 2009) and off the coast of Rhodes (Woodside et al., 2000), with some consistent earthquake first motions (Hall et al., 2009, their Figure 22). Shaw and Jackson (2010) concur with these assessments, indicating strike-slip along the bathymetric strike of the Pliny and Strabo Trenches, and oblique (more east-westerly) folds and thrusts. To the south, shortening is observed in the Mediterranean Ridge, interpreted as the accretionary wedge in front of the subduction zone (Mascle et al., 1986).

The Rhodes Basin lies in deep water (up to 4 km; Figure 6.2), has a relatively thick fill (over 1 km) of Pliocene-Quaternary sediments, but no Messinian evaporites (Hall et al., 2009; Woodside et al., 2000). Rapid subsidence in Pliocene-Quaternary is confirmed by the presence of stacked prograded delta packages at depth along the Turkish continental slope. Structures are dominated by SE-verging thrusts of Miocene and younger ages. Abundant normal faults also affect the Pliocene-Quaternary succession, but have very small displacements and do not appear to be basement controlled, because they do not cut the M-reflector at the base of the sequence. At the northern and northwestern margins of the basin, some of the SE-verging thrusts are coupled with oppositely verging thrusts to form positive flower structures; and a multitude of small steep faults is also present. Hall et al. (2009) interpreted these structures as indicative of Pliocene-Quaternary strike-slip, along a zone collinear with the onland Fethiye-Burdur Fault Zone. Toward the southeast margins of the Rhodes Basin, the thrusts have a more east-west trend and appear to link to a broadening zone of contraction involving the Anaximander Mountains. Hall et al. (2009) suggested that the Hellenic and Cyprus Arcs may have been col-linear in Late Miocene, prior to roll back of the Hellenic subduction slab, though reconstructions of van Hinsbergen and Schmid (2012) suggest that the rollback history extends much farther back in time to the late Eocene. Thereafter, in the Pliocene-Quaternary, the deformation, while still continuing contraction, shows significant evidence of strike-slip motions, compatible with the sinistral boundary conditions required of the STEP fault zone. The strike-slip deformation appears to be concentrated to the northwestern margins of the Rhodes Basin, indicating connections to the Pliny and Strabo Trenches to the southwest and to the Fethiye-Burdur Fault Zone to the northeast.

The Fethiye-Burdur Fault Zone is characterised by a 40-50 km wide zone running NE-SW across southern Turkey (Figures 6.1 and 6.2). It cuts through the eastern area of the Lycian nappes close to their boundary with the Beydağları para-autochthon to the east (Şenel, 1997a,1997b; Şenel and Bölükbaşı, 1997). In terms of present tectonism, in a regional sense, the fault zone lies along the boundary between the Aegean extensional domain and more stable central Anatolia (Barka and Reilinger, 1997; Dumont et al., 1979). The fault zone includes many short-segment near-vertical NE-SW-trending faults, many of which have demonstrable normal offsets, with some showing evidence of strike-slip, for example, dextral in the Holocene in the Çameli Basin (Alçiçek et al., 2006). Earthquake first motions in the area show mixed deformation (Hall et al., 2009, Figure 22): normal faults more commonly on the Aegean side of the zone, thrusting more commonly on the eastern side of the zone, and a variety of strike-slip motions, predominantly, but not universally, sinistral along NE-SW faults. Longer term strain is implicit in the 50 cm sinistral offset of the hippodrome in Cibyra along the fault zone (Akyüz and Altunel, 2001), though the existence of the latter offset is disputed according to co-authors, Elitez and Yaltırak, 2014a. What is missing from the Fethiye-Burdur Fault Zone is strong evidence for a large strike-slip offset: there does not appear to be a major single fault at the surface cutting right along the fault zone, but just a series of smaller faults, many of which appear to be dominantly normal faults, but which might together accumulate some net strike-slip.

It is doubtful, therefore, that the Fethiye-Burdur Fault Zone as presently exposed on land could accommodate the 60 km of sinistral displacement required by van Hinsbergen et al. (2010a) and van Hinsbergen (2010).

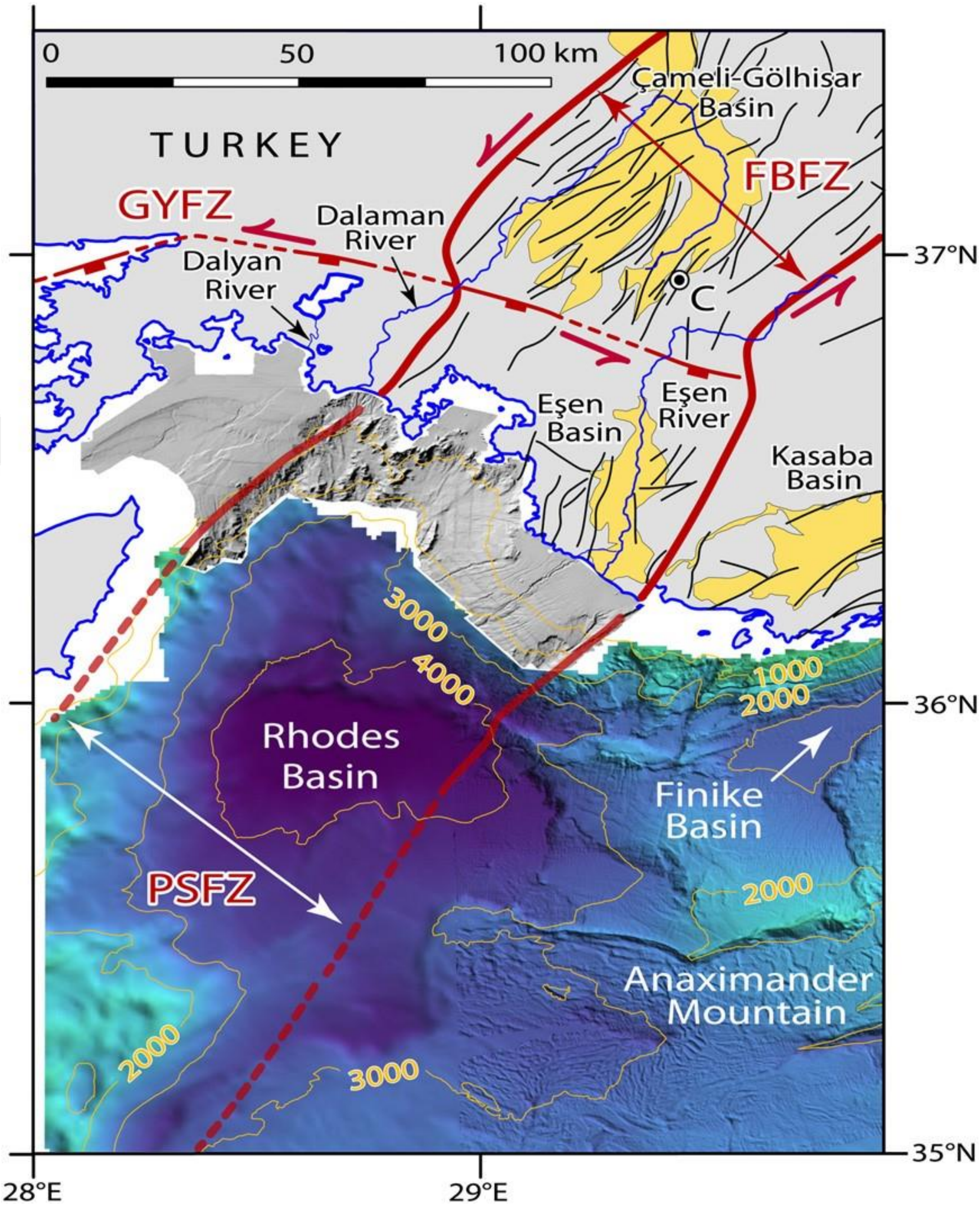

Figure 6.2 : Multibeam maps showing the detailed bathymetry of the Rhodes Basin and environs compiled using the 1 km grid in the west (MediMap Group, 2005), the 0.1 km grid in the east (i.e., the ANAXIPROBE 95 data, Woodside et al., 1997), and the grey base surface in the north (Ocakoğlu, 2012). The coastline and selected isobaths contours are from the Intergovernmental Oceanographic Commission (IOC) (1981). Also shown is the onland Fethiye-Burdur Fault zone, the ancient town of Cibyra (C) and the Neogene Kasaba, Eşen and Çameli-Gölhisar basins. FBFZ = Burdur Fethiye Fault Zone, GYFZ = Gökova-Yeşilüzümlü Fault Zone, PSFZ = Pliny-Strabo Fault Zone.

Whether the Fethiye-Burdur Fault Zone is collinear with the NE-extrapolation of the Pliny-Strabo Trench structures or mildly offset from them are alternatives postulated by Ocakoğlu (2012) who attempted to map the linkage from swath bathymetry and shallow re-flection seismic profiles in the region of Fethiye and Marmaris bays. Ocakoğlu (2012) observed several different NE-SW-trending fault sets in this region, including transtensional and normal faults below Marmaris Bay, and transpressional faults below Fethiye Bay. The latter faults are better aligned with the NE-extrapolation of the Pliny and Strabo Trench structures and are more consistent with them in terms of strain. The Marmaris Bay structures might appear to be transitional to the Aegean extensional province, as indicated by first motions of earth-quakes (Shaw and Jackson, 2010).

6.3 Data Acquisition and Processing

The principal data used in this paper consist of (a) ~720 km of multi-channel seismic reflection profiles collected in 2001 using the Memorial University of Newfoundland (MUN) systems on RV Koca Piri Reis of the Institute of Marine Sciences and Technology (IMST), Dokuz Eylül University, (b) ~1200 km of multichannel seismic reflection profiles using the MUN source and the IMST streamer on RV Koca Piri Reis in 2007, 2008 and 2010, and (c) the chronostratigraphic data from two on-shore exploration wells in the Kasaba Basin (Figure 6.3). The source for the MUN multichannel data consisted of a Halliburton sleeve gun array, employing gun sizes of 40, 20 and 10 in.^{3} (656, 328 and 164 cm^3), with the total volume varying during maintenance cycling of the guns, but typically 200 in.^{3} (3277 cm^3). Shots were fired every 25 m, and reflections were detected by the full 48 channels (group intervals = 12.5 m) in 2001, 96-channel (group interval = 6.25 m) in 2008 and 216 channels (group interval = 6.25 m) in 2010. The resultant 12-fold (2001 and 2008) and 27-fold (2010) data were recorded digitally for 3-5 s (with delay dependent on water depth) at 1 millisecond sample rate, using a DFS V instrument in 2001 and an NTRS2 seismograph in 2008 and 2010. The multichannel data were processed at Memorial University of Newfoundland, with automatic gain control, short-gap deconvolution, velocity analysis, normal move-out correction, stack, filter (typically 50-200 Hz bandpass), Kirchhoff time migration, and adjacent trace sum. Despite the relatively low source volume, reflections are imaged to at least 3-4 second two-way time (twt) below the seabed.

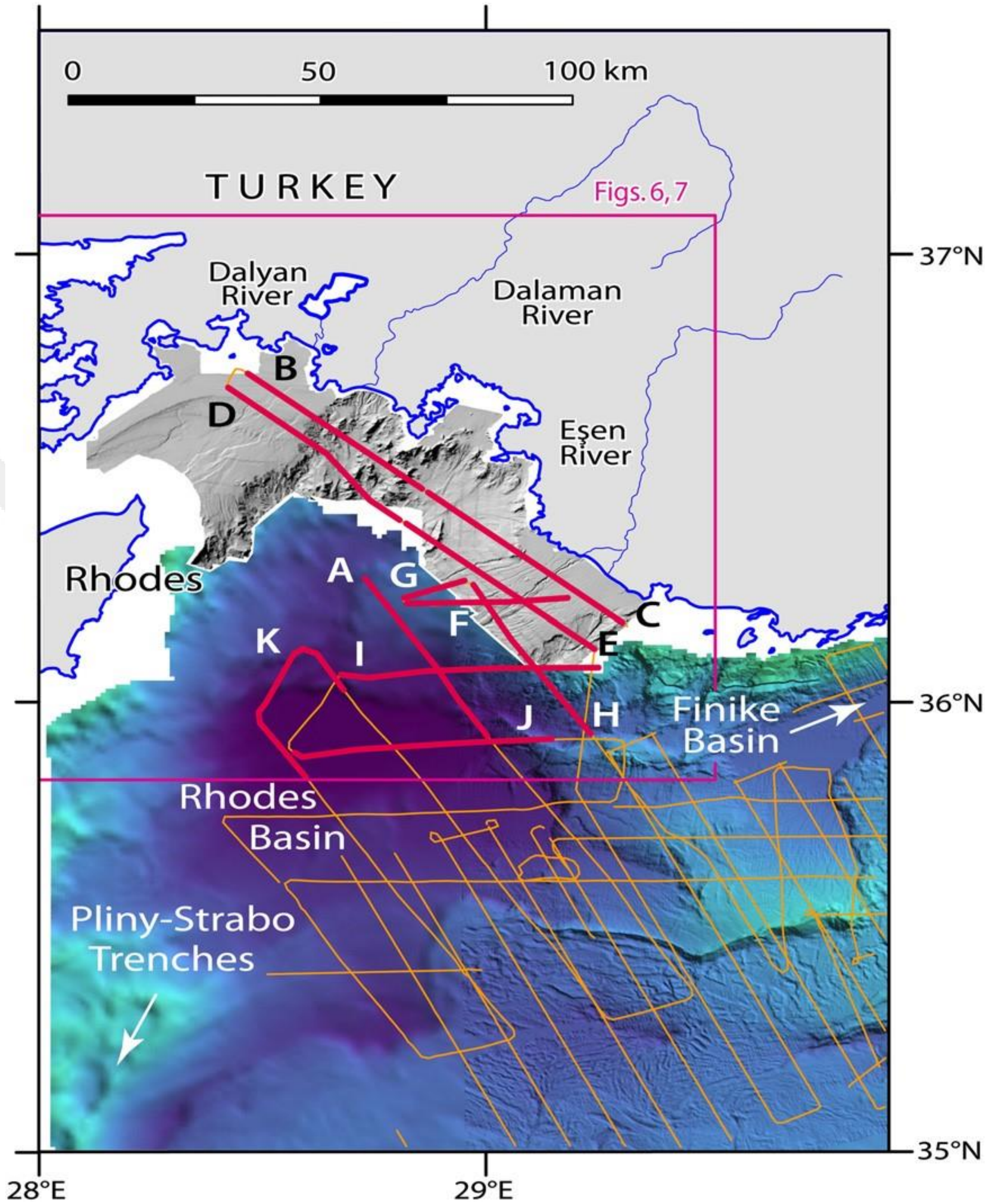

Figure 6.3 : Map of the Rhodes Basin and environs showing the locations of the multichannel seismic profiles used in this study. Thick red lines A through K are seismic reflection profiles illustrated in text figures. The inset is illustrated in Figures. 6.6-6.8. Also shown are the Eşen, Dalyan and Dalaman rivers (discussed in text). Multibeam details are given in Figure 6.2.

The sonic logs in the exploration wells in the Antalya Basin to the east show that the velocities in the Pliocene-Quaternary sediments increase from ~1500 m sat the sediment-water interface to ~2100-2300 m s^{-1} at the base of the succession. Similarly, borehole data reveal that the Miocene siliciclastic successions have interval velocities of 3000-3500 m s^{-1}. Interval velocities calculated during seismic data processing reveal that the Messinian evaporites of Unit 2 in the marine Antalya Basin often exhibit values ranging between 4200 and 5000 m s^{-1}.

6.4 Seismic Stratigraphy

Seismic profiles from the Rhodes Basin include two prominent seismic stratigraphic units (Units 1 and 3), separated from one another by a conspicuous angular unconformity, the M-reflector (Figure 6.4). Previous studies established the presence of a prominent and variably thick evaporite succession throughout the eastern Mediterranean (e.g., Unit 2 of Hall et al., 2005 and Işler et al., 2005). The evaporites were deposited during the desiccation of the Mediterranean associated with the Messinian salinity crises (e.g., Cita et al., 1978). Elsewhere in the eastern Mediterranean basins, two prominent seismic markers, the M and N reflectors, define the top and base of the Messinian evaporite succession, respectively (e.g., Aksu et al., 2005; Bridge et al., 2005; Işler et al., 2005). However, in regions where the evaporites are absent, such as the Rhodes and Finike basins, the hiatus is marked by the regionally continuous M-reflector, which often delineates a prominent angular unconformity at the base of the Pliocene-Quaternary succession (Aksu et al., 2009; Hall et al., 2009; Woodside et al., 2000).

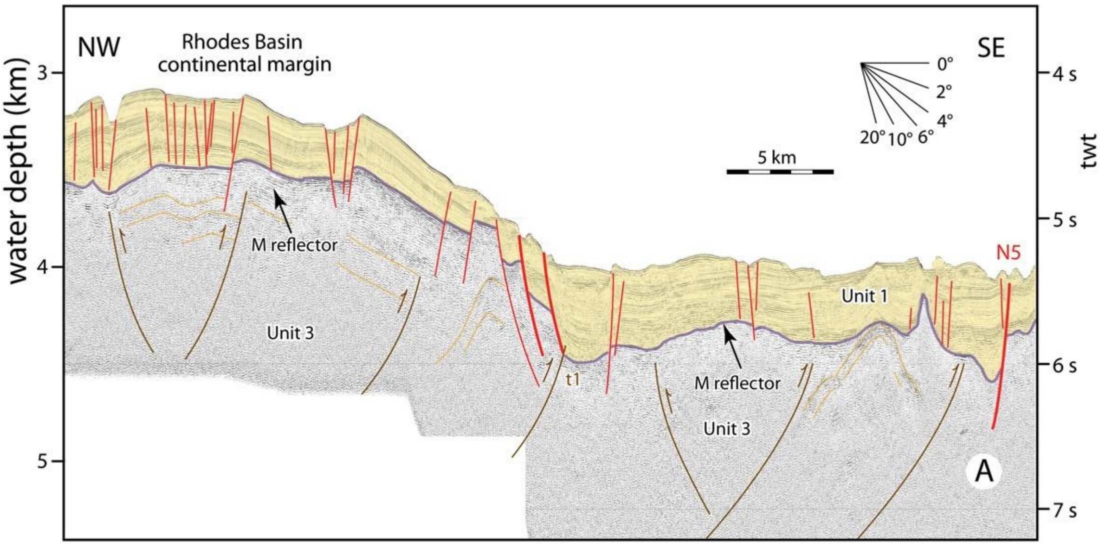

Figure 6.4 : Multi-channel seismic profile (A) across NW Rhodes Basin, showing seismic stratigraphic Units 1 and 3 and the prominent M-reflector delineating a major angular unconformity. Faults N5 and t1 are discussed in text. Location is shown in Figure 6.3.

In the northeastern portion of the eastern Mediterranean, such as in the Cilicia, Iskenderun, Latakia, Antalya basins, the Messinian deposits constitute our seismic stratigraphic Unit 2 (e.g., Aksu et al., 2005; Bridge et al., 2005; Hall et al., 2005; Işler et al., 2005). In order to maintain a consistent seismic stratigraphic nomenclature with the previous studies, in this paper, we labelled the successions above and below the M-reflector as Units 1 and Unit 3, respectively, despite the absence of evaporite successions in the Rhodes Basin and environs.

6.4.1 Unit 1: Pliocene-Quaternary

Unit 1 is composed of a regularly reflective package of acoustically strong and continuous reflectors that can be traced throughout the study area (Figure 6.4). Unit 1 is tentatively correlated with the Pliocene Değne Formation and Quaternary alluvial fans of the Çameli and Eşen Basins (Figure 6.5). It is further tentatively correlated with the Pliocene Yenimahalle and Alakilise formations and the Pleistocene Antalya Tufa and Belkış conglomerate of the onland Aksu, Köprü, and Manavgat basins (Figure 6.5). The base of Unit 1 is marked by the M-reflector.

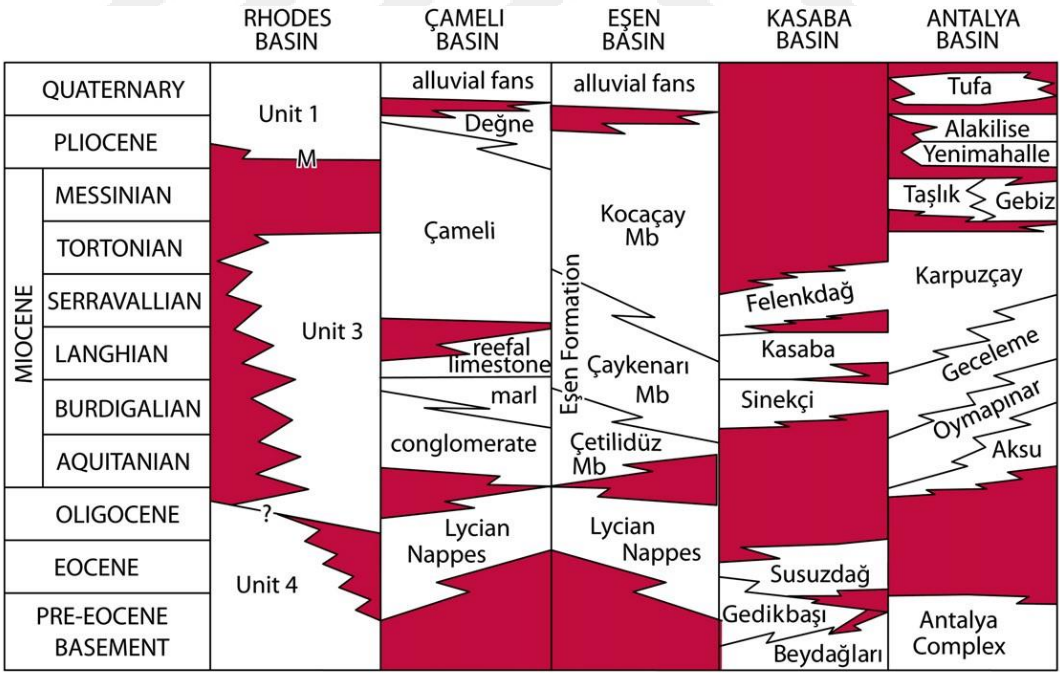

Figure 6.5 : Stratigraphy of the Rhodes Basin and environs showing the correlations between seismic stratigraphic units and the sedimentary successions on land, compiled from: (i) Çameli and Eşen (Çay) basins = Alçiçek et al. (2006), Alçiçek (2007);(ii) Kasaba Basin = Hayward (1984); Şenel (1997a,b); Şenel and Bölükbaşı (1997); and (iii) Antalya Basin, including the onland Aksu, Köprüçay and Manavgat basins = Akay and Uysal (1985); Akay et al. (1985); Flecker et al. (1998); Karabıyıkoğlu et al. (2000, 2005), Işler et al. (2005).

6.4.2 Unit 3: Pre-Messinian

Unit 3 underlies the M-reflector, and constitutes the deepest of the recognizable stratigraphic successions. It is characterised by lower frequency reverberatory reflections, locally showing moderate lateral continuity (Figure 6.4). It has a prominent reflective top delineated by the M-reflector, but the base of the unit is not imaged in our seismic reflection profiles. Unit 3 probably constitutes a diverse collection of regional lithostratigraphic units ranging from lower Mesozoic to upper Miocene in age, including the lateral equivalents of the Serravallian-Tortonian Felenkdağ Formation, mainly Langhian Kasaba Formation and Burdigalian Sinekçi Formation of the onland Kasaba Basin, as well as the lateral equivalents of the Aquitanian-Serravallian Aksu, Oymapınar and Geceleme formations and the predominantly Tortonian Karpuzçay Formation of the onland Aksu, Köprü and Manavgat Basins (Figure 6.5). This unit is further correlated with the lower Miocene conglomerates, marls and reefal limestones as well as the middle-upper Miocene Çameli Formation in the Çameli Basin and the Çetilidüz, Çaykenarı and Kocaçay members of the Eşen Formation in the Eşen Basin (Figure 6.5). Unit 3 may also include upper Mesozoic limestones and/or Oligocene flysch mapped in southern Turkey (e.g., Lycian Nappes and Beydağları Complex; Collins and Robertson, 1998), the Island of Rhodes (Hanken et al., 1996) and the Island of Cyprus (Robertson and Woodcock, 1986).

6.5 Morphological Architecture of the Northern Rhodes Basin

The northern sector of the Rhodes Basin is divided into two distinctive morpho-tectonic domains (Figure 6.6): (i) the Rhodes and Anatolian shelf slopes in the north and northeast and (ii) the deep Rhodes Basin in the south.

6.5.1 The Rhodes and Anatolian continental margins

The northern and northeastern margin of the Rhodes Basin includes a narrow shelf along southwestern Turkey, which widens considerably immediately north of the Island of Rhodes. The shelf-to-slope break occurs around 100-150 m and steep continental slopes lead into the deep Rhodes Basin, where the water depth exceeds 4300 m (Figure 6.6). The southern boundary of this domain vaguely corresponds with the base of the continental slope between 2000 and 3000 m water depths, whereas the northern boundary extends to the present-day coastline. We have no data from the western segment of the Rhodes Basin and its continental margin, therefore the following description is entirely focused to the Turkish continental margin. The Anatolian continental margin exhibits two distinctly different morpho-tectonic regions (Figures 6.3 and 6.6): (1) a rugged seafloor which occurs seaward of the Fethiye Bay and at the south-eastern end of the study area, and (2) a smooth sea-floor which occurs southwest of the Eşen River mouth and the prominent fresh water spring, as well as across the broad region that extends between the northeastern tip of the Island of Rhodes and the Marmaris Bay (Figure 6.6).

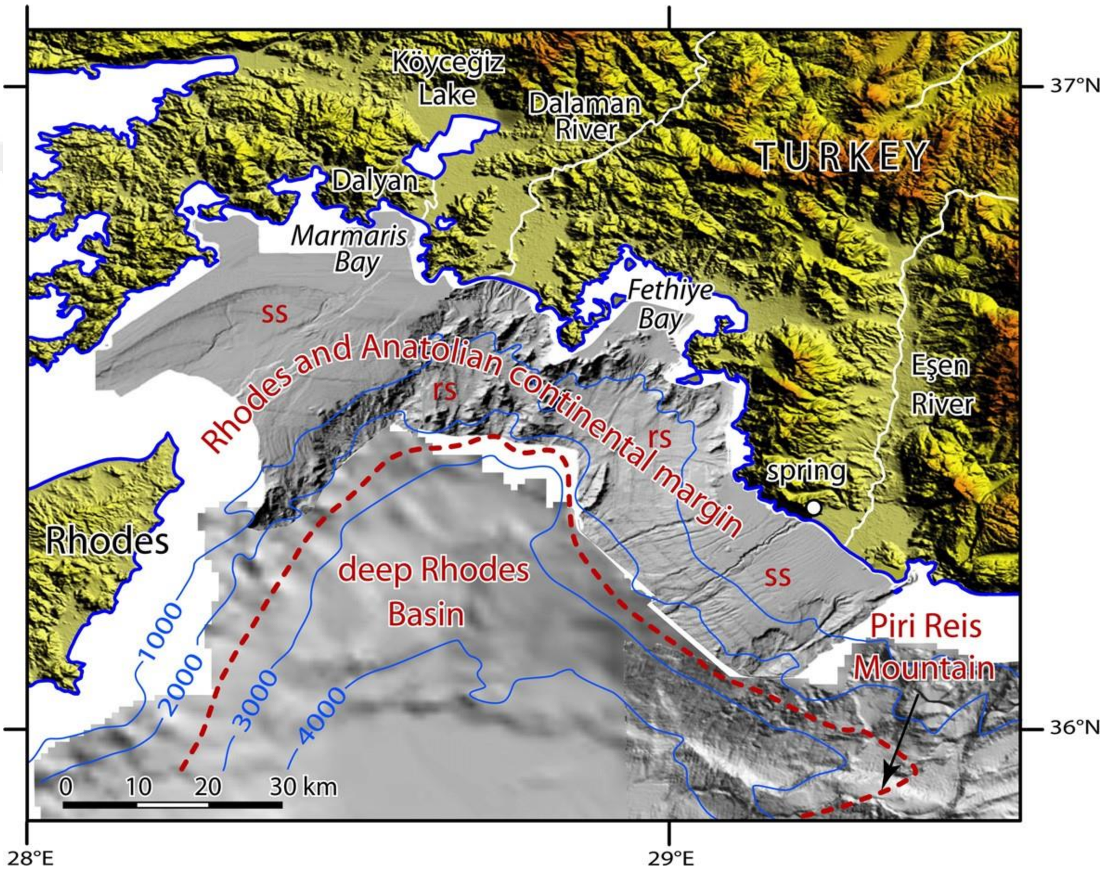

Figure 6.6 : Map of the study area showing the two morpho-tectonic domains: (i) the Rhodes and Anatolian continental margins and (ii) the deep Rhodes Basin. The topography is compiled from GeoMapApp (Ryan et al., 2009), the bathymetry is from MediMap Group (2005), Woodside et al. (1997) and Ocakoğlu (2012). The coastline and selected isobaths contours are from the Intergovernmental Oceanographic Commission (IOC) (1981). ss = smooth seafloor, rs = rugged seafloor (discussed in text).

6.5.2 Rugged seafloor

In the multibeam maps the region characterised by rugged seafloor morphology is delineated by prominent escarpments and curvilinear ridges and valleys which are reminiscent of the topography observed onland, immediately northeast of the rugged seafloor (Figure 6.6; also see Ocakoğlu, 2012). A major seafloor scar occurs near the shelf-edge in the central portion of the study area immediately seaward of the Dalaman River mouth and the Fethiye Bay. The associated escarpment extends to ~1000 m isobaths (Figure 6.6). In this region, the seafloor between 1000 and 2000 m isobath is relatively undeformed, but leads to another scar which occurs at around 2000 m isobath and its escarpment extends toward the deep Rhodes Basin (Figure 6.6). Here, the seafloor displays several internally parallel small linear ridges and their intervening valleys (Figures 6.3 and 6.6). The face of the escarpment is dissected by numerous small submarine canyons. The north-western portion of the scar that occurs southwest of the Fethiye Bay nearly extends to the present-day shoreline (Figure 6.6). Here the face of the escarpment is dissected by several small tributaries that link with the mouth of the present-day Dalaman River, immediately to the north. Along the north-western sector of the Anatolian continental margin there is a single scar on the seafloor, which occurs at ~1000 m isobath and the escarpment extends into the Rhodes Basin. The prominent scar that defines the northeastern and eastern margins of the Island of Rhodes can be traced confidently from the mouth of the Dalaman River toward the southwest, and gives the impression that it must extend a considerable distance paralleling the Island of Rhodes (Figures 6.3 and 6.6). However, there is no data in this region to confirm this.

Two northwest-southeast trending high-resolution seismic reflection profiles reveal the internal structural architecture of the rugged seafloor (Figures 6.7-6.10). The major slide scar is imaged as a prominent de-pression where several basement-cored ridges stick-out as prominent highs (e.g., Figures 6.7 and 6.9). Comparison of the seismic reflection profiles and the multibeam image shows that these basement-cored ridges exhibit broadly NE-SW orientations, which are in-turn parallel to the morphological elements of the elevated terrains bordering the Fethiye and Marmaris bays (Figure 6.6).

6.5.3 Smooth seafloor

The smoother seafloor morphology is clearly seen to the northwest and southeast of the region characterised by rugged seafloor morphology (Figures 6.3 and 6.6; also see Ocakoğlu, 2012). In the north-western smooth sea-floor region seaward of Marmaris Bay, the seafloor exhibits two distinctly different morphologies: (i) small bathymetric steps which trend broadly parallel to the regional trend of the coastline and (ii) small meandering and anastomosed channels which are incised into the seafloor. Although running oblique to the map trace of a small bathymetric step, a northwest-southeast trending seismic profile reveals the internal architecture of these bathymetric steps (Figure 6.7). Here there are several seaward prograded clinoform packages which are stacked on top of one another separated by internally parallel and continuous reflections. These packages are interpreted as deltas on the basis of strong morphological similarities between these packages and the previously described Pliocene-Quaternary delta successions in the eastern Mediterranean (e.g., Aksu et al., 1992a, b).

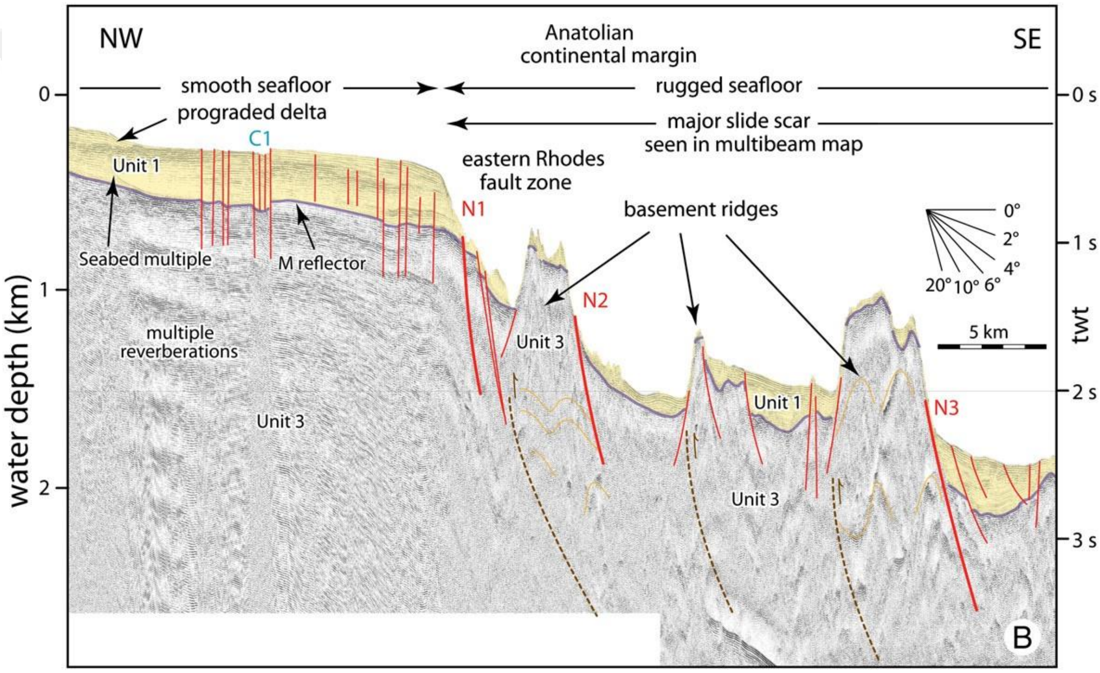

Figure 6.7 : Multichannel seismic reflection profile B showing the internal architecture of the north-western portion of the Turkish continental margin. Note the presence of prominent basement ridges in the region where the multibeam data shows a major seafloor scar and rugged seafloor topography (c.f., Figure 6.3). Faults N1-N3 and channel C1 are discussed in text. Location is shown in Figure 6.3.

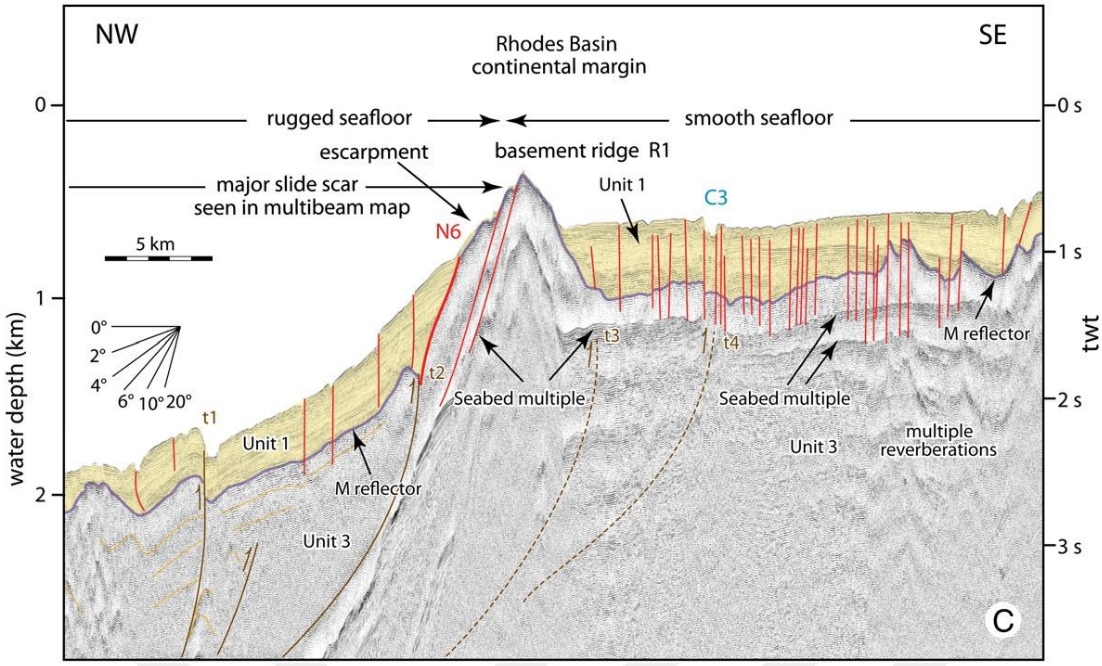

Figure 6.8 : Multichannel seismic reflection profile C showing the internal architecture of the southeastern portion of the Turkish continental margin. Faults N6 and t1-t4 and channel C3 are discussed in text. Note that the internal architecture of the region characterised by smooth seafloor morphology in the multibeam map is marked by numerous high-angle faults. Profile C is the southeast continuation of profile B. Location is shown in Figure 6.3.

These earlier studies show that the deltas were developed during the glacial periods when the global sea-level was 100-150 m lower and that the topset-to-foreset transitions of the seaward prograded clinoforms denote the last phase of delta progradation prior to the post glacial sea-level rise (Aksu et al., 1992a, b). The only possible river that can account for these stacked delta successions is the Dalyan River, which connects the Köyceğiz Lake to the Mediterranean Sea (Figure 6.6). Because the topset-to-foreset transitions in modern deltas in the eastern Mediterranean occurs at approximately 5-10 m water depth, the small steps on the sea- floor probably represent the former shoreline positions (Figure 6.6). slope face between the Marmaris Bay and the northeastern tip of the Island of Rhodes includes several northeast-southwest trending largely anastomosed channels (Figure 6.6). These channels appear to dissect the small seafloor steps interpreted as paleoshorelines, extending toward the present-day shoreline and the mouth of the Dalyan River, strongly suggesting that the Dalyan River was active during the Quaternary.

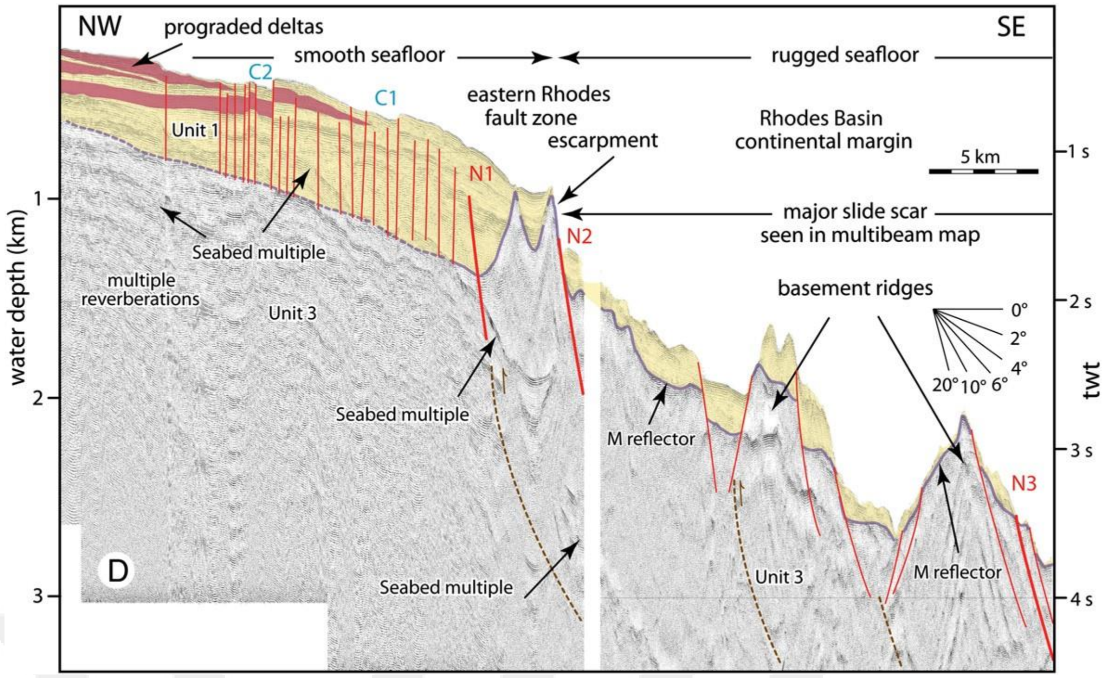

Figure 6.9 : Multichannel seismic reflection profile D showing the internal architecture of the northwestern portion of the Turkish continental margin. Note the presence of prominent basement ridges in the region where the multibeam data shows a major seafloor scar and rugged seafloor topography (c.f., Figure 6.3). Also note the presence of several stacked seaward prograded delta packages along the northwest segment of the profile. Faults N1-N3 and channels C1, C2 are discussed in text. Location is shown in Figure 6.3.

The south-eastern smooth seafloor region seaward of the Eşen River mouth is characterised by a series of northeast-southwest trending linear seafloor scars. Comparison between the multibeam image and the seismic reflection profiles shows that the seafloor scars are internally parallel small linear ridges and their intervening valleys developed over high-angle extensional faults (Figures 6.6, 6.8 and 6.10). In fact, these ridges and valleys are small horst and graben structures (discussed later). Two prominent channels are clearly visible, both of which also occupy two small grabens (Figures 6.8 and 6.10). The south-eastern of these two channels is either the marine extension of the Eşen River or the outflow from the prominent spring that is located near the shoreline. This channel is ~7 km to the northeast of the present-day Eşen River mouth, and requires that a distributary of the river must have existed during most of the Quaternary (Figure 6.6).

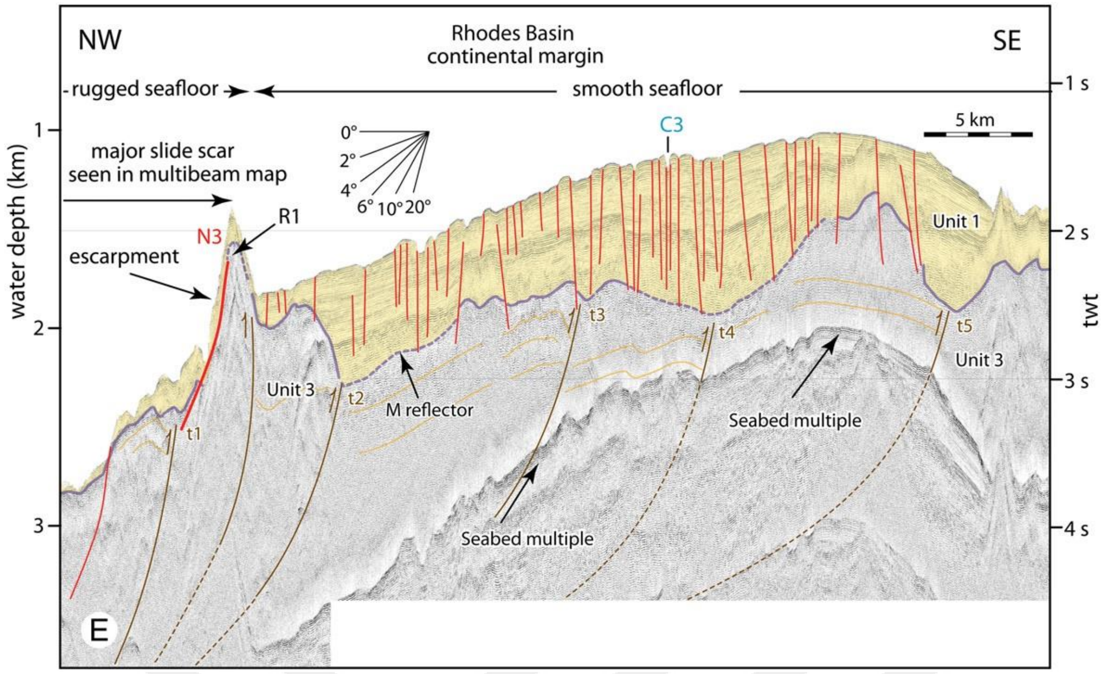

Figure 6.10 : Multichannel seismic reflection profile E showing the internal architecture of the south-eastern portion of the Turkish continental margin. Faults N3 and t1-t5 and channel C3 are discussed in text. Note that the internal architecture of the region characterised by smooth seafloor morphology in the multibeam map is marked by numerous high-angle faults developed over the backlimb of a prominent thrust culmination. Profile E is the southeast continuation of profile D. Location is shown in Figure 6.3.

6.6 Structural Architecture of the Northern Rhodes Basin

The structural architecture of the northern Rhodes Basin can best be described using two temporal phases, which are separated by the M-reflector: (1) the pre-Messinian Miocene and (2) Pliocene-Quaternary.

6.6.1 Pre-Messinian Miocene (Unit 3)

The pre-Messinian Miocene structural architecture of the northern segment of the Rhodes Basin underlying the M-reflector clearly demonstrates the basin-wide presence of a prominent NE-SW striking and in-variably SE verging fold-thrust belt (Figure 6.11). The fold-thrust belt is delineated by asymmetric anticline-syncline pairs, where the anticlines exhibit long, gently NW-dipping back limbs and shorter and more steeply SE-dipping forelimbs, suggesting that these structures define SE-verging fold system (Figures 6.12-6.15). The distance between the location of the hinge lines of any anticline and its leading syncline is closer than that between the anticline and the trailing syncline, expressing the consistent sense of asymmetry of the fold structures

(Hall et al., 2009). The belt is composed of 6-7 thrust panels, which are ~3-7 km apart from one another (Figures 6.11-6.15). Internally, the core of the ridges is characterised by strongly reflective, generally gently folded reflectors of Unit 3. The southern deeper water portion of this fold-thrust belt is previously described in Hall et al. (2009). This fold-thrust belt conspicuously extends from the southwestern segment of the Rhodes Basin immediately northeast of the Pliny-Strabo Trenches toward the Fethiye-Burdur Fault Zone in southwestern Anatolia (Hall et al., 2009).

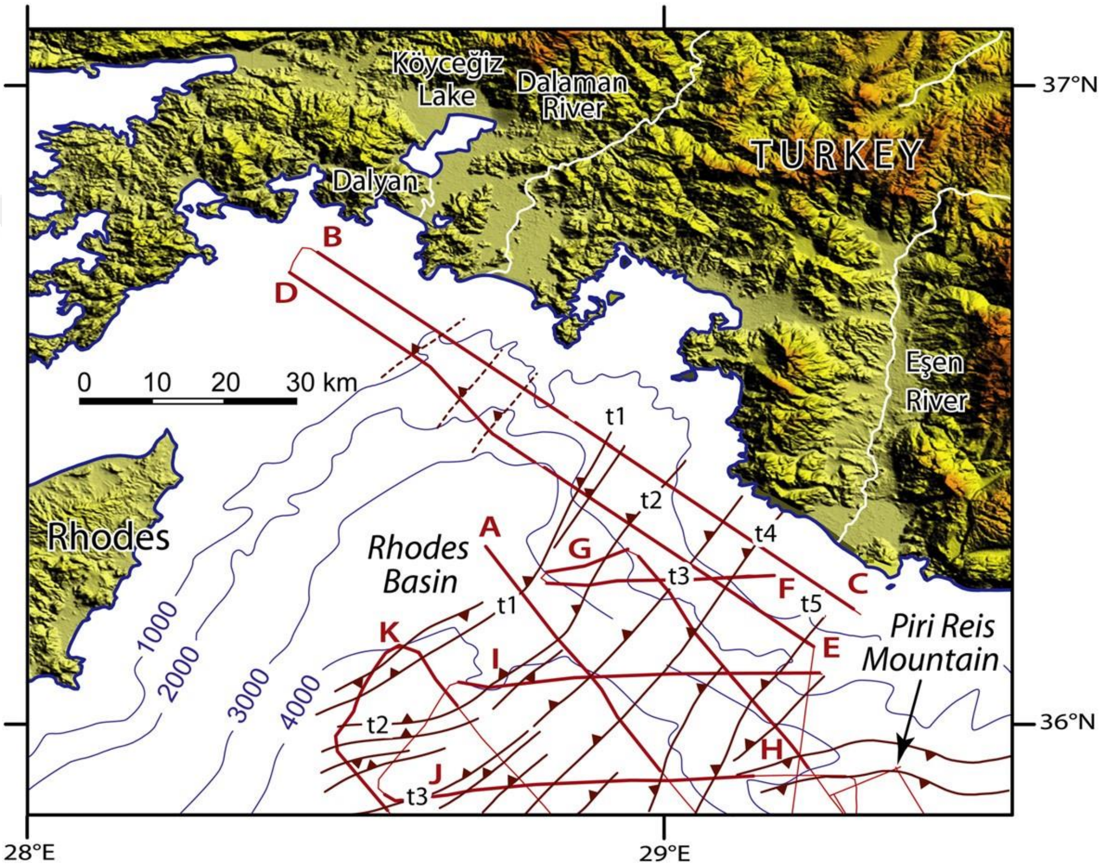

Figure 6.11 : Tectonic map of the Rhodes Basin and environs, showing the distribution of major Miocene thrust faults (ticks on hanging wall). Thrusts labelled t1-t5 are discussed in text. The topography is compiled from GeoMapApp (Ryan et al., 2009). The coastline and selected isobaths contours are from the Intergovernmental Oceanographic Commission (IOC) (1981).

In the eastern segment of the study area, seaward of the southern margin of the Anatolian continental slope there is an E-W trending ridge, informally referred to as the Piri Reis Mountain (Figures 6.11 and 6.12; Hall et al., 2009). The morphology of the Piri Reis Mountain is characterised by an asymmetric, northward-skewed two-crested antiformal structure, which is delineated by two north-verging thrust, which created a prominent steeply-north-dipping escarpments (Figure 6.12; Hall et al., 2009;

Aksu et al., 2009). Seismic profiles show that the core of the thrust panels is characterised by weakly folded discontinuous reflections of Unit 3. The escarpment creates ~900-1150 ms step on the seafloor (Figure 6.12). Multibeam bathymetry over this area clearly shows that the thrust culmination that delineates the Piri Reis Mountain is a broadly east-west trending arcuate structure (Figures 6.3 and 6.6).

6.6.2 Pliocene-Quaternary (Unit 1)

Across the northern portion of the Rhodes Basin the M-reflector delineates a major erosional surface where the folded and faulted successions of Unit 3 are decapitated at a profound unconformity (e.g., Figures 6.9, 6.10 and 6.12). Along the eastern and southern basin margins the Pliocene-Quaternary successions onlap, such as seen along the Sırrı Erinç Plateau to the south (Hall et al., 2009) or downlap, such as seen along the northern foothills of the Anaximander Mountain (sensu stricto; Aksu et al., 2009). However, Unit 1 appears as a large drape over a monoclinal structure along the northern margin of the basin (e.g., Figures 6.11 and 6.13).

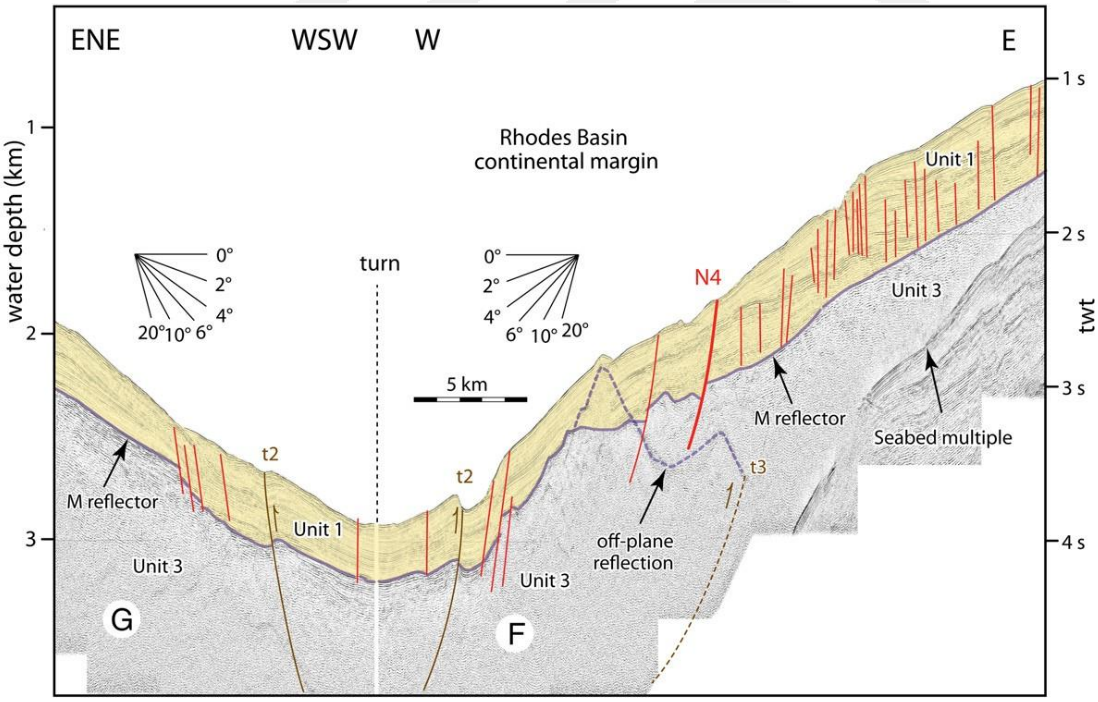

Figure 6.12 : Multichannel seismic reflection profiles F and G showing the internal stratigraphy of the northern Rhodes Basin margin. Note that the Pliocene-Quaternary Unit 1 forms a nearly isopachous drape over the M-reflector. Faults N4, t2 and t3 are discussed in text. Location is shown in Figure 6.3.

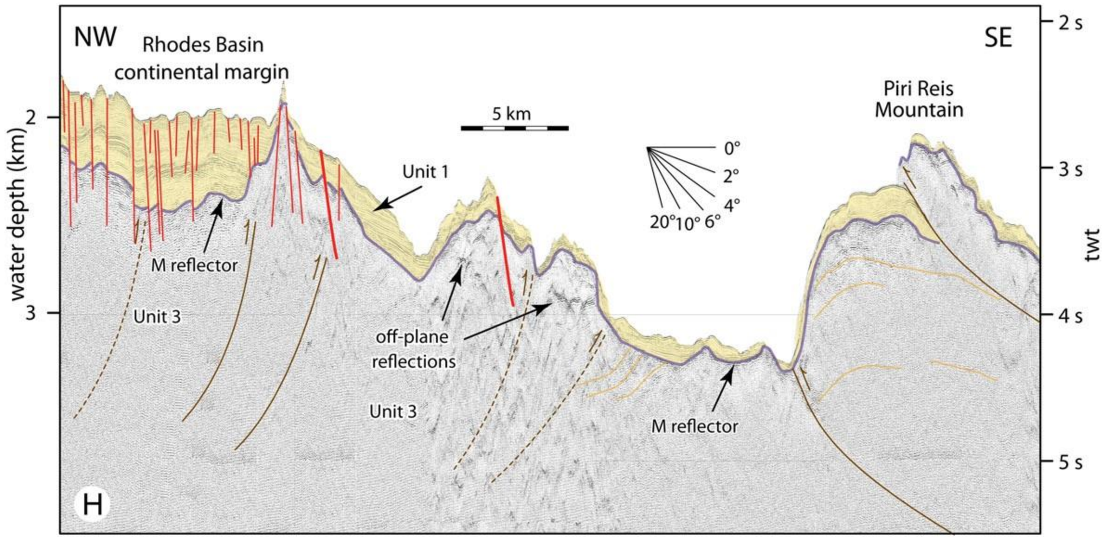

Figure 6.13 : Multichannel seismic reflection profile H showing the structural relationship between the prominent imbricate thrust panels that delineate the Piri Reis Mountains (also see Aksu et al., 2009) in the southeast and the Rhodes Basin continental margin in the northwest. Location is shown in Figure 6.3.

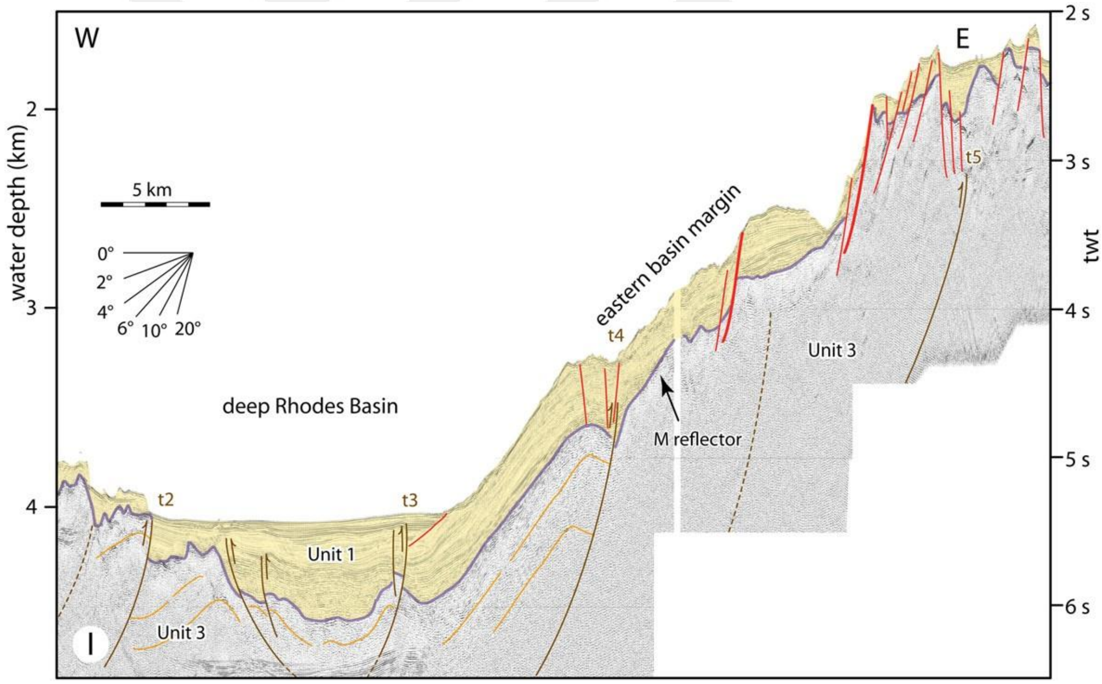

Figure 6.14 : Multichannel seismic reflection profile I showing the internal stratigraphy of the eastern Rhodes Basin margin. Note that the Pliocene-Quaternary Unit 1 forms a nearly isopachous drape over the M-reflector along the lower slope. Also note the stark contrast between the prominent thrusts that cut Units 1 and 3 within the deep Rhodes Basin versus the high-angle extensional faults that characterise the structural framework in the upper slope regions. Faults t2-t5 are discussed in text. Location is shown in Figure 6.3.

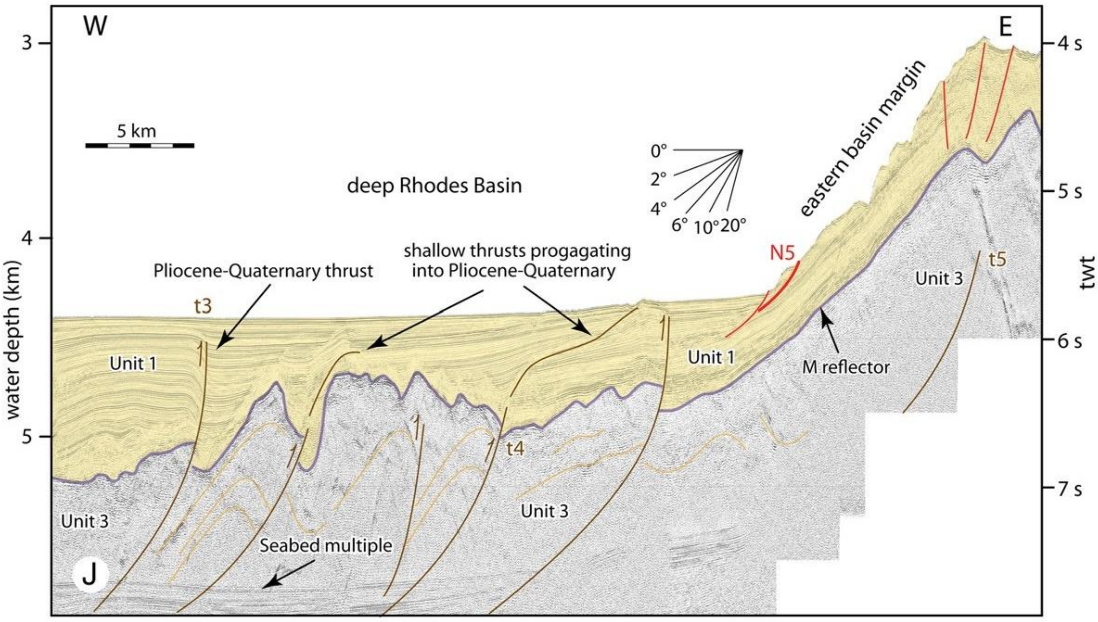

Figure 6.15 : Multichannel seismic reflection profile J showing the internal stratigraphy of the eastern Rhodes Basin margin. Note the similarities between the architecture of the Pliocene-Quaternary Unit 1 in the lower slope between profiles I and J. Also note that the structures within the deep Rhodes Basin are dominated by prominent thrusts. Faults N5, t3-t5 are discussed in text. Location is shown in Figure 6.3.

The architecture of the Pliocene-Quaternary successions of Unit 1 in the northern Rhodes Basin is characterised by a series of NE-SW trending ridges and their intervening basins, delineated by the morphology of the seafloor (Figure 6.16). In the southern (Hall et al., 2009), and the central portions of the Rhodes Basin (e.g., Figure 6.15) the Miocene thrust culminations also define Pliocene-Quaternary thrust culminations. Over these structures the thickness of the Pliocene-Quaternary succession is considerably reduced, and the axes of the anticlines and synclines observed within the Miocene successions of Unit 3 coincide well with major synclines developed in the Pliocene-Quaternary succession (Figure 6.15). This geometric coincidence together with the observed variations in the thickness of the Pliocene-Quaternary succession suggests that the Miocene fold-thrust structures were re-activated during the Pliocene-Quaternary.

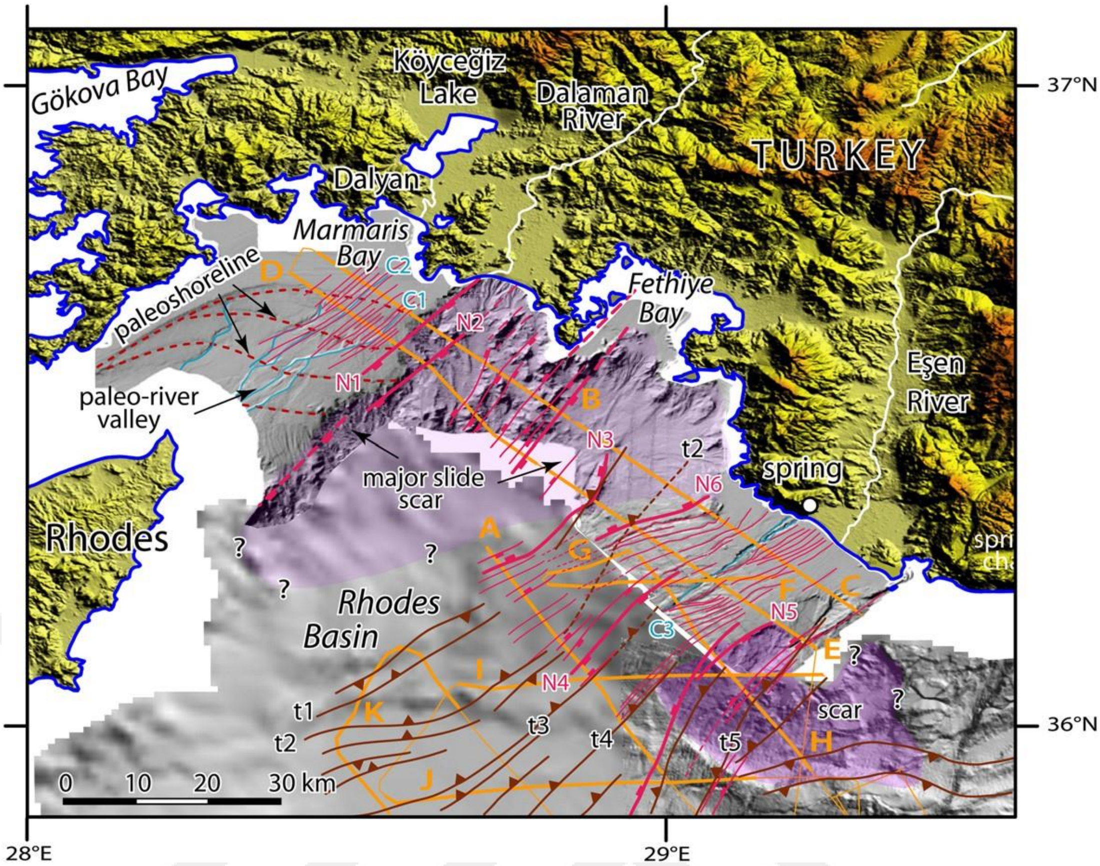

Figure 6.16 : Pliocene-Quaternary tectonic map of the Rhodes Basin and environs, showing the distribution of major thrust and normal faults (ticks on hanging wall). Normal faults N1-N6, thrust faults t1-t5 and channels C1-C3 are discussed in text. The topography is compiled from GeoMapApp (Ryan et al., 2009), the multibeam bathymetry is from MediMap Group (2005), Woodside et al. (1997), and Ocakoğlu (2012). The coastline is from the Intergovernmental Oceanographic Commission (IOC) (1981).

In the western portion of the study area, the NE-SW-striking thrusts are clearly imaged in seismic reflection profiles where they cut the entire Unit 3 and the M-reflector, further extending into the upper portion of Unit 1. Growth strata wedges are developed in the upper portion of Unit 1 on the backlimb of many of these thrust culminations (e.g., Figure 6.17). These wedges thicken toward the hanging wall of the adjacent thrust. This seismic stratigraphic architecture suggests that thrusting have been active since the late Pliocene. Tip points of many thrusts remain buried immediately below the depositional surface, but in others the thrusts extend to the seafloor where they create distinct steps (e.g., Figure 6.17). On the basis of dip direction of the fault plane, the relative offset of the basin fills across the faults and the drag of the Pliocene-Quaternary reflectors on their hanging walls Hall et al. (2009) argued that these thrusts are predominantly southeast-verging structures, with occasional northwest-verging thrusts. The sub-vertical dip of the fault planes (~70-80°NW), the abrupt sub-vertical juxtaposition of thick basin fill against Unit 3, the large discrepancies between the vertical offset of reflectors in the Pliocene-Quaternary basin fill versus that of the M reflector and the presence of positive flower structures, suggest that the Miocene fold-thrust belt has experienced NE-SW directed strike slip movements.

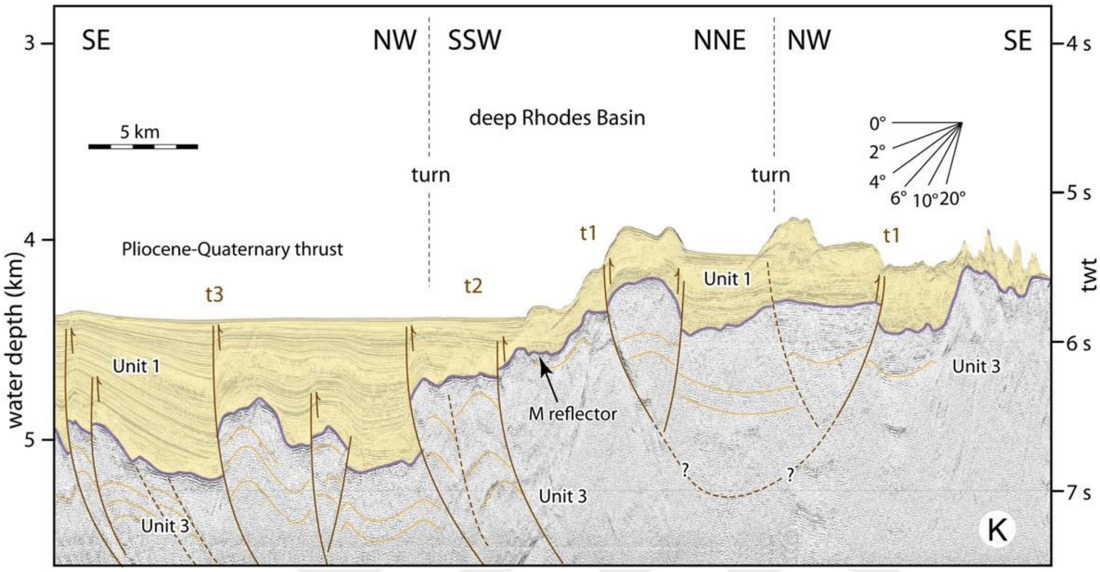

Figure 6.17 : Multichannel seismic reflection profile K showing the thrust structures affecting the Pliocene-Quaternary fill of the Rhodes Basin. Growth strata in the Pliocene Quaternary show that the thrusts were active during deposition and some of the thrusts affect the seabed, indicating their continuing activity. Thrust faults t1-t3 are discussed in text. Location is shown in Figure 6.3.

In the northeastern portion of the study area, the seafloor is corrugated, created by a series of basins and ridges (Figures 6.8 and 6.10). Multibeam bathymetry over this area (Ocakoğlu, 2012) shows that these basins and ridges display broadly NE-SW trends. Seismic profiles over this region illustrate that this undulating surface morphology is the expression of a numerous closely-spaced steep faults showing normal- and occasional reverse-sense displacements (Figure 6.8 and 6.10). The M-reflector is also affected, and displays as much as 200 ms of relief across adjacent faults (Figures 6.8 and 6.10). These high-angle faults appear to root in poorly imaged thrusts within Unit 3. Traced from the deep central Rhodes Basin toward the northeast, the Pliocene-Quaternary succession becomes increasingly affected by this system of steeply-dipping faults. In the northeastern portion of the study area, this zone delineates a 25-35 km wide belt (Figure 16), and is situated immediately southwest of the Eşen River valley and the eastern segment of the Fethiye-Burdur Fault Zone. One intriguing aspect of the Pliocene-Quaternary tectonism in the Rhodes Basin is the apparent correlation between the thrust faults in the southern and central portion of the

Rhodes Basin and the predominantly ex-tensional faults in the northeastern portion of the Rhodes Basin. This correlation suggests that during the Pliocene-Quaternary, the stress field was not isotropic and that it must have been strongly partitioned into regions dominated by transpression and others dominated by transtension. The close correlation between the faults mapped in the marine areas and those mapped in the onland Eşen and Dalaman river valleys strongly suggest that the Pliny-Strabo Fault Zone extends toward the northeast linking with the onland Fethiye-Burdur Fault Zone.

6.7 Discussion

6.7.1 Pre-late Messinian thrusting

The architecture of the pre-Messinian fold/thrust structures within the central and northern portions of the Rhodes Basin is characterised by large ramp anticlines above SE-verging thrusts developed within Unit 3. Hall et al. (2009) classified the Miocene fold/thrust belt as a trailing imbricate fan system which is deeply rooted at a level at least as deep as the lower portion of the imaged pre-Messinian successions. They proposed that during the early Miocene, this fold thrust belt had a broadly E-W trend, in agreement with data from Jongsma and Mascle (1981) and Mascle et al. (1986) who also showed the presence of E-W and NE-SW trending structures within the Rhodes Basin, and suggested that they may be correlated with the upper Miocene fold-thrust units of the Beydağları Mountains of southwest Turkey. The counter-clockwise rotation of the fold/thrust structures in the Rhodes Basin is similar to those demonstrated by Morris and Robertson (1993), Kissel and Poisson (1986) and van Hinsbergen et al. (2010b) for the Beydağları Mountains, and now dated at 16-5 Ma (Middle to Late Miocene).

6.7.2 Late Messinian-early Pliocene regional subsidence

Most eastern Mediterranean basins, such as the Antalya Basin (Işler et al., 2005), Cilicia Basin (Aksu et al., 2005; Bridge et al., 2005), and Latakia Basin (Hall et al., 2005) contain a thick sequence of late Miocene evaporites, deposited during the Messinian salinity crisis (e.g., Hsü et al., 1978). The absence of the evaporite facies in the Rhodes Basin strongly suggests that this region must have remained above the depositional base of the marine evaporite environment during the Messinian. It is difficult to see how the Rhodes Basin could have remained low and isolated from the rest of the Mediterranean Sea.

The absence of Messinian evaporites within the deepest basin in the present-day eastern Mediterranean is well documented by previous studies (Hall et al., 2009; Mascle et al., 1986; Woodside et al., 2000). This fact is puzzling and requires a geologically plausible explanation. Hall et al. (2009) used the absence of evaporites in the Rhodes Basin and the presence of several seaward prograded vertically stacked Quaternary delta successions resting at 2500-3500 m water depth to argue that the northern portion of the Rhodes Basin must have remained above the depositional base of the marine evaporite environment during the Messinian and that the region must have subsided very rapidly during the Pliocene-Quaternary. Hall et al. (2009) further suggested that the subsidence needed in the Rhodes Basin is created by the regional flexural response to the loading of the imbricate thrust sheets of the Taurus Mountains of southwestern Turkey, immediately to the north of Rhodes Basin. In support of their ideas Hall et al. (2009, their Figure 23) linked the continued thrusting observed in the Pliocene-Quaternary in the Rhodes Basin to thrusting and consequent uplift of Miocene marine sequences observed in boreholes in the Kasaba Basin, assuming that the thrusting observed in the boreholes is younger than that observed in exposed Beydağları Mountains. The shelf slope at the northern margin of the Rhodes Basin is a large Pliocene-Quaternary monocline with no evidence of large extensional faults that might indicate a pull-apart origin: we interpret the monocline as associated with blind SE-vergent thrusting of the Tauride margin, compatible with our model.

6.7.3 Offshore-onshore structural linkage

Any model that attempts to explain the Miocene to Recent evolution of the Rhodes Basin must account for the temporal and spatial relationships and correlations between the rock units and structures observed in the Rhodes Basin and those in southwestern Turkey, and the stark contrast between the post-Miocene uplift of southwestern Turkey, and the islands of Rhodes and Karpathos (see Zachariasse et al., 2008) versus the rapid subsidence observed in the Rhodes Basin.

Many of the Pliocene-Quaternary structures mapped offshore (Figure 6.16) trend toward the Turkish coastline and should link with onshore structures. The terrestrial geology is dominated by rocks, especially ophiolitic successions, which are as old as, or older than those imaged offshore. There are a limited number of basins of younger rocks onshore: one such basin is Çameli-Gölhisar Basin (Alçiçek et al., 2006) situated north of the Gökova-Yeşilüzümlü Fault Zone (Figure 6.2). In this basin, middle Miocene conglomerates and conformably overlying upper Miocene-lower Pliocene fluvio-lacustrine successions are syn-tectonically deposited in NE-SW striking fault blocks, where the faults show both sinistral strike slip and normal sense dip slip (Elitez, 2010; Elitez et al., 2009), although a phase of late dextral transtension is also inferred (Alçiçek et al., 2006). Detailed mapping of various basins along the Fethiye-Burdur Fault Zone by co-authors, Elitez and Yaltırak, 2014a, shows evidence for distributed oblique-slip faults, with sinistral strike-slip components, for example in the vicinity of Çameli (Figure 6.18). The faults have significant normal components of displacement but are of limited length, suggesting that sinistral strike-slip displacements are modest. Viewed on a regional scale (Figure 6.19), our mapping shows the broad zone of the Fethiye-Burdur Fault Zone with the predominance of NE-SW faults, many of which, like those shown in Figure 6.18 have sinistral components of displacement. Another prominent basin is the Eşen (Çay) Basin (Alçiçek, 2007; ten Veen, 2004), which is presently situated within the Eşen River valley (Figure 6.2). In this basin, upper Miocene conglomerates rest unconformably over the basement rocks, and pass up-section into an upper Miocene-lower Pliocene lacustrine carbonate series of rocks, which are in turn, unconformably overlain by late Pliocene-early Quaternary alluvial fan and braided river deposits. The Eşen River valley is characterised by N-S striking faults with prominent normal-sense dip slip, and as such gives the impression of a graben structure. Field mapping clearly documented the presence of numerous NW-SE striking and NE- and SW-dipping faults with considerable sinistral strike-slip component. These faults affected the younger basinal successions and are developed nearly at right angles to the NE-SW striking basin-bounding faults. Analyses of faults in the Eşen Basin analyses by Över et al. (2013b) show a Quaternary stress regime favouring extension in a NE-SW direction and sinistral strike-slip along faults trending NNE-SSW, though a different stress regime appears to have been operative in pre-Pliocene time. Another distinguishing feature of the Eşen River valley is the presence of an E-W striking normal fault situated at the contact between the late Pliocene-early Quaternary and the late Quaternary successions. This fault is clearly visible along the morphological contact between the valley and the hill where the ancient city of Xanthos is located. North of this fault, the upper Pliocene-early Quaternary successions are tilted to the northeast. Thus, in its architecture the Eşen River valley gives the impression that it is developed associated with an east-west dilation and north-south compression. Numerous conjugate faults within the Eşen Basin confirm this view (Alçiçek, 2007).

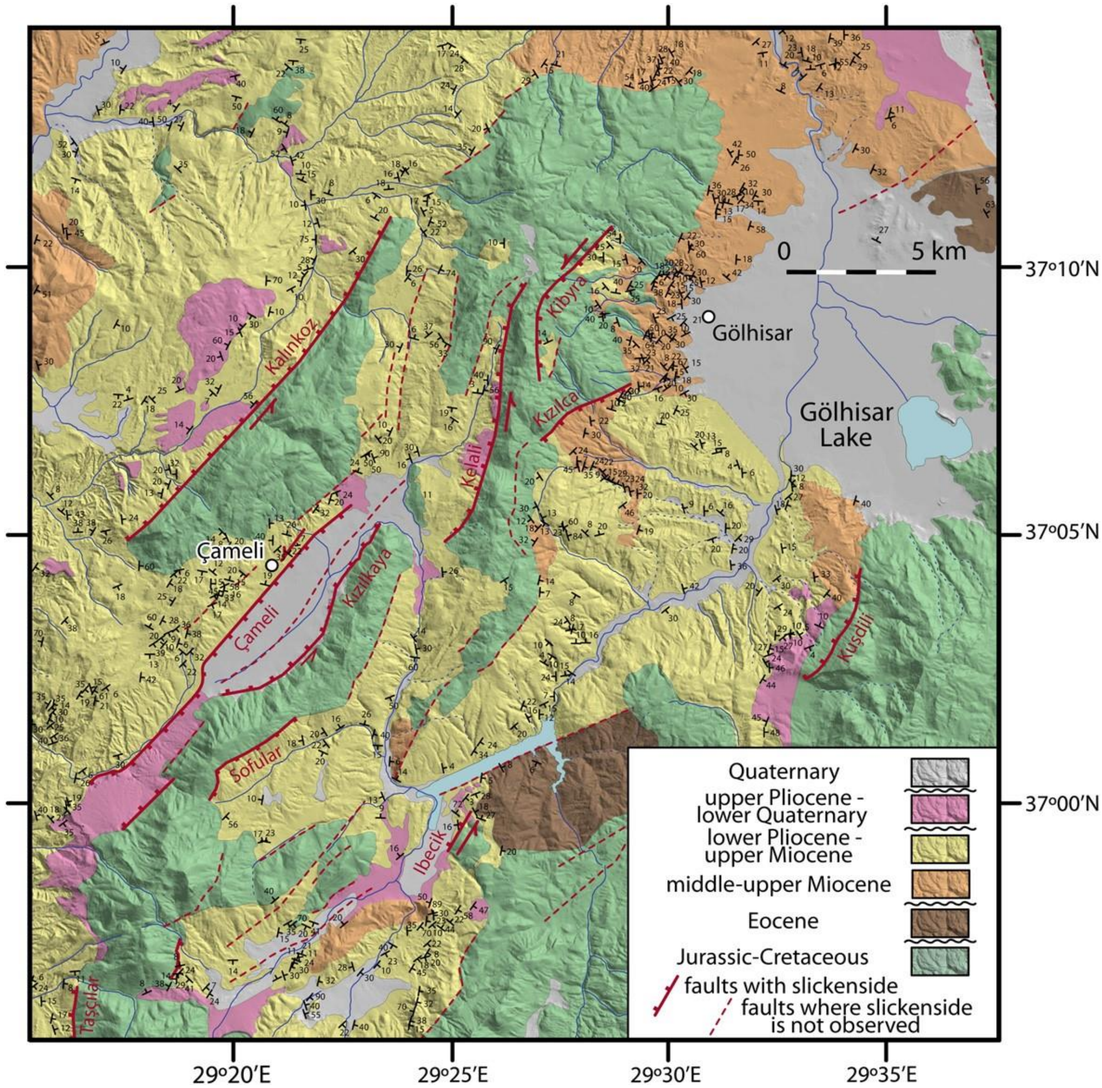

Figure 6.18 : Detailed geological map of the Çameli and Gölhisar basins mapped by co-authors Elitez and Yaltırak, showing major faults with dominant extensional slip but also sinistral strike-slip (after Elitez, 2010). Solid red lines = faults where clear slickenside is identified, dashed red lines = faults inferred from stratigraphic relationships, but slickenside is not seen in the field. Strike and dip of field measurements are also indicated. Red labels are faults names assigned by Elitez and Yaltırak during field mapping.

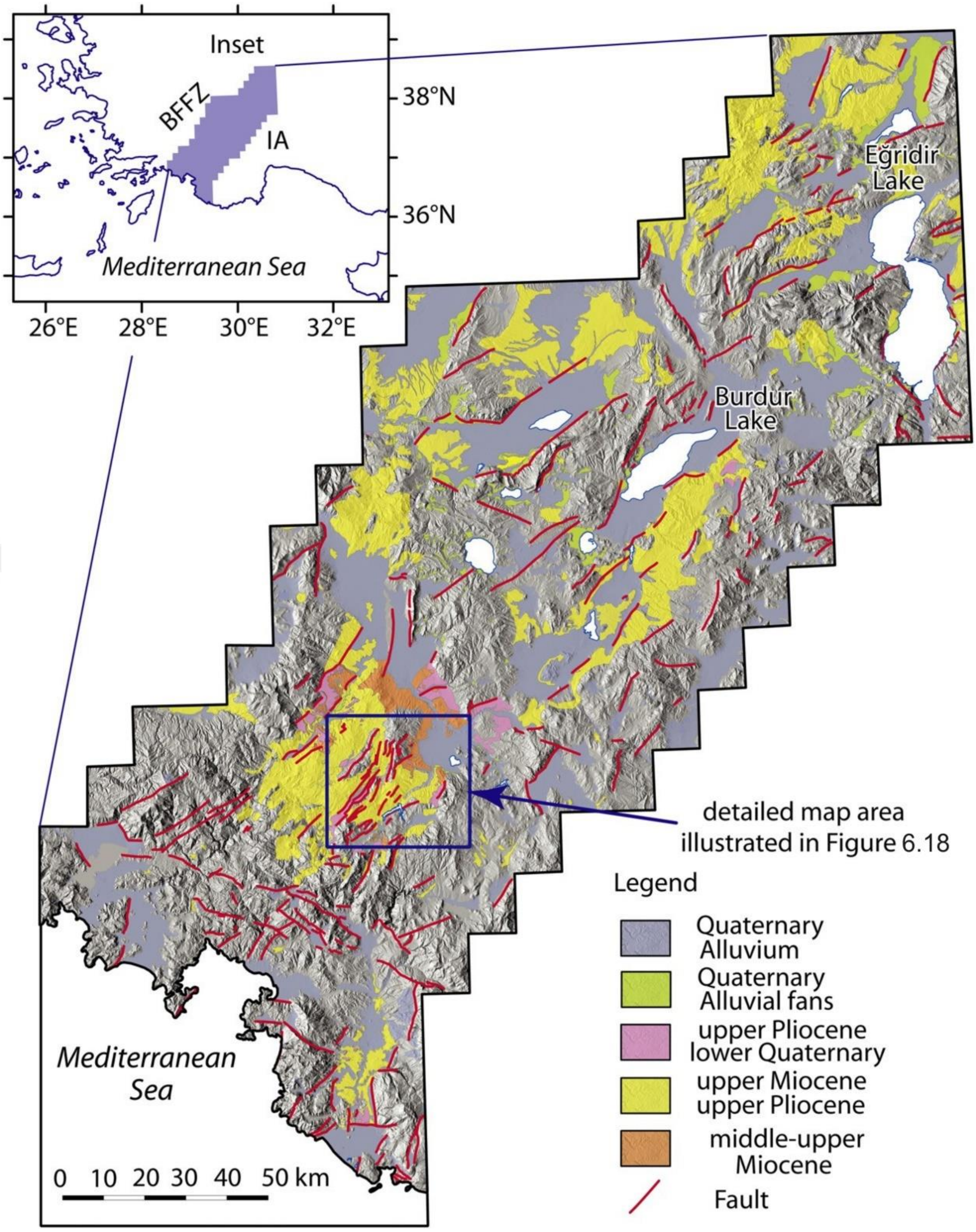

Figure 6.19 : Summary regional fault map associated with the Fethiye-Burdur Fault Zone compiled by co-authors Elitez and Yaltırak based on several seasons of field mapping. Inset shows the region of the map in southwestern Turkey. Small inset within the map area is illustrated in Figure 6.18.

A prominent structural element of the southwestern Turkey mapped by co-authors Elitez and Yaltırak, (2014a) is the presence of a major WNW-ESE striking fault zone, which is composed of numerous normal faults defining an en-échelon architecture. This fault zone is informally referred to as the Gökova-Yeşilüzümlü Fault Zone and it clearly transects the NE-SW striking basin-bounding strike slip faults, and exhibits sinistral strike slip component. It is noteworthy that all de-pressions containing notable Quaternary sediments are located south of this fault zone. Traced toward the south, particularly in the region of Köyceğiz and Dalaman valleys, the NE-SW striking sinistral strike slip system becomes hard to trace in the field, despite the fact that there are many small faults that show sinistral strike slip (e.g., the region north and northeast of Fethiye; Figure 6.2). The geology of this region is dominated by ophiolitic rocks and the numerous smaller faults showing sinistral strike slip probably represent a major shear zone in this region. The basins in this region are developed along broadly NE-SW striking faults formed at or near the contact between the ophiolitic series and the Mesozoic limestone successions. This architecture is characterised by numerous NE-SW trending small basins and ridges and is very similar to that observed in the multibeam maps and seismic reflection profiles in the marine areas. In particular, numerous hot-water springs near Köyceğiz and Dalaman further attest to the presence of faults along these small basins and ridges.

The Fethiye-Burdur Fault Zone extends from the deep Rhodes Basin as a major shear zone. The presence of the Çameli-Gölhisar Fault Zone and the Eşen River valley suggest that the Fethiye-Burdur Fault Zone is not a single zone extending from the Pliny-Strabo Trenches to the apex of the Isparta Angle, but must include a complex zone characterised by several internally parallel systems that collectively define a sinistral shear zone. The small change in orientation of the NE-SW faults north of the Gökova-Yeşilüzümlü Fault Zone to a more northerly trend on land to the south is interpreted as representing a swing in the overall Fethiye-Burdur Fault Zone (Figure 6.20). Farther southwest, the fault zone appears to swing back to its overall NE-SW trend, linking it to the Pliny-Strabo Fault Zone. The active faults appear to lie within the limits shown in Figure 6.18, with the parallel faults mapped in Marmaris Bay considered originally part of the same set but now apparently inactive, or mostly so (Ocakoğlu, 2012).

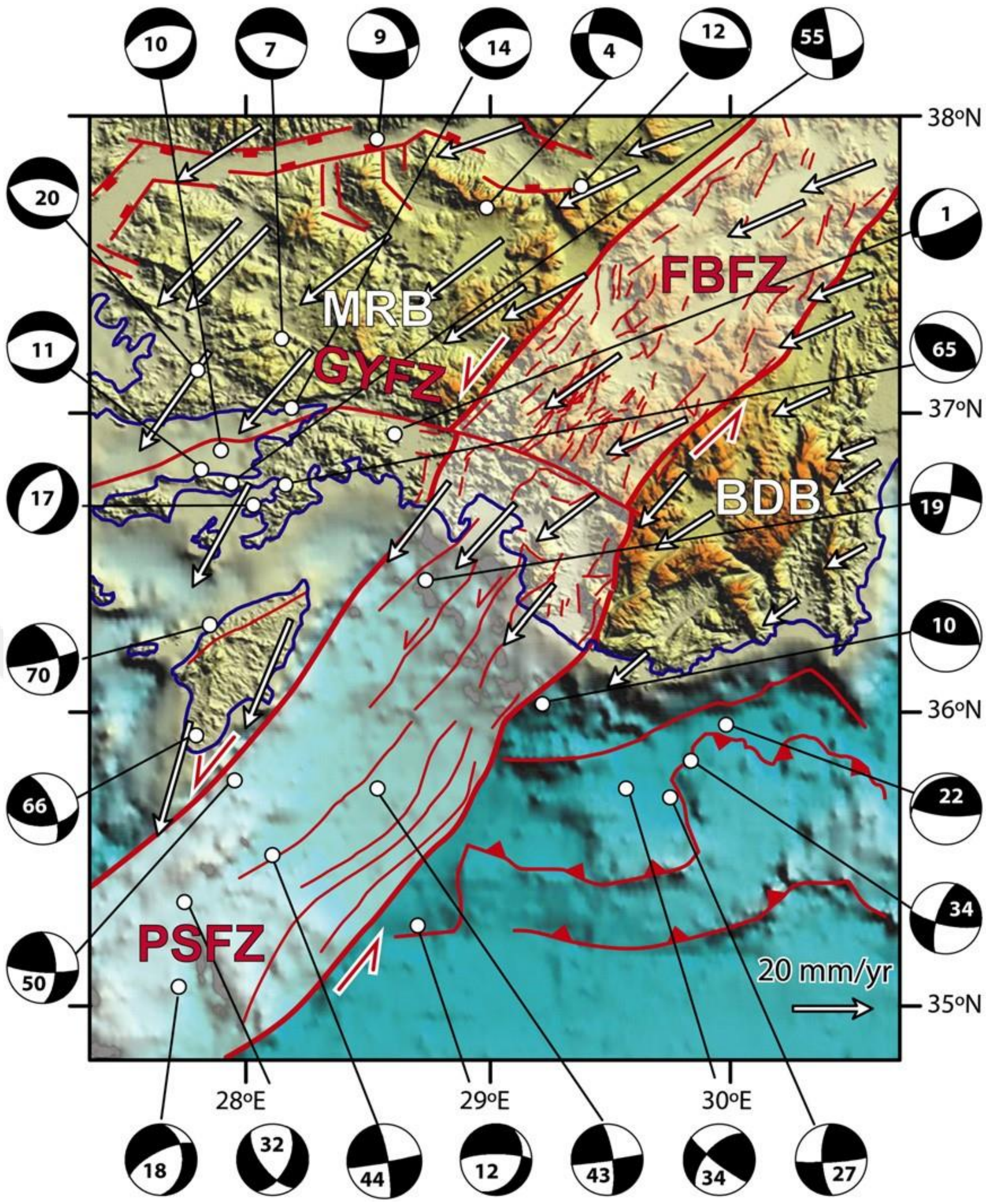

Figure 6.20 : Tectonic map of the Rhodes Basin and environs. Fault plane solutions are from Kiratzi and Louvari (2003), Benetatos et al. (2004), Yolsal et al. (2007), Yolsal and Taymaz (2010), Yolsal-Çevikbilen and Taymaz (2012); GPS vectors are from McClusky et al. (2000), Hollenstein et al. (2008), Aktuğ et al. (2009), and Floyd et al. (2010). FBFZ = Fethiye-Burdur Fault Zone, GYFZ = Gökova-Yeşilüzümlü Fault Zone = Elitez et al. (2009), PSFZ = Pliny-Strabo Fault Zone. Faults within the Fethiye-Burdur Fault Zone are from Elitez et al. (2009), those in the Anaximander Mountains and southern Rhodes Basin from Aksu et al. (2009) and Hall et al. (2009), respectively. MRB = Marmaris-Rhodes Block, BDB = Beydağları Block.

6.7.4 First motions of recent earthquakes

Recent earthquakes show a complex pattern of first motions (Figure 6.20). Normal faults abound to the northwest of the Fethiye-Burdur Fault Zone, but also occur within it: few are observed to the southeast of the fault zone. Most of the earthquakes with normal first motions have foci at shallow depth (<20 km). Thrust motions are less common in the whole area, but do occur on faults on both sides of the Fethiye-Burdur Fault Zone, though more rarely within it. Strike-slip motions often appear as oblique slip, and are uncommon to the northwest of the Fethiye-Burdur Fault Zone, but occur frequently both within and to the southeast of the fault zone. The oblique slip is predominantly transtensional in the Fethiye-Burdur Fault Zone and transpressional to the southeast of the zone. Earthquakes with thrust and strike-slip first motions occur at a range of depths up to 70 km, with very few at depths less than 20 km. There thus appears to be some degree of vertical partitioning of strain within the area, with the strains associated with the western edge of the Aegean graben system characterising the shallow crust and the transpressional strains associated with the Fethiye-Burdur Fault Zone and the western Antalya region dominating the deeper lithosphere. Recent compilation by Över et al. (2013b) tends to confirm the dominantly sinistral motions on faults tending from N-S through NE-SW to E-W.

6.7.5 Relationship to the Isparta Angle

The evolution of the Fethiye-Burdur Fault Zone is intrinsically linked with the evolution of the Isparta Angle. The Isparta Angle is bounded to the west and east by the allochthonous Lycian Nappes (Okay, 1989) and the Beyşehir-Hoyran-Hadim Nappes (Monod, 1977). The tectonic evolution of the Isparta Angle is controversial; however, there is general agreement that during the Miocene, the western limb of the Isparta Angle experienced a 30-40° counterclockwise rotation (Kissel and Poisson, 1986), whereas the eastern limb experienced a 20-40° clockwise rotation since the Eocene (Kissel et al., 1993, 2003). The Isparta Angle experienced a late Miocene phase of compression, (i.e., the Aksu Phase), with coeval eastward and westward thrusting along the western and eastern limbs, respectively (Barka and Reilinger, 1997; Barka et al., 1995). Thus, the syntaxis is developed during the Miocene by the northward buckling of the western Tauride Mountains. Palinspastic reconstructions show that when the western limb of the Isparta Angle is rotated back clockwise by ~20°, representing its position during the middle-late Miocene, the western limb (i.e., the Fethiye-Burdur Fault Zone) takes on an ENE-WSW orientation (Figure 6.20). During this time, the convergence vector between the African Plate and the Anatolian segment of then the Eurasian Plate was N-S, nearly orthogonal to this trend (e.g., Le Pichon and Angelier, 1979), so that the zone was then predominantly compressional. The counterclockwise rotation of the western Tauride Mountains and the Rhodes Basin, from the late Miocene to early-middle Pliocene (Kissel and Poisson, 1986), progressively changed the orientation of the fold-thrust belt, making it nearly parallel with the plate convergence vector, necessitating the development of a sinistral shear zone in this region (Figure 6.20). This tectonic phase utilized an older tectonic scar within the Lycian Nappes, and the rheological characteristics of the ophiolitic rocks within the Lycian Nappes created a 40-50 km wide fault zone between the Lycian Nappes and the Beydağları autochthon (Poisson et al., 2003).

6.7.6 Whither the STEP fault?

NNE-SSW-trending structures of the Rhodes Basin are shown to link the Pliny-Strabo Trenches to the Fethiye-Burdur Fault Zone, confirming the findings of Ocakoğlu (2012). The Fethiye-Burdur Fault Zone is only loosely defined as a linkage of broadly NE-SW-trending faults affecting Pliocene-Quaternary basins but with little evidence of its existence between the basins. Most of the faults are associated with NW-SE extension, but with sinistral, or sometimes dextral, components especially in Holocene time. It is difficult to estimate the overall offset across the fault zone: perhaps 20 km in the vicinity of the releasing bend at the Gökova-Yeşilüzümlü Fault Zone, and a maximum of 40 km in the Çameli Basin area mapped by us. There is no clear evidence of larger offsets as inferred from regional Miocene tectonism. While this casts doubt on the significance of the Fethiye-Burdur Fault Zone as a crustally significant structure, we note that magnetotelluric studies (Gürer et al., 2004) have been interpreted to show a deep high-conductivity zone associated with the fault zone, which suggests that there is a deeply-descending shear zone below the zone's surface expression.

We conclude that the Fethiye-Burdur Fault Zone is a component of the propagation of the STEP fault zone into the upper plate, but that other structures farther east also may share the strain. Thus the faulting observed in the Eşen Basin (Alçiçek, 2007; ten Veen, 2004), and the complex structures observed in the Anaximander Mountains (Aksu et al., 2009) may also contribute to the strain, perhaps even extending to the faults that delimit the western end of the Antalya basin (Hall et al., 2014b). The STEP fault zone is thus interpreted as a large flower structure, propagating upwards from a simple (who knows?) slab tear in the lower plate to a 50 km wide zone in the area of the Pliny-Strabo Trenches and then to a diffuse array of oblique slip faults across a 150-200 km wide zone extending from the Fethiye-Burdur Fault Zone to the western extremities of the Antalya Basin.

6.8 Conclusions

The Fethiye-Burdur Fault Zone is thus interpreted as part of a transition belt between the Aegean graben system that characterises the back arc region of the Hellenic Arc and the transpressionally-dominated forearc region of the Cyprus and Hellenic arcs. Rotation of small fault blocks within the region accounts for many of the variations in first motions observed from a simpler pattern (e.g., Aksu et al., 2009; Hall et al., 2009; van Hinsbergen et al., 2007). Many of the NE-SW-striking faults mapped offshore (and observed to have dip-slip) are likely extensions of faults onshore known to have normal dip-slip together with variable amounts of sinistral strike-slip. Therefore, it is concluded that the Fethiye-Burdur Fault Zone continues to the southwest but with an approximately 20 km of offset as shown in Figure 6.17, some of which may be taken up across the Gökova-Yeşilüzümlü Fault Zone. Assuming that the overall strike-slip motion across the Fethiye-Burdur Fault Zone is sinistral, the bend along the fault zone is a releasing bend, and likely accompanied by normal faults. In a juvenile fault system such normal faults might be expected to occur in an en échelon fashion and with a N-S orientation. Here, it appears that the strike-slip faults dominate the weak component of rheology of the fault zone imparting a strong anisotropy in strength, and so easily reactivated, rather than inducing new faults. Why the bend in the Fethiye-Burdur Fault Zone occurs here is unknown, perhaps hidden in the complex structures of the older ophiolitic basement. A two-stage history in Pliocene-Quaternary time is suggested, with an early phase of through-going NE-SW faults seen below Marmaris Bay becoming inactive as the Fethiye-Burdur Fault Zone bend developed, to form a simple link with the Pliny-Strabo Fault Zone to the southwest.

At a larger scale, we infer that the Fethiye-Burdur Fault Zone is just the most westerly component of a diffuse array of structures that represent the STEP fault zone in the underlying lower (African) plate. The STEP fault appears to propagate into the upper (Aegean-Anatolian) plate as a flower structure of crustal scale.

7. COMMENT ON ANALYSES OF SEISMIC DEFORMATION AT THE KIBYRA ROMAN STADIUM, SOUTHWEST TURKEY [6]

7.1 Introduction

In southwestern Turkey, a large number of ancient cities lie on the left-lateral Burdur-Fethiye Fault Zone and many of them have been damaged by ancient earthquakes. One of these important ancient cities is Kibyra where the most prominent ancient construction is the stadium. It has been argued that the collapsed rows of seats and damage to the columns in the stadium are directly related to an active NNE-SSW-trending left-lateral fault (Akyüz and Altunel, 1997, 2001; Karabacak, 2011). This view is repeated in the recent article published in Geoarchaeology by Karabacak et al. (2013).

In each summer since 2008, we have carried out field studies in this ancient city participating in the work of the archaeological excavation team. Our role is to map the geological features of Kibyra and the surrounding area and to investigate the earthquake damage. Our studies show that an active left-lateral fault cutting the stadium does not exist—the eastern part of the stadium was constructed on fill and the damage is related to earthquake shaking. We believe that the arguments and observations presented by Karabacak et al. (2013) are misleading in key respects. In this paper, we set out two main objections. The first is related to the evidence presented for the fault displacement and the second to numerous problems with the figures and interpretations. Our criticisms are set out below under two headings.

[6] This chapter is based on the paper “Elitez, İ., and Yaltırak, C. (2014). Comment on Analyses of Seismic Deformation at the Kibyra Roman Stadium, Southwest Turkey by Volkan Karabacak, Önder Yönlü, Eray Dökü, Nafiye Günenç Kıyak, Erhan Altunel, Şükrü Özüdoğru, Cahit Çağlar Yalçıner, and Hüsnü Serdar Akyüz (2014). Geoarchaeology, 29, 349-352”.

7.2 The Fault Cutting the Stadium

Karabacak et al. (2013) put forward three lines of evidence for the fault cutting the stadium: (1) vertical displacement in the trench excavated by Karabacak (2011) in the base of the stadium, (2) displacement of the seat rows, and (3) displacement of the eastern wall.

1. Karabacak et al. (2013) present LIDAR data measurements for a trench and assert a vertical displacement in the base of the stadium (Figure 5 in their paper). In order to check these data, a new trench was excavated in front of the half buried row of the southern seat rows with the help and permission of the archaeologists in summer 2013. Our observations show that there is no displacement on the lowermost row or deeper underground levels. Increasing separation of the southern seat rows at higher levels can be seen (Figure 7.1a) but it does not indicate a fault. These seat rows most likely collapsed as a result of the earthquake shaking effect.

2. As a result of the excavation and cleaning of the southern part of the collapsed seat rows, it is now clear that the stable seat rows are located on the bedrock (conglomerate) but not on a coarse grained, weakly cemented, and loose artificial fill (Figure 7.1b). At the point where the asserted fault is shown (Figure 4b in their paper), the soil on the bedrock was removed by us and no fault was found in the conglomerate bedrock (Figure 7.1c).

3. We carefully examined the location of the photograph that shows a displacement on the eastern wall (Figure 4d in their paper) and concluded that the asserted displacement is an artifact of the angle of the photograph. For this reason, a new photograph was taken from the same viewpoint and it is presented with the original one (Figure 7.1d and 7.1d). We also took two photographs both on and in front of the wall (Figure 7.1f and 7.1g). These photographs do not show any displacement of the wall.

According to the evidence given above, we argue that the views presented in Karabacak et al. (2013) about “the fault cutting the stadium” are incorrect—they are speculative and unsupported by data.

Figure 7.1 : (a) The trench excavated in front of the southern seat rows. The yellow dashed line indicates the supposed Kibyra Fault. The scale in the trench is 50 cm. (b) The southern entrance to the stadium. The yellow dashed line shows the boundary between the conglomerates and the artificial fill. The yellow rectangle shows Figure 7.1c. (c) The conglomerates of the bedrock. (d) The photograph of the asserted displacement on the eastern wall of the stadium taken by Karabacak et al. (2013). (e) The photograph taken for this study in order to show the viewpoint of the photograph. (f) The original position of the wall. The red arrow indicates the point of the asserted displacement. (g) The side view of the wall. The red arrow indicates the point of the asserted displacement.

7.3 Interpretation and Figure Errors

1. Karabacak et al. (2013) show a fallen block at the northern entrance (Figure 3D in their paper). It is asserted in their paper that this collapsed column is orientated in a westward direction. Considering the original shape of this column (Figure 7.2a), the fallen column must have collapsed in an eastward direction (Figure 7.2b).

2. The locations of Figures 4d and 9b shown in Figure 7.2b of Karabacak et al., 2013 are wrong. The true locations are marked as blue rectangles on the aerial photo (Figure 7.2c). Although Figure 2b in Karabacak et al. (2013) was described as a Google Earth satellite image in the caption, it is an aerial photo taken from a balloon by the archaeologists working in the ancient city of Kibyra.

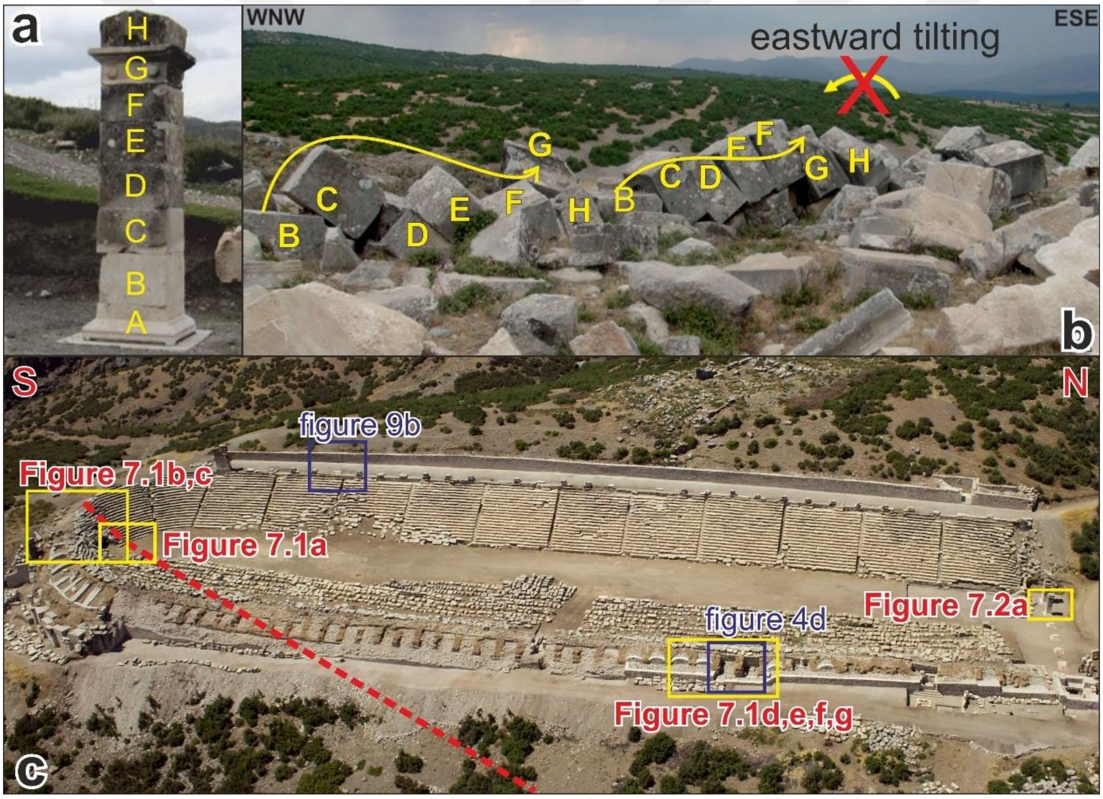

Figure 7.2 : (a) An original column of the northern entrance. The yellow letters show the array of the blocks on an original column. (b) A fallen column shown by Karabacak et al. (2013). The yellow letters show the array of the blocks on an original column. (c) The aerial photo of the ancient stadium. The red dashed line indicates the direction of the supposed Kibyra Fault. The yellow rectangles show the locations of the figures in this study. The blue rectangles show the locations of Figures 9b and 4d in Karabacak et al., 2013.

3. Karabacak et al. (2013) state that the stadium was built on bedrock (Figure 7 in their paper). The ground level of the eastern wall of the stadium is about 10 m below the

stadium floor (see Figure 7.2c). Özüdoğru et al. (2011) indicate that the blocks taken out of the western hill for the construction of the western seat rows were used during the construction of the eastern wall on which the eastern seat rows were placed. Therefore, it is clear that the reason for the damage to the eastern side of the stadium is the seismic response of the fill.

7.4 Conclusion

There is no doubt that earthquake damage has affected the ancient city of Kibyra. However, all of the damage described by Karabacak et al. (2013) has in fact been observed in the artificial fill. Other further damage was most likely caused by ground shaking but there is no evidence directly indicating a fault cutting the stadium. In conclusion, it is recommended that the arguments, observations, and interpretations in Karabacak et al. (2013) must be reviewed.

8. REPLY TO THE COMMENT ON "THE FETHIYE-BURDUR FAULT ZONE: A COMPONENT OF UPPER PLATE EXTENSION OF THE SUBDUCTION TRANSFORM EDGE PROPAGATOR FAULT LINKING HELLENIC AND CYPRUS ARCS, EASTERN MEDITERRANEAN" [7]

8.1 Reply to Comments by Alçiçek on the Hall et al. (2014) Manuscript

In his comments on the Hall et al. (2014a) paper (Chapter 6 in this thesis), Alçiçek (2015) focuses on the onland portion of our study area, and argues that there is no evidence — from GPS vectors, fault plane solutions of earthquakes, subsurface data, and field mapping including observed fault kinematics — for left-lateral strike-slip along the NE-trending zone which we describe as the Fethiye-Burdur Fault Zone (also known as the Burdur-Fethiye Fault Zone). He also disputes our interpretation of local stratigraphy. We provide counter arguments below and shown strong evidence for the presence of a 75-90 km wide Fethiye-Burdur Fault Zone developed as a left-lateral shear zone connecting toward the southwest with the offshore Pliny-Strabo Fault Zone.

8.1.1 GPS vectors

In Figure 8.1, we add information to Figure 6.20, using the same sources, to show that there is differential motion across our interpreted Fethiye-Burdur Fault Zone. Close to the Turkish coast, the GPS vectors directed to the southwest vary from 25 mm yr^{-1} on the northwest side of the zone to 13 mm yr^{-1} on the southeast side of the zone. The simplest interpretation of this is that there is a left lateral displacement of 12 mm yr^{-1} across the Fethiye-Burdur Fault Zone. Farther to the northeast, the differential motion across the Fethiye-Burdur Fault Zone (Aktuğ et al., 2009) would be 7 mm yr^{-1}. This supports our interpretation of left lateral displacement decreasing to the northeast, as would be expected of a break in the downgoing slab of the African plate as it

[7] This chapter is based on the paper "Elitez, İ., Yaltırak, C., Hall, J., Aksu, A. E., and Çifci, G. (2015). Reply to the comment by M.C. Alçiçek on "The Fethiye-Burdur Fault Zone: A component of upper plate extension of the subduction transform edge propagator fault linking Hellenic and Cyprus Arcs, Eastern Mediterranean," Tectonophysics, 635, 80-99, by J. Hall, A.E. Aksu, İ. Elitez, C. Yaltirak and G. Çifçi. Tectonophysics, 664, 5-13".

propagates into the upper Aegean-Anatolian Microplate. We note that such motion, if continued over 5 Ma, would give an overall displacement of a few tens of kilometres, distributed over the width of the Fethiye-Burdur Fault Zone (i.e., around 75-90 km). This strain, distributed over many faults, would only result in small offsets across individual faults (especially those seen in younger Quaternary strata).

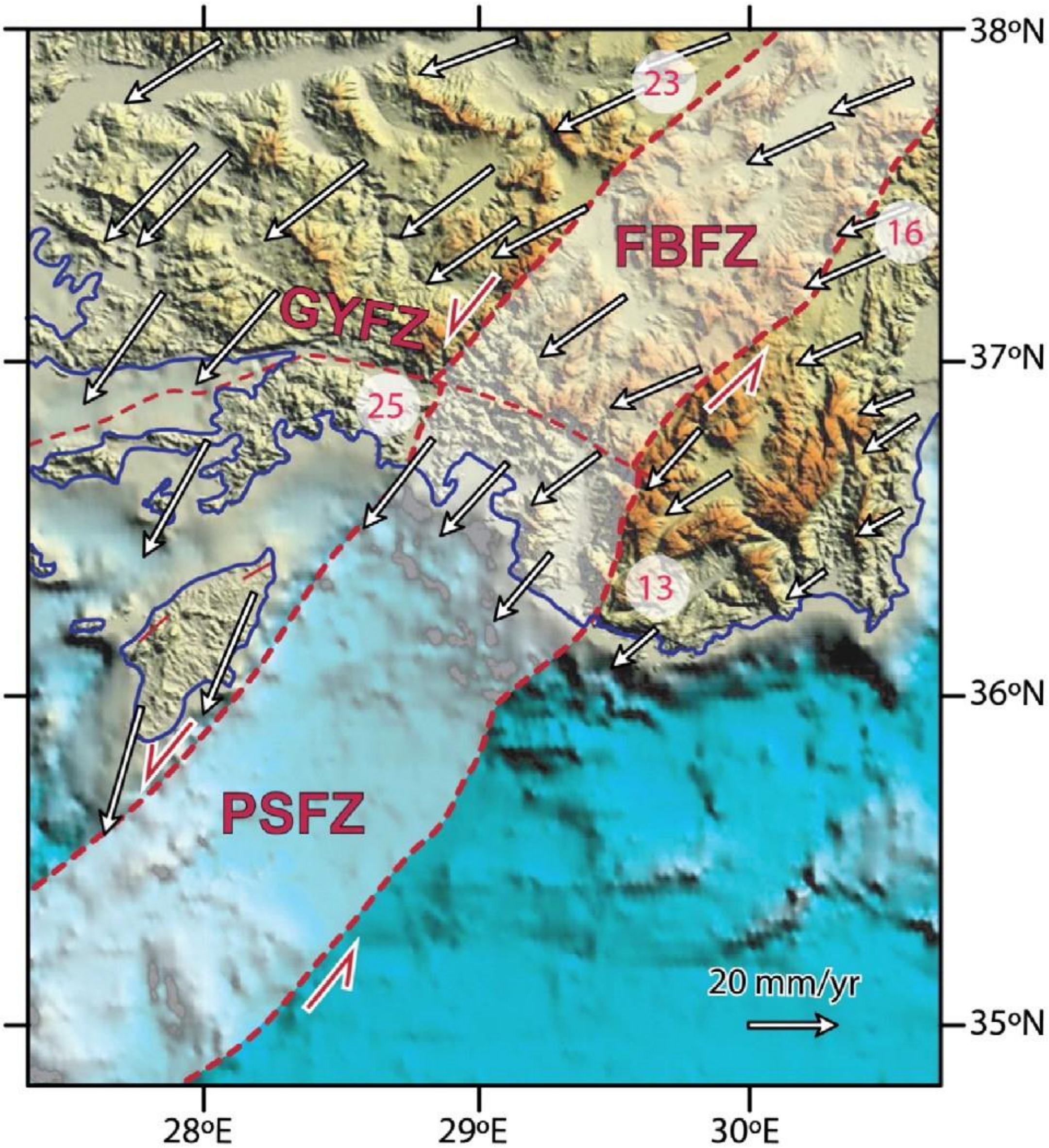

Figure 8.1 : GPS vectors relative to fixed Eurasian Plate. Data from Reilinger et al., 1997, 2010; McClusky et al., 2000; Hollenstein et al., 2008; Aktuğ et al., 2009; Floyd et al., 2010).

8.1.2 Fault plane solutions of earthquakes

The same Figure 6.20 shows a series of 26 'beach ball' first motion plots from earthquakes as interpreted in the five referenced source papers. These show a diversity of fault motions including a number of left-lateral strike-slip or oblique slip motions (including some within the Fethiye-Burdur Fault Zone), assuming the causative fault trend sub-parallel to the Fethiye-Burdur Fault Zone.

8.1.3 Subsurface data

The magnetotelluric studies of Gürer et al. (2004) show two deep high conductivity zones in the upper crust which lie centrally within our Fethiye-Burdur Fault Zone (Figure 8.2) in direct contradiction to Alçiçek's (2015) contention that the zones do not coincide. Alçiçek (2015) claims that the Burdur-Fethiye Fault Zone shown in Gürer et al. (2004) is in fact a separate fault (he calls it the Fethiye-Bucak fault zone), and shows, in support, the 070° strike-slip fault lines postulated by ten Veen (2004) running through Crete, Rhodes, and the Eşen Basin. We disagree with Alçiçek (2015): a comparison between Figure 6.19 and Figure 2 of Gürer et al. (2004) clearly shows that two deep high conductivity zones in the upper crust lie within the Fethiye-Burdur Fault Zone defined in Hall et al. (2014a; Chapter 6 in this thesis; Figure 8.2). We interpret these high conductivity zones to represent the deeper extensions of the Fethiye-Burdur Fault Zone (as also did Gürer et al., 2004), showing it to be a deeply-rooted structure in agreement with our original interpretation of this zone in Hall et al. (2014a; Chapter 6 in this thesis) as a structure related to the upward propagation of a break in the downgoing African Plate.

8.1.4 Field mapping

In Hall et al. (2014a; Chapter 6 in this thesis) we referenced Elitez (2010) MSc thesis and two conference papers (Elitez and Yaltırak, 2014a; Elitez et al., 2009) which were either early or brief descriptions of a substantial mapping campaign in the area of the Fethiye-Burdur Fault Zone, now more fully documented in Elitez and Yaltırak (2014c). Our field mapping at 1:25.000 scale included >3000 field measurements, >400 fault plane measurements, around 200 km of traversing and a spatial resolution as high as 1-3m.

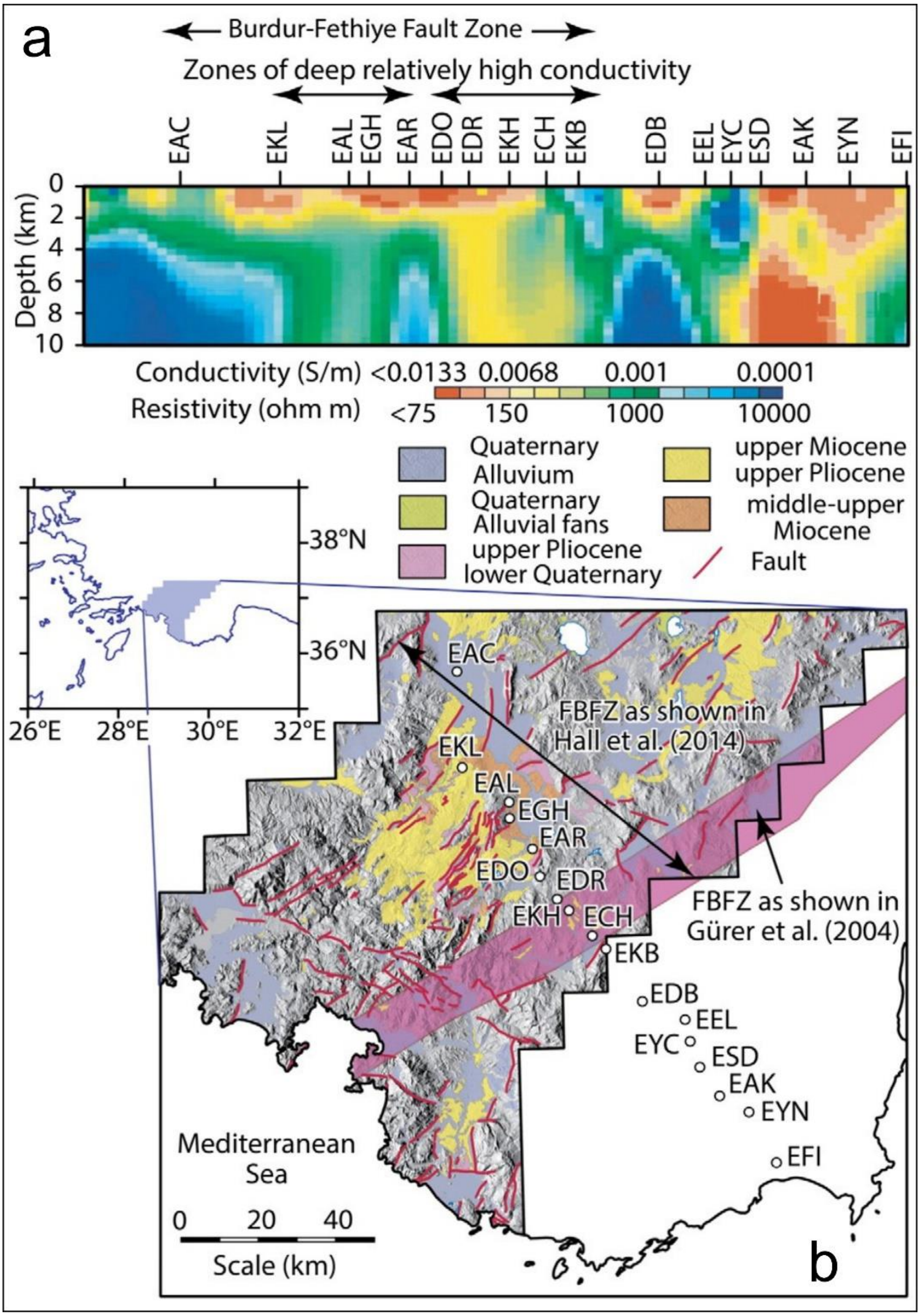

Figure 8.2 : (a) Summary magnetotelluric profile of Gürer et al. (2004) showing the zones of deep relatively high conductivity corresponding with (b) the Burdur-Fethiye Fault Zone published in Hall et al. (2014a; Chapter 6 in this thesis) and Elitez and Yaltırak (2014c)

Alçiçek (2015) stated that "… in their Figures 19 and 20, some manipulated faults are running NE-SW direction. However, in the complete map of the region compiled by MTA (Mineral Research and Exploration Directorate, i.e., Geological Survey of Turkey; Konak, 2002; Konak and Şenel, 2002; Şenel, 2002; Turan, 2002) band the papers dealing with the mapping particular areas of SW Anatolia (e.g. Alçiçek, 2007; Alçiçek et al., 2006; Price and Scott, 1994; ten Veen, 2004) document multidirectional faulting". The suggestion that we have manipulated data is an unfortunate and unprofessional allegation. Alçiçek (2015) claims that the map published in Figure 19 of Hall et al. (2014a; Figure 6.19 in this thesis) is "extracted" but "not cited" by the authors. We categorically disagree with Alçiçek (2015). Figure 8.3 shows a segment of the map published in Hall et al. (2014a; Chapter 6 in this thesis) and Elitez and Yaltırak (2014c). The reader can clearly see that our mapping is not plagiarised from MTA maps!

Alçiçek relies on the previously published low-resolution MTA maps which, in this area, are at 1:100.000 and 1:500.000 scale. The MTA maps are compiled by scanning various scale old paper maps and splicing of various map sheets to form the 1:100.000 and 1:50.000 scale maps. Subsequently, these spliced maps were re-digitised to create the presently available 1:100.000 and 1:500.000 scale map series. The resulting maps invariably have varying degrees of distortions particularly on the spatial resolution of the geological contacts and faults, but further lack the resolution to carry out detailed kinematic studies. Our mapping is on 1:25.000 scale digital terrain basemaps, incorporating the best available satellite imaging. The original maps that we produced and published in Hall et al. (2014a; Chapter 6 in this thesis) and Elitez and Yaltırak (2014c) have 1-3 m spatial resolution. We note that when we compare the geological contacts and/or specific locations with the previously published MTA maps, we see that there is between 500 m and 5 km spatial inconsistencies with our measurements. The lack of reliability of the MTA maps and the difficulties of correlating structures observed in the field with the previously published maps were the primary motivation for carrying out the detailed geological mapping exercise that we started in 2008. Alçiçek appears to be unaware of these distortion issues, spatial resolution difficulties and correlation inconsistencies between the MTA maps and the GPS-guided field observations, thus used the MTA maps in his doctorate (Alçiçek, 2001) and continues to use these maps in his subsequent studies (e.g., Alçiçek, 2007; Alçiçek et al., 2004,

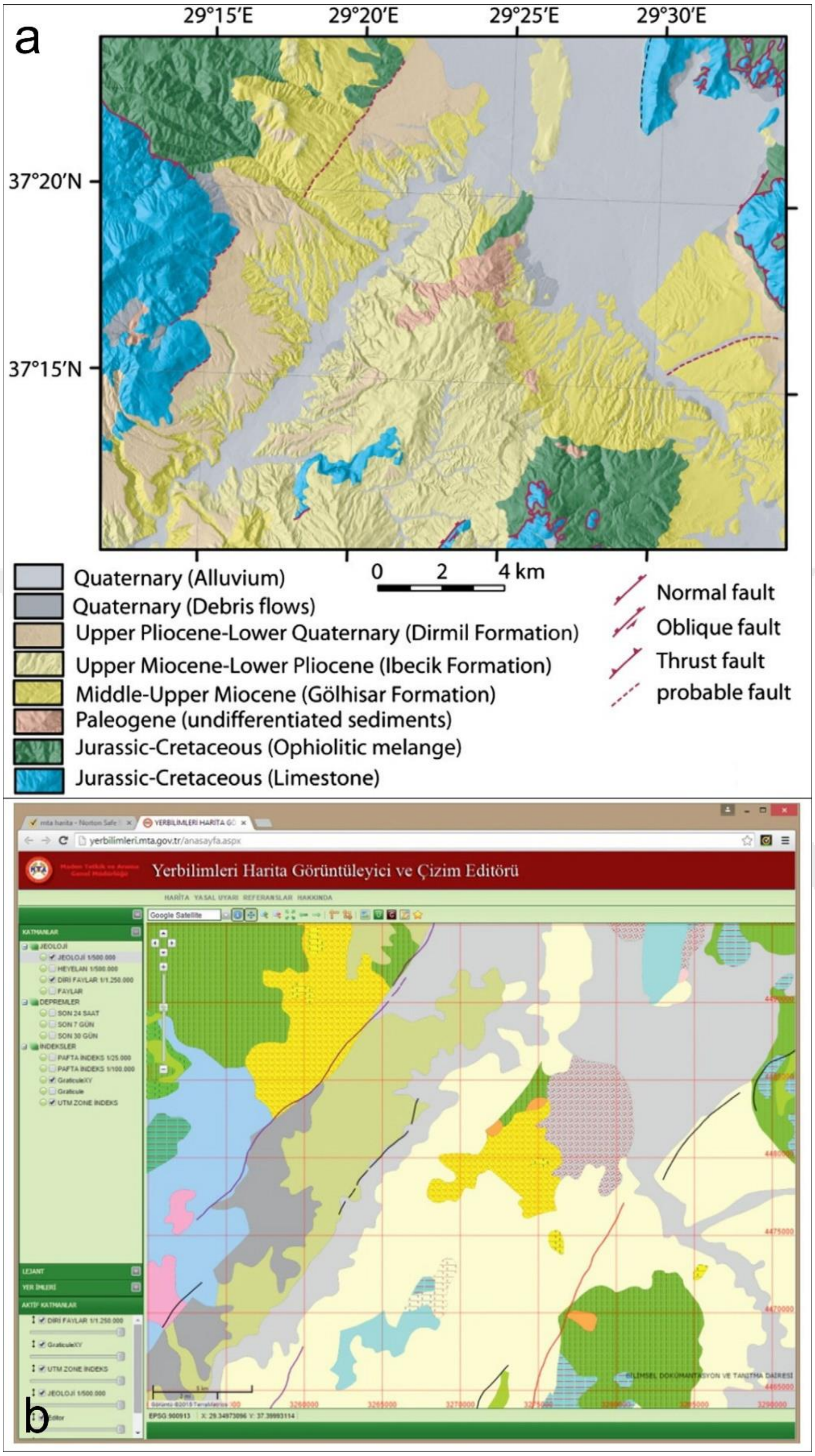

Figure 8.3 : Comparison between the (a) the geological map compiled by Elitez (2010) and Elitez and Yaltırak (2014c) and (b) the map published by the Mineral Research and Exploration Directorate of Turkey — MTA (http://yerbilimleri.mta.gov.tr/anasayfa.aspx). The geological map in (a) is claimed by Alçiçek (2015) as taken from the MTA map; however, the details of the map by Elitez (2010) and Elitez and Yaltırak (2014c) are clearly not seen in the MTA map, in stark contrast of the claim by Alçiçek (2015).

2005, 2006, 2012). It is noteworthy to point out that the maps that we published in Hall et al. (2014a; in this thesis) and Elitez and Yaltırak (2014c) have considerably more fault traces but furthermore, only a very small percentage (<20%) of the faults shown in Alçiçek et al. (2004, 2005, 2006, 2012) and Alçiçek (2007) can be confirmed in our detailed mapping. Alçiçek (2015) refers to our work as “manipulation”: we call it detailed mapping!

8.1.5 Lineations

Alçiçek (2015) presented the lineament map published by ten Veen et al. (2009) and claimed that faulting is “multidimensional”. We do not dispute that, but we do claim that there is a distinct set of northeast-southwest trending fault lineations in the area. The map presented by ten Veen et al. (2009) is produced by satellite-based 30 m resolution DEM (30 m × 30 m = 1 pixel) where the SRTM data were obtained from the USGS Seamless Data Distribution System.On the other hand, we produced a 1:25.000 scale map, using the 1:10.000 scale air photos (6 m × 6 m = 25 pixels) from the General Command of Mapping (Harita Genel Komutanlığı), thus our data base has 5 times higher spatial resolution than the map published by ten Veen et al. (2009). The SRTM data are compilations of images obtained by satellites looking at Earth at different angles and the DEM obtained fromsuch data often creates artificial lineaments that do not exist in topography (de Oliviera and de Fatima, 2012; Gómez et al., 2012). Thus, it is clear that not all the lineaments obtained in SRTM data are real and that care must be exercised in comparing and contrasting the lineations obtained by SRTM with topographic and geological field observations. Recent comparisons between the SRTM and higher resolution satellite imagery clearly documented that many of the lineations mapped using the SRTM data are found to be artificially created when compared to higher resolution satellite data (e.g., de Oliviera and de Fatima, 2012; Gómez et al., 2012). Figure 8.4a shows the digital elevation model of southwestern Turkey published by ten Veen et al. (2009) where the onshore elevation data come from the SRTM data obtained from USGS Seamless Data Distribution System (seamless.usgs.gov). Here we colour-coded three prominent lineament orientations (Figure 8.4a). We subsequently separated these three colours and plotted them together with the view direction (solid coloured lines, Figures 8.4b, c, d). It is clear that there are three distinct bundles of coherent lineations in the map published in ten Veen et al. (2009). Considering the fact that the SRTM data can readily create artificial lineations, the validity of the lineaments of the map published by ten Veen et al. (2009) must be confirmed by field studies. Our detailed field study confirmed the presence of the northeast-southwest trending lineations as the imprints of the similarly striking faults within the Fethiye-Burdur Fault Zone: however, the east-northeast lineations (i.e., 070°) postulated by ten Veen (2004) remain untested in detailed field mapping.

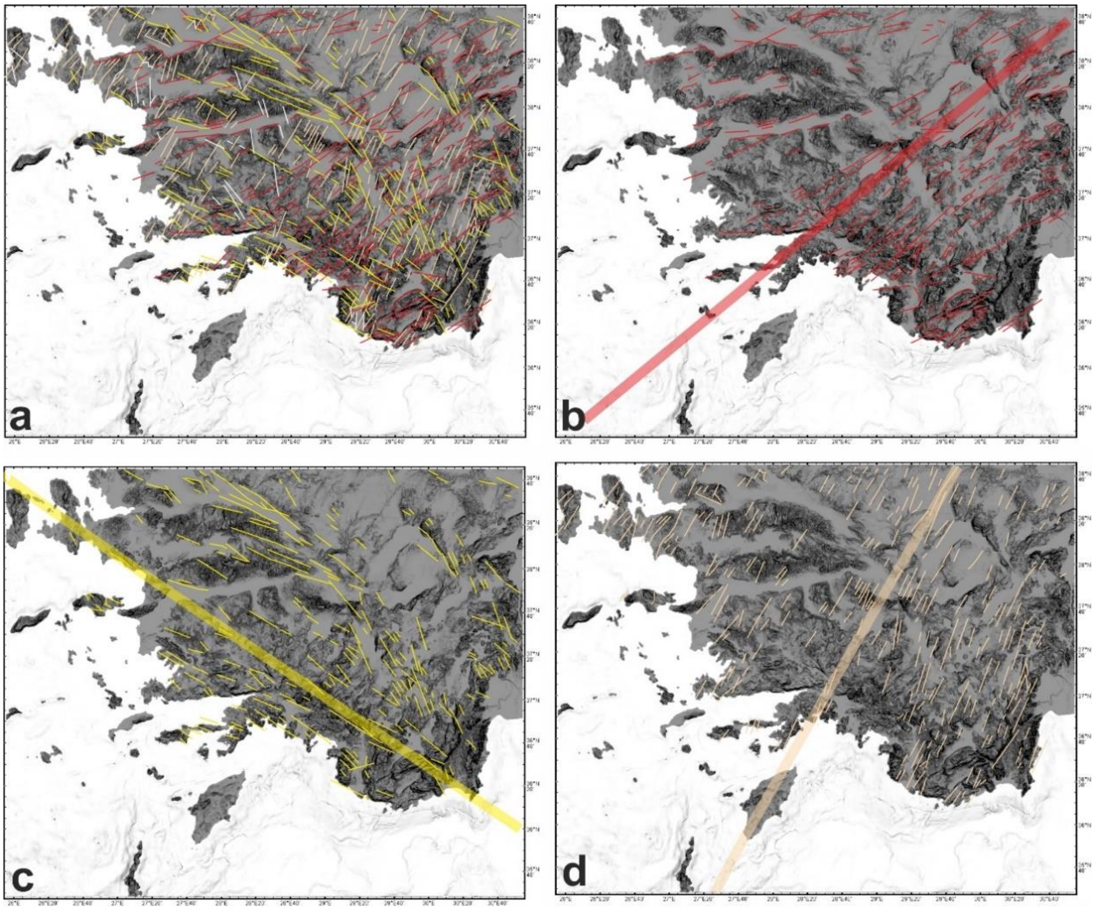

Figure 8.4 : (a) Lineation map published by ten Veen et al. (2009), compiled using the SRTM data obtained from USGS Seamless Data Distribution System. (b, c, d) Three distinct bundles of coherent lineations of the map shown in (a).

8.1.6 Fault kinematics and paleomagnetic data

We have measured over 400 major and over 1350 minor faults, to determine their kinematics in our onland mapping area. Slickensides show variable pitches, some steep, some quite shallow (Figure 8.5). The shallow pitch indicates oblique slip, so that many of the ‘normal’ faults in the area have a strong strike-slip component of displacement.

Alçiçek (2015) stated that seismological and kinematic observations by Över et al. (2010) support his tectonic interpretations. Över et al. (2010) measured the slickensides of 20 fault planes and used the fault plane solutions of 12 Mw 4.1-5.3 earthquakes in their study of the Çameli Basin. On the other hand, Elitez (2010) and Elitez and Yaltırak (2014c) measured the slickensides of 432 fault planes within the Çameli, Acıpayam, Gölhisar and Atlınyayla and other Neogene basins, and clearly documented that the tectonic evolution of these basins is controlled by a large northeast-southwest striking left-lateral shear zone. These data are not reconcilable with the horst and graben model of Alçiçek et al. (2004, 2005, 2006). Furthermore, the fault plane solutions published by Över et al. (2010, 2013a, b) can be clearly used to support tectonic development associated with a left lateral shear zone.

Figure 8.5 : Photograph showing slickensides of a fault at 36°59′29.46″ and 29°25′4.26″E. Note the slickensides pitch at a shallow angle down to the right, demonstrating oblique slip with a strong horizontal component.

Alçiçek (2015) cites two new publications by Özkaptan et al. (2014) and Kaymakçı et al. (2014) to further his claim that there is no left lateral strike slip across the Fethiye-Burdur Fault Zone. He specifically stated that "… more recently the left lateral transtensional feature has put doubt by Kaymakçı et al. (2014) whose observed no change in the rotations senses and amounts on either side of the proposed Fethiye-Burdur Fault Zone implying no differential rotation on the basis of paleomagnetic and kinematics. The slickensides and paleostress configurations along the proposed zone are consistent with focal mechanisms indicating normal sense and no data supporting strike-slip but dominated by extensional deformation…" Barka et al. (1997) suggested that there is a narrow northeast-southwest trending left-lateral fault zone in southwestern Turkey, naming it as the Burdur-Fethiye Fault Zone. Kaymakçı et al. (2014) and Özkaptan et al. (2014) used paleomagnetic and fault kinematic data across the region shown in Barka et al. (1997) and indicated that their data do not support the presence of the Fethiye-Burdur Fault Zone. However, the reader must be reminded that the Fethiye-Burdur Fault Zone is a broad 75-90 km wide and 300 km long zone that extends from the present-day shoreline to the Burdur Lake in west-central Anatolia. Thus, it is not surprising that the narrow band of ~10 km that Kaymakçı et al. (2014) and Özkaptan et al. (2014) studied, in the middle of the ~75-90 km Fethiye-Burdur Fault Zone, did not show significant rotations or paleomagnetic anomalies. These authors were simply looking for the Fethiye-Burdur Fault Zone in the wrong place.

8.1.7 Summary of evidence for left-lateral strike slip in the Fethiye-Burdur Fault Zone

As repeated above, GPS vectors, earthquake first motions and fault kinematics support the existence of left-lateral strike-slip across the Fethiye-Burdur Fault Zone. Magnetotelluric data (Gürer et al., 2004) suggest that the Fault Zone may extend down into at least the midcrust (Figure 8.2), in support of our notion that it might connect downwards with the slab tear in the downgoing plate.

8.1.8 Other points of dispute

8.1.8.1 Dinar Fault Zone

Alçiçek states that we ignored the NW-trending Dinar Fault Zone in Figure 8.19 (Hall et al., 2014a; Chapter 6 in this thesis) and suggests that there is no offset in the Dinar Fault by the proposed Fethiye-Burdur Fault Zone. He is correct that we have inadvertently omitted the Dinar Fault Zone, southwest of the similarly striking Keçiborlu-Çobansaray Fault Zone (Figure 8.6). The left lateral offsets are difficult to see in the regional map published by Hall et al. (2014a; Chapter 6 in this thesis); however, they are clearly visible when a smaller area is presented (Figure 8.6). This shows exactly what is expected to be seen in a left-lateral shear zone where the northwest-southeast striking faults naturally develop. We show several such faults in our regional map such as that seen between Salda and Akgöl, the southwest margin of the Eğridir Lake, the Dinar Fault Zone, the Keçiborlu-Çobansaray Fault as well as numerous northwest-southeast striking faults across the southwestern segment of the map area (Hall et al., 2014a; Chapter 6 in this thesis).

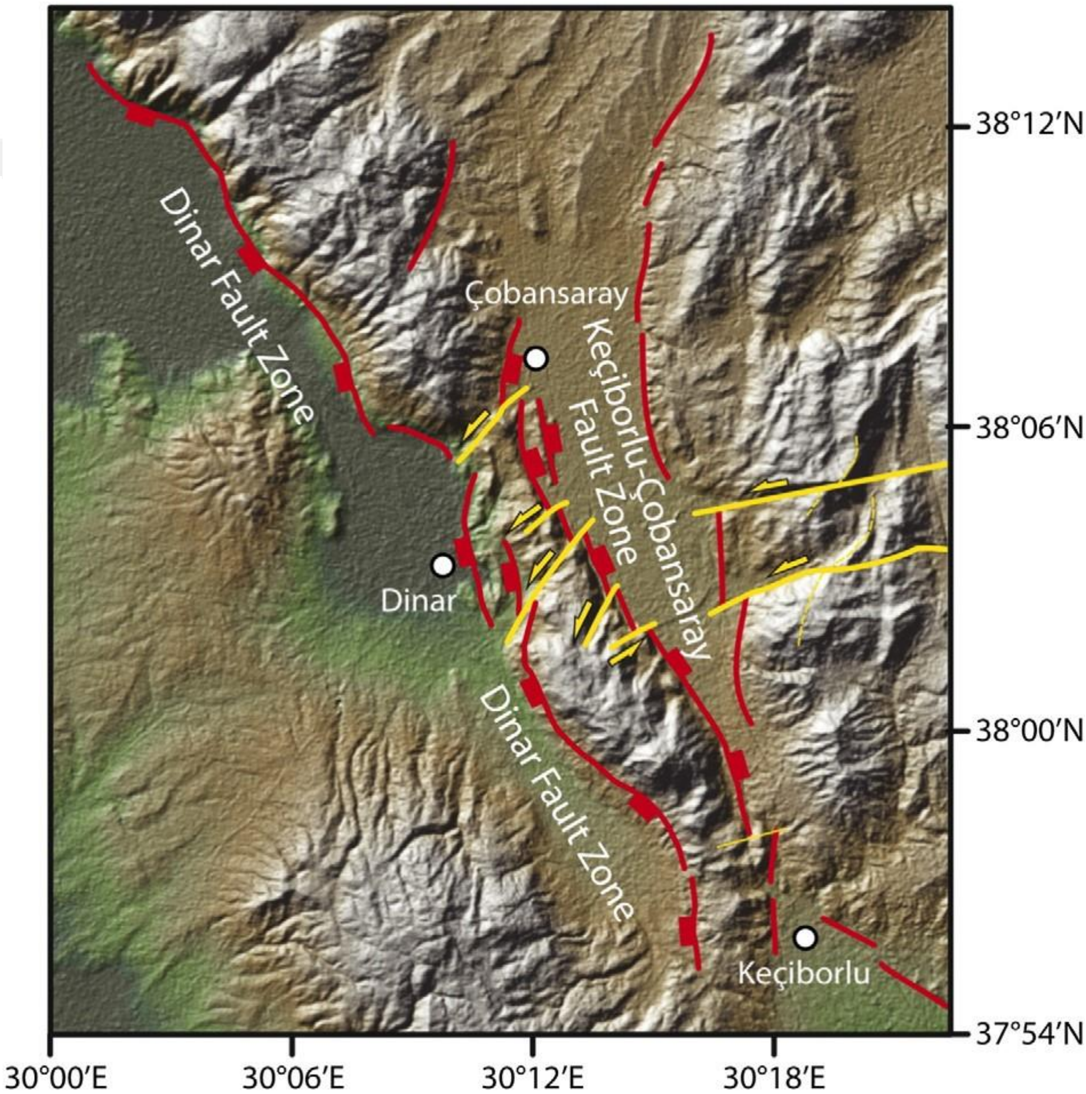

Figure 8.6 : Morphotectonic map of the Dinar and the Keçiborlu-Çobansaray Fault Zones.

8.1.8.2 Stratigraphy

Alçiçek (2015) criticises our age re-assignment of the terrestrial Gölhisar Formation to middle-upper Miocene, because he believes based on the MTA map that the middle

Miocene successions in the Çameli Basin are marine (Figure 8.7). However, field observations and detailed mapping in the vicinity of the Köke town (37.343875° N, 29.384249° E) show that the succession described as marine middle Miocene is indeed characterised by conglomerate, fine sandstone and marl interbeds, physically indistinguishable from the upper Miocene-lower Pliocene Ibecik Formation described and mapped elsewhere. In fact, the same middle Miocene succession is shown to be present in the MTA maps south of Acıpayam along the western shores of the Dalaman River, yet the succession along the eastern shores of the river is strangely labelled as Pliocene. Marine middle Miocene is not reported anywhere in southwestern Anatolia, including the Büyük Menderes Graben and the region surrounding the city of Denizli (Alçiçek, 2010; Alçiçek et al., 2007; Wesselingh et al., 2008).

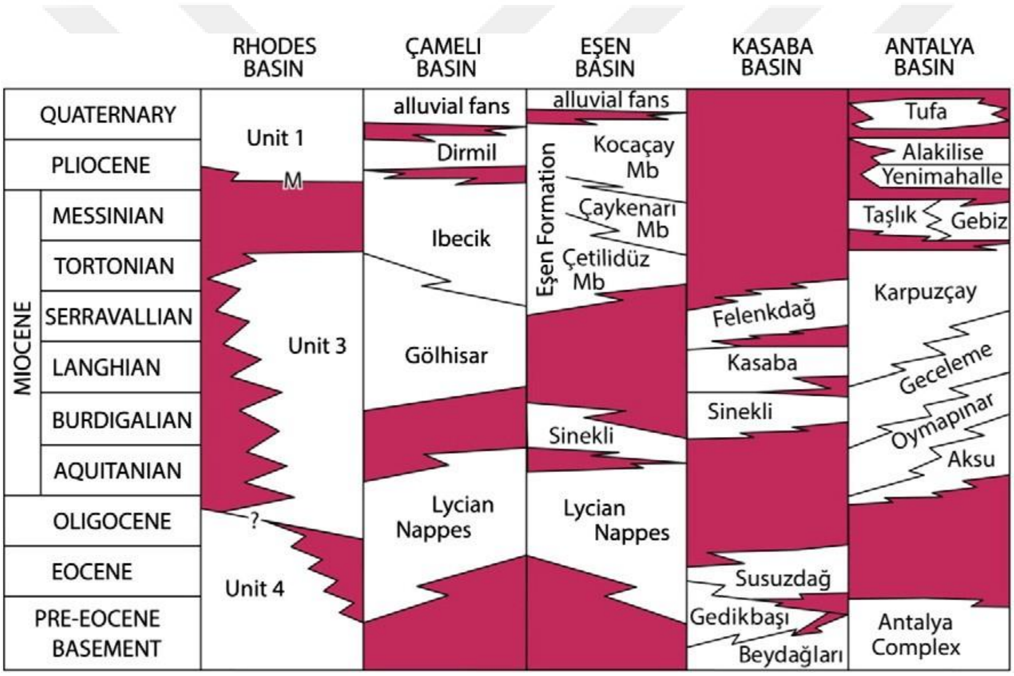

Figure 8.7 : Revised chronostratigraphy of the marine Rhodes Basin and the onland Çameli and Eşen basins, compiled from: Çameli Basin = Elitez and Yaltırak (2014c), Eşen (Çay) Basin = Alçiçek et al. (2006); Alçiçek (2007); Kasaba Basin = Hayward (1984); Şenel (1997a,b); Şenel and Bölükbaşı (1997); and Antalya Basin, including the onland Aksu, Köprüçay and Manavgat basins = Akay and Uysal (1985); Akay et al. (1985); Flecker et al. (1998); Karabıyıkoğlu et al. (2000, 2005); Işler et al. (2005).

Alçiçek (2001, 2010) provided a Tortonian (MN9-10; 9-11.1 Ma; Valessian) age for the uppermost 200 m of the Ibecik Formation based on a vertebrate fossil found in a coal mine at the base of lagoonal limestones in Elmalıyurt within the Gölhisar Basin at an elevation of 2000 m above datum (personal communication Alçiçek, 2015). At this site the Ibecik Formation is ~850 m thick. The total thickness of the Gölhisar and Ibecik formations are ~1500 m (Elitez, 2010; Elitez and Yaltırak, 2014a, c). The upper age of the Ibecik Formation is determined by two $^{40}Ar/^{39}Ar$ radiometric dates of 6.28 ± 0.48 and 6.00 ± 1.54 on the lamproite volcanics (Paton, 1992). Thus, the upper ~200 m sediments in the Ibecik Formation were deposited in ~3-5 Myr, suggesting a sedimentation rate of 40-70 m per Myr. These two ages bracket the depositional interval for the upper Ibecik Formation to between 9-11.1 Ma and 6.0-6.3 Ma, thus, an upper Miocene age for the Ibecik Formation as suggested by Elitez (2010) and Elitez and Yaltırak (2014a, c). Alçiçek (2001) and Alçiçek et al. (2004) also consider the remaining ~1300 m of the Gölhisar and Ibecik formations as Tortonian (Vallesian) age, which requires an unrealistic sedimentation rate of 300-500 m per Myr for lacustrine deposits, which is more typical of sedimentation within flysch-molasse basins. Considering the 200 m thickness of the Tortonian limestone overlying the ~1050 m thick middle-upper Miocene succession near Denizli (Alçiçek, 2010; Alçiçek et al., 2007; Wesselingh et al., 2008), immediately north of the Acıpayam-Çameli-Gölhisar basins, the proposed middle-upper Miocene age for the Gölhisar Formation (Elitez, 2010; Elitez and Yaltırak, 2014a, c) is not unrealistic. Alçiçek (2015) refers to Figure 8.5 of Hall et al. (2014a; Chapter 6 in this thesis) and correctly points out that there is no lower Miocene in the Eşen Basin. We include a revised chronostratigraphic chart correcting this error (Figure 8.7).

8.1.9 Models of deformation in the Fethiye-Burdur Fault Zone

8.1.9.1 NW-SE extensional system

Alçiçek (2001) and Alçiçek et al. (2004, 2005, 2006, 2013) suggested that the northeast-southwest striking faults in the Çameli Basin (Figure 8.8a) are developed as the result of a northwest-southeast oriented extensional system. However, these studies do not explain the rhombohedric geometric relationships between these faults and the proposed extensional system, nor do they account for the oblique slip observed.

8.1.9.2 Pull-apart basin

The abrupt termination of the northeast-southwest striking faults across the northeastern and southwestern margins of the Çameli Basin (Figure 8.8a) requires that the basin is bounded in the northeast and southwest by prominent right-lateral transfer faults, as shown in Figure 8.8b. This is a classic pull-apart structure, however, there is no evidence for the required northwest-southeast striking bounding faults in our detailed field maps (Elitez and Yaltırak, 2014c) and such faults are also not shown in Alçiçek et al. (2004, 2005), suggesting that the Çameli Basin did not evolve as the result of pull-apart.

8.1.9.3 NE-SW-oriented compression

An alternative possibility is a northeast-southwest oriented regional compression which would ultimately result in secondary northwest-southeast extension (Figure 8.8c). However, the absence of northwest-southeast oriented folding and/or thrusting in the field studies preclude this alternative as a viable option for the evolution of the Çameli Basin.

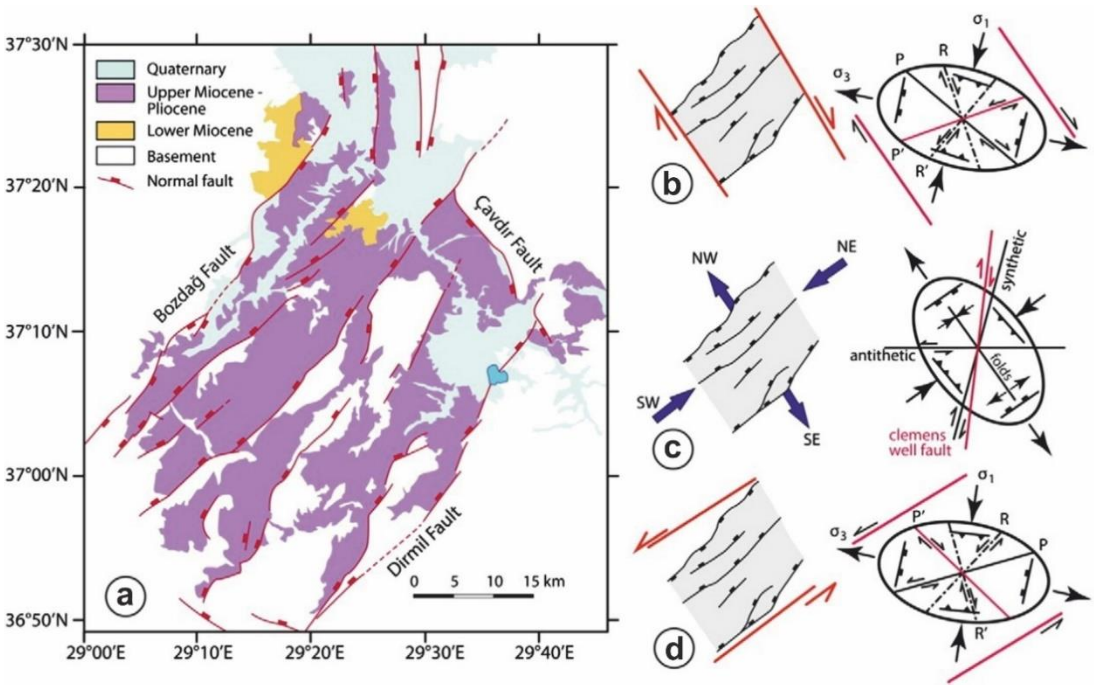

Figure 8.8 : (a) Simplified tectonic map of Alçiçek et al. (2004); and strain ellipsoids showing possible basin development and fault orientations associated with (b) right-lateral strike-slip system, (c) NE-SW directed compression and (d) left-lateral strike slip system (our preferred model).

8.1.9.4 NE-SW-trending left-lateral shear zone

Hall et al. (2014a; Chapter 6 in this thesis) proposed that the horst-graben structures of Alçiçek et al. (2004, 2005), i.e., the northeast-southwest striking normal faults with left-lateral strike slip components, are developed within a prominent northeast-southwest trending left-lateral shear zone that created parallel faults that exhibit both normal and strike slip components (Figure 8d; also see Elitez and Yaltırak, 2014c). The development of such faults within a shear zone is also experimentally shown by

Schreurs and Colletta (1998, 2003). The northeast-southwest trending large open folding that is observed in the Çameli Basin (Elitez and Yaltırak, 2014c) is a notable feature that is observed in such shear zones (e.g., Fossen et al., 2013).

8.2 Conclusion

In contradiction of the claims of Alçiçek (2015-in this volume), we have shown strong evidence for a 75-90 km wide Fethiye-Burdur Fault Zone, generated as a left-lateral shear zone, and likely connected vertically at depth with a tear in the downgoing African plate slab. As would be expected of a fault zone propagating upwards and outwards from a tear in the southerly lower plate, the shear zone diminishes northwards in the upper plate.

Because we suggest that the fault propagates upwards and northwards through the upper plate, and so diminishes in significance from Fethiye towards Burdur, we call it the Fethiye-Burdur Fault Zone, although it has also been called the Burdur-Fethiye Fault Zone in the literature. The terms are intended to be synonymous at least in the works of our group.

9. VEGETATION AND CLIMATE CHANGES DURING THE LATE PLIOCENE AND EARLY PLEISTOCENE IN SW TURKEY - COMMENT TO THE PUBLISHED PAPER BY JIMÉNEZ-MORENO ET AL., QUATERNARY RESEARCH, 84 (2015), 448-456[8]

9.1 Introduction

There are several Miocene to recent terrestrial and lacustrine basins along the NE-SW-trending Burdur-Fethiye Shear Zone in southwestern Turkey (Elitez and Yaltırak, 2014c; Hall et al., 2014a; Elitez et al., 2015). The stratigraphic positions of the sequences in these basins are controversial (e.g., Alçiçek, 2015; Elitez et al., 2015). Jimenez-Moreno et al. (2015) interpreted the late Pliocene-early Pleistocene climate based on the vegetation changes at the Ericek and Bıçakçı localities south of the Çameli town. Our observations at these localities (e.g., Elitez et al., 2015) revealed that there are three important geological problems with Jiménez-Moreno et al. (2015): (1) the geographic locations of the samples used in this manuscript are inaccurate, (2) the lithologies and the associated thicknesses of the sequences reported in the manuscript are inconsistent, and (3) the positions of the fossils and pollens in an allochthonous stratigraphic succession has no stratigraphic control. The primary aim of this comment is to correctly identify the precise positions of the fossil and pollen data in the stratigraphic sequence rather than an objection to the interpretation of the vegetation and climate data in southwestern Turkey.

9.2 Localities, Observations, and Field Problems

9.2.1 Bıçakçı locality

It is impossible to find the Bıçakçı locality by using the coordinates (37°00′53″ N, 29°17′57″ E) given in the manuscript by Jiménez-Moreno et al. (2015). Furthermore,

[8] This chapter is based on the paper “Elitez, İ., Yaltırak, C., and Şahin, M. (2016). Vegetation and climate changes during the late Pliocene and early Pleistocene in SW Turkey e Comment to the published paper by Jiménez-Moreno et al., Quaternary Research, 84 (2015), 448-456. Quaternary Research, 85, 471-475.

no outcrop photograph exists in the paper. The precise Bıçakçı locality is situated in a valley in the village of Cevizli, ~3.2 km away from Bıçakçı (Figure 9.1a; 37°1′27.21″ N 29°18′8.20″ E).We communicated with Drs. Hüseyin Erten and Nurdan Yavuz at the end of 2015, who have also extensively worked in this area, and obtained field photographs of the outcrops of the Bıçakçı locality. We determined the location used by Jiménez-Moreno et al. (2015) by comparing our detailed field photographs together with two photographs presented in the MSc thesis of Erten (2002; Figure 9.1c), one photograph provided to us by Drs. Hüseyin Erten and Nurdan Yavuz. The coordinates of the Bıçakçı locality given by the authors is ~3.3 km east of the locality on their geological map (Figure 9.1b; Jiménez-Moreno et al., 2015, their Figure 2). Comparison of the lithologic log given by Jiménez- Moreno et al. (2015) and these photographs, it became obvious that the thickness of the outcrop is 6.3 m and the lithological characteristics of the sedimentary successions described in this manuscript are entirely different (Figures 9.1c, d and e). Jiménez-Moreno et al. (2015) present this outcrop as a 15-m-thick succession. And our detailed study in exactly the same location clearly shows that the thickness of this measurable section is 4.6 m (Figures 9.1c and e). Furthermore, our study shows that the lithologies reported by Jiménez-Moreno et al. (2015) and van den Hoek Ostende et al. (2015a) are largely incorrect (Figure 9.1).

9.2.2 Ericek locality

The coordinates of the Ericek locality provided in the Jiménez-Moreno et al. (2015) do not indicate the precise location of the sedimentary successions described in the manuscript. Our detailed field studies and mapping clearly document that the location where the stratigraphic section was created by Jiménez-Moreno et al. (2015) and a field photograph of the same location referenced in van den Hoek Ostende et al. (2015b; their Figure 2) the coordinates of the location is inaccurate (Figures 9.1a and b). Both van den Hoek Ostende et al. (2015b; their Figure 2) and Jiménez-Moreno et al. (2015; their Figure 4) present the same measured sections, reporting its coordinates as 37°04′12″ N 29°11′55″ E. However, the exact coordinates of this locality is at 37°3′56.89″ N 29°11′47.62″ E, ~502 m southeast of the location (Figure 9.1a) indicated by Jiménez-Moreno et al. (2015). The thickness of this outcrop is reported to be 18 m by Jiménez-Moreno et al. (2015; their Figure 4).

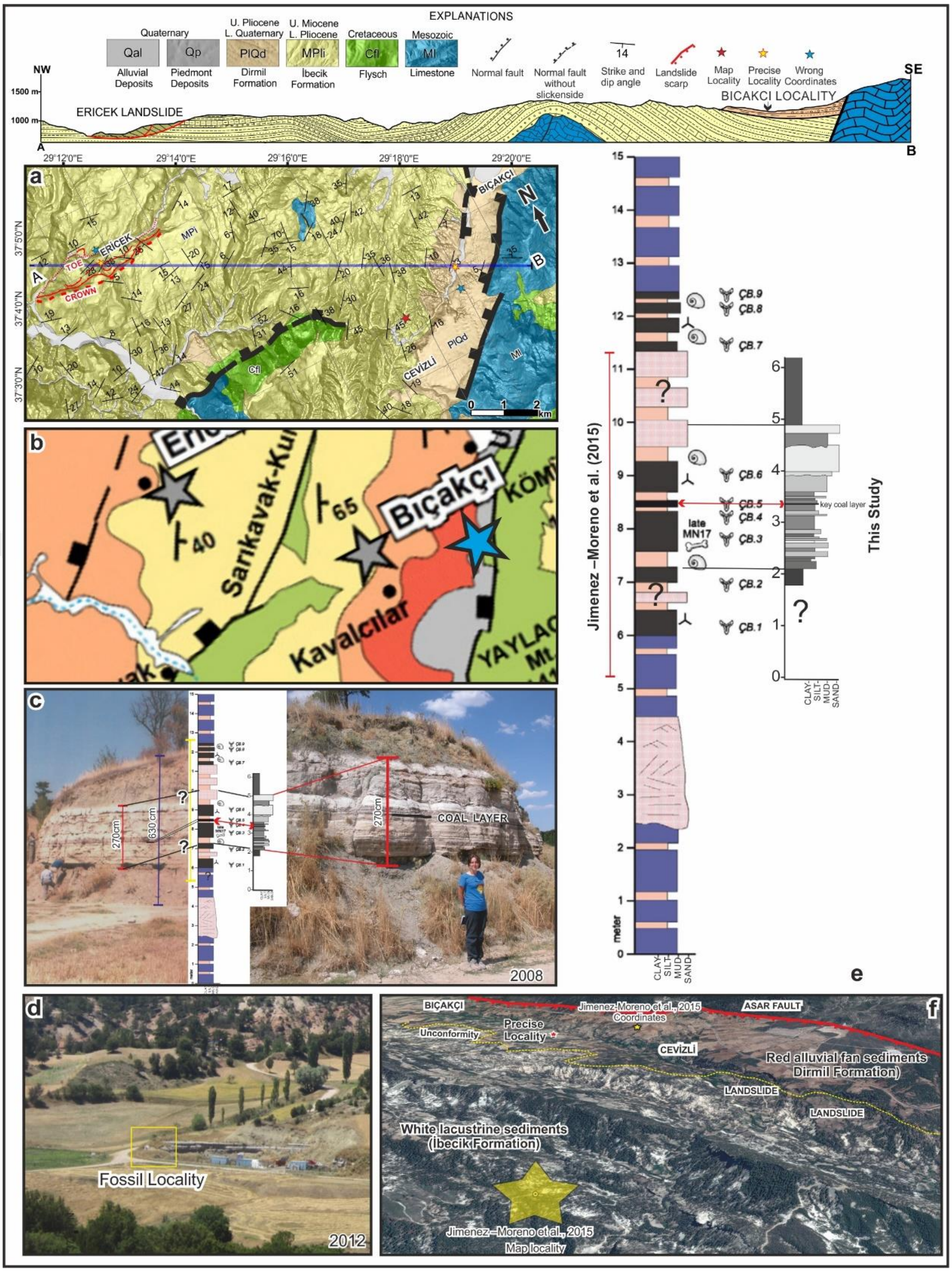

Figure 9.1 : a. The geological map and A-B cross-section of the study area. b. Ericek and Bıçakçı localities on the geological map of Jiménez-Moreno et al. (2015). Blue star shows the Bıçakçı locality coordinates suggested by Jiménez-Moreno et al. (2015). c. The photographs and measured sections of Cevizli (Bıçakçı) locality. Left from Erten (2002) and right from our archives. d. Photograph of the Cevizli (Bıçakçı) locality from our archives. e. Correlation between measured sections of Jiménez-Moreno et al. (2015) and this study. f. 3D view of the Bıçakçı-Cevizli area and localities. Small yellow star indicates the coordinates of the Bıçakçı locality and big yellow star indicates the Bıçakçı locality on the geological map in Jiménez-Moreno et al., 2015. Red star shows the precise locality.

This section was previously published as a 13-m-thick succession by van den Hoek Ostende et al. (2015b; their Figure 2). However, our study in exactly the same location clearly shows that the thickness of this section is 8.8 m. Furthermore, our study shows that the lithologies reported by Jiménez-Moreno et al. (2015) and van den Hoek Ostende et al. (2015b) are also incorrect (Figures 9.2a-d). Although the time interval indicated by these fossils (Rhagapodemus, Orientalomys, Mimomys occitanus) are between 3.6 and 3.8 Ma at the Ericek locality (van den Hoek Ostende et al., 2015b; their Figure 8), these authors suggest a 3.4 Ma age as a best estimate (van den Hoek Ostende, personal communication, 2015a, b). The locality studied by Jiménez-Moreno et al. (2015) is situated in front of a minor scarp of a landslide (Figure 9.2e). This outcrop is a block that dragged both horizontally and vertically for 200-300 m and tilted (Figure 9.2e). The 38° dip to the east indicative of rotational slides tilted to the landslide scarp (Figures 9.1a and 9.2e).

9.3 Regional Stratigraphy and Fossil Ages

9.3.1 Problems in the stratigraphic sequences

Jiménez-Moreno et al. (2015) use the stratigraphy published in M.C. Alçiçek's Ph.D. thesis (i.e., Alçiçek, 2001), and the measured sections in this thesis are shown by the authors as proof of this stratigraphy. We examined all measured sections individually and realized that the coordinates of the sections contradict with the localities in the geological map and most of the localities are not topographically and geologically suitable for the construction of measured stratigraphic sections (e.g., Figures 9.1a, e, f and detailed section localities: https://www.researchgate.net/publication/296327942) However, all subsequent papers use this stratigraphy (e.g., Alçiçek et al., 2004, 2005, 2006; van den Hoek Ostende et al., 2015a, b; Jiménez-Moreno et al., 2015), which shows numerous inconsistencies, thus confusing the reader. Although they suggested that this sequence is a part of Değne Member (Late Pliocene-Early Pleistocene), the coordinates of this locality are placed into the Derindere Member. On the west portion of the map area the stratigraphy from the older to younger is the Derindere, Kumafşarı, Değne members (Jiménez-Moreno et al., 2015; their Figure 2). However, on the east portion of the map area, the stratigraphy is chronologically reversed and is shown as Değne, Kumafşarı, Derindere members (Jiménez-Moreno et al., 2015; their Figure 2). This situation can only be encountered when there a recumbent synclinal folding developed. Our geological cross-sections and mapping show that there is no such structure in this area (Figure 9.1a). Therefore, the only alternative is that the sequences in the region between Bıçakçı and Suçatı villages were mapped incorrectly by Jiménez-Moreno et al. (2015; their Figure 2). One inevitably asks the question as to which one is correct? The Bıçakçı locality is given an age range between 2.6 and 1.8 Ma by Alçiçek et al. (2004, 2005, 2006). However, the same location is given a different age of 2.25 and 2.1 Ma by Jiménez-Moreno et al. (2015). So, why is the Derindere Member the oldest unit as indicated by Alçiçek et al. (2004, 2005, 2006)? Within this framework, the time, environment and climate relationships attributed to this stratigraphy becomes questionable. Furthermore, our field observations and mapping clearly show that the Ericek and the Bıçakçı localities occur in two different formations, exhibiting an unconformable relationship with a 1.2 Ma hiatus (Figure 9.1a).

9.3.2 When and how was the Miocene-Pliocene sequence eroded and where did it deposit?

The suggested age for the top of the sequence Jiménez-Moreno et al. (2015) is 2.2 Ma. If the sequence was continuous, the end of the lacustrine-river environment would correspond with the beginning of the alluvial fan environment. Thus, the middle Miocene-Pliocene unit would begin eroding at ~2.2 Ma ago. Today there is a semi-formed drainage that causes the erosion of this sequence. The recent Dalaman River Basin is a big part of the Miocene-Pliocene basin. Data published by the General Directorate of Renewable Energy (Elektrik İşleri Etüt İdaresi Genel Müdürlüğü, EİE, 2005) show that ~205 x 10^{-6} km^3 sediment was accumulated at the Suçatı sediment trap in the upper Dalaman Basin between 1969 and 2005. Our calculations based on the stratigraphic position of the Miocene sediments, suggest that the volume of the sediments eroded is ~772 km^3. In order to obtain the recent topography, a minimum time of 3.76 Ma is required. The amount of the eroded sediment shows that 1-km-thick sediment should be accumulated on a 27 x 27 km area during 2 Ma as from the

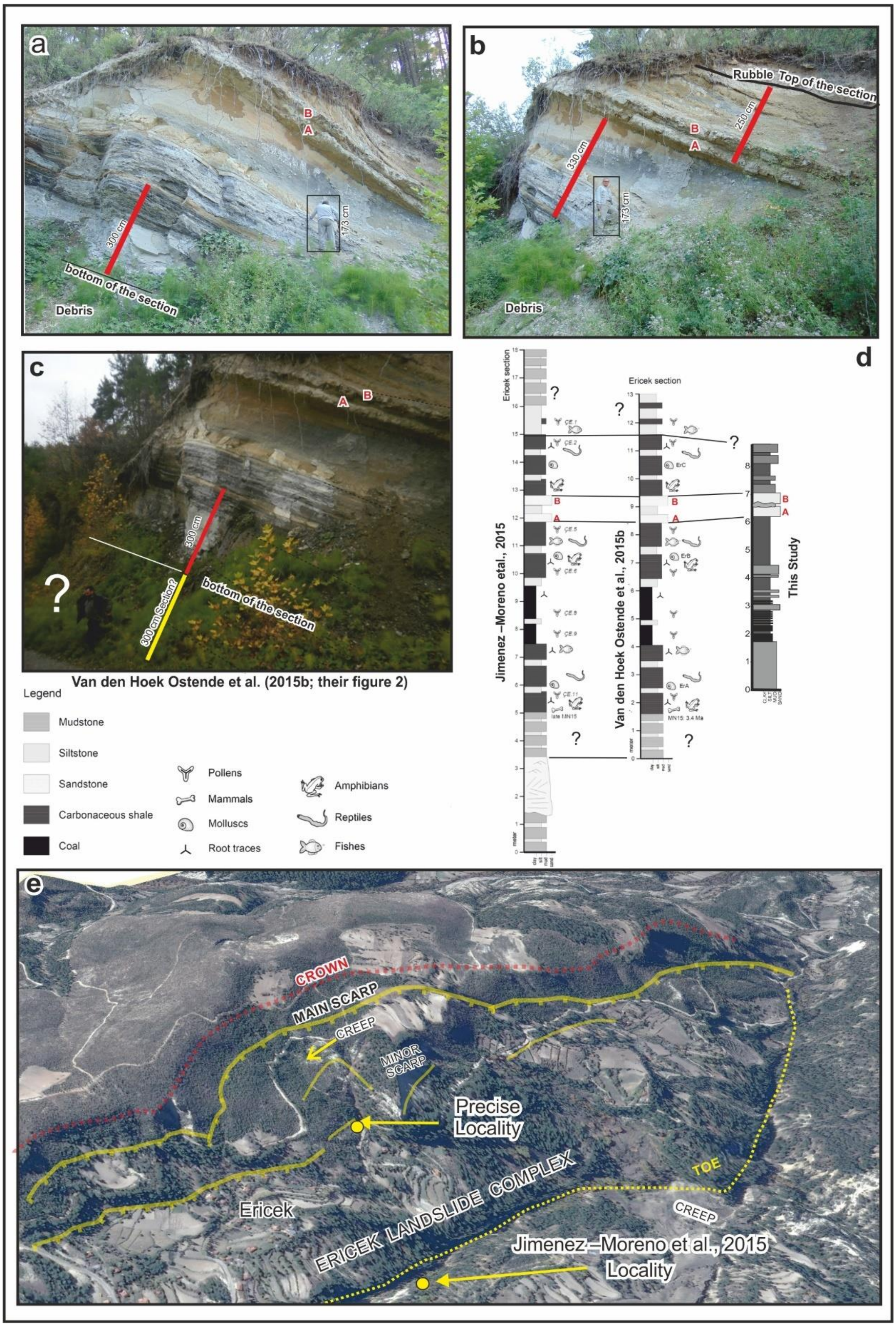

Figure 9.2 : Photographs and measured sections of the outcrop in the Ericek locality: a. Ericek locality view direction west to east. b. Ericek locality view direction south to north. c. Ericek locality from van den Hoek Ostende et al., 2015b; their Figure 2. d. Correlation of the stratigraphic sections measured in the Ericek locality. e. 3D Ericek landslide complex and localities suggested by Jiménez-Moreno et al. (2015) and this study.

beginning of the Dalaman River. The Dalaman plain is ~110 km^2. In this case, the sediment thickness must be more than 6 km and the age must be 2 Ma. Ocakoğlu (2012) suggests that a Quaternary delta does not exist in on the continental shelf. According to Hall et al. (2009, 2014a; Chapter 6 in this theses), some amount of ~500-m-thick (200-800 m) sequence accumulated above the M-reflector during 5 Ma and located in front of the Dalaman River towards the Rhodes Basin was transported from the eroded basin.

9.4 Conclusion

There are several stratigraphic and lithological problems with Jiménez-Moreno et al. (2015). As the nature of the scientific discussion, the stratigraphic construct suggested in this publication should be reviewed by the help of this comment.

10. REPLY TO THE COMMENT ON “MIOCENE TO QUATERNARY TECTONOSTRATIGRAPHIC EVOLUTION OF THE MIDDLE SECTION OF THE BURDUR-FETHIYE SHEAR ZONE, SOUTHWESTERN TURKEY: IMPLICATIONS FOR THE WIDE INTER-PLATE SHEAR ZONES”[9]

10.1 Introduction

Most of the criticisms raised by Alçiçek et al. (2017) have been addressed before (see Alçiçek, 2015; Elitez et al., 2015). Furthermore, we have written a detailed comment about their suggested ages and purported positions of the sedimentary units in the field (see Elitez et al., 2016a; Jiménez-Moreno et al., 2016). The authors represent a geological map and suggest a stratigraphic construction of the Neogene deposits. The most important claim of this construction is that there is a period of 2.2 Ma of sedimentation gap between Langhian and Vallesian (13.8-11.6 Ma). Alçiçek et al. (2017) criticise our study by referring their geological map and fossil data. In this reply, we refute their assertions by discussing their geological section localities which they use as the basis for their criticisms in their article.

10.2 Questions and Answers

10.2.1 Is there a relationship between the stratigraphic sequences of both northern and southern sides of the Acıpayam Basin?

It is not possible to compare the stratigraphic architectures of the northern and southern sides of the Acıpayam Basin by using the geological map of the authors (see red dashed line in Figure 10.1; Alçiçek et al., 2017, their Figure 1). The terrestrial conglomerates of the Gölhisar Formation which underlie the lacustrine marls of the İbecik Formation

[9] This chapter is based on the paper “Elitez, İ. and Yaltırak, C. (2018). Reply to the comment on “Miocene to Quaternary tectonostratigraphic evolution of the middle section of the Burdur-Fethiye Shear Zone, south-western Turkey: Implications for the wide inter-plate shear zones”. Tectonophysics, 722, 601-606.

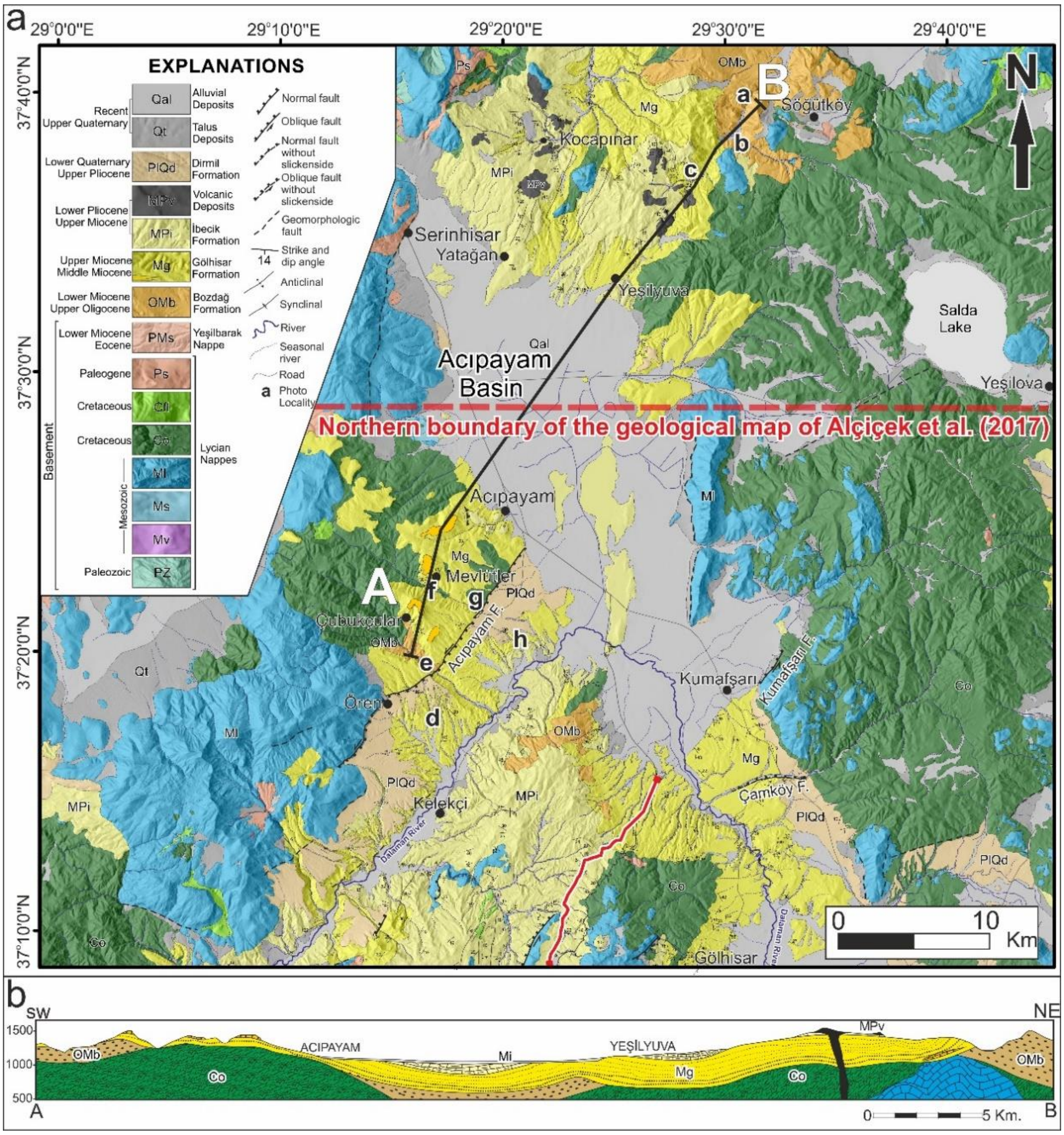

Figure 10.1 : (a) Geological map of the study area. Contacts bounding the basement rocks were drawn by integrating the 1:500000 Denizli sheet geological map by the General Directorate of Mineral Research and Exploration (Şenel, 2002), field observations, DEMs and satellite images. (b) A-B geological cross section through the study area.

are not shown on their geological map (Alçiçek et al., 2017, their Figure 1). However, the Miocene sequence is observed north of the Acıpayam Basin (Figure 10.1a). The geological cross-section clearly shows the stratigraphic continuity in both sides of the Acıpayam Basin (Figure 10.1b). Alçiçek et al. (2017) assert that the units located around Acıpayam and the Miocene sequence north of Yatağan and Yeşilova have no relation to each other (Figure 10.1a). In these regions, there are two different conglomeratic sequences. One is the upper Oligocene-lower Miocene Bozdağ Formation and the other is the middle-upper Miocene Gölhisar Formation. In the absence of a detailed geological map, it is hard to realize that the conglomerates around the Mevlütler locality (i.e., the Gölhisar Formation) are composed of the pebbles of the Oligo-Miocene conglomerates of the Bozdağ Formation (Figure 10.2). This is the reason why the authors confuse these conglomerates with the Oligo-Miocene conglomerates. However, Oligo-Miocene conglomeratic unit can be easily separated from the middleupper Miocene conglomerates in the field (Figure 10.2). For example, there is an angular unconformity between the tilted conglomerates of the Bozdağ Formation located in the stream bed south of the village of Çubukçular and the conglomerates of the Gölhisar Formation intercalating with upper Burdigalian-lower Langhian limestones around the Mevlütler locality (Figure 10.1).

The conglomerates of the Bozdağ Formation is composed of a 15 m thick, massive, dark-grey to grey to light-brown sequence (Figure 10.2a, b, e). The Gölhsiar Formation is characterized by thick-bedded conglomerates with reddish sandstone and mudstone intercalations (Figure 10.2c, d, f, g, h). The same lithologies and facies are observed in both sides of the Acıpayam Basin (Figures 10.1a and 10.2). Langhian limestones are observed on the Kaleburnu Hill south of Acıpayam and on the hills north of the Mevlütler locality (Figure 10.2f) and the Çubukçular village (Figure 10.1a). These limestone levels are an intercalation located in the lowest parts of the Gölhisar Formation and it is associated with a marine inflow from west of the study area (i.e., the Kale Basin) during the early-middle Miocene. Although Alçiçek et al. (2017) suggest as different formations, the localities in c, d, f, g and h are indeed the same formation (Figure 10.2). In their geological map Alçiçek et al. (2017) show our localities h and d within the fluvial unit and our localities e, f and g within the terrestrial marine deposits. However, these deposits represent a single unit in the basin. The existence of the marine sediments in the Kaleburnu Hill suggested by the authors does not affect our study. The gradual transition between Gölhisar and İbecik formations can be observed along the Çameli road (thick red line in Figure 10.1). Same transition can be observed along the road between Kocapınar and Yeşilyuva.

10.2.2 What are the ages of the Gölhisar and İbecik formations?

The corresponding author has grouped all sediments under the name of the Çameli Formation and dated these as Vallesian-Villanian in all of his publications (e.g. Alçiçek et al., 2017; their Figure 4). In the geological map of Alçiçek et al. (2017), there are three sequences from the older to younger represented by three colours

Figure 10.2 : Conglomerates and sandstones of the Bozdağ Formation (a,b,e in Figure 10.1) and Gölhisar Formation (c,d,f,g,h in Figure 10.1)

Derindere Member (orange), Kumafşarı (pink) and Değne (yellow) (Figure 10.3a). According to their geological map, all these units are dipping eastward (red circles in Figure 10.3a). When considering the strikes and dips of these units, the stratigraphy is chronologically reversed around their Bıçakçı fossil locality, south of Çameli. So, the question is: which of these chronologies is correct? Or, is there a recumbent synclinal folding in the region? We can also see this contradiction in the stratigraphic sections they used in all their publications (Figure 10.3b). While the age of the Derindere Member is older than 10.5-8.5 Ma in the stratigraphic section of Elmalıyurt, it is 2.6-1.5 Ma in the stratigraphic section of Kavalcılar (Bıçakçı, Figure 10.3b; Alçiçek et al., 2005, 2007). In this case, according to the fossils of the corresponding author, it is not possible that these two deposits are the same unit. In an attempt to solve the age problem of Neogene sequence, we have obtained zircon crystals from a tuff level in the lacustrine deposits of the İbecik Formation on a road between Yolçatı and Narlı south of Çameli. These zircons gave an age of ~7 Ma (Elitez et al., 2017a).

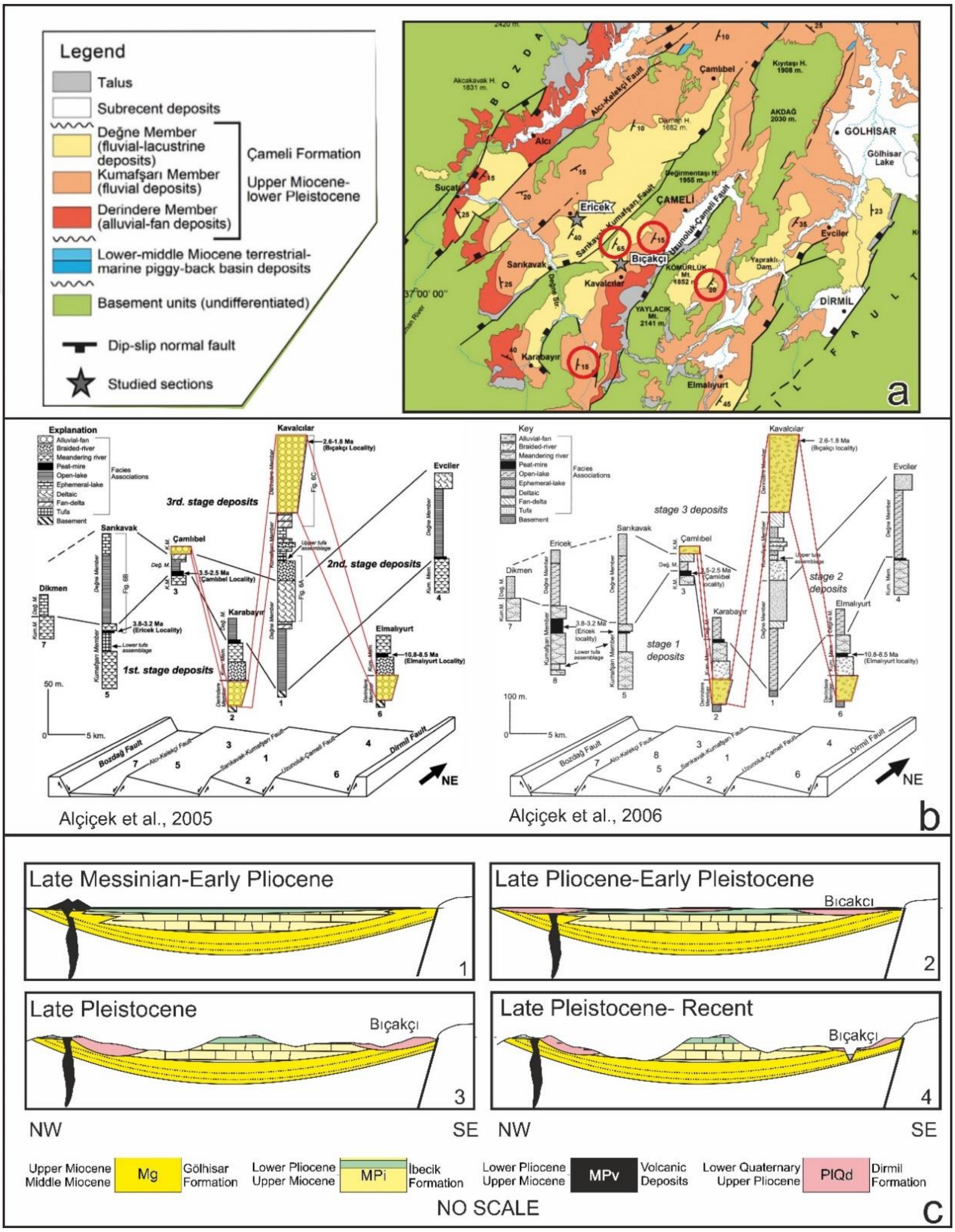

Figure 10.3 : (a) Geological map and (b) stratigraphic sections of Alçiçek et al. (2005, 2006, 2017) (c) Sedimentological and morphological evolution of the Bıçakçı area from early Pliocene to recent.

Furthermore, we have obtained 39Ar/40Ar ages from the lamproites located in the northern side of the Acıpayam Basin, which are compatible with the zircon age (Elitez et al., 2017a). In short, the upper Miocene units which are covered or cut by the lamproites north of Acıpayam Basin and the Plio-Pleistocene Değne Member of Alçiçek et al. (2017) are essentially same deposits of the İbecik Formation.

So, what does the Pleistocene fossil record of Alçiçek et al. (2017, in this volume) tell us? As mentioned above, the stratigraphic sections of M.C. Alçiçek indicate two different ages for the Derindere Member in most of his studies (Figure 10.3b). These two ages were obtained from two different units. A detailed discussion on this issue has already been published as a discussion by Elitez et al. (2016b).

According to the vertebrate fossils in the village of Elmalıyurt, the lowermost age of the İbecik Formation is Vallesian (10.7-8.5 Ma) and according to the radiometric dating, the age of the uppermost parts of the succession is between 5 and 7 Ma. In this case, the age of the 900 m thick Gölhisar Formation is older than 10.7 Ma. The Gölhisar Formation was deposited in the Langhian-early Tortonian (14-10 Ma). The gradual transition in the sequence can be obviously observed along the Gölhisar-Altınyayla (Dirmil) road (Elitez and Yaltırak, 2016).

10.2.3 Can this basin erode and develop the recent topography in 1.5 my?

The recent Dalaman River Basin includes a great part of our study area. This basin exhibits a semi-developed drainage (Figure 10.4). According to the data obtained from the General Directorate of Renewable Energy (EİE, 2005), there is an accumulation of ~205×10-6 km^3 sediment at the Suçatı sediment trap during a 40-year period. Previous studies point out a fossil age of 2.2 Ma in a locality close to Suçatı (e.g. Jiménez-Moreno et al., 2015). It is excepted to observe nearly horizontal lacustrine sediments in the basin. The topographic horizontal plane that represents the upper level of the lacustrine sediments indicates the ancient lake bottom. The volume between this plane and recent topography gives the eroded volume in the region. In order to examine this age, we calculated the volume of the eroded Miocene sediments. The result is ~772 km^3. This result shows that the recent topography has been formed during the last 3.76 my. When considering the area of the Dalaman Basin (~110 km^2), a 6 km-thick sediment must be observed for an age of 2 my (see also Elitez et al., 2016a, 2016b).

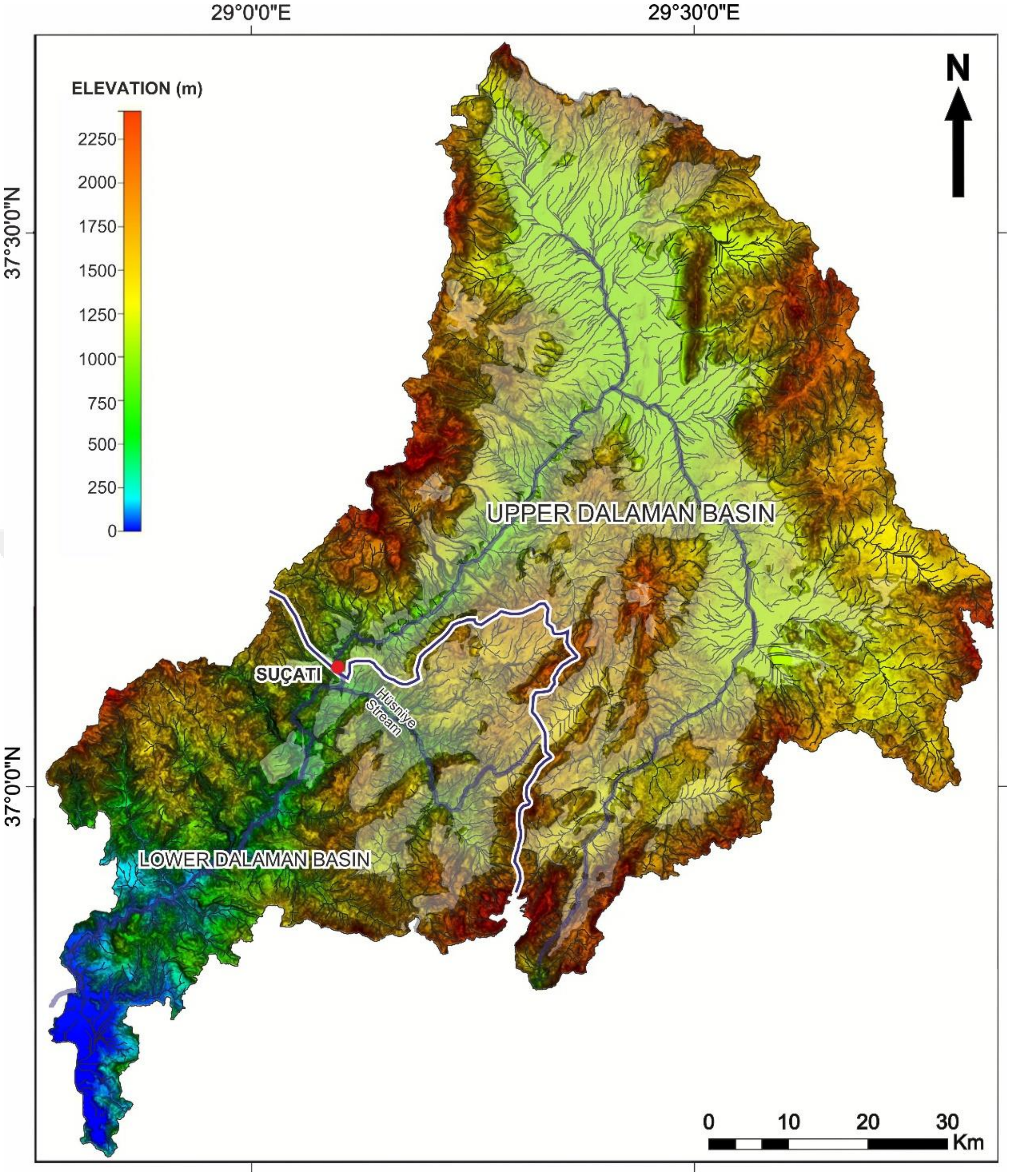

Figure 10.4 : Digital elevation model of the Dalaman River Basin.

10.2.4 Are all references accessible and relevant to the study area?

Alçiçek et al. (2017) criticise our study and indicate observation mistakes and incorrect stratigraphic construction in the study area. In order to negate our studies (Hall et al., 2014a; Elitez et al., 2015, 2016a, 2016b, 2017a, 2017b), they suggest their repetitious publications (e.g. Alçiçek, 2001; Alçiçek et al., 2005) and also many studies that were not conducted in the study area. Alçiçek et al. (2017) refer 57 studies in order to support their claims. But,

• Seven of these studies are 1/100000-scale geological maps and explanation texts, and only two of them are related to the study area.

• Nine of these studies are unpublished and inaccessible mining and petroleum exploration reports that include wide areas and do not contain detailed Neogene stratigraphy. Only three of them partly overlap the study area.

• Two of these studies are the Ph.D. theses and only one of them is about the study area.

• Only 11 studies of the corresponding author are about the study area.

• Only 17 studies of 57 references are related to the study area.

As mentioned above, there are many references that readers cannot access and that are not relevant to the study area. In spite of their misleading geological map and stratigraphic sections, the authors disregard all studies that conflict with their views by severely criticizing these.

10.3 Conclusions

The Gölhisar Formation is a 900 m-thick middle-late Miocene sequence and grades horizontally and vertically to the İbecik Formation. This sequence shows continuity between the northern and southern sides of the Acıpayam Basin. According to radiometric ages obtained from the lamproites and a tuff level, the lacustrine sediments of the İbecik Formation were deposited in the middle-upper Miocene. The Dirmil Formation unconformably overlies Gölhisar and İbecik formations and its age is upper Pliocene-early Quaternary according to the fossil data in the Bıçakçı locality. The source of the confusion that causes the misinterpretation of the age of the İbecik Formation is the misinterpretation of the deposits in which fossils are observed in the Bıçakçı locality.

The uppermost parts of the İbecik Formation indicate a Messinian-early Pliocene playa environment. Alçiçek et al. (2017, in this volume) confuse the fine-grained sequence (Dirmil Formation) derived from the materials of the İbecik Formation during the erosion regime with the lacustrine sediments (İbecik Formation). This confusion has an evolutionary explanation (Figure 10.3c).

• In the early stage, in the Messinian-early Pliocene period (7-3.6 Ma), the İbecik Lake evaporated and left behind a playa (1 in Figure 10.3c). This playa had been periodically turned into a lake. The red-wine-coloured caliche and mudstones in the uppermost levels of the İbecik Formation are the products of this period (Figure 5f in Elitez and Yaltırak, 2016).

• In the second stage, in the late Pliocene-early Pleistocene (3.6-1.8 Ma), the basin began to erode depending on the tectonic uplift, and a fluvio-lacustrine (Dirmil Formation) environment which includes the carbonates and marls of the İbecik Formation was formed (2 in Figure 10.3c).

• In the third stage, in the late Pleistocene, the valleys began to form along the margin of the basin depending on the tectonic uplift, the İbecik Formation remained topographically high and the materials of the Dirmil Formation tended to be coarser (3 in Figure 10.3c).

• After the late Pleistocene, the Dirmil Formation began to erode and the alluvium has begun to deposit in the deep valleys and basins. In conclusion, they have been eroded by the recent drainage system (4 in Figure 10.3c).

This evolution is clearly observed in the Bıçakçı locality and Quaternary valley cutting this locality. We will be happy to share our field experience and observations to further clarify these issues.

11. CONCLUSIONS

In this thesis, three main problems are addressed; (1) age and stratigraphy of the Neogene sequence, (2) structural properties of the region, (3) Miocene to recent tectonostratigraphic evolution of south-western Turkey.

During the field studies, the first remarkable point is the stratigraphy of the region. In the previous studies, all the Neogene units were described as the Çameli Formation (Erakman et al., 1982; Bilgin et al., 1990). Additionally, these Neogene sediments were assigned a Pliocene age around the basins in the region (e.g. Şenel, 1997c, 2002). In some of the studies, the Çameli Formation was divided into members (Alçiçek, 2001; Alçiçek et al., 2004, 2005, 2006). Here, the main problem was the stratigraphic positions of these members. Considering the fossil data and interpretations related to these fossils, it was obvious that there were inconsistencies in these studies. Mostly, the younger alluvial fan conglomerates were confused with the river conglomerates and also this situation caused contradictory age assignments. Therefore, a new stratigraphy based upon a combination of fossil data and new radiometric ages is built in this thesis.

The study area is located between the Aegean extensional province and the Western Taurides Block in south-western Turkey. In most of the previous studies, this tectonically active region was characterized related to a narrow NE-SW-trending left-lateral Burdur-Fethiye Fault Zone (e.g. Barka et al., 1997) and also an evolution controlled by pure normal faults (e.g. ten Veen et al., 2008). During the field studies, nearly two thousand major and minor faults were measured. Contrary to previous opinions, many of these faults have strong strike-slip components of displacement.

During thesis studies, structural similarities between the region and the experimental transtensional model by Schreurs and Colletta (1998) were noticed. According to this experimental model, the strike-slip faults develop at early stages of a transtensional system. While the deformation increases, the normal and oblique normal faults and also small basins develop between these strike-slip faults. In the framework of this thesis, it is known that there are many 1- to 10-km-long normal and left-lateral oblique normal faults, limited reverse and strike-slip faults and several basins in the study area. Starting from this point of view, it was deduced that the tectonic evolution of the basins along the region is controlled by a large NE-SW-trending left-lateral shear zone: the Burdur-Fethiye Shear Zone.

The evolution of the Burdur-Fethiye Shear Zone is controlled by the Western Taurides compressional regime, the roll-back effect of the Hellenic Trench and the westward tectonic escape of the Anatolian Microplate along the North Anatolian and East Anatolian Transform Faults. Also, the zone is closely linked with the evolution of the Isparta Angle. According to the radiometric ages obtained from lamproite upwelling in the Acıpayam region and lavas of the Afyon Volcanic Complex (e.g. Prelević et al., 2015), the Burdur-Fethiye Shear Zone has been active since the middle Miocene.

The Burdur-Fethiye Shear Zone is bounded by the Aegean extensional province in the west and the Western Taurides Block in the east. According to the GPS velocities, the Aegean extensional province moves south-westward faster than the Western Taurides Block. This velocity difference between two blocks has caused a left-lateral shear and formed the Burdur-Fethiye Shear Zone. Along the Burdur-Fethiye Shear Zone, the GPS velocities decrease from northwest toward southeast and the GPS vectors become nearly parallel to the zone on the southern part of the zone. While the velocity difference is 3-4 mm/yr on the northern part of the zone, this difference increase to 8-10 mm/yr toward the southern side. This is the reason why the southern part is wider than the northern part of the zone.

The Burdur-Fethiye Shear Zone is located on a Cretaceous ophiolitic basement. Therefore, most of the major faults were formed at or near the contacts between this basement and younger successions. Both major and minor faults indicate different stress directions. These stress directions are in fact the sign of shearing, internal rotation and counter-clockwise rotation of the Anatolian Microplate.

It is obvious that there is a progressive deformation in the south-western Anatolia and eastern Mediterranean. The lineaments observed in the digital elevation models of the land morphology has same directions of the lineaments in the marine area. The strike-slip traces found in the extensional left-lateral shear regime of the Burdur-Fethiye Shear Zone are preserved in the marine area. Therefore, the Burdur-Fethiye Shear Zone can be defined as the northeastern onland continuation of the Pliny-Strabo

Trenches which are associated with the STEP fault zone (Aksu et al., 2009; Barka and Reilinger, 1997; Elitez et al., 2009; Hall et al., 2009, 2014; Huguen et al., 2001; Ocakoğlu, 2012; Taymaz and Price, 1992; ten Veen et al., 2004, 2009; Woodside et al., 2000; Yaltırak et al., 2010; Zitter et al., 2003).

REFERENCES

Akal, C., Helvacı, C., Prelevic, D., and van den Bogaard, P. (2013). High-K volcanism in the Afyon region, western Turkey: from Si-oversaturated to Si-undersaturated volcanism, *International Journal of Earth Sciences, 102,* 435-453.

Akay, E., and Uysal, S. (1985). Orta Torosların batısındaki (Antalya) Neojen çökellerininstratigrafisi, sedimantolojisi ve yapısal jeolojisi (Report No: 7799). Ankara: Mineral Research Exploration Institute (MTA).

Akay, E., Uysal, S., Poisson, A., Cravette, J., and Müller, C. (1985). Antalya Neojen havzasının stratigrafisi, *Bulletin of the Geological Society of Turkey, 28,* 105-119.

Akdeniz, N. (2011). *Geological Map of Denizli, N21 quadrangle, No: 163, in 1:100.000 scale sheet,* General Directorate of Mineral Research and Exploration, Ankara, Turkey.

Aksu, A. E., Calon, T. J., Piper, D. J.W., Turgut, S., Izdar, E. (1992a). Architecture of late orogenic Quaternary basins in northeastern Mediterranean Sea, *Tectonophysics, 210,* 191-213.

Aksu, A. E., Uluğ, A., Piper, D. J. W., Konuk, Y.T., Turgut, S. (1992b). Quaternary sedimentary history of Adana, Cilicia and Iskenderun Basins, northeastern Mediterranean Sea, *Marine Geology, 104,* 55-71.

Aksu, A. E., Calon, T. J., Hall, J., Mansbridge, S., Yaşar, D. (2005). The Cilicia-Adana Basin complex, Eastern Mediterranean: Neogene evolution of an active fore-arc basin in an obliquely convergent margin, *Marine Geology, 221,* 121-159.

Aksu, A. E., Hall, J., and Yaltırak, C. (2009). Miocene-Recent evolution of Anaximander Mountains and Finike Basin at the junction of Hellenic and Cyprus Arcs, eastern Mediterranean, *Marine Geology, 258*(1), 24-47.

Aksu, A. E., Hall, J., Yaltırak, C., Çınar, E., Küçük, M., and Çifçi, G. (2014). Late Miocene-Recent evolution of the Finike Basin and its linkages with the Beydağlari complex and the Anaximander Mountains, eastern Mediterranean, *Tectonophysics, 635,* 59-79.

Aktuğ, B. and Kılıçoğlu, A. (2006). Recent crustal deformation of Izmir, western Anatolia and surrounding regions as deduced from repeated GPS measurements and strain field, *Journal of Geodynamics, 41,* 471-484.

Aktuğ, B., Nocquet, J. M., Cingo, A., Parsons, B., Erkan, Y., and England, P. (2009). Deformation of western Turkey from a combination of permanent and campaign GPS data: limits to block-like behaviour, *Journal of Geophysical Research, 114,* 1-22.

Aktuğ, B., Parmaksız, E., Kurt, M., Lenk, O., Kılıçoglu, A., Gürdal, M. A., and Özdemir, S. (2013). Deformation of Central Anatolia: GPS implications, *Journal of Geodynamics, 67*, 78-96.

Akyüz, H. S., and Altunel, E. (1997). The 417 A.D. Cibyra earthquake: Evidences of left-lateral motion along the Burdur-Fethiye fault zone (SW Anatolia-Turkey). In ATAG-1. *First Meeting of Active Tectonics Research Group Abstracts (in Turkish with English abstract),* ITU, Istanbul, Turkey, December 8-9.

Akyüz, H. S., and Altunel, E. (2001). Geological and archaeological evidence for post-Roman earthquake surface faulting at Cibyra, SW Turkey, *Geodinamica Acta, 14,* 95-101.

Alçiçek, H. (2010). Stratigraphic correlation of the Neogene basins in southwestern Anatolia: regional palaeogeographical, palaeoclimatic and tectonic implications, *Palaeogeography, Palaeoclimatology, Palaeoecology, 291,* 297-318.

Alçiçek, M. C. (2001). *Sedimentological Investigation of Çameli Basin (Late Miocene-Late Pliocene, Denizli, SW Anatolia).* (Ph.D. Thesis). Ankara University, Department of Geological Engineering, Ankara (in Turkish with English abstract).

Alçiçek, M. C. (2007). Tectonic development of an orogen-top rift recorded by its terrestrial sedimentation pattern: the Neogene Eşen Basin of southwestern Anatolia, Turkey, *Sedimentary Geology, 200,* 117-140.

Alçiçek, M. C. (2015). Comment on "The Fethiye-Burdur Fault Zone: A component of upper plate extension of the subduction transform edge propagator fault linking Hellenic and Cyprus Arcs, Eastern Mediterranean. Tectonophysics 635, 80-99" by J. Hall, A.E. Aksu, İ. Elitez, C. Yaltırak, G. Çiftçi, *Tectonophysics, 128,* 1-4.

Alçiçek, M. C., Kazancı, N., Özkul, M., and Şen, Ş. (2004). Sedimentary Infill and Geological Evolution of Çameli Neogene Basin, Denizli-SW Turkey, *Bulletin of the Mineral Research and Exploration, 128,* 99-123.

Alçiçek, M. C., Kazancı, N., and Özkul, M. (2005). Multiple rifting pulses and sedimentation pattern in the Çameli Basin, southwestern Anatolia, Turkey, *Sedimentary Geology, 173,* 409-431.

Alçiçek, M. C., ten Veen, J. H. T., and Özkul, M. (2006). Neotectonic development of the Çameli Basin, southwestern Anatolia, Turkey. In: Robertson, A.H.F., Mountrakis, D. (Eds), Tectonic Development of the Eastern Mediterranean Region. *Geological Society, London, Special Publications, 260,* 591-611.

Alçiçek, H., Varol, B., and Özkul, M. (2007). Sedimentary facies, depositional environments and palaeogeographic evolution of the Neogene Denizli Basin of SW Anatolia, Turkey, *Sedimentary Geology, 202,* 596-637.

Alçiçek, M. C., and ten Veen, J. H. (2008). The late Early Miocene Acıpayam piggy-back basin: refining the last stages of Lycian nappe emplacement in SW Turkey, *Sedimentary Geology, 208*(3), 101-113.

Alçiçek, M. C., Mayda, S., and Alçiçek, H. (2012). Faunal and palaeoenvironmental changes in the Çal Basin, SWAnatolia: implications for regional stratigraphic correlation of late Cenozoic basins, *Comptes Rendus Geoscience, 344*, 89-98.

Alçiçek, M. C., Brogi, A., Capezzuoli, E., Liotta, D., and Meccheri, M. (2013). Superimposed basins formation during the Neogene-Quaternary extensional tectonics in SW-Anatolia (Turkey): Insights from the kinematics of the Dinar Fault Zone, *Tectonophysics, 608*, 713-727.

Aleksandrowski, P. (1985). Graphical determination of principal stress directions for slickenside lineation populations: an attempt to modify Arthaud's method, *Journal of Structural Geology, 7*(1), 73-82.

Allmendinger, R. W., Cardozo, N. C., and Fisher, D. (2012). *Structural Geology Algorithms: Vectors and Tensors*, Cambridge, England, Cambridge University Press.

Alpar B., and Yaltırak, C. (2002). Characteristic features of the North Anatolian Fault in the Eastern Marmara region and its tectonic evolution, *Marine Geology*, *190*, 329-350.

Angelier, J., and Mechler, P. (1977). Sur une méthode graphique de recherche des contraintes principales également utilisable en tectonique et en séismologie: la méthode des dièdres drits, *Bulletin de la Société géologique de France, 6*, 1309-1318.

Angelier, J. (1979). Determination of the mean principle directions of stress for a given fault population, *Tectonophysics, 56*, 17-26.

Angelier, J. (1984). Tectonic analysis of fault-slip data set, *Journal of Geophysical Research 89*, 5835-48.

Arthaud, F. (1969). Methode de determination graphique des directions de raccourcissement, d’allongement et intermediaire d’une population de failles, *Bulletin Geological Sociéte de France, 7*(11), 729-37.

Barka, A., Reilinger, R., Şaroğlu, F., and Şengör, A. M. C. (1995). The Isparta Angle: Its importance in the neotectonics of the eastern Mediterranean region. In: Pişkin, O., Ergun, M., Savaşçın, Y., Tarcan, G. (Eds.), *International Earth Sciences Colloquium on the Aegean Region*, Güllük, İzmir, Turkey, October 9-14.

Barka, A., and Reilinger, R. (1997). Active tectonics of the Eastern Mediterranean region: deduced from GPS, neotectonic and seismicity data, *Annals of Geophysics, 40*, 587-610.

Benetatos, C., Kiratzi, A., Papazachos, C., and Karakaisis, G. (2004). Focal mechanisms of shallow and intermediate depth earthquakes along the Hellenic Trench, *Journal of Geodynamics, 37*, 253-296.

Bilgin, Z. R., Karaman, T., Öztürk, Z., Şen, M. A., and Demirci, A. R. (1990). Yeşilova-Acıgöl civarının jeolojisi (Report No. 9071). Ankara: General Directorate of Mineral Research and Exploration Report.

Biryol, C. B., Beck, S. L., Zandt, G., Özacar, A. A. (2011). Segmented African lithosphere beneath the Anatolian region inferred from teleseismic P-wave tomography, *Geophysical Journal International*, *184*, 1037-1057.

Bozcu, M., Yağmurlu, F., and Şentürk. M. (2007). Some Neotectonic and Paleoseismological features of the Fethiye-Burdur Fault zone, SW Anatolia, *Geological Engineering, 31*(1), 25-48.

Bozkurt, E., and Park, R. G. (1994). Southern Menderes Massif: an incipient metamorphic core complex in western Anatolia, Turkey, *Journal of the Geological Society of London, 151*, 213-216.

Brachert, T. C., Betzler, C., Braga, J. C., and Martin, J. M. (1998). Microtaphofacies of a warm-temperate carbonate ramp (uppermost Tortonian/lowermost Messinian, southern Spain), *Palaios, 13*, 459-475.

Braga, J. C. (2016). *Neogene Rhodoliths in the Mediterranean Basins, In: Riosmena-Rodríguez R., Nelson W., Aguirre J. (eds) Rhodolith/Maërl Beds: A Global Perspective*. Coastal Research Library, 15. Springer, Cham**.**

Brandano, M., Tomasetti, L., Sardella, R., and Tinelli, R. (2016). Progressive deterioration of trophic conditions in a carbonate ramp environment the lithothamnion, Majella Mountain (Tortonian-Erly Messinian, Central Apennines, Italy), *Palaios, 31*, 125-140.

Bridge, C., Calon, T. J., Hall, J., Aksu, A. E. (2005). Salt tectonics in two convergent margin basins of the Cyprus Arc, Eastern Mediterranean, *Marine Geology, 221*, 223-259.

Brunn, J. H., de Graciansky, P. C., Gutnic, M., Juteau, T., Lefevre, R., Marcoux, J., Monod, O., and Poisson, A. (1970). Structures majeures et corrélations stratigraphiques dans les Taurides occidentales, *Bulletin de la Societe geologique de France, 3*, 515-556.

Buchbinder, B. (1979). Facies and Environments of Miocene Reef Limestones in Israel, *Journal of Sedimentary Petrology, 49*, 1323-1344.

Cita, M. B., Wright, R. C., Ryan, W. B. F., Longinelli, A. (1978). Messinian Paleoenvironments. In: Hsü, K., Montadert, L., et al. (Eds.), Initial Reports of the Deep Sea Drilling Project XLII, Part I. U.S. Government Printing Office, Washington, pp. 1003-1035.

Cornée, J. J., Münch, P., Achalhi, M., Merzeraud, G., Azdimousa, A., Quillévéré, F., ….. Moissette, P. (2016). The Messinian erosional surface and early Pliocene reflooding in the Alboran Sea: New insights from the Boudinar basin, Morocco, *Sedimentary Geology, 333*, 115-129.

Collins, A. S., and Robertson, A. H. F. (1997). Lycian melange, southwestern Turkey: An emplaced Late Cretaceous accretionary complex, *Geology, 25*(3), 255-258.

Collins, A. S., and Robertson, A. H. F. (1998). Processes of Late Cretaceous to Late Miocene episodic thrust-sheet translation in the Lycian Taurides, SW Turkey, *Journal of the Geological Society, 155*, 759-772.

Çemen, I., Catlos, E. J., Göğüş, O., and Özerdem, C. (2006). Post-collisional extensional tectonics and exhumation of the Menderes Massif western Anatolia extended terrain, Turkey, in Post-collisional Tectonics and Magmatism in the Eastern Mediterranean Region, *Geological Society of America Special Papers, 409*, 353-379.

de Boorder, H., Spakman, W., White, S. H., Wortel, M. J. R. (1998). Late Cenozoic mineralization, orogenic collapse and slab detachment in the European Alpine Belt, *Earth and Planetary Science Letters, 164*, 569-575.

Delvaux, D., and Sperner, B. (2003). Stress tensor inversion from fault kinematic indicators and focal mechanism data: the TENSOR program. In: New Insights into Structural Interpretation and Modelling (D. Niewland Ed.), *Geological Society, London, Special Publications, 212*, 75-100.

de Oliviera, F.C., and de Fatima, R. (2012). Effectiveness of SRTM and ALOS-PALSAR data for identifying morphostructural lineaments in northeastern Brazil, *International Journal of Remote Sensing, 33*, 1058-1077.

Dewey, J. F., and Şengör, A. M. C. (1979). Aegean and surrounding regions. Complex multiplate and continuum tectonics in a convergent zone, *Geological Society of America Bulletin, 90*, 84-92.

Dewey, J. F., Hempton, M. R., Kidd, W. S. F., Şaroğlu, F., Şengör, A. M. C. (1986). Shortening of continental lithosphere: the neotectonics of eastern Anatolia — a young collision zone. In: Coward, M. P., Ries, A. C. (Eds.), Collision Tectonics. *Geological Society Special Publication, 19*, 3-36.

Dumont, J. F., Poisson, A., and Şahinci, A. (1979). Sur l'existence de coulissement sénestres récent a l'extrémité orientale de l'arc Égéen (sud-ouest de la Turquie), *Comptes Rendus de l'Académie des Sciences, 289*, 261-264.

EİE (2005). Suspended Sediment Data for Surface Waters in Turkey, p. 451.

Elitez, İ. (2010). *Miocene-Quaternary Geodynamics of Çameli and Gölhisar Basins, Burdur-Fethiye Fault Zone, SW Turkey*. (Master Thesis). İstanbul Technical University, Eurasia Institute of Earth Sciences, İstanbul (in Turkish with English abstract).

Elitez, İ., and Yaltırak, C. (2014a). Burdur-Fethiye shear zone (Eastern Mediterranean, SW Turkey). *General Assembly European Geosciences Union (EGU-2014)*, Vienna, Austria, 27 April-2 May.

Elitez, İ., and Yaltırak, C. (2014b). Comment on Analyses of Seismic Deformation at the Kibyra Roman Stadium, Southwest Turkey by Volkan Karabacak, Önder Yönlü, Eray Dökü, Nafiye Günenç Kıyak, Erhan Altunel, Şükrü Özüdoğru, Cahit Çağlar Yalçıner, and Hüsnü Serdar Akyüz, *Geoarchaeology, 29*, 349-352.

Elitez, İ., and Yaltırak, C. (2014c). Miocene-Quaternary Geodynamics of Çameli Basin, Burdur-Fethiye Shear Zone (SW Turkey), *Geological Bulletin of Turkey, 57*(3), 41-67.

Elitez, İ., and Yaltırak, C. (2016). Miocene to Quaternary tectonostratigraphic evolution of the middle section of the Burdur-Fethiye Shear Zone, southwestern Turkey: Implications for the wide inter-plate shear zones, *Tectonophysics, 690*, 336-354.

Elitez, İ., Yaltırak, C., and Sunal, G. (2017a). A new chronostratigraphy (40Ar-39Ar and U-Pb Dating) for the Middle Section of the Burdur-Fethiye Shear

Zone, SW Turkey. *General Assembly European Geosciences Union (EGU-2014)*, Vienna, Austria, 23-28 April.

Elitez, İ., Yaltırak, C., Kürçer, A., Özdemir, E., and Uygun Güldoğan, Ç. (2017b). A critical review of the Kibyra Fault (Burdur-Fethiye Shear Zone, SW Turkey), *Geodinamica Acta, 29*(1), 91-102.

Elitez, İ., and Yaltırak, C. (2018). Reply to the comment on "Miocene to Quaternary tectonostratigraphic evolution of the middle section of the Burdur-Fethiye Shear Zone, south-western Turkey: Implications for the wide inter-plate shear zones", *Tectonophysics*, *722*, 601-606.

Elitez, İ., Yaltırak, C., and Akkök, R. (2009). Morphotectonic evolution of the Middle of Fethiye-Burdur Fault Zone: Acıpayam, Gölhisar and Çameli Area, SW Turkey. *International Symposium on Historical Earthquakes and Conservation of Monuments and Sites in the Eastern Mediterranean Region, 500th Anniversary Year of the 1509 September 10, Marmara Earthquake*, Istanbul Technical University, Istanbul, 10-12 September, pp. 296-297.

Elitez, İ., Yaltırak, C., Hall, J., Aksu, A. E., and Çifçi, G. (2015). Reply to the comment by M.C. Alçiçek on "The Fethiye-Burdur Fault Zone: A component of upper plate extension of the subduction transform edge propagator fault linking Hellenic and Cyprus Arcs, Eastern Mediterranean," Tectonophysics, 635, 80-99, by J. Hall, AE Aksu, İ. Elitez, C. Yaltırak and G. Çifçi, *Tectonophysics, 664*, 5-13.

Elitez, İ., Yaltırak, C., and Şahin, M. (2016a). Vegetation and climate changes during the late Pliocene and Early Pleistocene in SW Turkey -- Comment to the published paper by Jiménez-Moreno et al, Quaternary Research, 84 (2015), 448-456, *Quaternary Research, 85*, 471-475.

Elitez, İ., Yaltırak, C., and Aktuğ, B. (2016b). Extensional and compressional regime driven left lateral shear in the Southwestern Anatolia: Burdur-Fethiye Shear Zone (Eastern Mediterranean), *Tectonophysics, 688*, 26-35.

Erakman, B., Meşhur, M., Gül, M. A., Alkan, H., Öztaş, Y., and Akpınar, M. (1982). Toros projesine bağlı Kalkan-Köyceğiz-Çameli-Tefenni arasında kalan alanın jeolojisi ve hidrokarbon olanakları raporu (Report No: 1732). Ankara: TPAO Technical Report.

Erdoğan, S., Şahin, M., Tiryakioğlu, İ., Gülal, E., and Telli, A. K. (2009). GPS velocity and strain rate fields in southwest Anatolia from repeated GPS measurements, *Sensors, 9*, 2017-2034.

Ersoy, Ş. (1990). The analysis of evolution and structural items of the western Taurus-Lycian Nappes. *Geol Eng (Bulletin Chamber of Geological Engineer, Turkey), 37*, 5-16.

Ersoy, E. Y., Cemen, I., Helvaci, C., and Billor, Z. (2014). Tectono-stratigraphy of the Neogene basins in Western Turkey: Implications for tectonic evolution of the Aegean Extended Region, *Tectonophysics, 635*, 35-58.

Erten, H. (2002). *Stratigraphy and micromammal investigation of the Acıpayam-Çameli Area.* (Master Thesis). Pamukkale University, Denizli, Turkey (in Turkish with English abstract).

Eyidoğan, H., and Barka, A. (1996). The 1 October 1995 Dinar earthquake, SW Turkey. *Terra Nova, 8*(5), 479-485.

Faccenna, C., Jolivet, L., Piromallo, C., and Morelli, A. (2003). Subduction and the depth of convection of the Mediterranean mantle, *Jornal of Geophysical Research, 108* (B2), 2099.

Faccenna, C., Bellier, O., Martinod, J., Primallo, C., and Regard, V. (2006). Slab detachment beneath eastern Anatolia; a possible cause for the formation of the North Anatolian Fault, *Earth Planetary Science Letters, 242*, 85-97.

Flecker, R., Ellam, R. M., Müller, C., Poisson, A., Robertson, A. H. F., and Turner, J. (1998). Application of Sr isotope stratigraphy and sedimentary analysis to the origin and evolution of the Neogene basins in the Isparta Angle, southern Turkey, *Tectonophysics, 298*, 83-101.

Floyd, M. A., Billiris, H., Paradissis, D., Veis, G., Avallone, A., Briole, P., McClusky, S., ….. England, P.C. (2010). A new velocity field for Greece: implications for the kinematics and dynamics of the Aegean, *Jornal of Geophysical Research, 115* (B10), 2156-2202.

Fossen, H., Teyssier, C., and Whitney, D. L. (2013). Transtensional folding, *Journal of Structural Geology, 56*, 89-102.

Frigui, M., Youssef M. B., and Ouaja, M. (2016) Evidences of "Lago-Mare" episode around the Messinian-Pliocene boundary in eastern Tunisia (central Mediterranean), *Journal of African Earth Sciences, 123*, 57-74.

Gautier, P. M., Brun, J. -P., Moriceau, R., Sokoutis, D., Martinod, J., and Jolivet, L. (1999). Timing, kinematics and cause of Aegean extension: a scenario based on a comparison with simple analogue experiments, *Tectonophysics, 315*, 31-72.

Glover, C., and Robertson, A. (1998). Neotectonic intersection of the Aegean and Cyprus tectonic arcs: extensional and strike-slip faulting in the Isparta Angle, SW Turkey, *Tectonophysics, 298*, 103-132.

Gómez, M. F., Lencinas, J. D., Siebert, A., and Díaz, G. M. (2012). Accuracy assessment of ASTER and SRTM DEMs: a case study in Andean Patagonia, *GIScience and Remote Sensing, 49*, 71-91.

Govers, R., and Wortel, M. J. R. (2005). Lithosphere tearing at STEP faults: response to edges of subduction zones, *Earth and Planetary Science Letters, 236*(1), 505-523.

Göktaş, F., Çakmakoğlu, A., Tarı, E., Sütçü, Y. F., and Sarıkaya, H. (1989). Çivril-Çardak arasının jeolojisi (Report No 8701). Ankara: General Directorate of Mineral Research and Exploration Report.

Graciansky, P. C. (1972). Recherches géologiques dans le Taurus Lycien occidental. (Ph.D. Thesis). Univ. Paris-Sud, Orsay.

Guerra-Merchán, A., Serrano, F., Hlila, R., El Kadiri, K., de Galdeano, C. S., and Garcés, M. (2014). Tectono-sedimentary evolution of the peripheral basins of the Alboran Sea in the arc of Gibraltar during the latest Messinian-Pliocene, *Journal of Geodynamics*, 77, 158-170.

Guidoboni, E., Comastri, A., and Traina, G. (1994). *Catalogue of ancient earthquakes in the Mediterranean area up to the 10th century*: Istituto Nazionale di Geofisica.

Guillong, M., von Quadt, A., Sakata, S., Peycheva, I., and Bachmann, O. (2014). LA-ICP-MS Pb-U dating of young zircons from Kos-Nisyros volcanic centre, SE Aegean arc, *Journal of Analytical Atomic Spectrometry, 29*, 963-970.

Gürer, A., Bayrak, M., and Gürer, Ö. F. (2004). Magnetotelluric images of the crust and mantle in the southwestern Taurides, Turkey, *Tectonophysics, 391*, 109-120.

Hack, J. T. (1973). Stream-profiles analysis and stream-gradient index, *Journal of Research of the U.S. Geological Survey*, *1* (4), 421-429.

Hafkenscheid, E., Wortel, M. J. R., and Spakman, W. (2006). Subduction history of the Tethyan region derived from seismic tomography and tectonic reconstructions, *Jornal of Geophysical Research*, *111*, B08401.

Hall, J., Aksu, A. E., Calon, T. J., and Yaşar, D. (2005). Varying tectonic control on basin development at an active microplate margin: Latakia Basin Eastern Mediterranean, *Marine Geology, 221*, 15-60.

Hall, J., Aksu, A. E., Yaltırak, C., and Winsor, J. D. (2009). Structural Architecture of the Rhodes Basin: A Deep Depocentre that Evolved since the Pliocene at the Junction of Hellenic and Cyprus Arcs, Eastern Mediterranean, *Marine Geology, 258*, 1-23.

Hall, J., Aksu, A. E., Elitez, İ., Yaltırak, C., and Çifçi, G. (2014a). The Fethiye-Burdur Fault Zone: A component of upper plate extension of the subduction transform edge propagator fault linking Hellenic and Cyprus Arcs, Eastern Mediterranean, *Tectonophysics, 635*, 80-99.

Hall, J., Aksu, A. E., King, H., Gogacs, A., Yaltırak, C., and Çifçi, G. (2014b). Miocene-Recent evolution of the western Antalya Basin and its linkage with the Isparta Angle, eastern Mediterranean, *Marine Geology, 349*, 1-23.

Hanken, N., Bromley, R. G., and Miller, J. (1996). Plio-Pleistocene sedimentation in coastal grabens, north-east Rhodes, Greece, *Geological Jornal, 31*, 393-418.

Hayward, A. B. (1984). Sedimentation and basin formation related to ophiolite nappe emplacement; Miocene, SW Turkey, *Sedimentary Geology, 40*, 105-129.

Hollenstein, Ch., Müller, M. D., Geiger, A., and Kahle, H. G. (2008). Crustal motion and deformation in Greece from a decade of GPS measurements, 1993-2003, *Tectonophysics, 449*, 17-40.

Hsü, K. J., Ryan, W. B. F., and Cita, M. B. (1973). Late Miocene desiccation of the Mediterranean, *Nature, 242*, 240-244.

Huguen, C., Mascle, J., Chaumillon, E., Woodside, J. M., Benkhelil, J., Kopf, A., and Volkonskaïa, A. (2001). Deformational styles of the eastern Mediterranean Ridge and surroundings from combined swath mapping and seismic reflection profiling, *Tectonophysics, 343*(1), 21-47.

Hull, J. (1988). Thickness-displacement relationships for deformation zones, *Journal of Structural Geology, 10*, 431-435.

Hüsing, S. K., Kuiper, K. F., Link, W., Hilgen, F. J., and Krijgsman, W. (2009). The upper Tortonian-lower Messinian at Monte dei Corvi (Northern Apennines, Italy): Completing a Mediterranean reference section for the Tortonian Stage, *Earth and Planet Science Letters, 282*, 140-157.

Intergovernmental Oceanographic Commission (IOC). (1981). *International Bathymetric Chart of the Mediterranean.* Published by the Head Department of Navigation and Oceanography, Russia under the authority of IOC, 10 sheets.

İşler, F. I., Aksu, A. E., Hall, J., Calon, T. J., and Yaşar, D. (2005). Neogene development of the Antalya Basin, Eastern Mediterranean: an active fore-arc basin adjacent to an arc junction, *Marine Geology, 221*, 299-330.

Jacobs, E., Wessia, H., and Shields, G. (1996). The Monterey event in the Mediterranean: A record from shelf sediments of Malta, *Paleoceanography and Paleoclimatology, 11*, 717-728.

Jiménez-Moreno, G., Alçiçek, H., Alçiçek, C., van den Hoek Ostende, L., and Wesselingh, F.P. (2015). Vegetation and climate changes during the late Pliocene and early Pleistocene in SW Anatolia, *Quaternary Research, 84* (3), 448-456.

Jiménez-Moreno, G., Alçiçek, H., Alçiçek, M.C., Van den Hoek Ostende, L.W., and Wesselingh, F.P. (2016). Letter to Editor "Vegetation and climatic cycles during the late Pliocene and early Pleistocene in SW Anatolia" Response to comments, *Quaternary Research, 85*, 476-477.

Jolivet, L., Faccenna, C., Huet, B., Labrousse, L., Le Pourhiet, L., Lacombe, O., ….. Driussi, O. (2013). Aegean tectonics: strain localisation, slab tearing and trench retreat, *Tectonophysics, 597-598*, 1-33.

Jongsma, D., and Mascle, J. (1981). Evidence for northward thrusting south-west of the Rhodes Basin, *Nature, 293*, 49-51.

Kahle, H. G., Straub, C., Reilinger, R., McClusky, S., King, R., Hurst, K., Veis, G., Kastens, K., and Cross, P. (1998). The strain rate field in the eastern Mediterranean region, estimated by repeated GPS measurements, *Tectonophysics, 294*, 237-252.

Karabacak, V. (2011). Geological, Geomorphological and Archaeoseismological Observations Along the Cibyra Fault and Their Implications for the Regional Tectonics of SW Turkey, *Turkish Journal of Earth Sciences, 20*(4), 429-447.

Karabacak, V., Yönlü, O., Dökü, E., Kıyak, N. G., Altunel, E., Özüdoğru, S., Yalçıner, C. Ç., and Akyüz, H. S. (2013). Analyses of Seismic

Deformation at the Kibyra Roman Stadium, Southwest Turkey, *Geoarchaeology, 28*(6), 531-543.

Karabıyıkoğlu, M., Çiner, A., Monod, O., Deynoux, M., Tuzcu, S., and Örçen, S. (2000). Tectonosedimentary evolution of the Miocene Manavgat Basin, western Taurides, Turkey. In: Bozkurt, E., Winchester, J.A., Piper, J.D.A. (Eds.), Tectonics and Magmatism in Turkey and the Surrounding Area, *Geological Society, London, Special Publication, 173,* 271-294.

Karabıyıkoğlu, M., T-zcu, S., Çiner, A., Deynoux, M., Örçen, S., and Hakyemez, A. (2005). Facies and environmental setting of the Miocene coral reefs in the Late-Orogenic fill of the Antalya Basin, Western Taurids, Turkey. In: Kelling, G., Robertson, A.H.F., van Buche, F. (Eds.), Cenozoic Sedimentary Basins of SouthCentral Turkey, *Sedimentary Geology, 173,* 345-371.

Kaymakçı, N., Özacar, A., Özkaptan, M., Koç, A., Gülyüz, E., Lefebvre, C., ….. Sözbilir, H. (2014). Fethiye-Burdur Fault Zone: a myth?*, The 8th International Symposium on Eastern Mediterranean Geology (ISEMG-8)*, Muğla, Turkey, October 13-17.

Kazancı, N., Boyraz, S., Özkul, M., Alçiçek, M. C., and Kadıoğlu, Y. K. (2012). Late Holocene terrestrial tephra record at western Anatolia, Turkey: possible evidence of an explosive eruption outside Santorini in the eastern Mediterranean, *Global and Planetary Change, 80,* 36-50.

Kiratzi, A., and Louvari, E. (2003). Focal mechanisms of shallow earthquakes in the Aegean Sea and the surrounding lands determined by waveform modelling: a new database, *Journal of Geodynamics, 36,* 251-274.

Kissel, C., and Poisson, A. (1987). Étude paléomagnetique préliminaire des formations cénozoïques des Bey Daglari (Taurides occidentales, Turquie), *Comptes Rendus Acadademie Science Paris, 304* (II), 343-348.

Kissel, C., Averbuch, O., Frizon de Lamotte, D., Monod, O., and Alberton, S. (1993). First paleomagnetic evidence for a post-Eocene clockwise rotation of the Western Taurides thrust belt east of the Isparta rentrant (Southwestern Turkey), *Earth Planetary Science Letters, 117,* 1-14.

Kissel, C., Laj, C., Poisson, A., and Görür, N. (2003). Paleomagnetic reconstruction of the Cenozoic evolution of the Eastern Mediterranean, *Tectonophysics, 362,* 199-217.

Krijgsman, W., Blanc-Valleron, M. M., Flecker, R., Hilgen, F. J., Kouwenhoven, T. J., Merle, D., Orszag-Sperber, F., Rouchy, J. M. (2002). The onset of the Messinian salinity crisis in the Eastern Mediterranean (Pissouri Basin, Cyprus), *Earth and Planet Science Letters, 194* (3-4), 299-310.

Koç, A., van Hinsbergen, D. J. J., Kaymakçı, N., and Langereis, C. G. (2016). Late Neogene oroclinal bending in the central Taurides: A record of terminal eastward subduction in southern Turkey?, *Earth and Planetary Science Letters, 434*, 75-90.

Konak, N. (2002). *Geological map of Turkey in 1:500.000 scale İzmir sheet*. General Directorate of Mineral Research and Exploration, Ankara, Turkey.

Konak, N., and Şenel, M. (2002). *Geological map of Turkey in 1:500.000 scale Denizli sheet*. General Directorate of Mineral Research and Exploration, Ankara, Turkey.

Kreemer, C., Blewitt, G., and Klein, E. C. (2014). A geodetic plate motion and Global Strain Rate Model, *Geochemistry, Geophysics, Geosystems, 15*(10), 3849-3889.

Kürçer, A., Özdemir, E., Güldoğan, Ç. U., and Duman, T. Y. (2016). Paleoseismic Trenching along the Central part of Fethiye Burdur Fault Zone, SW Turkey, *General Assembly European Geosciences Union (EGU-2016),* Vienna, Austria, April 17-22.

Le Pichon, X., and Angelier, J. (1979). The Hellenic Arc and trench system: a key to the evolution of the eastern Mediterranean area, *Tectonophysics, 60*, 1-42.

Le Pichon, X., and Kreemer, C. (2010). The Miocene-to-present kinematic evolution of the eastern Mediterranean and Middle East and its implications for dynamics, *Annual Review of Earth and Planetary Science, 38,* 323-351.

Le Pourhiet, L., Huet, B., May, D. A., Labrousse, L., and Jolivet, L. (2012). Kinematic interpretation of the 3D shapes of metamorphic core complexes, *Geochemistry, Geophysics, Geosystems, 13* (9), 1-17

Ludwig, K. R. (2003). *User's manual for Isoplot 3.00. A Geochronological Toolkit for Microsoft Excel*. Berkeley Geochronology Center Special Publication.

Marrett, R. A., and Allmendinger, R. W. (1990). Kinematic analysis of fault-slip data, *Journal of Structural Geology, 12*, 973-986.

Martín, J. M., Braga, J. C., Aguirre, J., and Puga-Bernabéu, A. (2009). History and evolution of the North-Betic Strait (Prebetic Zone, Betic Cordillera): A narrow, early Tortonian, tidal-dominated, Atlantic-Mediterranean marine passage, *Sedimentary Geology, 216*, 80-90.

Mascle, J., Le Cleach, A., and Jongsma, D. (1986). The eastern Hellenic margin from Crete to Rhodes: example of progressive collision, *Marine Geology, 73*, 145-168.

McClusky, S., Balassanian, S., Barka, A., Demir, C., Ergintav, S., Georgiev, I., Gurkan, O., ….. Veis, G. (2000). Global Positioning System constraints on plate kinematics and dynamics in the eastern Mediterranean and Caucasus, *Journal of Geophysical Research, 105*(B3), 5695-5720.

McKenzie, D. (1972). Plate tectonics in the Mediterranean region, *Nature, 226*, 239-243.

McKenzie, D. (1978). Active tectonics of the Alpine-Himalayan belt: the Aegean Sea and surrounding regions, *Geophysical Journal International*, *55*(1), 217-254.

Means, W. D. (1984). Shear zones of types I and II and their significance for reconstruction of rock history, *Geological Society of America Abstracts, 16*, 50.

Means, W. D. (1995). Shear zones and rock history, *Tectonophysics, 247*, 157-160.

MediMap Group (2005). *Morpho Bathymetry of the Mediterranean*. CIESM/Ifremer Special Publication, Atlases and Maps, two maps at 1:2,000,000.

Mitra, G. (1992). Deformation of granitic basement rocks along fault zones at shallow to intermediate crustal levels. In S. Mitra, G. W. Fisher (Eds), *Structural Geology of Fold and Thrust Belts* (pp. 123-144). Baltimore: Johns Hopkins University Press.

Meulenkamp, J. E., Wortel, W. J. R., Van Wamel, W. A., Spakman, W., and Strating, E. H. (1988.) On the Hellenic Subduction Zone and the Geodynamic Evolution of Crete in the Late Middle Miocene, *Tectonophysics, 146*, 203-215.

Moissette, P., Cornée, J. J., Antonarakou, A., Kontakiotis, G, Drinia, H., Koskeridou, E., ….. Karakitsios, V. (2018). Palaeoenvironmental changes at the Tortonian/Messinian boundary: A deep-sea sedimentary record of the eastern Mediterranean Sea, *Palaeogeography, Palaeoclimatology, Palaeoecology, 505*, 217-233.

Monod, O. (1977). *Recherces géologiques dans le Taurus occidentales au sud de Beyşehir (Turquie)*. (Ph.D. Thesis). Université de Paris-Sud, Thèse de Doctorat d'État ès Sciences, Orsay, France.

Morris, A., and Robertson, A. H. F. (1993). Miocene remagnetisation of carbonate platform and Antalya Complex unitswithin the Isparta Angle, SW Turkey, *Tectonophysics, 220*, 243-266.

Ocakoğlu, N. (2012). Investigation of Fethiye-Marmaris Bay (SW Anatolia): seismic and morphologic evidences from the missing link between the Pliny Trench and the Fethiye-Burdur Fault Zone, *Geo-Marine Letters, 32*, 17-28.

Okay, A.I. (1989). Geology of the Menderes Massif and the Lycian Nappes south of Denizli, western Taurides, *Bulletin of The Mineral Research and Exploration (MTA), 109*, 37-51.

Önalan, M. (1979). *Elmalı-Kaş (Antalya) arasındaki bölgenin jeolojisi*. (Ph.D. Thesis). İstanbul Üniversitesi Fen Fakültesi Monografileri, İstanbul.

Över, S., Pınar, A., Özden, S., Yılmaz, H., Ünlügenç, U. C., and Kamacı, Z. (2010). Late Cenozoic stress field in the Cameli Basin, SW Turkey, *Tectonophysics, 492*(1), 60-72.

Över, S., Yılmaz, H., Pınar, A., Özden, S., Ünlügenç, U. C., and Kamacı, Z. (2013a). Plio-Quaternary Stress State in the Burdur Basin, SW-Turkey, *Tectonophysics, 588*, 56-68.

Över, S., Özden, S., Yılmaz, H., Pınar, A., Unlügenç, U. C., and Kamacı, Z. (2013b). Plio-Quaternary stress regime in Eşen Çay Basin, SW Turkey. Geological Development of Anatolia and the Easternmost Mediterranean Region, *Geological Society of London Special Publications, 372*(1), 547-560.

Özbakır, A. D., Şengör, A. M. C., Wortel, M. J. R., and Govers, R. (2013). The Pliny-Strabo trench region: A large shear zone resulting from slab tearing, *Earth and Planetary Science Letters, 375,* 188-195.

Özeren, M. S., and Holt, W. E. (2010). The dynamics of the eastern Mediterranean and eastern Turkey, *Geophysical Journal International, 183,* 1165-1184.

Özkaptan, M., Koç, A., Lefebvre, C., Gülyüz, E., Uzel, B., Kaymakci, N., ….. Sözbilir, H. (2014). Kinematics of SW Anatolia implications on crustal deformation above slab tear, *General Assembly European Geosciences Union (EGU-2014),* Vienna, Austria, 27 April - 2 May.

Özüdoğru, Ş., Dökü, F. E., Dikbaş, G., and Vanhavarbeke, H. (2011). Kibyra 2010, *ANMED, 9,* 36-43.

Papazachos, B. C., and Papaioannou, Ch. A. (1999). Lithospheric boundaries and plate motions in the Cyprus area, *Tectonophysics, 308,* 193-204.

Paton, S. (1992). *The relationship between extension and volcanism in western Turkey, the Aegean Sea and central Greece*. (Ph.D. Thesis). University of Cambridge, UK.

Pe-Piper, G., and Piper, D. J. W. (2007). Neogene back arc volcanism of the Aegean: new insights into the relationship between magmatism and tectonics. In, L. Beccaluva, G. Bianchini (Eds.), *Cenozoic Volcanism in the Mediterranean Area (Vol. 418, 17-31).* Geological Society of America.

Piromallo, C., and Morelli, A. (2003). P wave tomography of the mantle under the Alpine-Mediterranean area, *Journal of Geophysical Research, 108* (B2), 2065.

Poisson, A., Yağmurlu, F., Bozcu, M., and Şentürk, M. (2003). New insight on the tectonic setting and evolution around the apex of the Isparta Angle (SW Turkey), *Geological Journal, 38,* 257-282.

Popov, S. V., Shcherba, I. G., Ilyina, L. B., Nevesskaya, L. A., Paramonova, N. P., Khondkarian, S. O., and Magyar, I. (2006). Late Miocene to Pliocene palaeogeography of the Paratethys and its relation to the Mediterranean, *Palaeogeography, Palaeoclimatology, Palaeoecology, 238,* 91-106.

Prelević, D., Akal, C., Romer, R. L., Mertz-Kraus, R., and Helvacı, C. (2015). Magmatic response to slab tearing: constraints from the Afyon Alkaline Volcanic Complex, Western Turkey, *Journal of Petrology, 56*(3), 527-562.

Price, S. P., and Scott, B. (1994). Fault-block rotations at the edge of a zone of continental extension; southwest Turkey, *Journal of Structural Geology, 16*(3), 381-392.

Ramsay, J. G., and Huber, M. I. (1983). *The Techniques of Modern Structural Geology. Strain Analysis.* Vol. 1. Academic Press, London.

Reilinger, R., McClusky, S., Oral, M., King, R., Toksöz, M., Barka, A., ….. Sanlı, I. (1997). Global positioning system measurements of present-day crustal movements in the Arabia-Africa-Eurasia plate collision zone, *Journal of Geophysical Research: Solid Earth, 102*(B5), 9983-9999.

Reilinger, R., McClusky, S., Vernant, P., Lawrence, S., Ergintav, S., Cakmak, R., Ozener, ….. Karam, G. (2006). GPS constraints on continental deformation in the Africa-Arabia-Eurasia continental collision zone and implications for the dynamics of plate interactions, *Journal of Geophysical Research, 111*(B5), 1-26.

Reilinger, R., McClusky, S. C., Paradissis, D., Ergintav, S., and Vernant, P. (2010). Geodetic constraints on the tectonic evolution of the Aegean region and strain accumulation along the Hellenic subduction zone, *Tectonophysics, 488*, 22-30.

Robertson, A., and Woodcock, N. (1986). The role of the Kyrenia Range linement, Cyprus, in the geological evolution of the Eastern Mediterranean area, *Philosophical Transactions of the Royal Society London Serie A, 317*, 141-177.

Rossi, M., Minervini, M., Ghielmi, M., and Rogledi, S. (2015). Messinian and Pliocene erosional surfaces in the Po Plain-Adriatic Basin: Insights from allostratigraphy and sequence stratigraphy in assessing play concepts related to accommodation and gateway turnarounds in tectonically active margins. *Marine and Petroleum Geology, 66*, 192-216.

Ryan, W. B. F., Carbotte, S. M., Coplan, J. O., O'Hara, S., Melkonian, A., Arko, R., ….. Zemsky, R. (2009). Global multi-resolution topography synthesis, *Geochemstry, Geophysics, Geosystems, 10*(3), 1-9.

Sakınç, M., Yaltırak, C., and Oktay, F. Y. (1999). Palaeogeographical evolution of the Thrace Neogene Basin and the Tethian-Paratethian relations at northwest Turkey (Thrace), *Palaeogeography, Palaeoclimatology, Palaeoecology, 153*, 17-40.

Sakınç, M., Yaltırak, C., and Oktay, F. Y. (2000). Messinian palaeogeography and Messinian crisis effect of the North Aegean Sea. In 1. National Marine Science Conference. *Proceedings of the 1. National Marine Science Conference*, Ankara, Turkey, pp. 208-213.

Sakınç, M., and Yaltırak, C. (2005). Messinian Crisis: What Happened around the Northeastern Aegean?, *Marine Geology, 221*(1-4), 423-436.

Samson, S. D., and Alexander, E. C. (1987). Calibration of the interlaboratory ^{40}Ar/^{39}Ar dating standard, Mmhb-1, *Chemical Geology: Isotope Geoscience Section, 66*, 27-34.

Saraç, G. (2003). Türkiye omurgalı fosil yatakları (Report No. 10609). Ankara: General Directorate of Mineral Research and Exploration (MTA) Report.

Schreurs, G., and Colletta, B. (1998). Analogue modelling of faulting in zones of continental transpression and transtension. In: Holdsworth, R.E., Strachan, R.A., Dewey, J.F. (Eds.), Continental Transpressional and Transtensional Tectonics, *Geological Society Special Publications, 135*, 59-79.

Schreurs, G., and Colletta, B. (2003). Analogue modelling of continental transpression. In: Schellart, W.P., Passchier, C. (Eds.), Analogue

Modelling of Large-scale Tectonic Processes, *Journal of the Virtual Explorer*, *7*, 103-114.

Seyitoğlu, G., Işık, V., and Çemen, I. (2004). Complete Tertiary exhumation history of the Menderes massif, western Turkey: an alternative working hypothesis, *Terra Nova, 16*(6), 358-364.

Shanker, D., Paudyal, H, and Singh, H. N. (2011). Discourse on Seismotectonics of Nepal Himalaya and Vicinity: Appraisal to Earthquake Hazard, *Geosciences, 1*(1), 1-15.

Shaw, B., and Jackson, J. (2010). Earthquake mechanisms and active tectonics of the Hellenic subduction zone, *Geophysical Journal International*, *181*(2), 966-984.

Smith, W. H. F, and Wessel, P. (1990). Gridding with continuous curvature splines in tension, *Geophysics, 55*, 293-305.

Snel, E., Mărunţeanu, M., and Meulenkamp, J. E. (2006). Calcareous nannofossil biostratigraphy and magnetostratigraphy of the Upper Miocene and Lower Pliocene of the Northern Aegean (Orphanic Gulf-Strimon Basin areas), Greece, *Palaeogeography, Palaeoclimatology, Palaeoecology, 238*, 125-150.

Sözbilir, H. (2001). Extensional tectonics and the geometry of related macroscopic structures: field evidence from the Gediz Detachment, Western Turkey, *Turkish Journal of Earth Sciences*, *10*, 51-67.

Şaroğlu, F., Emre, M., and Kuşçu, M. (1992). *Active Fault Map of Turkey*. General Directorate of Mineral Research and Exploration (MTA), Ankara, Turkey.

Şenel, M. (1997a). *Geological Map of Fethiye, L8 quadrangle, No:2, in 1:100.000 scale sheet*. General Directorate of Mineral Research and Exploration (MTA), Ankara, Turkey, 22 pp.

Şenel, M. (1997b). *Geological Map of Fethiye, M8 quadrangle, No:4, in 1:100.000 scale sheet*. General Directorate of Mineral Research and Exploration (MTA), Ankara, Turkey.

Şenel, M. (1997c). *Geological Map of Denizli, J9 quadrangle, No: 16, in 1:100.000 scale sheet*. General Directorate of Mineral Research and Exploration (MTA), Ankara, Turkey.

Şenel, M. (2002). *Geological Map of Turkey, Denizli 1:500.000 scale sheet*. General Directorate of Mineral Research and Exploration (MTA), Ankara, Turkey.

Şenel, M., and Bölükbaşı, A. S. (1997). *Geological Map of Fethiye, M9 quadrangle, No:5, 1:100.000 scale sheet*. General Directorate of Mineral Research and Exploration (MTA), Ankara, Turkey.

Şenel, M., Selçuk, H., Bilgin, Z. R., Şen, A. M., Karaman, T., Dinçer, M.A., ….. Bilgi, C. (1989). Geology of the Region around Çameli (Denizli)-Yeşilova (Burdur)-Elmalı (Antalya) (Report No. 9429). Ankara: General Directorate of Mineral Research and Exploration (MTA) Report.

Şengör, A. M. C. (1979). The North Anatolian Transform Fault: its age, offset and tectonic significance, *Journal Geological Society London*, *136*, 269-282.

Şengör, A. M. C., Görür, N., and Şaroğlu, F. (1985). Strike-slip faulting and related basin formation in zones of tectonic escape: Turkey as a case study. In: K. Biddle, N. Christie-Blick (Eds.), *Society of Economic Paleontologists and Mineralogists, Special Publications*, *37*, 227-264.

Taymaz, T., and Price, S. (1992). The 1971 May 12 Burdur earthquake sequence, SW Turkey: a synthesis of seismological and geological observations, *Geophysical Journal International*, *108*(2), 589-603.

ten Veen, J. H. (2004). Extension of Hellenic forearc shear zones in SW Turkey: the Pliocene-Quaternary deformation of the Esen Cay Basin, *Journal of Geodynamics*, *37*, 181-204.

ten Veen, J. H., and Kleinspehn, K. L. (2002). Geodynamics along an increasingly curved convergent plate boundary: Late Mioicene-Pleistocene Rhodes, Greece, *Tectonics*, *21*(3), 8-1-8-21.

ten Veen, J. H., Woodside, J. M., Zitter, T. A. C., Dumont, J. F., Mascle, J., and Volkonskaia, A. (2004). Neotectonic evolution of the Anaximander Mountains at the junction of the Hellenic and Cyprus arcs, *Tectonophysics*, *391*, 35-65.

ten Veen, J. H., Boulton, S. J., and Alçiçek, M. C. (2009). From palaeotectonics to neotectonics in the Neotethys realm: The importance of kinematic decoupling and inherited structural grain in SW Anatolia (Turkey), *Tectonophysics*, *473*, 261-281.

Tiryakioğlu, I., Floyd, M., Erdoğan, S., Gülal, E., Ergintav, S., McClusky, S., and Reilinger, R. (2013). GPS Constraints on Active Deformation in the Isparta Angle Region of SW Turkey, *Geophysical Journal International*, *195*, 1455-1463.

Tsaparas, N., and Marcopodouluo-Dicantoni, A. (2005). Tortonian Scleractinian Corals from the island of Gavdos (South Greece), *Revue de Paléobiologie, 24*, 629-637

Tur, H., Yaltırak, C., Elitez, İ., and Sarıkavak, K. T. (2015). Pliocene-Quaternary tectonic evolution of the Gulf of Gökova, southwest Turkey, *Tectonophysics*, *638*, 158-176.

Turan, N. (2002). *Geological map of Turkey in 1:500.000 scale Ankara sheet*. General Directorate of Mineral Research and Exploration, Ankara, Turkey.

Url-1 <http://earthquake.usgs.gov/earthquakes/search/>, date retrieved 2015.

van den Hoek Ostende, L. W., Diepenveen, F., Tesakov, A., Saraç, G., Mayhew, D., and Alçiçek, M. C. (2015a). On the brink: micromammals from the latest Villanyian from Bıçakçı (Anatolia), *Geological Journal*, *50*, 230-245.

van den Hoek Ostende, L. W., Gardner, J. D., van Bennekom, L., Alçiçek, M. C., Murray, A., Wesselingh, F. P., Alçiçek, H., and Tesakov, A. (2015b). Ericek, a new Pliocene vertebrate locality in the Çameli Basin (southwestern Anatolia, Turkey), *Palaeobiodiversity and Palaeoenvironments*, *95*(3), 305-320.

van Hinsbergen, D. J. J. (2010). A key extensional metamorphic core complex reviewed and restored: the Menderes Massif on western Turkey, *Earth Science Reviews, 102*, 60-76.

van Hinsbergen, D. J. J., and Boekhout, F. (2009). Neogene brittle detachment faulting on Kos during formation of the Cycladic-Menderes metamorphic core complex (Greece/ Turkey). In: van Hinsbergen, D.J.J., Edwards, M.A., Govers, R. (Eds.), *Collision and Collapse at the Africa-Arabia-Eurasia Subduction Zone: Geological Society, London, Special Publications, 311*, 311-320.

van Hinsbergen, D. J. J., and Schmid, S. M. (2012). Map view restoration of Aegean-West Anatolian accretion and extension since the Eocene, *Tectonics, 31*(5), 1-40.

van Hinsbergen, D. J. J., Hafkenscheid, E., Spakman, W., Meulenkamp, J. E., and Wortel, R. (2005). Nappe stacking resulting from subduction of oceanic and continental lithosphere below Greece, *Geology, 33*, 325-328.

van Hinsbergen, D. J. J., Krijgsman, W., Langereis, C. G., Cornée, J. -J., Duermeijer, V. E., and van Vugt, N. (2007). Discrete Plio-Pleistocene phases of tilting and counterclockwise rotation of the southeastern Aegean Arc (Rhodos, Greece): early Pliocene formation of the south Aegean left-lateral strike-slip system, *Journal of the Geological Society London, 164*, 1133-1144.

van Hinsbergen, D. J. J., Kaymakci, N., Spakman, W., and Torsvik, T. H. (2010a). Reconciling the geological history of western Turkey with plate circuits and mantle tomography, *Earth Planetary Science Letters, 297*, 674-686.

van Hinsbergen, D. J. J., Dekkers, M. J., and Koç, A. (2010b). Testing Miocene remagnetization of Bey Dağları: timing and amount of Neogene rotations in SW Turkey, *Turkish Journal of Earth Sciences, 19*, 123-156.

van Hinsbergen, D. J. J., Dekkers, M. J., Bozkurt, E., and Koopman, M. (2010c). Exhumation with twist: Palaeomagnetic constraints on the evolution of the Menderes metamorphic core complex (western Turkey), *Tectonics, 29*, 1-33.

Verhaert, G., Muchez, P., Sintubin, M., Similox-Tohon, D., Vandycke, S., Keppens, E., Hodge, E. J., and Richards, D. A. (2004). Origin of palaeofluids in a normal fault setting in the Aegean region, *Geofluids, 4*(4), 300-314.

Verhaert, G., Similox-Tohon, D., Vandycke, S., Sintubin, M., and Muchez, P. (2006). Different stress states in the Burdur-Isparta region (SW Turkey) since Late Miocene times: a reflection of a transient stress regime, *Journal of Structural Geology, 28*, 1067-1083.

Vitale, S., and Mazzoli, S. (2008). Heterogeneous shear zone evolution: the role of shear strain hardening/softening, *Journal of Structural Geology, 30*(11), 1383-1395.

Wesselingh, F. P., Alçiçek, H., and Magyar, I. (2008). A Late Miocene Paratethyan mollusc fauna from the Denizli Basin (southwestern Anatolia, Turkey) and its regional palaeobiogeographic implications, *Geobios, 41*, 861-879.

Woodside, J. M., lvanov, M. K., and Limonov, A. F. (1997). Neotectonics and fluid flow through seafloor sediments in the Eastern Mediterranean and Black Seas, *Intergovernmental Oceanographic Commission Technical Series, 48*, No. I&II.

Woodside, J., Mascle, J., Huguen, C., and Volkonskaia, A. (2000). The Rhodes Basin, a post-Miocene tectonic trough, *Marine Geology, 165*, 1-12.

Yaltırak, C. (2002). Tectonic evolution of the Marmara Sea and its surroundings, *Marine Geology, 190*, 493-529.

Yaltırak, C., and Alpar, B. (2002). Evolution of the Middle Strand of North Anatolian Fault and Shallow Seismic Investigation of the Southestern Marmara Sea (Gemlik Bay), *Marine Geology*, *190*, 307-328.

Yaltırak, C. (2003). *Geodynamic evolution of the Gulf of Edremit and northern area.* (Ph.D. thesis). Istanbul Technical University, İstanbul, Turkey.

Yaltırak, C., Elitez, İ., Aksu, A., Hall, J., Çifçi, G., Dondurur, D., ….. Güneş, P. (2010). The relationship and evolution of the Burdur-Fethiye Fault/Shear Zone, the Rhode Basin, Anaximander Seamounts, the Antalya Gulf, and the Isparta Angle since Miocene to Recent in tectonics of the Eastern Mediterranean. *63th Geology Congress of Turkey*, Ankara, Turkey, 5-9 April.

Yılmaz, Y., Genç, S. C., Gürer, O. F., Bozcu, M., Yılmaz, K., Karacık, Z., Altunkaynak, Ş., and Elmas A. (2000). When did the western Anatolian grabens begin to develop? E. Bozkurt, J.A. Winchester, J.D.A. Piper (Eds.), *Geological Society, London, Special Publications, 173*, 353-384.

Yolsal, S., and Taymaz, T. (2010). Sensitivity Analysis on Relations between Earthquake Source Rupture Parameters and Far-Field Tsunami Waves: Case Studies in the Eastern Mediterranean Region, *Turkish Journal of Earth Sciences, 19*, 313-349.

Yolsal, S., Taymaz, T., and Yalçıner, A. C. (2007). Understanding tsunamis, potential source regions and tsunami prone mechanisms in the Eastern Mediterranean. In: The Geodynamics of the Aegean and Anatolia, Taymaz, T., Yılmaz, Y. and Dilek, Y. (eds.), *Geological Society, London, Special Publications, 291*, 201-230.

Yolsal-Çevikbilen, S., and Taymaz, T. (2012). Earthquake source parameters along the Hellenic subduction zone and numerical simulations of historical tsunamis in the Eastern Mediterranean, *Tectonophysics, 536-537*, 61-100.

Zachariasse, W. J., van Hinsbergen, D. J. J., and Fortuin, A.R. (2008). Mass wasting and uplift on Crete and Karpathos during the early Pliocene related to initiation of south Aegean left-lateral strike-slip tectonics, *Bulletin of Geological Society, 120*, 976-993.

Zitter, T. A., Woodside, J. M., and Mascle, J. (2003). The Anaximander Mountains: a clue to the tectonics of southwest Anatolia, *Geological Journal, 38*(3-4), 375-394.

APPENDICES

APPENDIX A: Geological map of the study area and geological cross-sections through the study area (in the CD, Chapter 3).

APPENDIX B: Supplementary materials of the simplified palinspastic model of the Burdur-Fethiye Shear Zone (in the CD, Chapter 3).

APPENDIX C: Geological map and geological cross-section of the study area (in the CD, Chapter 4).

APPENDIX D: Supplementary materials of the supposed Kibyra Fault (Chapter 4).

APPENDIX E: Supplementary materials of the morphotectonic analysis of the Kibyra Fault (Chapter 4).

APPENDIX F: Geological map of the study area and geological cross-sections through the study area (in the CD, Chapter 5).

APPENDIX G: The measured Ar gas fractions released by laser-step heating for each of the 5 Ar isotopes in units of 1×10^{-13} ccSTP. Also included are the "J" factors and calculated ages. Measured volumes have been corrected for K, Ca AND Cl interference. All errors ARE ±1 sigma. (in the CD, Chapter 5).

APPENDIX D: Supplementary materials of the supposed Kibyra Fault

APPENDIX D1:

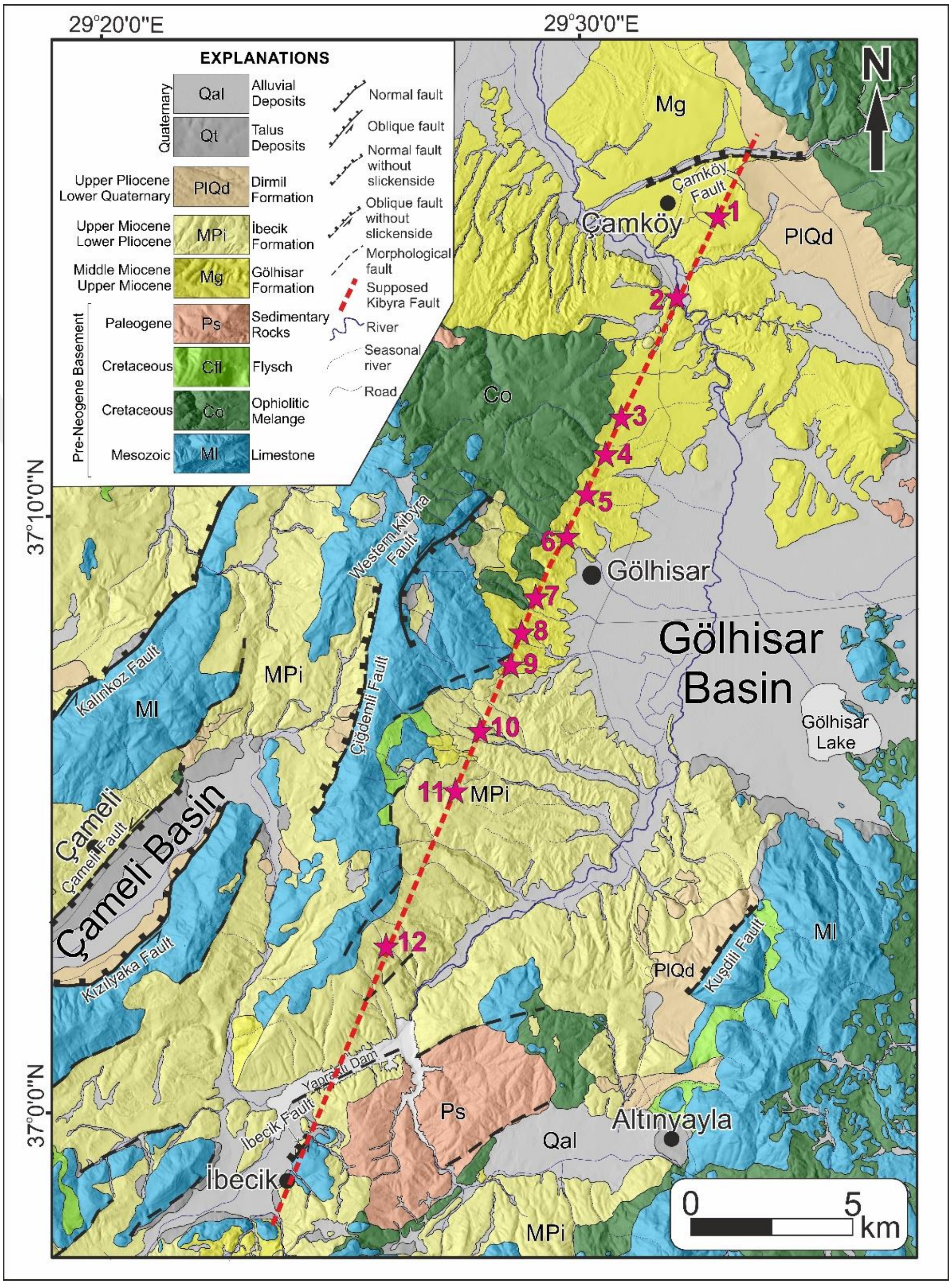

Figure D.1 : Geological map of the study area. The lithological properties and ages of the basement rocks were modified from 1/500000 Denizli sheet geological map of General Directorate of Mineral Research and Exploration (Şenel, 2002) and the contacts were redrawn by using field observations, DEMs and satellite images. Purple stars indicate the approximate locations of 1-12.

APPENDIX D2: The satellite images, digital elevation models and topographic profiles of the ridges and rivers along the supposed Kibyra Fault (see Appendix D1). Blue lines show the rivers, pink dashed lines show the ridges and orange dashed lines show the supposed Kibyra Fault.

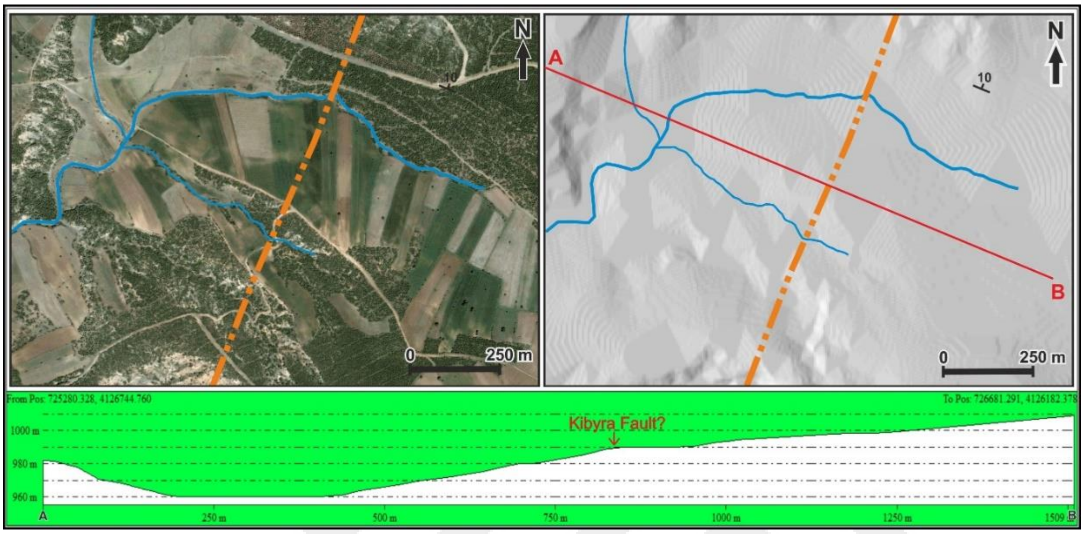

Figure D.2 : Location 1. Approximate coordinates: 37°15'17.86"N 29°32'55.28"E

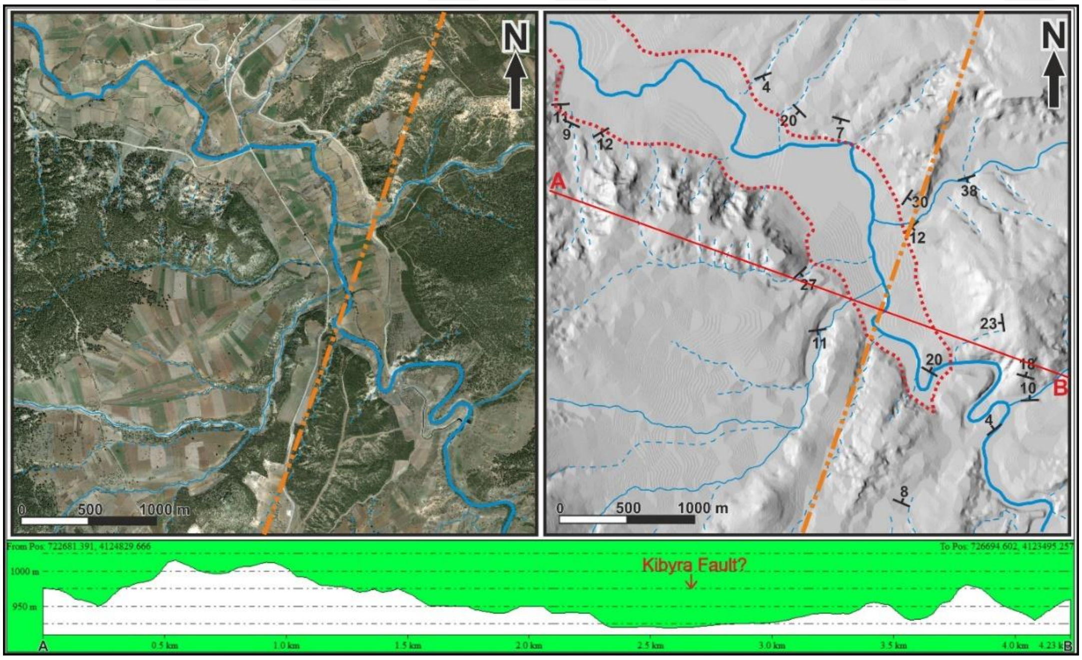

Figure D.3 : Location 2. Approximate coordinates: 37°13'57.18"N 29°32'15.39"E. The red dashed line shows the boundary of the bedrock on the edge of the valley.

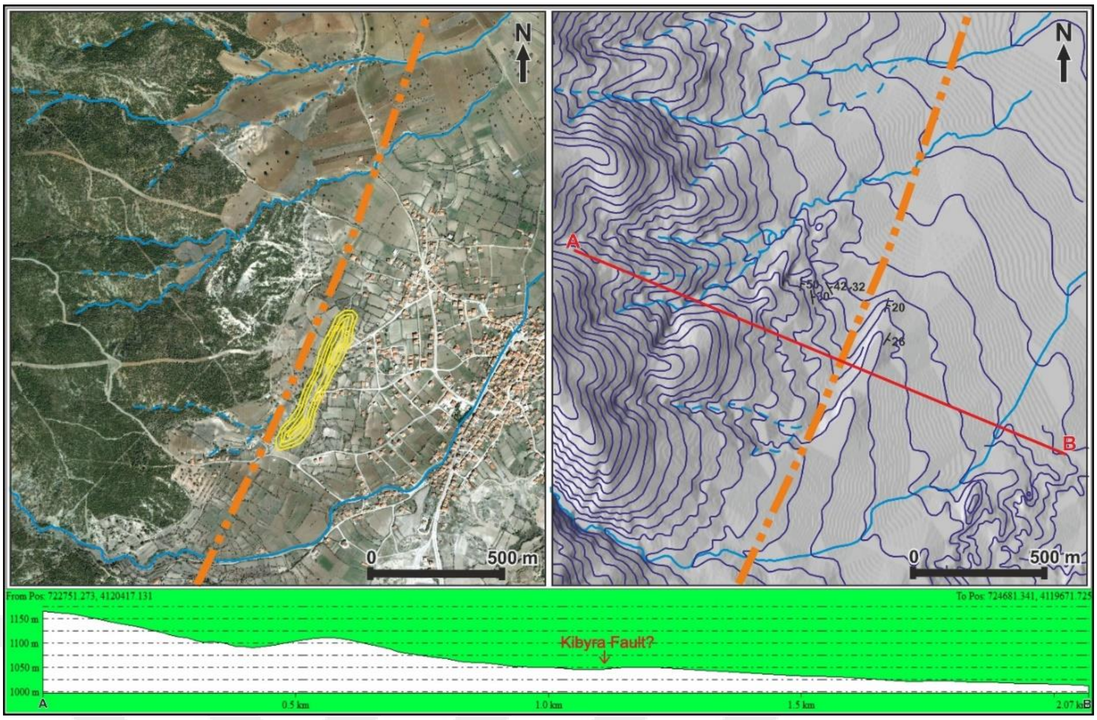

Figure D.4 : Location 3. Approximate coordinates: 37°11'51.68"N 29°31'19.12"E. The yellow lines show supposed contours of the ridge (Karabacak 2011).

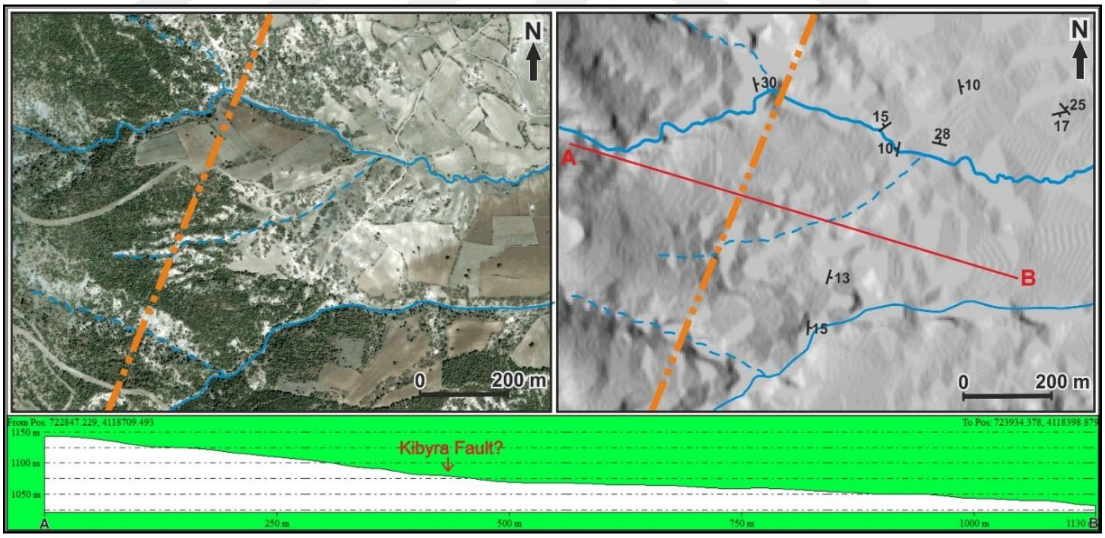

Figure D.5 : Location 4. Approximate coordinates: 37°11'10.73"N 29°30'48.82"E

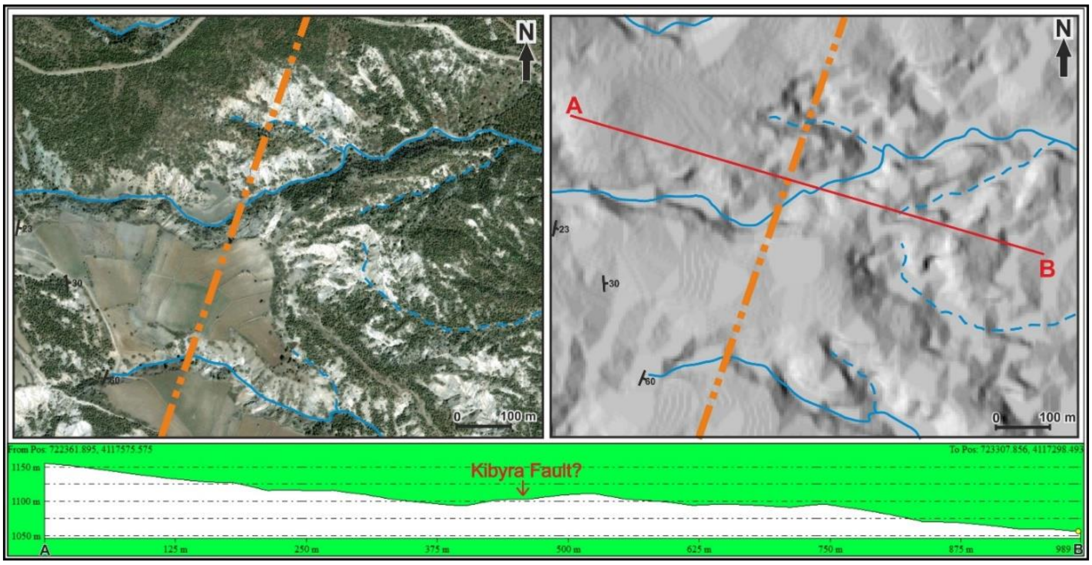

Figure D.6 : Location 5. Approximate coordinates: 37°10'30.88"N 29°30'24.93"E

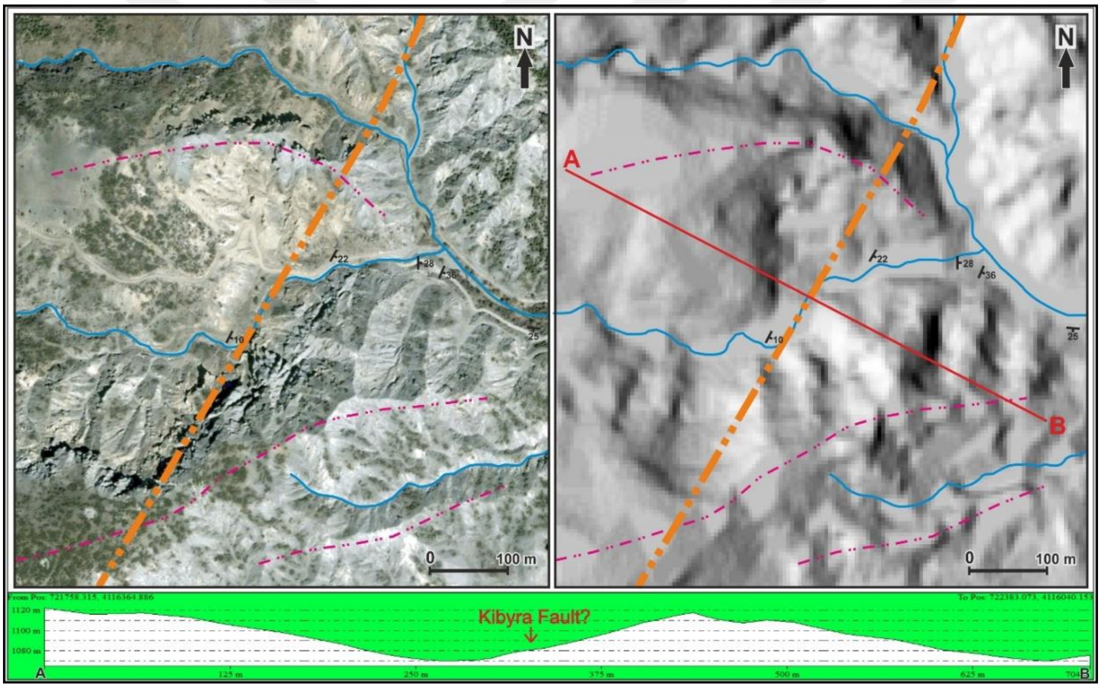

Figure D.7 : Location 6. Approximate coordinates: 37°9'53.90"N 29°30'2.17"E

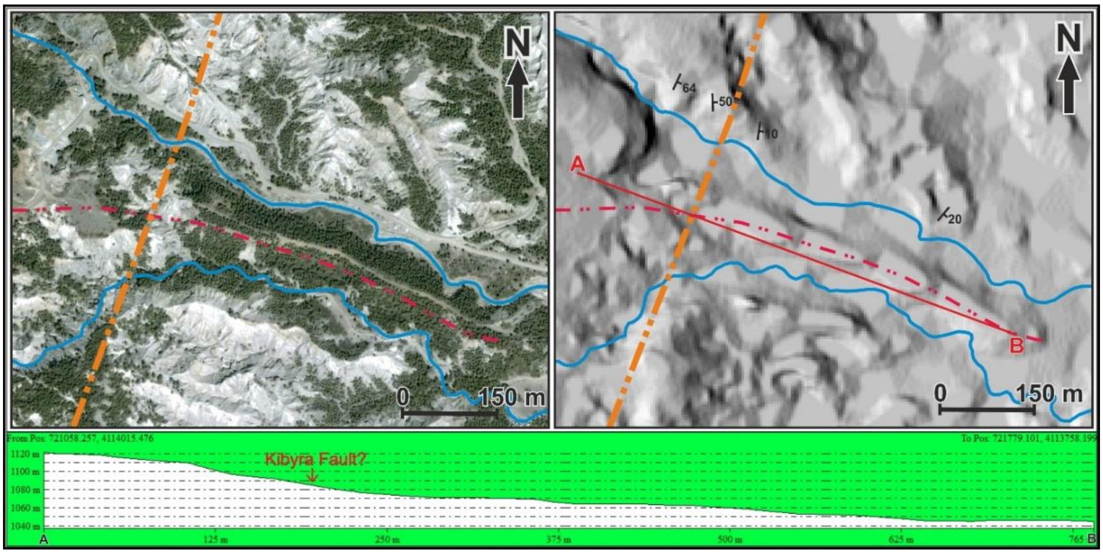

Figure D.8 : Location 7. Approximate coordinates: 37°8'44.58"N 29°29'27.26"E

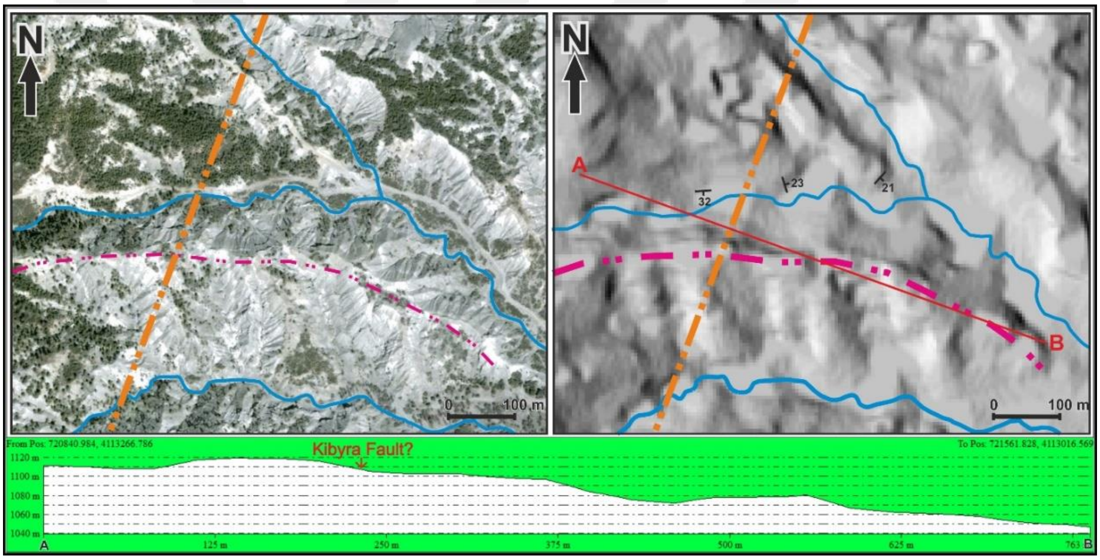

Figure D.9 : Location 8. Approximate coordinates: 37°8'16.63"N 29°29'17.33"E

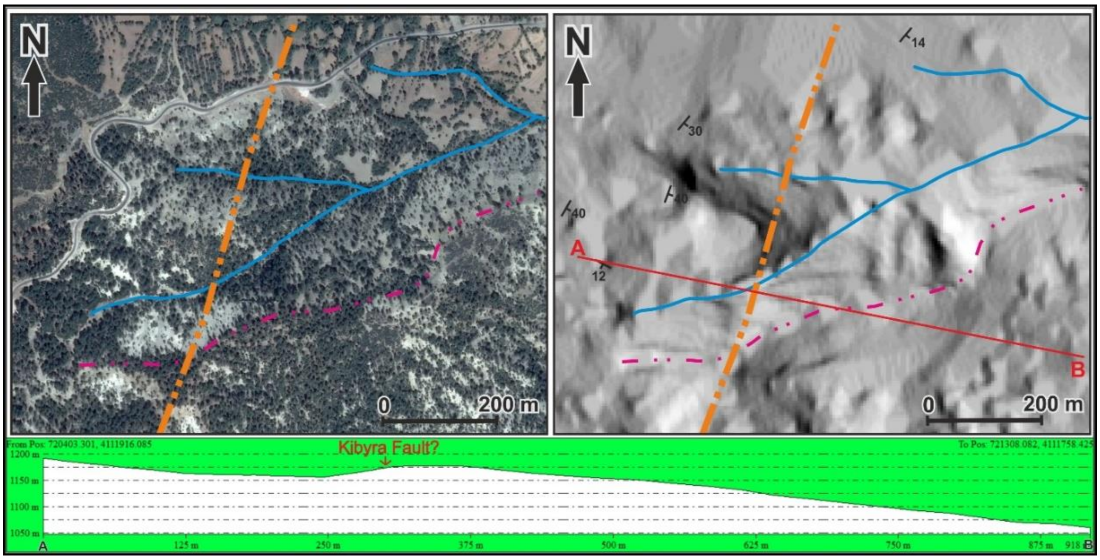

Figure D.10 : Location 9. Approximate coordinates: 37°7'43.27"N 29°29'6.05"E

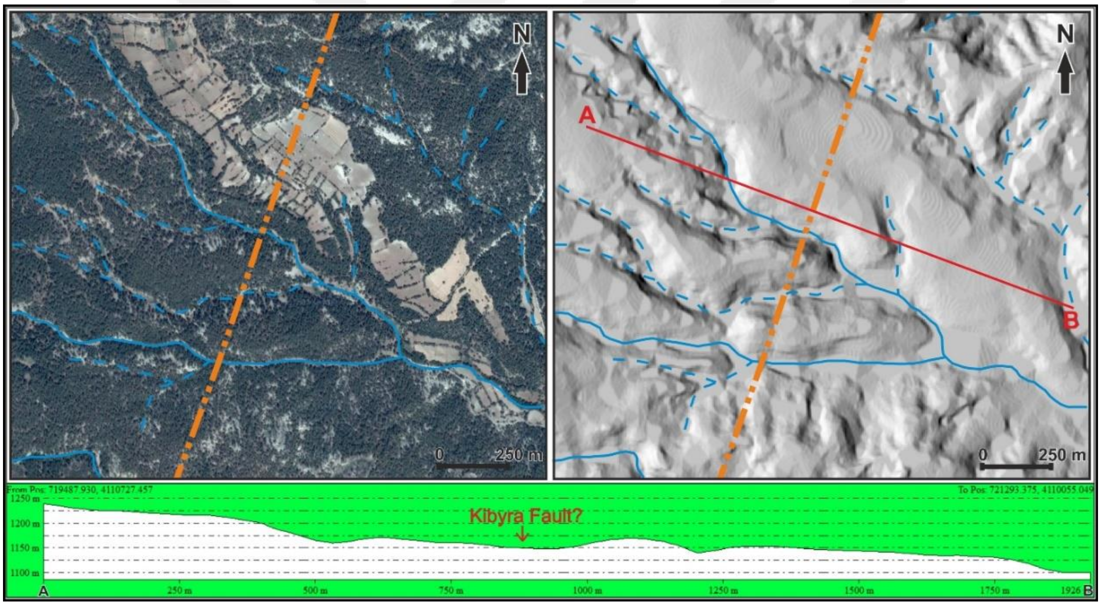

Figure D.11 : Location 10. Approximate coordinates: 37°6'46.80"N 29°28'31.59"E

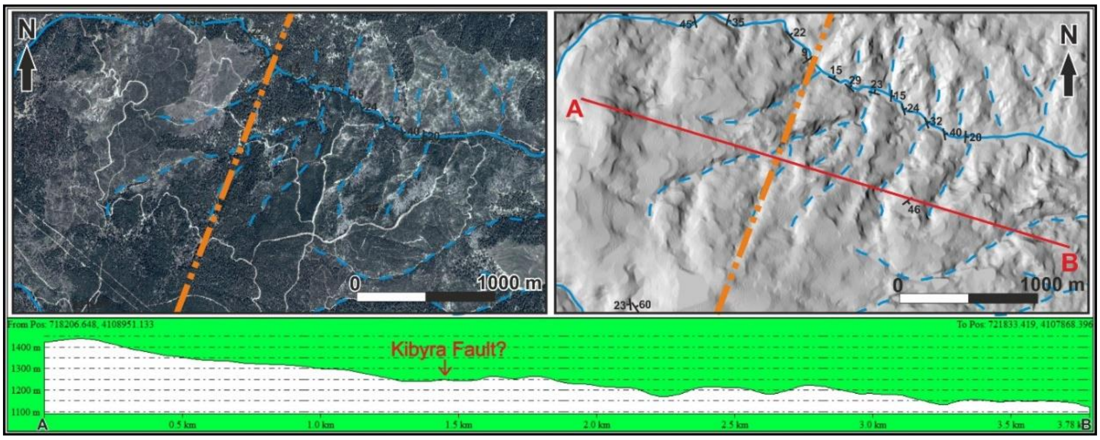

Figure D.12 : Location 11. Approximate coordinates: 37°5'56.27"N 29°28'6.74"E

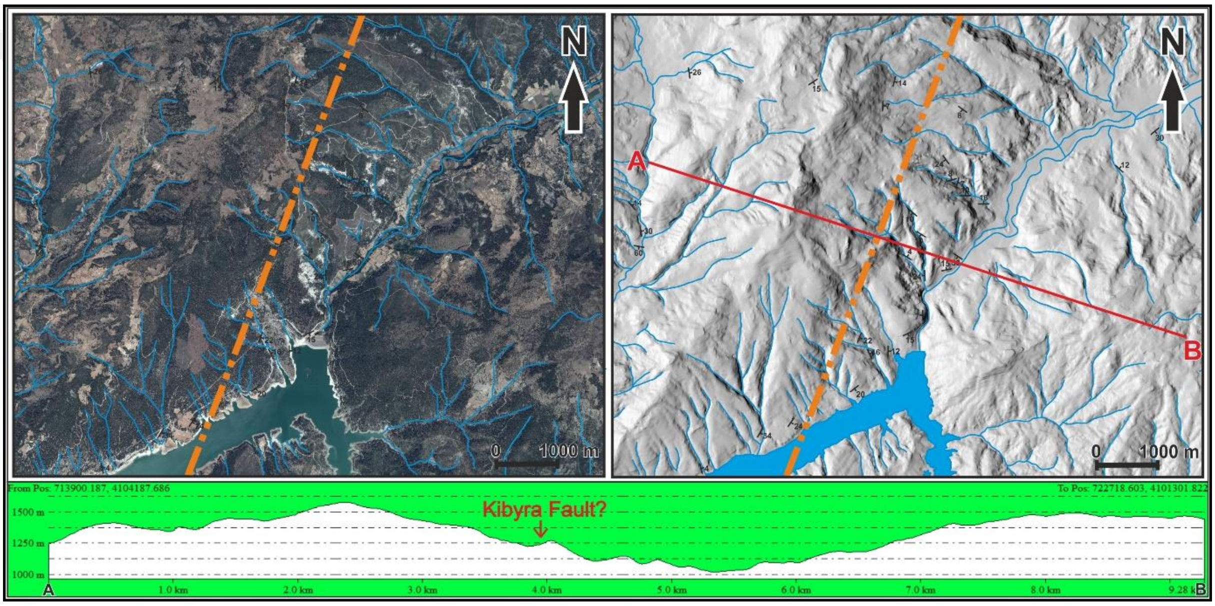

Figure D.13 : Location 12. Approximate coordinates: 37°2'13.52"N 29°26'15.35"E

APPENDIX E: Supplementary materials of the morphotectonic analysis of the Kibyra Fault

APPENDIX E1: Geological map of the study area showing the SL (stream length-gradient index) indices at 12 locations (from r1 to r12) along the supposed Kibyra Fault

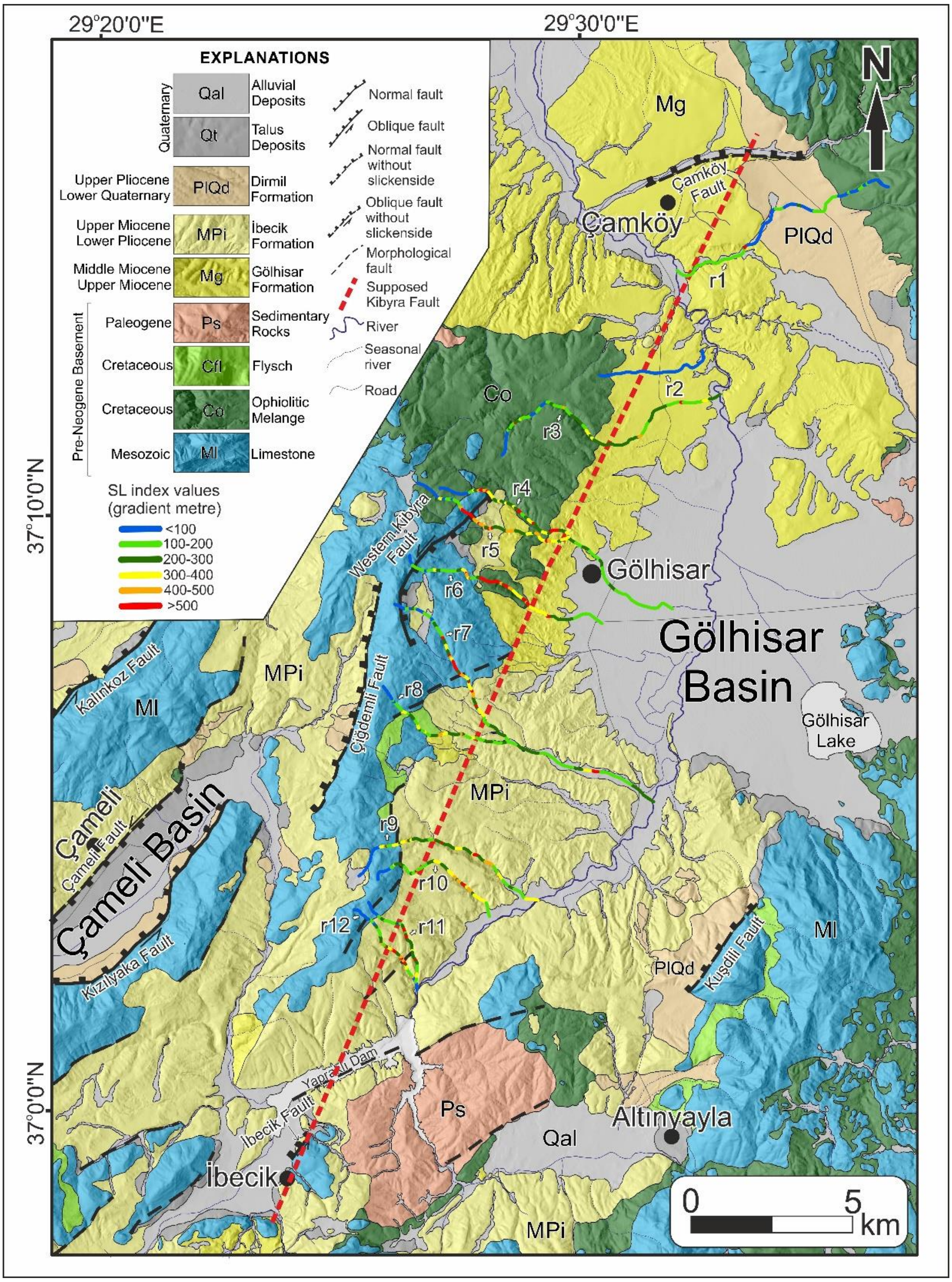

APPENDIX E2: Some longitudinal river profiles (coloured lines) along the supposed Kibyra Fault (see Appendix E1) and the measured SL index (dashed lines)

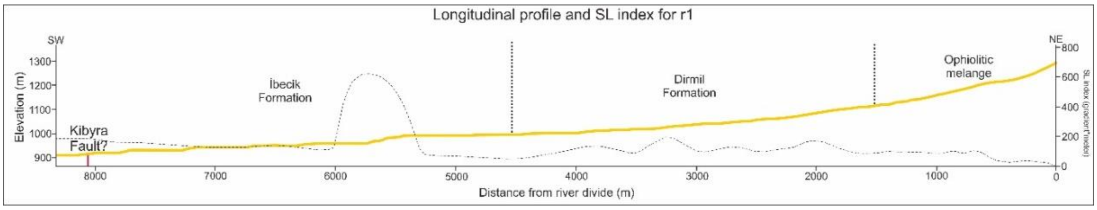

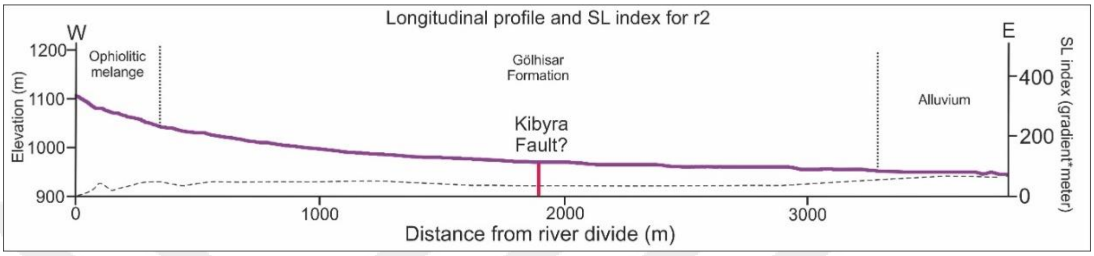

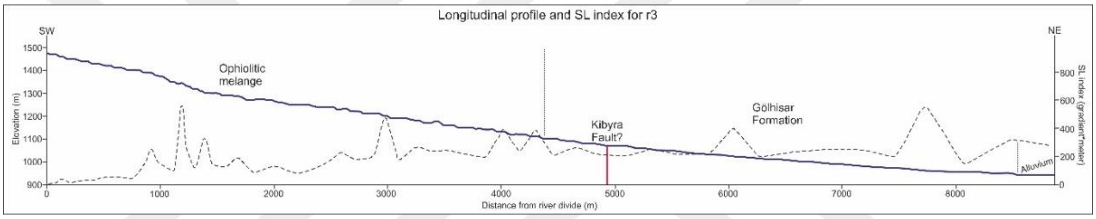

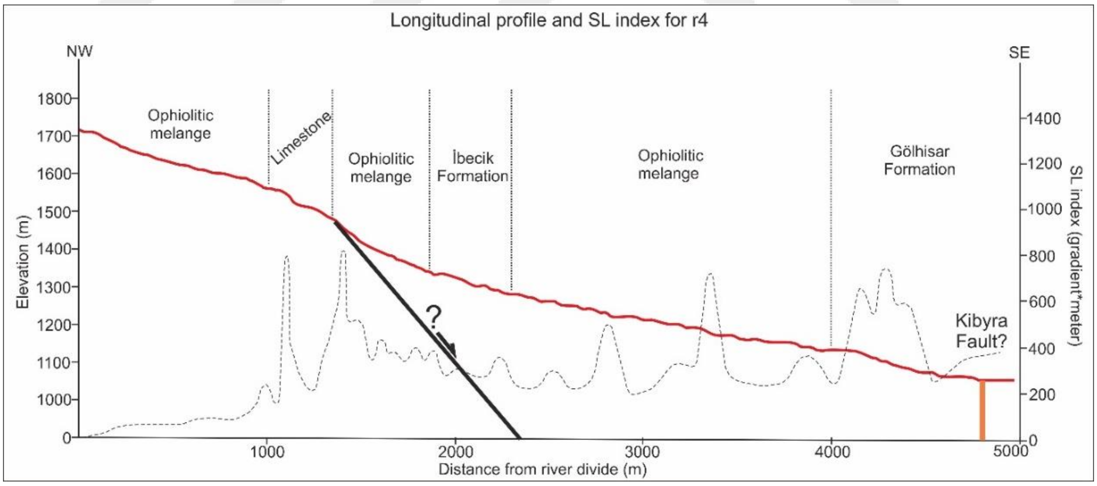

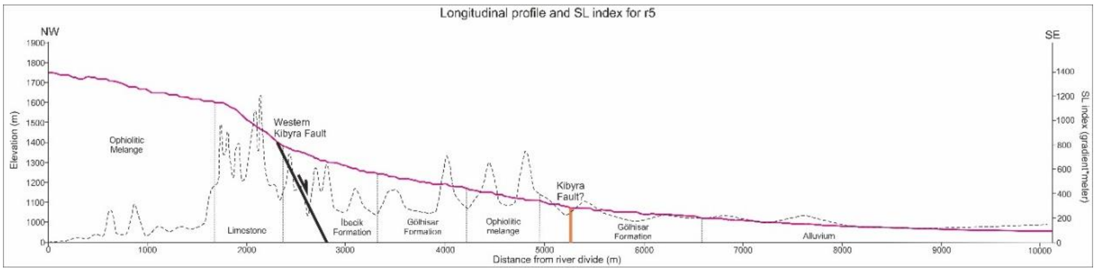

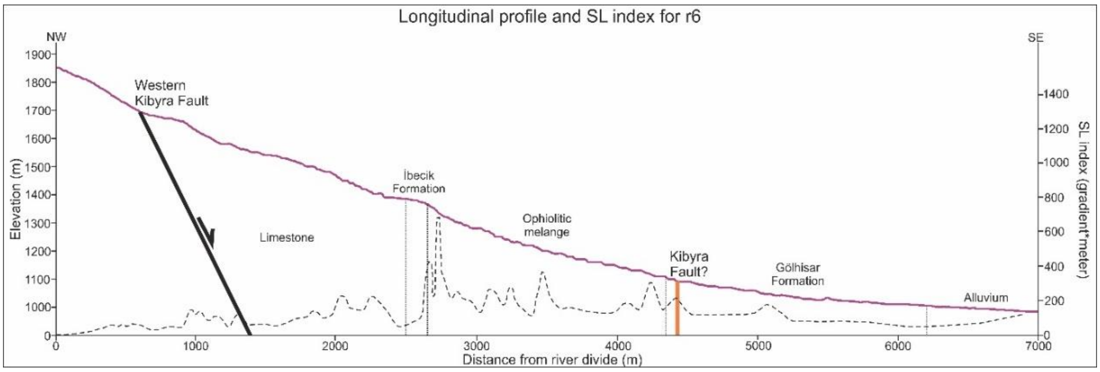
Longitudinal profile and SL index for r6
NW
SE
Western Kibyra Fault
İbecik Formation
Limestone
Ophiolitic melange
Kibyra Fault?
Gölhisar Formation
Alluvium
Elevation (m)
SL index (gradient*meter)
Distance from river divide (m)

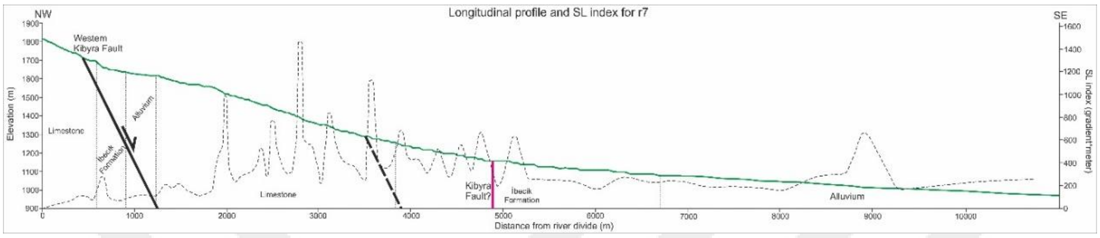
Longitudinal profile and SL index for r7
NW
SE
Western Kibyra Fault
Limestone
Alluvium
Kibyra Fault?
Alluvium
Distance from river divide (m)

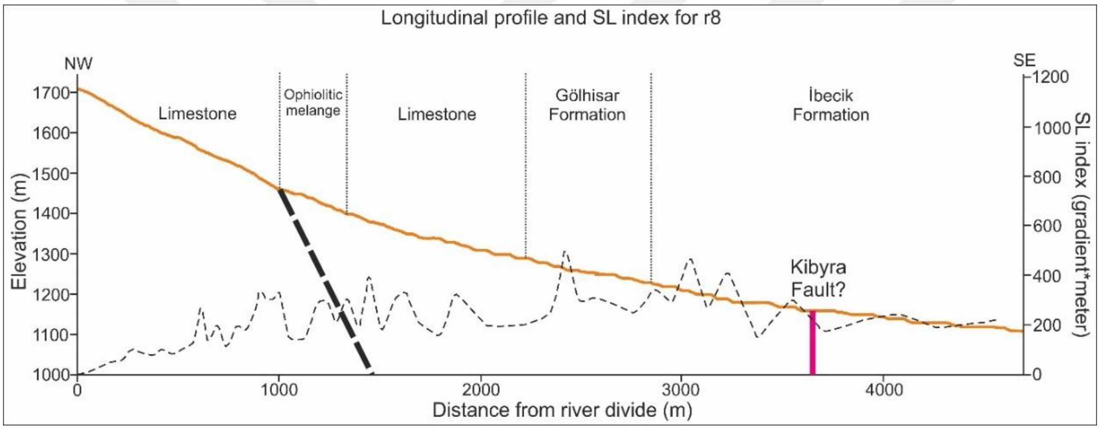
Longitudinal profile and SL index for r8
NW
SE
Limestone
Ophiolitic melange
Limestone
Gölhisar Formation
İbecik Formation
Kibyra Fault?
Elevation (m)
SL index (gradient*meter)
Distance from river divide (m)

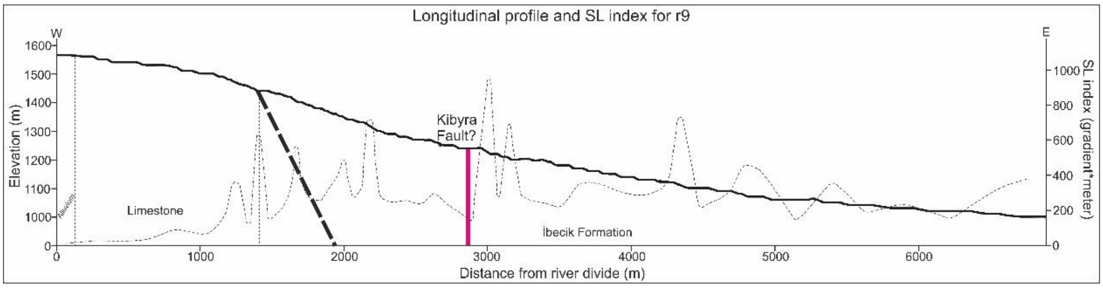
Longitudinal profile and SL index for r9
W
E
Kibyra Fault?
Limestone
İbecik Formation
Elevation (m)
SL index (gradient*meter)
Distance from river divide (m)

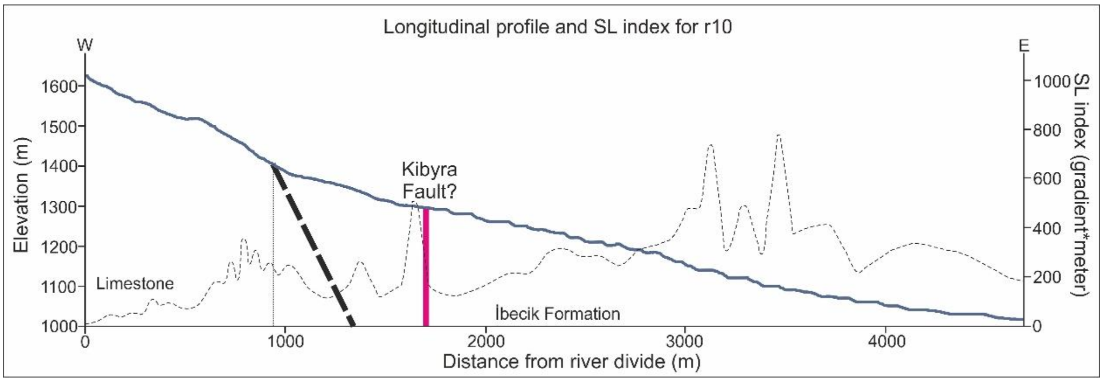
Longitudinal profile and SL index for r10
W
E
Kibyra Fault?
Limestone
İbecik Formation
Elevation (m)
SL index (gradient*meter)
Distance from river divide (m)

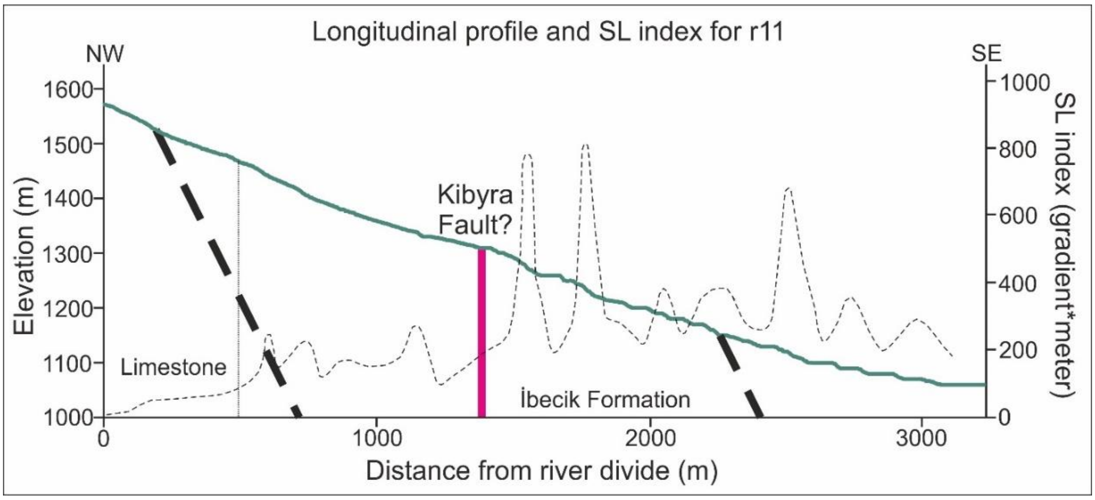
Longitudinal profile and SL index for r11
NW
SE
Kibyra
Fault?
Limestone
İbecik Formation
Elevation (m)
SL index (gradient*meter)
Distance from river divide (m)
1000
1100
1200
1300
1400
1500
1600
0
200
400
600
800
1000
0
1000
2000
3000

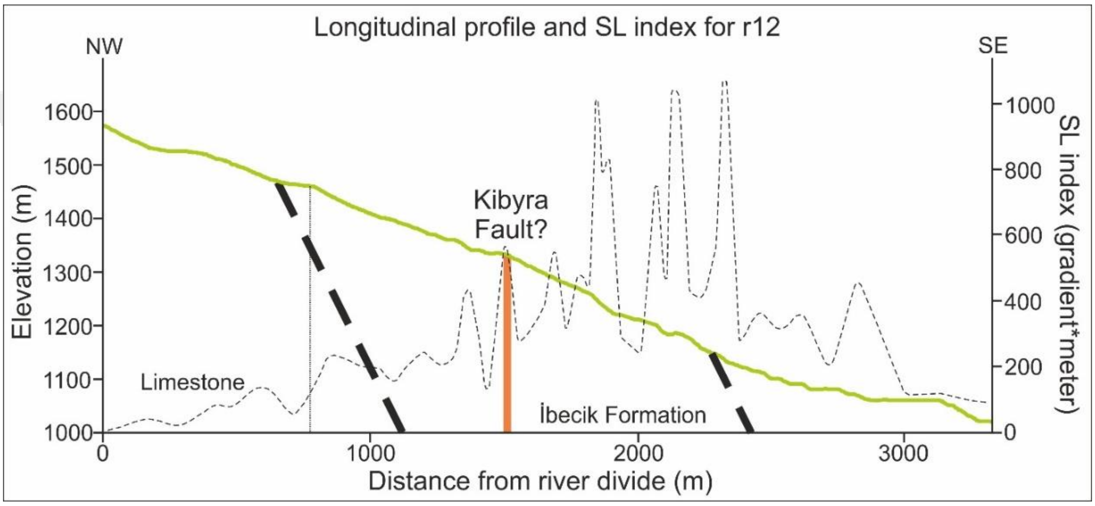
Longitudinal profile and SL index for r12
NW
SE
Kibyra
Fault?
Limestone
İbecik Formation
Elevation (m)
SL index (gradient*meter)
Distance from river divide (m)
1000
1100
1200
1300
1400
1500
1600
0
200
400
600
800
1000
0
1000
2000
3000

CURRICULUM VITAE

Name Surname : İrem Elitez

Place and Date of Birth : Zonguldak, 1984

E-Mail : elitezi@itu.edu.tr

EDUCATION :

- **B.Sc.** : 2007, İstanbul Technical University, Faculty of Mines, Geological Engineering Department
- **M.Sc.** : 2010, İstanbul Technical University, Eurasia Institute of Earth Sciences, Earth System Science

PROFESSIONAL EXPERIENCE AND REWARDS:

- April 2018 - currently : Senior Energy Consultant, Yeni Yapı Konut Sanayi ve Ticaret A.Ş. LTD. ŞTİ., İzmir, Turkey
- July 2017 - April 2018 : Research Assistant, Department of Geological Engineering, Istanbul Technical University, Turkey
- February 2011 - September 2016 : Research Assistant, Department of Geological Engineering, Istanbul Technical University, Turkey
- 2016 : Project Coordinator (Field geology, ArcGIS based geological and hydrogeological mapping and modelling, radiometric dating), “The Role of Burdur-Fethiye Shear Zone in the Neotectonics of the SW Turkey: Radiometric Dating of Volcanic Rocks Intercalated with Miocene-Pliocene Lacustrine and Terrestrial Sedimentary Units and Revealing of Real Chronostratigraphic Positions of the Sequences”, TUBITAK 1002 Project No: 115Y424
- 2014 : Researcher (Field geology, ArcGIS based geological and hydrogeological mapping and modelling), “Preparation of Beyşehir Lake Basin Protection Plan and Determination of Special Provision”, T.C. Ministry of Environment and Forestry, TUBITAK MAM-İTÜ Joint Project, Turkey

- 2014 : Researcher (Field geology, ArcGIS based geological and hydrogeological mapping and modelling) “Preparation of Karacaören I and II Dam Lakes Protection Plan and Determination of Special Provision”, T.C. Ministry of Environment and Forestry, TUBITAK MAM-İTÜ Joint Project, Turkey
- 2011 : Researcher (Field geology, ArcGIS based geological and hydrogeological mapping and modelling), “Bursa 1/100.000-scaled Environmental Arrangement Plan, Climate and Earth Sciences Project”, İTÜ Geological Engineering Research Group
- January 2010 - May 2010 : Field Engineer, İzmit Gulf Crossing Project, FUGRO-SIAL Geosciences Consulting and Engineering Ltd., Turkey
- 2009 : Scholarship student (Field geology, ArcGIS based geological and hydrogeological mapping and modelling), “Miocene-Recent Tectonic and Sedimentary Evolution of the Hellenic and Cyrus Arc Junction (including the Pliny-Strabo Trenches, Rhodes, Finike and Antalya Basins and Anaximander Mountains) and Its Comparison With the Tectonic Evolution of the Western Tauride Mountains, Eastern Mediterranean”, TUBITAK Project, Turkey

PUBLICATIONS, PRESENTATIONS AND PATENTS ON THE THESIS:

- **Elitez, İ.,** Yaltırak, C., Sunal, G. 2018. A new chronostratigraphy (^{40}Ar-^{39}Ar and U-Pb dating) for the middle section of the Burdur-Fethiye Shear Zone, SW Turkey (eastern Mediterranean), *Turkish Journal of Earth Sciences*, 27, 405-420.
- **Elitez, İ.,** Yaltırak, C., Aksu, A. E., Hall, J., Çifçi, G. 2018. The Continuation of the Burdur-Fethiye Shear Zone in the Marine Area between Dalaman and Patara. 3rd National Marine Sciences Conference, 9-12 May, 2018, İzmir, Turkey.
- **Elitez, İ.,** Yaltırak, C. 2018. Reply to the comment on “Miocene to Quaternary tectonostratigraphic evolution of the middle section of the Burdur-Fethiye Shear Zone, south-western Turkey: Implications for the wide inter-plate shear zones”, *Tectonophysics*, 722, 601-606.
- **Elitez, İ.,** Yaltırak, C., Kürçer, A., Özdemir, E., Güldoğan, Ç. U., 2017. A Critical Review of the Kibyra Fault (Burdur-Fethiye Shear Zone, SW Turkey), *Geodinamica Acta*, 29(1), 91-102.
- **Elitez, İ.,** Yaltırak, C., and Sunal, G. 2017. A new chronostratigraphy (40Ar-39Ar and U-Pb Dating) for the Middle Section of the Burdur-Fethiye Shear Zone, SW Turkey. General Assembly European Geosciences Union (EGU), 23-28 April, 2017, Vienna, Austria.
- **Elitez, İ.,** Yaltırak, C. 2016. Miocene to Quaternary tectonostratigraphic evolution of the middle section of the Burdur-Fethiye Shear Zone, south-western Turkey: Implications for the wide inter-plate shear zones, *Tectonophysics*, 690, 336-354.
- **Elitez, İ.,** Yaltırak, C., Aktuğ, B. 2016. Extensional and compressional regime driven left-lateral shear in southwestern Anatolia (eastern Mediterranean): The Burdur-Fethiye Shear Zone, *Tectonophysics,* 688, 26-35.
- **Elitez, İ.,** Yaltırak, C., Şahin, M. 2016. Vegetation and climate changes during the late Pliocene and early Pleistocene in SW Turkey-Comment to the published paper by Jiménez-Moreno et al., Quaternary Research, 84 (2015), 448-456, *Quaternary Research*, 85(3), 471-475.

- **Elitez, İ.,** and Yaltırak, C. 2016. Recent deformation of a left-lateral shear zone developed between extensional and compressional tectonic regimes: Burdur Fethiye Shear Zonu, SW Turkey. ATAG 20, 13-15 October, 2016, Pamukkale University, Denizli, Turkey.
- **Elitez, İ.,** and Yaltırak, C. 2016. Shear zones developed between extensional and compressional tectonic regimes: recent deformation of the Burdur-Fethiye Shear Zone as a case study. General Assembly European Geosciences Union (EGU), 17-22 April, 2016, Vienna, Austria.
- **Elitez, İ.,** Yaltırak, C., Hall, J., Aksu, A. E., Çifçi, G. 2015. Reply to the comment by M.C. Alçiçek on "The Fethiye-Burdur Fault Zone: A component of upper plate extension of the subduction transform edge propagator fault linking Hellenic and Cyprus Arcs, Eastern Mediterranean," Tectonophysics, 635, 80-99, by J. Hall, AE Aksu, İ. Elitez, C. Yaltirak and G. Çifçi, *Tectonophysics*. 664, 5-13.
- **Elitez, İ.** and Yaltırak, C. 2015. A different approach to age range of Neogene sediments in SW Turkey. General Assembly European Geosciences Union (EGU), 12-17 April, 2015, Vienna, Austria.
- **Elitez, İ.,** Yaltırak, C., Zabcı C., and Şahin, M. 2015. The integrated analyses of digital field mapping techniques and traditional field methods: implications from the Burdur-Fethiye Shear Zone, SW Turkey as a case-study. General Assembly European Geosciences Union (EGU), 12-17 April, 2015, Vienna, Austria.
- Yaltırak, C., Aksu, A. E., Hall, J., and **Elitez, İ.** 2015. Old stories and lost pieces of the Eastern Mediterranean puzzle: a new approach to the tectonic evolution of the Western Anatolia and the Aegean Sea. General Assembly European Geosciences Union (EGU), 12-17 April, 2015, Vienna, Austria.
- Hall, J., Aksu, A.E., **Elitez, İ.,** Yaltırak, C., Çifçi, G. 2014. The Fethiye-Burdur Fault Zone: A component of upper plate extension of the subduction transform edge propagator fault linking Hellenic and Cyprus Arcs, Eastern Mediterranean, *Tectonophysics*, 635, 80-99.
- **Elitez, İ.,** Yaltırak, C. 2014. Comment on Analyses of Seismic Deformation at the Kibyra Roman Stadium, Southwest Turkey by Volkan Karabacak, Önder Yönlü, Eray Dökü, Nafiye Günenç Kıyak, Erhan Altunel, Şükrü Özüdoğru, Cahit Çağlar Yalçıner, and Hüsnü Serdar Akyüz, *Geoarchaeology*, 29, 349-352.
- **Elitez, İ.,** Yaltırak, C. 2014. Miocene-Quaternary Geodynamics of Çameli Basin, Burdur-Fethiye Shear Zone (SW Turkey), *Geologial Bulletin of Turkey*, 57/3, 41-67.
- **Elitez, İ.,** and Yaltırak, C. 2014. Burdur-Fethiye Shear Zone (Eastern Mediterranean, SW Turkey). General Assembly European Geosciences Union (EGU), 27 April-2 May, 2014, Vienna, Austria.
- Yaltırak, C., **Elitez, İ.,** and Erkoç, S. A. 2013. Earthquake-Generating Structures: The Geology of Burdur-Fethiye Fault Zone, Finike and Rodos Basins with Relation to Ancient Cities. 25 Years of Patara Excavations, 11-13 November, 2013, Antalya, Turkey.
- **Elitez, İ.,** and Yaltırak, C. 2013. Cibyra Fault: From a Hypothetic Approach to Reality. 66th Geological Congress of Turkey, 1-5 April, 2013, Ankara, Turkey.

- **Elitez, İ.,** and Yaltırak, C. 2013. Is there really an active fault (Cibyra Fault?) cutting the Stadion of the ancient city of Cibyra? (Burdur-Fethiye Fault Zone, Turkey). General Assembly European Geosciences Union (EGU), 7- 12 April, 2013, Vienna, Austria.
- **Elitez, İ.,** and Yaltırak, C. 2012. Does the active Cibyra Fault cut the ancient Stadion? (Burdur-Fethiye Fault Zone, Turkey). PANAF, 08-10 October, 2012, İTÜ, İstanbul, Turkey.
- **Elitez, İ.,** Yaltırak, C., and Akkök, R. 2011. The Miocene-Quaternary Geodynamıcs of Çameli, Gölhisar and Acıpayam basins, Burdur-Fethiye Fault Zone, SW Turkey. 64th Geological Congress of Turkey, 25-29 April, 2011, Ankara.
- Yaltırak, C., **Elitez, İ.,** Aksu, A., Hall, J., Çiftçi, G., Dondurur, D., Akkök, R., Küçük, M., and Güneş, P. 2010. The Relationship and Evolution of the Burdur-Fethiye Fault Zone, the Rhodes Basin, Anaximander Seamounts, the Antalya Gulf and the Isparta Angle since Miocene to Recent in Tectonics of the Eastern Mediterranean. 63th Geological Congress of Turkey, 5-9 April, 2010, Ankara, Turkey.
- **Elitez, İ.,** Yaltırak, C., and Akkök, R. 2009. Morphotectonic Evolution of the Middle of Burdur-Fethiye Fault Zone: Acıpayam, Gölhisar and Çameli Area, SW Turkey. International Symposium on Historical Earthquakes and Conservation of Monuments and Sites in the Eastern Mediterranean Region 500th Anniversary Year of the 1509 September 10 Marmara Earthquake, 10-12 September, 2009, İstanbul, Turkey.

OTHER PUBLICATIONS, PRESENTATIONS AND PATENTS:

- Gültekin, D. İ., Karakoç, O., Şahin, M., **Elitez, İ.,** and Yaltırak, C. 2017. Influence of the Saros Fault on the Periodicity of Earthquake Activity (Gelibolu Peninsula, NW Turkey). General Assembly European Geosciences Union (EGU), 23-28 April, 2017, Vienna, Austria.
- Karakoç, O., Gültekin, D. İ., Şahin, M., **Elitez, İ.,** and Yaltırak, C. 2017. The Anafartalar Thrust Fault and its Effect on Mega-Constructions (Çanakkale Strait, NW Turkey). General Assembly European Geosciences Union (EGU), 23-28 April, 2017, Vienna, Austria.
- Şahin, M., **Elitez., İ.,** and Yaltırak, C. 2017. How angry was the ancient Greek god Poseidon in 141/142 A.D.?. General Assembly European Geosciences Union (EGU), 23-28 April, 2017, Vienna, Austria.
- Şahin, M., **Elitez., İ.,** Özmen, A., and Yaltırak, C. 2016. Historical Earthquake Scenarios and Effects on the Ancient City of İstanbul (A.D. 478-1999). General Assembly European Geosciences Union (EGU), 17-22 April, 2016, Vienna, Austria.
- Tur, H., Yaltırak, C., **Elitez, İ.,** Sarıkavak, K. T. 2014. Pliocene-Quaternary tectonic evolution of the Gulf of Gökova, southwest Turkey, *Tectonophysics,* 638, 158-176.
- Şenol, Ş., Biberoğlu, S., Poşluk, E., and **Elitez, İ.** 2014. The Comparison of Blasting Excavation and TBM Performance in the Running Tunnel Being

Excavated Through Dolayoba Formation. 67th Geological Congress of Turkey, 14-18 April, 2014, Ankara, Turkey.

- Yaltırak, C., Alpar, B., Altınok, Y., **Elitez, İ.,** Tur, H., Kıyak, N., and Zabcı, C. 2012. Kinematic features, fault segmentation and historical earthquakes of the Ganos Fault Zone. PANAF, 08- 10 October, 2012, İTÜ, İstanbul, Turkey.
- Vardar, D., Öztürk, K., Yaltırak, C., Alpar, B., Tur, H., and **Elitez, İ.** 2012. The geometry and activity of the North Anatolian Fault's middle strand at the southern shelf of the Sea of Marmara. PANAF, 08- 10 October, 2012, İTÜ, İstanbul, Turkey.